PIEZOELECTRIC POLYMER FILMS MADE OF POLY-L-LACTIC ACID FOR BIOMEDICAL USE

Lea Gazvoda

Doctoral Dissertation
Jožef Stefan International Postgraduate School
Ljubljana, Slovenia

Supervisor: DDr. Marija Vukomanović, Jožef Stefan Institute, Ljubljana, Slovenia

Evaluation Board:
Prof. Dr. Janez Štrancar, Chair, Jožef Stefan Institute and Jožef Stefan International Postgraduate School, Ljubljana, Slovenia
Prof. Dr. Ida Poljanšek, Member, Biotechnical Faculty, University of Ljubljana, Ljubljana, Slovenia
Prof. Dr. Simonida Tomić, Member, Faculty of Technology and Metallurgy, University of Belgrade, Serbia

MEDNARODNA PODIPLOMSKA ŠOLA JOŽEFA STEFANA
JOŽEF STEFAN INTERNATIONAL POSTGRADUATE SCHOOL

Lea Gazvoda

PIEZOELECTRIC POLYMER FILMS MADE OF POLY-L-LACTIC ACID FOR BIOMEDICAL USE

Doctoral Dissertation

PIEZOELEKTRIČNI POLIMERNI FILMI IZ POLIMLEČNE KISLINE ZA BIOMEDICINSKO UPORABO

Doktorska disertacija

Supervisor: DDr. Marija Vukomanović

Ljubljana, Slovenia, Januar 2024

To my energetic children,
to my dear husband,
to my father.

I want to make you proud!

Acknowledgments

I sincerely thank my supervisor DDr. Marija Vukomanović for sharing her knowledge with me, she is an excellent researcher and always ready to help. She gave me the freedom with directing the course of my research and gave me constructive and honest comments on my work, which helped me become a better researcher and also paper writer. Thank you for your guidance, suggestions, discussions and honesty.

I appreciate the help of Prof. Danilo Suvorov and Prof. Dr. Matjaž Spreitzer for the opportunity that allowed me to do the research, for always having open doors for questions, for advice, and the way of management that made the workplace very pleasant.

I also wish to thank Dr. Nemanja Aničić and Dr. Mario Kurtjak, who were in my shoes beforehand. Thank you Nemanja for your help with the orientation and start with my research, for all the advice and shared work practice about bacteria and polymers, for introduction to SEM microscopy and working with microplate reader and how to perform FTIR measurements. Thank you, Mario, for sharing your experience with bacteria and cells, for brainstorming ideas and problems with me and for relaxed conversations. Thank you both for introducing me to the established work practice in BiomatLab.

I also thank all of my fellow Young Researchers from the Advanced Materials Department. Thank you all for contributing to the relaxed and friendly atmosphere. Special thanks to Urška and Nina for the help with the specific XRD measurements on monocrystal.

I appreciate all the help from the co-workers from the Advanced Materials Department who are always ready to listen to my presentations, problems and ideas and give advice. Many helped me with the knowledge about measuring systems I performed analyses on during my research, I would like to thank Marjeta Maček for teaching me how to use DSC, Srečo Škapin for showing me how the XRD is used, Damjan Vengust for teaching me and helping me with the Raman spectrometer. Also, a big thank you to David Fabijan for his piezoelectric measurement and his programming skills.

I would also like to thank my family, my husband and his family for all the support given during the course of my PhD.

Special thanks go to the Jožef Stefan International Postgraduate School, and to the Slovenian Research and Innovation Agency for the provided funding (grant numbers PR-08338 and P2-0091).

Abstract

In the field of biomedical materials, conventional approaches to tissue engineering and wound healing face limitations that encourage the exploration of innovative treatments. This work presents multifaceted exploration of piezoelectric polylactic acid (PLA) films intended for biomedical applications, from the optimization of the conditions for efficient film preparation to the investigation of the degradation processes, the development of nanotextured (NT) PLA films, and presents the evaluated performance for wound healing as an applicative view of use.

The study firstly presents the polymer physical, chemical and piezoelectric properties and behavior at different temperatures to successfully optimize the preparation of piezoelectric polymer film by uniaxial tensile stretching. As part of this study, piezoelectric measurements of the whole film were directly correlated to the newly formed properties of the polymer, such as crystallinity and orientation, and more importantly, how additional modifications (annealing and surface etching, topography) affect piezoelectricity through modified method of measurements. The surface was additionally alkali etched due to poor hydrophilic properties, which noticeably improves the surface. Accelerated degradation using proteinase K reveals that enhanced surface hydrophilicity alters the degradation process from bulk to surface-oriented erosion, maintaining mechanical stability and, consequently, piezoelectric properties for extended durations.

The study also introduces a template-assisted method for preparing NT PLA films. The nano-sized topography significantly enhances piezoelectric properties, offering promising biological responses. A new method for assessing piezoelectric properties which employed the decomposition of an organic dye as a measure was proposed, which enables a complete evaluation of piezoelectric properties by considering materials with complex surface texture.

The antibacterial effects of piezoelectric PLA films on both Gram negative and Gram positive bacteria were explored. Notably, the research identifies (piezo)electric stimulation, activated externally via ultrasound (US), to lead to bactericidal effects for bacteria in contact with piezoelectric NT film. The study also dismisses concerns of toxicity to non-adherent (red blood cells) or adherent cells (epithelia skin cells), establishing the films as promising candidates for antibacterial agents or wound healing applications.

Cellular (keratinocytes) and immune response (macrophages) to piezoelectric and non-piezoelectric PLA films were also investigated. Mechanical stimulation through US activates (piezo)electric stimulation on cells and reveals improved cell attachment, enhanced actin filament production, improved cell-to-cell connections, and indicates towards improved cell differentiation. The immune response, evaluated through monocyte differentiation into macrophages, suggests minimal immune reaction towards the PLA polymer films, with different polarization responses observed for different film types.

In conclusion, this comprehensive exploration establishes the potential of piezoelectric PLA films in biomedical applications. The findings offer valuable insights into the material's degradation, antibacterial properties, and cellular responses, providing a foundation for future advancements in electro-stimulated regeneration and wound healing technologies.

Povzetek

Na področju biomedicinskih materialov se konvencionalni pristopi k tkivnemu inženirstvu in celjenju ran soočajo z omejitvami, ki spodbujajo raziskovanje inovativnega zdravljenja. To delo predstavlja večplastno raziskovanje piezoelektričnih filmov PLA, namenjenih biomedicinskim aplikacijam, od optimizacije pogojev za učinkovito pripravo filma do raziskovanja procesov biorazgradnje, razvoja nanotekstuiranih (NT) PLA filmov in predstavlja ocenjeno učinkovitost za celjenje ran kot aplikativni pogled uporabe.

V študiji so najprej predstavljene fizikalne, kemijske in piezoelektrične lastnosti PLA ter obnašanje polimera pri različnih pogojih za uspešno optimizacijo priprave piezoelektričnega polimernega filma z enoosnim raztezanjem, saj isti polimer z manjšo ali večjo molekulsko maso različno reagira na temperaturo in pogoje vlečenja. V tej študiji so piezoelektrične meritve celotnega filma neposredno povezane z nastajajočimi lastnostmi polimera, kot sta kristaliničnost in orientacija, in še pomembneje, kako dodatne modifikacije (segrevanje pri visokih temperaturah in površinsko jedkanje, topografija) vplivajo na piezoelektričnost, izmerjeno s predelano merilno metodo. Zaradi slabih hidrofilnih lastnosti je površina filma dodatno kemijsko jedkana, kar opazno izboljša površinske lastnosti. Pospešena razgradnja z uporabo encima proteinaze K razkriva, da izboljšana površinska hidrofilnost spremeni proces razgradnje iz globinske v površinsko usmerjeno erozijo, zaradi tega film ohranja mehansko stabilnost in posledično piezoelektrične lastnosti dlje časa.

Študija prikaže tudi metodo priprave NT filmov s pomočjo templata z definiranimi nano porami. Topografija nano velikosti znatno izboljša piezoelektrične lastnosti in ponuja obetavne biološke odzive. V delu je predstavljena tudi nova metoda za ocenjevanje piezoelektričnih lastnosti, merjeno preko razgradnje organskega barvila, ki omogoča celostno oceno piezoelektričnih lastnosti materialov s kompleksno površinsko topografijo.

Raziskovan je antibakterijski učinek piezoelektričnih PLA filmov na Gram negativne in Gram pozitivne bakterije. Raziskava identificira predvsem (piezo)električno stimulacijo, aktivirano od zunaj z ultrazvokom, da vodi do baktericidnega učinka na bakterije v stiku s piezoelektričnim NT filmom. Študija prav tako zavrača pomisleke o toksičnosti za ne-adherentne (rdeče krvne celice) ali adherentne celice (epitelijske kožne celice), kar filme uvršča med obetavne kandidate za antibakterijska sredstva ali aplikacije za celjenje ran.

Raziskani so bili tudi različni odzivi celic (keratinociti) in imunski odziv (makrofagi) na piezoelektrične in ne-piezoelektrične PLA filme. Mehanska stimulacija z ultrazvokom aktivira (piezo)električno stimulacijo na celice in pokaže izboljšano pritrditev celic, povečano proizvodnjo aktinskih filamentov, izboljšane povezave med celicami in nakazuje na povečanje celične diferenciacije. Imunski odziv, ovrednoten z diferenciacijo monocitov v makrofage, kaže na minimalno imunsko reakcijo proti polimernim filmom PLLA, z različnimi polarizacijskimi stanji makrofagov (vnetna ali protivnetna polarizacija).

Skratka, ta celovita raziskava predstavlja potencial piezoelektričnih PLA filmov v biomedicinskih aplikacijah. Ugotovitve ponujajo dragocen vpogled v razgradnjo materiala, antibakterijske lastnosti in celične odzive, ki zagotavljajo osnovo za nadaljnje raziskave pri elektro-stimulacijski tehnologiji regeneracije in celjenja ran.

Contents

List of Figures

List of Tables

Abbreviations

PLA	... polylactic acid polymer
PLLA	... poly-L-lactic acid polymer
PVDF	... polyvinylidene fluoride
PI	... polyimide
ECM	... extracellular matrix
FDA	... Food and Drug Administration
EMA	... European Medicines Agency
NT	... nanotextured
AAO	... anodized aluminum oxide template
PZP	... piezoelectric patch
Akt	... protein kinase B
PI3K	... phosphoinositide 3-kinase
ERK ½	... extracellular signal-regulated kinase
M0	... non-activated macrophages
M1	... inflammatory phenotype of macrophage
M2	... anti-inflammatory phenotype of macrophage
ROS	... reactive oxygen species
US	... ultrasound
XRD	... X-ray diffraction
DSC	... differential scanning calorimetry
FTIR	... Fourier transform infrared spectroscopy
DR	... draw ratio
HP	... hot pressed amorphous film
Tg	... temperature of glass transition
Tc	... temperature of cold crystallization
Tm	... temperature of polymer melt
ANN	... annealing
SEM	... scanning electron microscope
MB	... methylene blue organic dye
LB	... Luria-Bertani growth medium
OD	... optical density
CFU	... colony forming units
E. coli	... *Escherichia coli*, ATCC 47076
SE	... *Staphylococcus epidermidis*, ATCC 12228
RBC	... red blood cells
DAPI	... diamidino-2-phenylindole, fluorescent dye
PDLLA	... poly(D,L-lactide-co-glycolide
DC	... direct current
PC	... pulsed current

AC ... alternating current
PS ... polystyrene
FBS ... feta bovine serum
DMEM ... glucose-rich cell medium
BSA ... bovine serum albumin
DPBS ... physiological solution for cells
RP ... Rhodamine Phalloidin
HaCaT ... keratinocyte immortal cells, ATCC PCS-200-011
PB ... PrestoBlue™ viability reagent
THP-1 ... monocyte cells ATT TIB-202
GA ... glutaraldehyde
PMA ... phorbol 12-myristate 13-acetate
HMDS ... hexamethyldisilazane
PFM ... piezoelectric force microscopy

Chapter 1

Introduction

In the modern world, medical practice is still limited to conventional standardized methods of treating a wide variety of medical conditions, especially tissue engineering and wound healing. These methods with their own limitations may affect the effectiveness of treatment in certain cases and could be addressed using innovative treatment procedures, which are intensively researched today. Given my interest in specific topics such as wound healing, tissue engineering and antibacterial properties of biomaterials, some new materials and/or new treatment methods have already been proposed, but are in a state towards the clinical practice. External physical stimuli such as magnetic field, electric field, mechanical stimulation are new and interesting methods that showed some advancement towards accelerating the healing process. The piezoelectric property of the material provides one of the aforementioned stimulations, which is electrical stimulation, and can aid in wound healing.

Piezoelectricity, as a property of materials to accumulate an electric charge as a response to mechanical deformation, is a well-known property of inorganic materials, mostly used in electronics. However, some of the organic materials (including polymers, proteins, DNA, etc.) can also exhibit piezoelectric properties, which are usually with at least one order of magnitude smaller strength and are relevant for interactions that exist inside the living organism [1]. For wound healing, electrical potential gradient at the wound site is a mayor signal for cells to start regeneration [2]. Following this natural phenomenon, the critical role of electrical signals in regeneration can be effectively used to design a new generation of biomaterials for tissue engineering. A particularly interesting class of materials are organic piezoelectric biomaterials. As piezoelectric coefficients of polymers are more comparable to the piezoelectric properties of organic materials than to ceramic, and their mechanical properties are significantly compliable to soft human tissue, in interactions with human cells they can promote their growth, which classifies them as promising biomaterials for use in wound healing stimulation [3].

In addition to stimulating human cell growth, piezoelectric stimulation has also a potential for targeting bacterial infections, particularly during wound healing and tissue regeneration. Bacteria respond to electric potential in different ways, including damaging cell wall which leads to bacterial cell death, inhibition of growth or changing the surface potential leading to surface repulsion [4]. As currently used medical protocols are based on excessive use of antibiotics to prevent or fight bacterial infections which may lead to bacterial resistance to frequently used antibiotics and decreasing their efficacy, novel approach based on piezoelectric stimulation has a large capacity to offer significantly more effective alternative.

According to the presented aspects, I focused my dissertation on the investigation of piezoelectric polymer, specifically polylactic acid (PLA) and its possible generated

piezoelectric potential on the surface to benefit human keratinocyte cells, exhibit antimicrobial properties or some other possible uses due to mechanical/electrical properties of the polymer, hydrophobic/hydrophilic surface, biodegradability and biocompatibility.

1.1 Wound Healing and Electrical Potential

Every tissue scarring results in an immediate response of the organism, starting with the inflammatory phase which initiates a healing process, proceeding with proliferation (repair) and maturation phase (remodeling) [5]–[7]. Fig. 1a (adapted from the article [6]) demonstrates the wound healing process over a period of time. In the first hemostasis phase, which starts immediately after the injury, the initial blood clotting occurs. It is caused by accumulation of released platelets adhered on collagen fibers which come from blood vessels to the wound site, stop further bleeding and limit a spread of pathogens into the blood system [5], [8]. Generated signals from platelets and wound debris (growth factors, chemical mediators) recruit immune cells to the wound site, starting the inflammation phase, which usually lasts for a few days. In this phase, injury-causing agents are neutralized (due to dilution) and tissue's normal physiological state is restored [5], [8]. Chemical mediators, which promote wound healing and prevent infections, are usually released in low concentrations by macrophages (cells of the immune system), lymphocytes (provide body with immune capabilities), fibroblasts (produce collagen and elastin) and plasma cells [5]. During this phase, some tissue is already formed, however tissue does not regain normal functional strength yet. After removal of tissue debris and pathogens, cell proliferation is initiated in the following phases (repair and remodeling processes), which last much longer (weeks to months) than prior steps and result in new tissue formation [7]. Repair, also called proliferation phase, is important to determine the necessary properties of the scaffolds used to support, rebuild or stimulate damaged tissues. In this phase the wound defect is filled with granulation tissue (highly vascular connective tissue), the process of angiogenesis (formation of new blood vessels) occurs and epithelization (migration of cells towards wound closure) over the vascular wound surface, the extracellular matrix (ECM) is formed to fill the gap when needed and main cell proliferation and migration occur, which usually ends with scar tissue [8], [9]. During the remodeling phase, which can possibly last a year or more, the old or damaged ECM is degraded by fibroblast regulation in proteolytic events (cleavage of proteins into smaller components) and replaced by the formation of a new one, during which the tensile strength increases, but usually not more than 80% of the strength of the intact tissue [9].

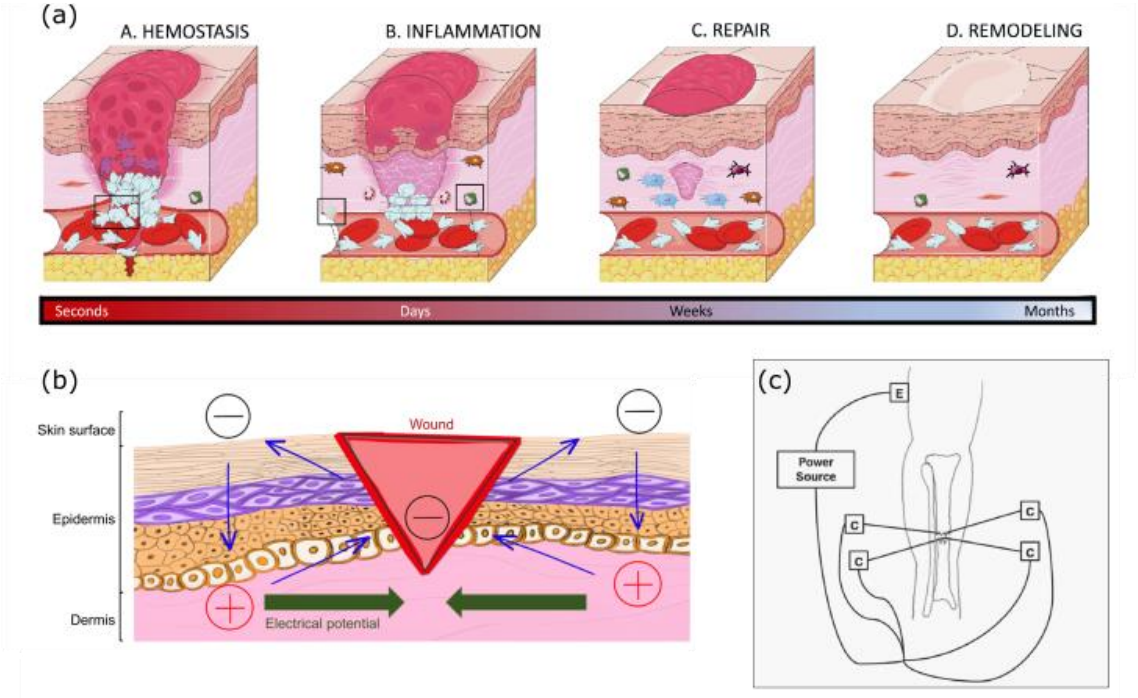

Figure 1: Image shows (a) steps during the tissue repair process (hemostasis, inflammation, repair and remodeling) in chronological order, adapted after ref. [6]; (b) altered endogenous electrical potential formed after the tissue damage, where direct current is generated towards the wound area, adapted after ref. [10]; (c) the use of direct inside electrical stimulation for broken leg, which is an invasive method that uses cathodes directly at the wound site, labeled C, connected to an energy source and electrode (labeled E), located on the outside of the leg, adapted after ref. [11].

Prior factor in wound healing processes and tissue regeneration is endogenous electric field, as a directional electrical potential that guides migration of macrophages, keratinocytes, neutrophils (type of white blood cells) at the wound site [12]. This field is a natural electrical potential formed in epithelia layers composing the epidermis of surrounding organs, which generate steady voltage across themselves. And in case of disruption, lateral electric field has been measured around 40-200 mV/mm, demonstrated in Fig. 1b, leading to initial reaction on the cells, which have the ability to detect electric field and respond with migration towards the wound [13]. The local electric field also stimulates cellular activity through the opening of ion channels via inducing intracellular calcium transients, resulting in better cell proliferation and differentiation [14]. Similarly, an electric field applied through an external material (nanogenerator or piezoelectric [14]) could modulate cellular activity and thus mimic the natural healing process.

Tissue gradually assumes normal functions, however complete recovery is rare [8], therefore it can result in chronic wound (incomplete repair and remodeling stage). Any of the phases can be suppressed due to the bacterial infection, diseases, systemic problems, therefore, some new methods or materials that can activate or accelerate healing process in different stages are welcome/needed to continue delayed or unfinished healing. One of the researched methods is the use of growth factors which cause many additional complications (including low availability, high instability, short half-life, dose-related complications), where optimization is required for each particular wound [15]. The other already used but invasive method is electric current wound healing of injured tissue, schematically presented in Fig. 3c. Its invasiveness is primarily related to the requirement of surgically implemented cathode that can be a source of infection, mechanical mismatch

with surrounding tissue, toxicity and formation of oxidation-reduction products [11]. Therefore, the passive stimulation of endogenous electric field is required for noninvasive method, and it can be achieved through novel functional/smart materials. The alternative noninvasive method is the use of piezoelectric material at site to trigger the voltage difference, when the material is mechanically deformed by body movement or externally by applied ultrasonic field [16]. By choosing the appropriate biocompatible and piezoelectric material, their noninvasive nature (self-sufficient powering as lack of needed wires to induce electricity), great biocompatibility and in case of biodegradable properties no removal is needed after their use, have great potential for use in the wound healing process.

In medicine, electrotherapy is already established and daily used practice in physiotherapy for improved blood circulations, acceleration of bone fracture healing, stimulates the peripheral nervous system, for chronic pain, muscle disorders, as a stress reliever, which mainly has analgesic, anti-inflammatory and tissue-forming effects [17], [18]. Therefore, the use of electrical stimulation inside the body, directly at the wound site, is a promising idea for the regeneration of chronic wounds.

1.2 Piezoelectricity

Piezoelectricity of some natural crystals was discovered in 1880 by Curie brothers and it was named after a Greek word ″piezein″ which literally means pressure. Some ceramics, polymers and composites, which lack a macroscopic center of symmetry in their crystalline structure [15], have piezoelectric properties (Fig. 2a). Piezoelectrics are described as anisotropic dielectric materials, where the applied stress triggers internal polarization (the arrangement/orientation of ions in the non-centrosymmetric crystal structure) and causes an electric field to develop across the material boundary, known as direct piezoelectricity [19]. In the case of indirect piezoelectric effect, electric field causes mechanical deformation on material [20]. A dielectric material has no free electrical charge in basic (random dipole orientation), so external electrical field is usually applied to orient electric dipoles, due to the interaction of the electrical field with the dielectric structure, also called poling or polarizing the material, presented in Fig. 2b [20].

Piezoelectricity is demonstrated with piezoelectric tensor d_{ij}, i defined as the direction of generated electric polarization in the material in response to applied mechanical stress in direction j [19]. Also important but usually not mentioned is piezoelectric voltage constant g_{ij}, defined as the electric field generated by a piezoelectric material per unit of mechanical stress applied, with units Vm/N [19]. We encounter several ways of stimulating piezoelectric property in material, due to the many possible different crystalline structures, known as longitudinal (d_{33}, direction of mechanical deformation and measured generated voltage graphically presented in Fig. 2c), transverse (d_{13}, Fig. 2d), and shear (d_{14}) piezoelectricity. They can act as actuators (doing mechanical work), where d constant is important, or sensors (sending the electrical signal after deforming), where g constant is in focus.

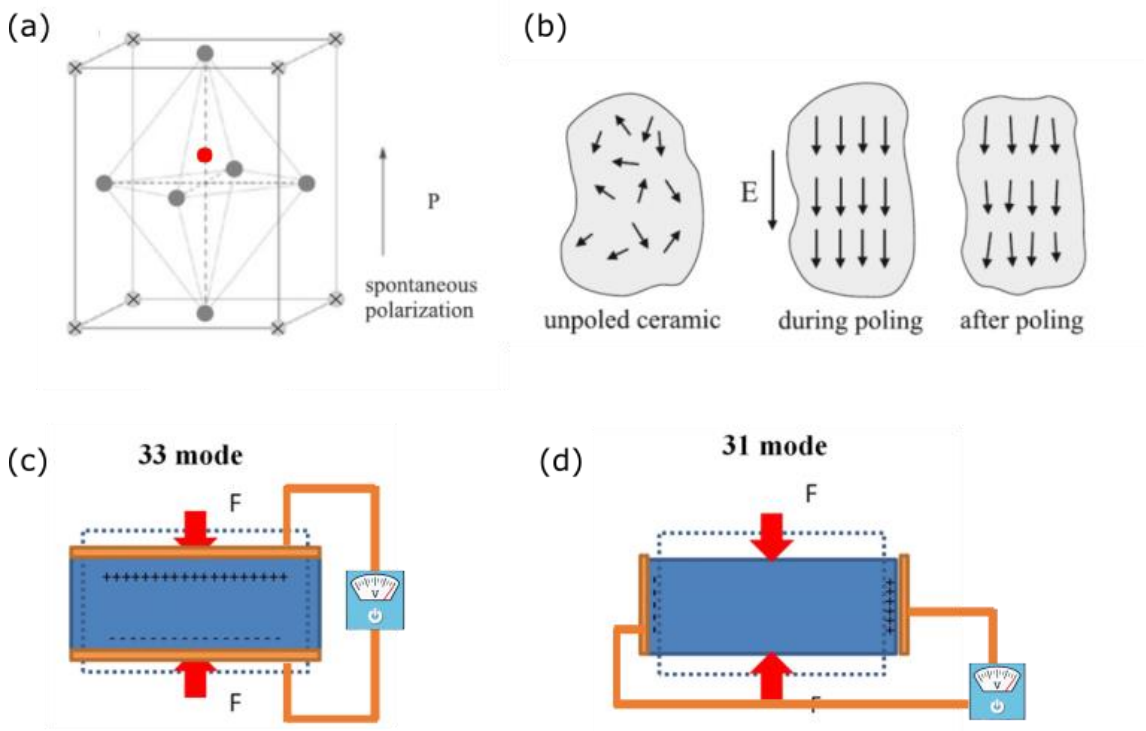

Figure 2: (a) Non-centrosymmetric crystal structure with direction of natural polarization, adapted after ref. [20]; (b) changes in direction of polarization after poling of dielectric by application of high electric field, adapted after ref. [20]; showing the direction of mechanical deformation and the responding voltage in (c) parallel d_{33} and (d) longitudinal d_{31} direction, adapted after ref. [19].

Polymers are long organic chains, composed of chemically bonded series of monomers. Most polymers are considered insulators, which is true for non-polar polymers. These polymers have tightly and covalently bonded electrons to the center of a long main chain with evenly distributed electrons (unavailability of free electrons to create conductivity) [21]. However polar polymers, with slight imbalance in the electronic charge, can be dielectric, therefore also piezoelectric [21]. In order to have piezoelectric properties, polymers need some structural properties including: the presence of permanent molecular dipoles, ability to orient molecular dipoles, ability to sustain achieved dipole alignment and ability of material to undergo large strains upon mechanical stress (polar semi-crystalline polymers) [19]. Semi-crystalline polymers act similarly as piezoelectric ceramic materials, where the polar groups are arranged in crystalline form, allowing for a change in polarization with applied mechanical stress. To enhance the piezoelectricity in semi-crystalline polymers, orientation of crystalline parts is necessary, achieved usually through poling [19]. Poling is done by application of high electric field at the working temperature above the glass transition temperature (increased moldability), where polymer can change shape and dipoles can effectively be aligned with the applied electric field, and then quenched to lower temperatures to maintain most of the orientation [19]. To simplify, only the crystalline parts in oriented semi-crystalline polymer are most affected by mechanical stress, so it contributes the most to the piezoelectric properties.

In general, ceramic materials have 1-2 orders higher piezoelectric values compared to biologic or polymer piezoelectrics. However, g constant of polymers is similar or higher compared to ceramic, therefore are more suitable for sensor application (generating charge due to small mechanical deformations), which is also the property of interest studied in this work. Polymers which possess piezoelectric properties are polyvinylidene fluoride

(PVDF, d_{33}= 20-28 pC/N, already commercially available in different forms) and its copolymers (addition of trifluoroethylene enhances the crystallinity, d_{33}= 25-38 pC/N), polyimide (PI, d_{33}= 5-16 pC/N), poly-L-lactic acid (PLLA, d_{14}= 10 pC/N) and some with lower values (polycaprolactone, polyurethane, polyhydroxybutyrate [22], nylon) [23]. Among the piezoelectric polymers, PLLA is the polymer with the highest piezoelectric coefficient among the biodegradable and biocompatible options. It has a similar spiral or helix crystal structure as biological polymers (collagen). Fig. 3a illustrates the proposed molecular dipole orientation of collagen (red arrows) in helix structure and Fig. 3b shows generated charge on collagen surface after the bone is compressed [23].

Biological materials usually have a spiral structure at different levels of organization, so almost all biological matter possesses piezoelectric properties because spirals do not have a center of symmetry [24]. It was accepted by many researchers that crystallization of material and growth of living tissue are similar phenomena since periodic pattern formation is expressed in crystals and also observed in living organisms (additional units are continuously added with growth, so they orient depending on the previous state) [24].

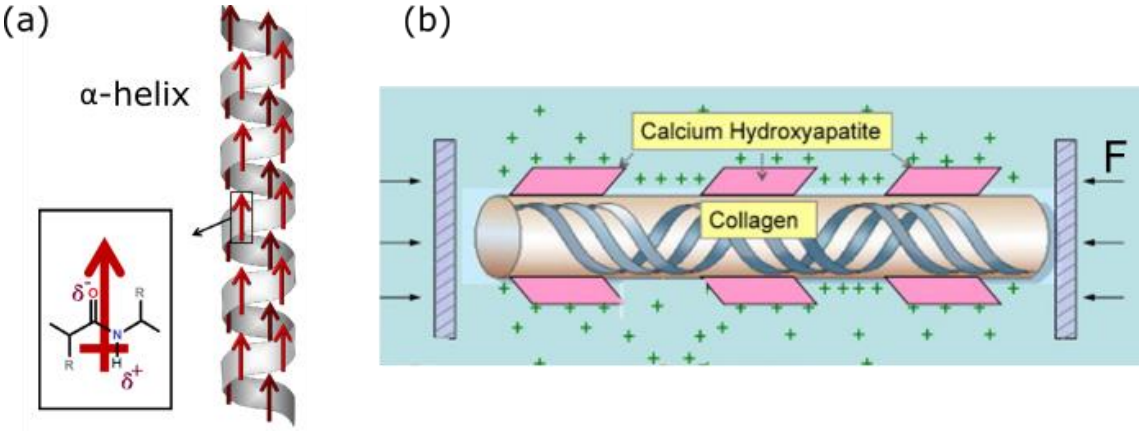

Figure 3: (a) Schematic illustration of permanent polarization in α-helix, demonstrated with red arrows; (b) presentation of generated surface charges as a response to applied stress (F) on bone (collagen fiber with calcium hydroxyapatite), adapted from ref. [23].

1.3 Piezoelectric Poly-L-Lactic Acid Polymer

PLA is a bio-based (biologically derived and biodegradable) thermoplastic polymer, which exists in three conformations, depending on the monomer optical isomer condition (L- clockwise rotation and D- counterclockwise rotation), which are semi-crystalline poly-L-lactic acid, poly-D-lactic acid or amorphous poly-DL-lactic acid [25], [26]. The most preferred/mentioned stereoisomer of PLA for use in medicine with the highest piezoelectric properties is semi-crystalline poly-L-lactic acid (PLLA) [27]. PLLA is a synthetic, biodegradable and biocompatible polyester (monomer presented in Fig. 4a) with α left-handed helix crystal structure, characterized by shear piezoelectric responsiveness. It is also approved by Food and Drug Administration (FDA) and European Medicines Agency (EMA) as appropriate for medical applications [28]. Piezoelectricity in PLLA originates from orientation of C=O molecular dipoles. Due to helical structure and lack of center of symmetry in the crystal structure (a chiral center in monomer) polymer exhibits shear piezoelectricity in all crystal forms, including α, β, and γ [29]. The most stable structure of PLLA is α with orthorhombic unit cell and 10_3 helix conformation, illustrated in Fig. 4b. It is formed upon crystallization above 120°C [25]. Its unit cell contains two antiparallel chains [30]. Frequently observed is also α'crystal form, which has disordered packaging of

10_3 helix conformation, with pseudo-hexagonal unit cell [30]. An α' is formed with temperature crystallization under 120°C.

Shear piezoelectrics act differently compared to parallel, therefore methods for measuring piezo coefficients are more complicated, poling is not necessary since all conformations of PLLA are piezoelectric due to chirality. When PLLA polymer is mechanically deformed, C=O groups (carriers of charge) around the polymer backbone orient in the same direction which creates molecular dipole through the whole polymer chain [29], schematically illustrated in Fig. 4c. Crystallites still need to be oriented in the same direction to exhibit charge on the bulk polymer surface upon deformation, otherwise generated charges are canceled out inside the bulk polymer film. Therefore, the magnitude of the piezoelectric constant of PLLA polymer is proportional to the degree of orientation of molecular chains and crystallinity [31]. Because of low dielectric constant value (ε=2.7) [3], PLLA films have a small charge (d) but high voltage piezoelectric coefficient (g). This means that its sensitivity is very high, therefore small changes instantly invoke charge generation on the surface.

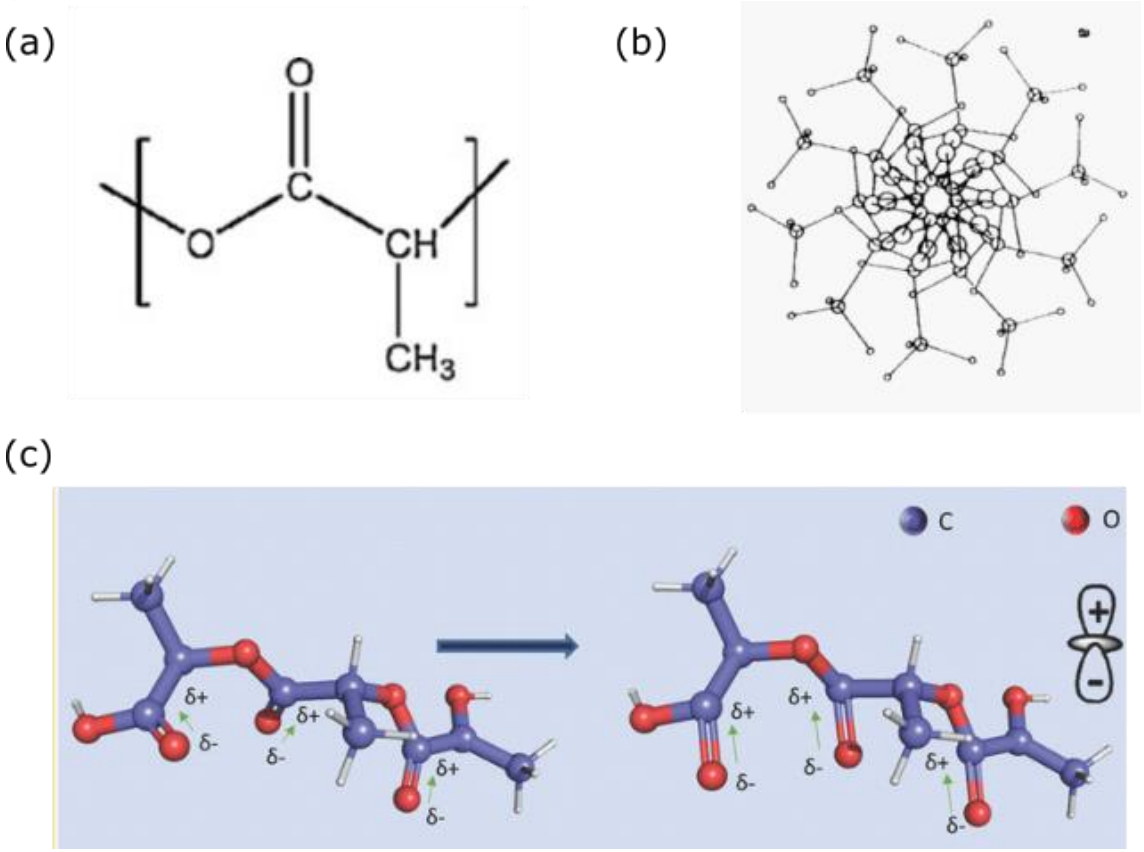

Figure 4: (a) Monomer unit of PLLA; (b) typical 10_3 helix conformation of α crystalline PLLA, adapted after ref. [32]; (c) dipole orientation after mechanical stretching, adapted after ref. [33].

The main drawback for the mentioned polymer is mostly its hydrophobic and inert surface [28]. PLA polymers do not contain functional groups through the main chain, such as carboxyl (COOH) and hydroxyl (OH) groups, which increase surface hydrophilicity. These groups are present only at the long ends of the polymer chain, therefore the polymer exhibits more hydrophobic properties. However, surface hydrophilicity can be improved to be more attractive for cell attachment by surface modification/functionalization such as plasma etching [34] or alkali etching [35], [36], functionalization by attaching

macromolecules (improves biocompatibility and biomaterial integration *in vivo* [37]), changing the topography [38]. During my research, I have shown that the use of chemical surface etching (alkaline etching) of the PLLA polymer surface results in an increase in surface roughness and improved hydrophilicity due to the surface degradation of amorphous polymer chains into short chains with more exposed polymer hydrophilic end groups on the surface, without deterioration of mechanical properties [39]. Also, PLA is characterized with slow degradation rate, which can be beneficial or not, depending on the proposed application. When I investigated the degradation of PLLA polymer, I found that despite the rapid degradation in the presence of enzymes, the piezo-properties do not decrease immediately but are preserved for some time, so that they can still support certain critical levels of regeneration [40].

1.3.1 Methods to prepare piezoelectric poly-l-lactic acid films

A simple and efficient method to impart orientation and crystallinity into the polymer is uniaxial drawing of polymer films or fibers above the glass transition temperature [41], [42]. Drawing process leads to the molecular orientation of crystalline and amorphous regions, which also influences mechanical properties, and induces structural changes such as crystallinity and orientation, due to the strain-induced crystallization [43]. Mechanism of stretching process is schematically illustrated in Fig. 5a. The additional post-processing heat treatment can improve crystallinity, and consequently also piezoelectric properties. The largest value of piezoelectric coefficient d_{14} for oriented polymer film (bulk) is 10 pC/N, [44], however, I mostly encounter lower values in the literature for differently prepared samples (micro or nano fibers). Using a tensile-like stretching machine to draw the amorphous PLLA polymer film, I optimized conditions such as draw ratio, draw speed, stretching temperature, preheating time to achieve the maximum chain orientation/relaxation ratio, stretched at temperature above the glass transition with confirmed and measured piezoelectric properties [39].

Another method for producing piezoelectric films, however with a much different morphology (nanotextured (NT) surface), is the template-assisted method. Anodized aluminum oxide plate (AAO) with well-defined nanosized pores is used as a template, in which polymer is imprinted from the melt or the solution [25], [45]. When using AAO template, oriented and slightly crystalline nanofibers are achieved on a polymer substrate. With this approach, stretching of the polymer fiber occurs due to capillary flow inside the tube in a template, therefore orientation in longitude direction was observed [45]. Polymers in the form of liquid have low-energy surface and spread rapidly on high energy surfaces (solid material), therefore pore walls are wetted instantly, while the complete filling of the pore takes much more time [46]. After solidification of the polymer (cooling below the crystallization or glass transition temperature for melt or by evaporation of solvent for solutions), tubes or pillars are formed [46]. Crystallinity can be improved with annealing. Due to the selected conditions (time, temperature, pressure, solvent), nanorods or nanotubes with different lengths can be formed [45], [47]. Due to the template properties (pore size, pore length, spacing between pores), different NT films are formed, where properties are just as different (mechanical, antibacterial) [48]. Fig. 5b presents a principle of template-assisted method (pressing the template on to polymer melt, polymer protected with aluminum (Al) foil and glass slides, compressed between two metallic blocks, heated near the melting temperature of the polymer) and proposed appearance of the exposed NT polymer film after template removal [45]. I was able to prepare a NT film as nanotubes attached to a polymer surface after the AAO template was chemically removed, without

the use of toxic organic solvents, with confirmed and improved piezoelectric properties compared to stretched PLLA film and with confirmed bactericidal properties against Gram negative and Gram positive representatives [49].

Interesting and frequently used methods for producing polymer fibers/films are also electrospinning and melt-drawing of polymer. Electrospinning is a cost-effective method of producing nano or micro fibers, when using the conductive collector to attract/catch fibrous mesh. The mechanism behind electrospinning is using the electric field (15kV) to drive positively charged polymer solution which emerges from the tip of the needle towards the negative charged rotating or static collector, drying the polymer solution and producing the fibers [50]. For melt spinning or melt drawing, polymer melt is extruded on the substrate and is air quenched at the exit, later being drawn using a series of heated rotating drums to improve crystallinity and orientation of the microfibers [51]. Using an extruder, thin films or fibers with more uniform mechanical properties over the sample are prepared, and additional stretching of the extruded samples greatly improves the mechanical properties of the polymer films [51], [52]. With electrospinning, soft films are obtained with poor crystallinity and orientation, which is then improved in the post-processing steps by annealing and stretching. Similar with the melt-spinning, where additionally, large amounts of polymer are required for continuous production of large samples, therefore unable to prepare small specific samples (hard to simultaneously extrude and draw small samples) for easier optimization or modifications of the polymer preparation process.

Piezoelectric properties and preparation conditions of differently prepared films, using electrospinning [28], melt-drawing [29], and template-assisted method [19] for PLLA were already researched. However, direct correlations of bulk piezoelectric properties through direct measurements with processing conditions are rarely presented, piezoelectricity is mostly concluded through improved crystallinity and orientation characteristic of the prepared films.

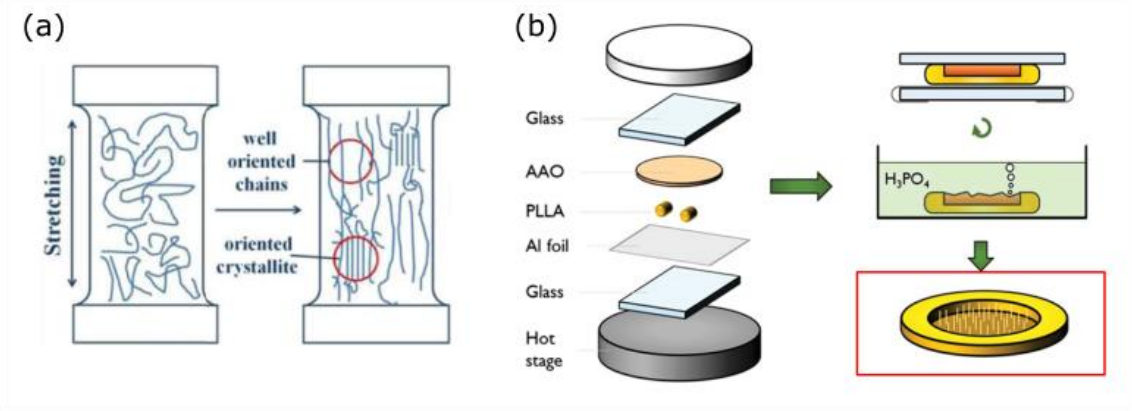

Figure 5: (a) Schematic illustration of how stretching of amorphous polymer film elicits orientation of long polymer chains and therefore also crystallinity within the amorphous matrix (strain-induced crystallization, adapted after ref. [42]); (b) presentation of the template-assisted method: PLLA granules are compressed with two metal blocks on hot stage between AAO and Al foil, protected with glass slides, later on the AAO template is removed by phosphoric acid (H_3PO_4) to expose NT polymer film highlighted with red border (adapted after ref. [45]).

1.4 Prospective Applications of Piezoelectric Polymers in Medicine

Although polymers, specifically PLLA, have been intensively applied in many areas of biomedicine, including designing implants for tissue regeneration (meshes, patches, plasters, scaffolds), forming tools for surgery, as a drug delivery system or only as coatings [53], [54], piezoelectric property of PLLA for biomedical applications is very poorly explored. Because of the biodegradability of PLLA in water (which takes place for the period of up to three years and depends on many properties including polymer crystallinity, molecular weight, chain size polydispersity, crosslinking, etc.), no later removal from inside the body is needed [55] which presents important advantage of PLLA in comparison to other biocompatible piezoelectrics.

Preparing and modifying PLLA biodegradable polymer films with different piezoelectric properties leads to many uses, as for therapeutic use for improved wound healing (placing film in the form of piezoelectric patch (PZP) on wound surface, presented in Fig. 6a or for antibacterial properties.

1.4.1 Using piezoelectric polymers for wound healing

There is much evidence in the literature on how electrical stimulation improves healing and affects cell behavior (cell proliferation, migration, differentiation or increases protein/growth factor production [55]–[58]) through imitations of the natural process of wound healing, where small electric fields are already present. In case when a piezoelectric patch was used in *in vivo* study on mice (patch put on artificially created wound, presented in Fig. 6b), significantly smaller wound size was observed compared to non-treated wound after 10 days of stimulation/piezo-activation by mouse movement, presented in Fig. 6c [58]. Previous findings suggest that piezoelectric potential induces intracellular signaling pathways (phosphorylation of protein kinase B (Akt), phosphoinositide 3-kinase (PI3K) and extracellular signal-regulated kinase (ERK ½), determined with western blot analysis) to direct cell migration and proliferation in keratinocyte cells, schematically presented in Fig. 6d [58]. In general, cells in close contact with piezoelectric material can also respond to electrical stimulation through changes in voltage-gated channels (Ca^{2+} influx affecting cytoskeleton changes to direct cell migration [59]) and with additional activation of signaling pathways [60], improved cell migration, proliferation or differentiation is observed. For keratinocytes, suppressed proliferation was also observed as a result of mechanical/electrical (5V) stimulation at the expense of improved cell differentiation, activated by changes in transepidermal extracellular calcium gradient, which plays a key role as a regulator for cell maturation and differentiation [61], [62]. When observing the effect of electrical stimulation on keratinocyte cells in my study, a significant effect was observed mainly on the increased formation of F-actin filaments and altered cell shape into more elongated filopodia-like shapes on piezoelectric PLLA films, both important in cell adhesion and cell migration during wound healing.

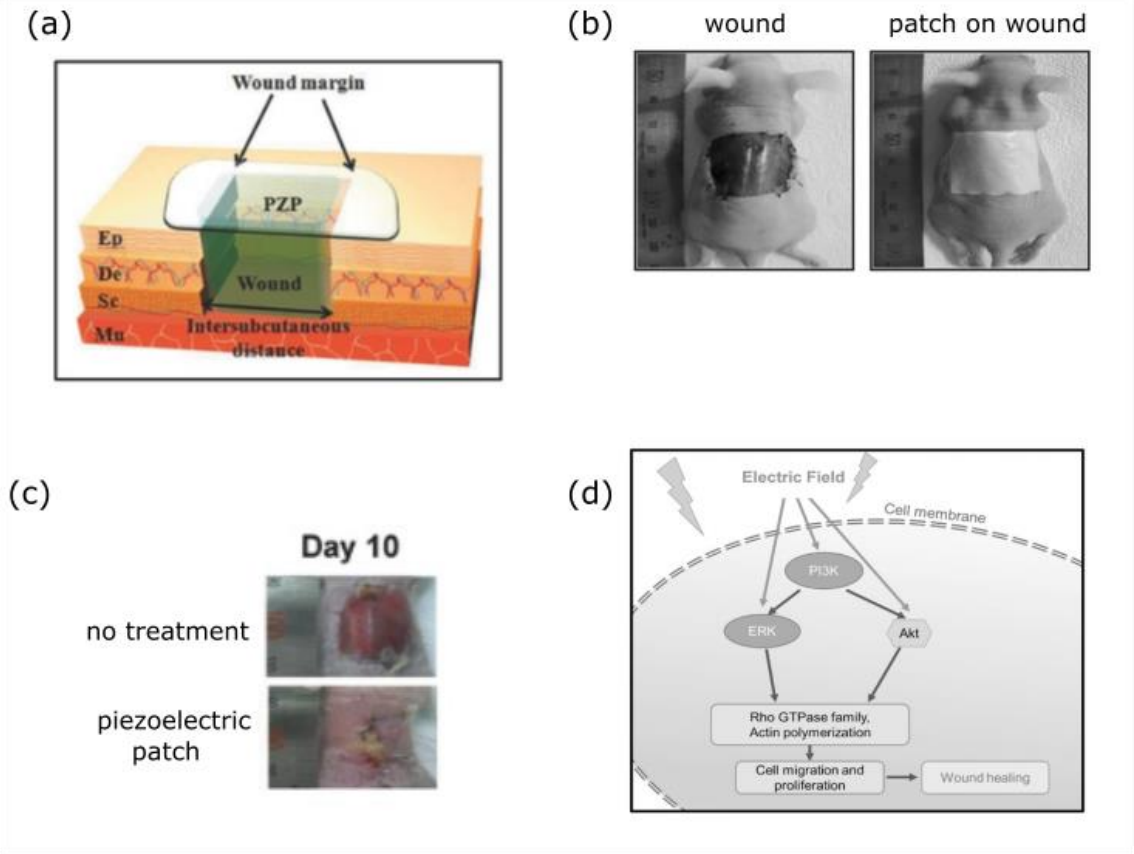

Figure 6: (a) Presentation of PZP on artificially created wound; (b) artificially created wounds on mouse and the coverage with PZP film; (c) changes in the area of wound reduction after 10 days of stimulating PZP film for mice with or without the patch; (d) proposed signaling pathway activated due to electrical stimulation, where electric field activates ERK and Akt signals to increase actin polymerization, resulting in increased cell migration and proliferation.

However, in the case of biodegradable PLLA, only recent studies have been focused on exploiting piezoelectric properties as the main beneficial property of the polymer aimed at enhancing wound healing. Most literature regarding the piezoelectric polymers is done for PVDF piezoelectric scaffolds [12], [33], [38], however the excitation of piezoelectricity is different for PLLA (shear vs. parallel piezoelectric), therefore the mechanism of charge generation and excitation in combination with cells needs some more detailed explanation. Fig. 7a presents crystal structures of PVDF polymer (α, β, γ), with piezoelectric β phase (polarity due to the strong electro-negativity of fluorine atoms on one side and electro-positivity of hydrogen on the other side) with highest piezoelectric properties and difficult-to-achieve γ piezoelectric phase [63]. Since molecular dipoles are uniformly oriented through the chain, which can be achieved mostly through poling, the crystal can exhibit a non-zero dipole moment [63]. Fig. 7b presents the two classes of polymer piezoelectrics, divided by the type of necessary treatment to achieve polarization (Class 1- high electric field; Class 2- uniaxial mechanical stretching) [64]. PVDF belongs to class 1 with oriented dipoles (upon polarization), presenting point group $C_{\infty v}$ in crystallography and PLLA belongs to the second class of polar chiral molecules, presenting helix chains (point group D_{∞} in crystallography) [64]. I believe that upon mechanical deformation in case of twisting the film, constant positive charge is present on positive side of poled PVDF film, due to polymer dipole polarization, when compared to oriented PLLA, charge is shifting from

positive on stretched and negative on compressed side, due to shear piezoelectric properties (Fig. 7c).

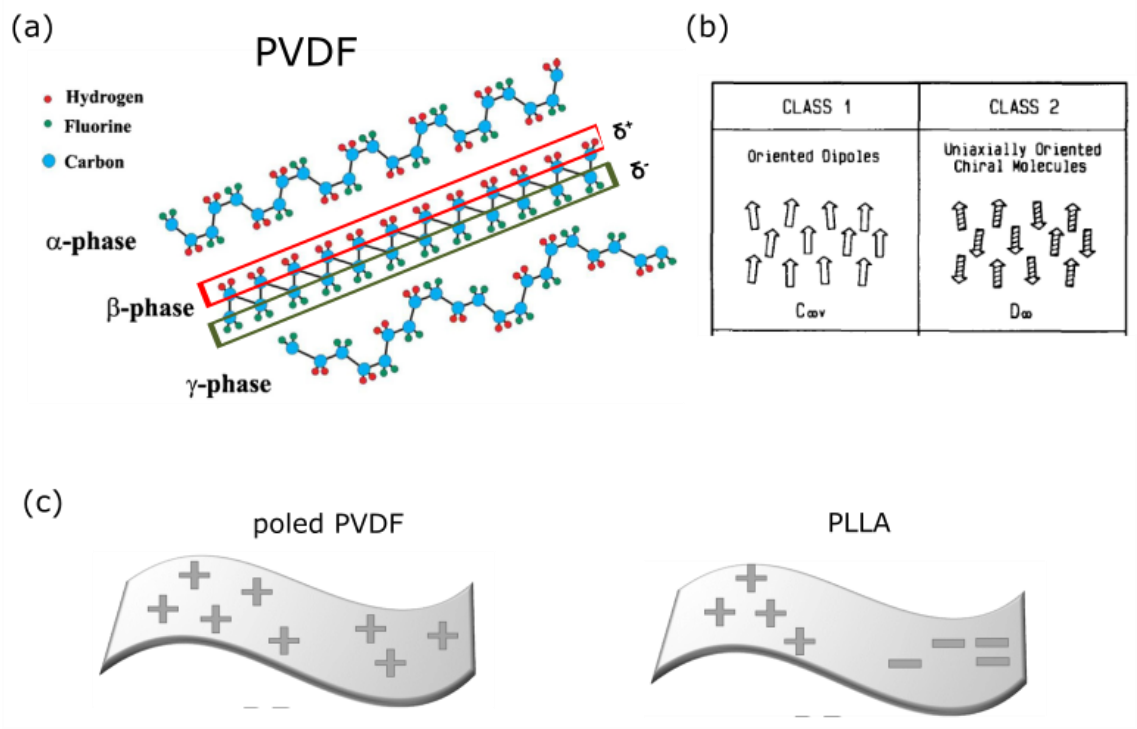

Figure 7: (a) Schematic representation of the chain conformation for the α, β and γ phases of PVDF with the added electro-active potential of fluorine or hydrogen atoms of the most piezoelectric β-phase (adapted from ref. [63]); (b) two classes of oriented polymers, according to the type of necessary treatment, where the first class presents orientation of molecular dipoles with application of high electric field (poling) associated with C symmetry and the second class presents orientation imparted by uniaxial mechanical drawing of chiral polymers, associated with D symmetry (adapted from ref. [64]); (c) schematic understanding of charge generation upon mechanical twisting of PVDF and PLLA thin film.

Fig. 8a illustrates attached cell on thin piezoelectric film, where due to close contact, the cell can feel electrical stimulation activated through mechanical deformation of the film. For the attachment of the material with cells, the topography of the material is also extremely important, as it serves as the first interaction with the biomaterial. By using NT material (displayed pores, fibers or ridges in the nanometer scale), mimicking the natural ECM with nanosized topography is achieved, improving the initial cell attachment [65], [66]. ECM, usually conducted from nanosized immobilized biomacromolecules (collagen, glycoproteins, glycosaminoglycans and proteoglycans), serves as structural support and provides together with signaling molecules the cues for cell adhesion, migration, proliferation and differentiation [65]. Due to the NT morphology, many advantages can be expected, such as improved cell adhesion due to mimicking ECM, increased specific surface area, and additional antimicrobial properties (discussed in Chapter 1.4.2). In case of nanosized pillars on polymer surface (Fig. 8b), cellular weight can be enough to activate piezoelectric properties of polymer fibers [20].

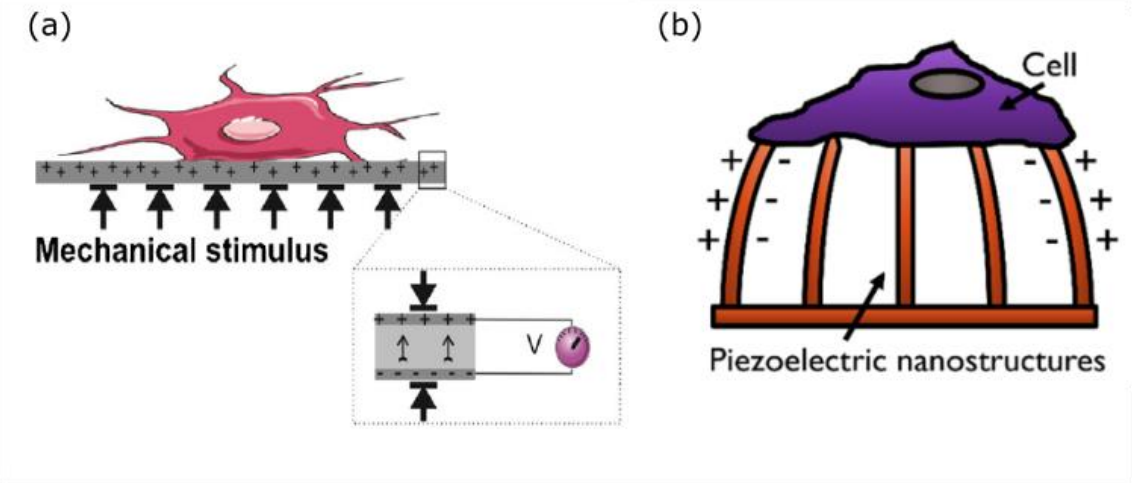

Figure 8: (a) Cell seeded on polarized piezoelectric film, mechanically triggered to activate electric stimulation on cells, adapted after ref. [15]; (b) cell seeded on nanotubes triggers polymers PLLA piezoelectric properties (adapted after ref. [48]).

1.4.1.1 Inflammatory response to implemented material

In case of wound damage, monocytes provide the first line of defense. Monocytes are short-lived non-proliferating cells which die after 1-2 days and are replaced with the new ones, if not recruited into a tissue for facing the danger [67]. For viruses, bacteria, foreign material implementation, tissue damage, non-adherent monocyte from blood differentiate into macrophages, which attach to specific material and try to digest it via phagocytosis, reactive oxygen species (ROS), nitric oxide, and inflammatory cytokines (cell signaling molecules that modulate the immune system response) in case of inflammatory response [67], [68]. In short, macrophages are differentiated from white blood cells (monocytes) which are present in blood stream, and for the injury or implementation they migrate to the wound area [69]. They play a vital role in immune response through different polarization states, including the proinflammatory (M1) or anti-inflammatory phenotype (M2) [69]. In case of implementation of the scaffolds (cell supporting biocompatible material), both types of responses can be triggered, an immune reaction against the material or activation of tissue repair mechanism of the injury [70]. In both cases, inflammation is essential to promote cell recruitment and initiate wound healing. Differentiation is activated with inflammatory signaling molecules after the injury. If the inflammatory response is not excessive, therefore implemented material is not rejected, macrophages enable the injured site to transition into healing phase by releasing growth factors which promote proliferation of fibroblast and blood vessel formation [69]. Therefore, macrophages can be mostly recruited from blood for inflammatory response, while after the differentiation into type 2 polarization (M2) when re-establishment of tissue integrity is enhanced, the number of macrophages in this stage usually increases by proliferation of non-active tissue-resident macrophages (M0) rather than migration from the blood [67].

Proinflammatory response can be exploited for immunotherapy, mostly for cancer/tumor cells, for stem cell recruitment and differentiation, where proliferation and differentiation into M1 is beneficial to stimulate immune response [70], [71]. Using electric stimulation on seeded macrophages on piezoelectric PVDF film, enhanced gene expression of M1 markers was observed, as a result of changing Ca^{2+} influx through voltage-gated channels, compared to not stimulated samples [71]. Due to the biodegradability of PLLA, degradation products and the presence of monomeric l-lactic acid, which lowers the pH to an acidic microenvironment, can present a problem, as they lead to a reactive immune

microenvironment. Only with long-term exposure to monomeric lactic acid have the simulated degradation products been observed to remodel metabolism in cells, leading to elevated proinflammatory cytokines (signaling proteins to stimulate, recruit and proliferate immune cells) as an immune response [72]. Through change from M1 to M2 macrophage polarization it was shown that electric stimulation can be beneficial toward wound healing, since M2 differentiation increased for stimulated samples [73]. Otherwise, surface functionalization/modification can also improve biomaterial integration with the sample.

1.4.2 Antimicrobial properties of piezoelectric materials

The main problem we have been facing for some time is the excessive use of antibiotics, in case of preventive use or in large dosages or for treatment of chronic wounds, where continuous use is required. This leads to the development of bacterial resistance to antibiotics, which motivates researchers to seek new approaches to combat them. Also, the implementation of active substrate on the wounded tissue brings the possibility of infection when implants are inserted, which prolongs the healing process. Therefore, it is important to access the issue of bacteria present.

An alternative method is to exploit electro-stimulation on bacteria through piezoelectric property of material (polymer, ceramic, composite). For material to gain antibacterial properties, three mechanisms are proposed, such as repelling effect (these surfaces resist bacteria attachment), leachable surface (surface is treated with antibacterial agents that are able to leach into the medium) or contact-kill surface [74].

In the case of piezoelectric materials with a high piezoelectric coefficient (>100 pC/N, [75]), a toxic effect on bacteria is observed, which is mostly explained by the formation of ROS. ROS are highly reactive molecules and free radicals, such as hydroxyl radicals ($\cdot OH$), superoxide ($\cdot O_2^-$), originating from molecular oxygen and water molecules [75]. Even though ROS are naturally present and are engaged in many cell activities (signaling for molecules to control normal cell physiological functions activates inflammation response), their overproduction causes damage to cell structures [76]. Piezoelectric barium titanite (BTO) nanoparticles, activated through US stimulation and forming ROS via redox reactions, show high antibacterial efficiency against Gram negative and Gram positive representatives [77], [78]. Powerful piezoelectric material produces ROS directly from water molecules through the reaction of generated charge on the material surface with water and oxygen present in surrounding medium, schematically presented in Fig. 9a [75], [77]–[79]. Overproduction of ROS leads to bacterial membrane damage (oxidizing membrane-bound protein), its fragmentation, leakage of intracellular material, damage to cell organelle (mitochondria and DNA), therefore leading to bacteria death [78], [79]. In this case, the contact between the bacteria and the material is not that important, since ROS is formed in molecules from the liquid. However, ROS are non-selective, therefore they attack bacteria and human cells at the same time, and they are therefore not appropriate for wound healing application.

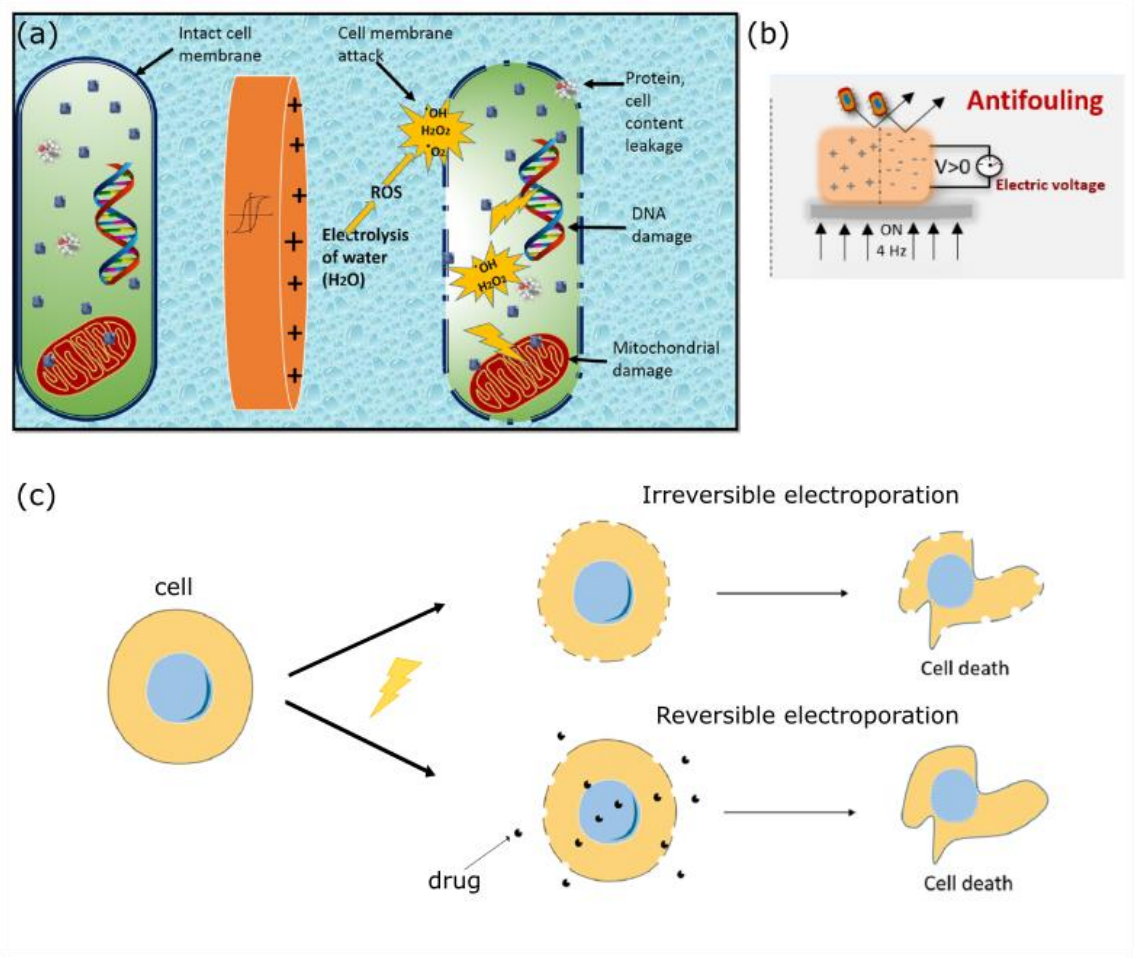

Figure 9: (a) Schematic illustration of the piezo-catalytic generation of ROS from water by piezoelectric material and proposed mechanism for bacteria inactivation (adapted by the ref. [79]); (b) antifouling effect of bacteria due to electric polarization of piezoelectric film, activated by ultrasound (adapted after ref. [80]); (c) process of electroporation (pore formation), leading to cell death through irreversible electroporation due to the high electric polarization or reversible electroporation with a combination of antibacterial drug, where the drug is able to enter the cell due to pore formation (adapted after ref. [81]).

Using polymers with much smaller piezoelectric coefficient, ROS production is usually not possible. In this case, for electro-stimulation, close contact between piezoelectric material and cells/bacteria is important since no active species are released into the medium, therefore the mechanism is fully contact-based. One observed effect (presented in Fig. 9b) as a response to electrical stimulation using US mediated PVDF film is antifouling, which prevents bacteria to attach on the surface [80]. Possible electrical-based killing mechanism is also irreversible electroporation (formation of pores in membrane, Fig. 9c), where cell membrane permeability is increased, which is possible when the induced voltage through piezoelectric exceeds the threshold transmembrane voltage (0.2-1 V) [4]. For materials exceeding the potential difference of 1 V, each bacterium undergoes electroporation, regardless of the type and size of cell [82]. Suppressed growth and death of the bacteria was observed for PLLA fibers, based on the electric field generated from piezoelectric polymer fibers [82], [83], which was explained as a result of electroporation. While using less powerful piezoelectrics with a combination of active agents (antibiotics, antibacterial nanoparticles, drugs), membrane depolarization (the electro-permeabilization effect as a response to electrostimulation) can boost the effect of agent, diminishing the

concentration of material needed to work (Fig. 9c) [4]. Even when I stimulated the PLLA piezoelectric polymer samples with ultrasound (US) to activate electric properties, there was no direct generation of ROS from water detected by the possible oxidation/degradation of the organic methylene blue dye [49]. Using the same procedure to determine ROS formation, the piezoelectric properties were compared between non-measurable NT and smooth samples when hydrogen peroxide was added to piezo-catalyze the formation of ROS, which degrades the MB dye, observed as a decrease in MB absorbance values measured spectroscopically. Comparing the piezo-catalyzed properties of films, a new method was presented to compare and confirm piezoelectric properties of surface-challenged samples [49].

1.4.2.1 Effect of topography

Recent research shows that films without antibacterial properties prepared with NT pattern on the surface (effect of topography) mechanically disturb bacteria (cell rupture, membrane disfiguring), mimicking the natural antibacterial surfaces, like cicada-wing nano-pillars or taller nano-structures of dragonfly wings [48], [84]–[86]. Bacteria can be in contact with nano-pillars by being adhered on the surface or suspended between the pillars, due to the bigger size of the bacteria (micrometer range) compared to the pillars. For strongly attached bacteria, nano-pillar movement stretch the cell membrane (mechanical effect), leading to membrane rapture, provoking the cytoplasm leakage, followed by the complete cell rapture [85], [87]. As observed, cell death is mostly dependent on the rigidity of the bacterial cell membrane, where it is less affective on rigid and smaller Gram positive bacteria (resistant to topography) compared to less rigid Gram negative bacteria strains, schematically presented in Fig. 10a [85]. Height of the structure is also important, since taller structures tend to bend, therefore bacteria strongly attach to nano-pillars, since more surface is exposed to bacteria, leading to membrane separation due to the effort of bacteria to move away from the material, increasing the antibacterial effect, with maximum stretching of bacteria on the top of the nano-pillar [85]. Also the shape of the pillars can affect bacteria membrane distortion, where the mechanism of killing for blunt and short pillars (Fig. 10b) is adhesion of bacteria followed by stretching of the membrane or piercing, in case of sharp and long pillars (Fig. 10c) [87], leading to complete cell rapture. The first step in killing the bacteria is attracting the bacteria to adhere to the surface, therefore material's physical characteristics (hydrophilicity) are important.

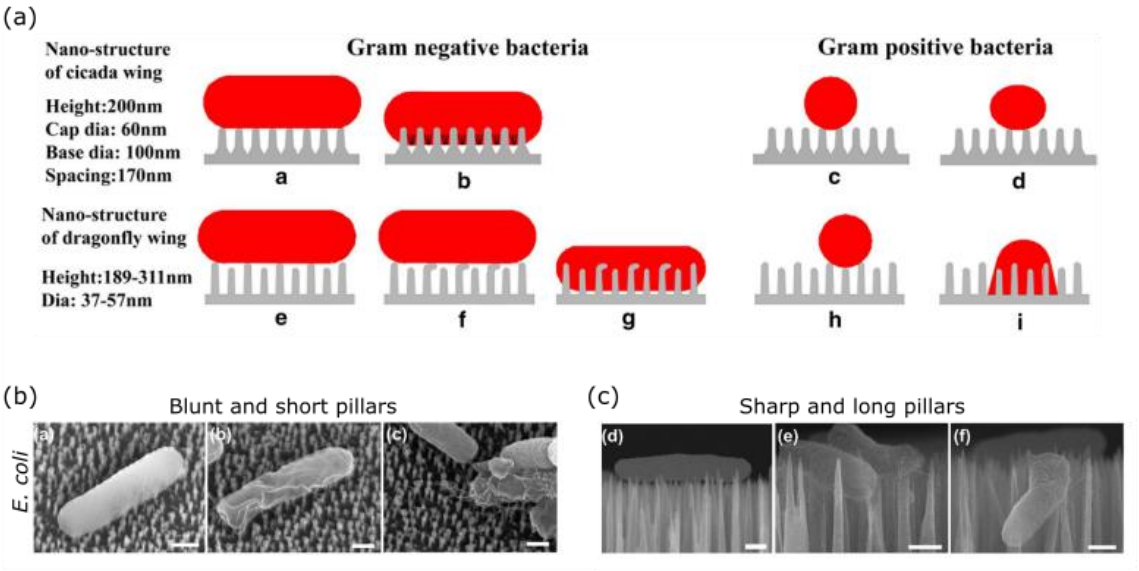

Figure 10: (a) Schematic of interaction of Gram negative (a, b, e, f, g) and Gram positive bacteria (c, d, h, i) with NT surface of cicada-wing (a, b, c, d) or dragonfly wing (e, f, g, h, i) as representatives for natural defense against bacteria (adapted after ref. [85]); microscopic images of Gram negative bacteria (*E. coli*) at various stages of interactions with nano-structures with: (b) blunt and short pillars or (c) sharp and long pillars (adapted after ref. [87]).

Using a simple method like "template wetting", NT films can be prepared as piezoelectric pillars on the thin substrate. PLLA with NT form are also characterized by increased piezoelectricity due to a much greater active surface area. Consequently, it could be expected that charge-induced membrane deformation due to piezo-stimulation combined with mechanical deformation by specific morphology in NT PLLA surfaces will lead toward effective antimicrobial protections [49]. In my research, I rejected the effect of NT topography as the main effect of antibacterial properties, which may be due to too long and compressed nanotubes on the polymer substrate, which are not strong/sharp enough to penetrate the bacterial membrane. However, my research was the first study/evidence in the literature that directly confirms the harmful effect of electrical stimulation through an US-activated piezoelectric NT PLLA film against the membrane of bacteria in contact [49].

1.5 Excitation of Piezoelectric Property of Material

Since electrical stimulation shows great promise in biomedical applications (regenerative medicine, neuromodulation, cancer treatment), controlled and external/wireless electrostimulation is highly desirable as a solution to connected electrodes or batteries, which dramatically hamper the translation of electrical stimulation [88]. By using piezoelectrics, electrostimulation on biomaterial in contact can be achieved through mechanical deformation of piezoelectric material. This piezoelectric property of material can be activated by mechanical forces to which the body is normally subjected (implemented inside body on bones or muscles by compression, vibrations, sounds), or externally triggered by using US, which is able to deeply penetrate biological tissue with low-energy attenuation [16], [89], [90]. By using US, wireless, local and minimally invasive electrical stimulation is achieved [88], which is possible due to its biocompatibility and deeply focused penetration into biological tissues [91]. The appropriate range of using US

for medical purpose is 1-3 MHz, which can provide an effective way for deep power transmission under FDA safety limits, since due to the weak acoustic scattering in soft tissues, activation of implemented piezoelectric devices is possible [91].

Piezoelectric properties of polymers were successfully activated by using US bath within *in vitro* (PVDF, at 137 kHz, cells seeded on film, [16]) or low power US probe (1 MHz) *in vivo* studies (biodegradable piezo composites PLLA/KNN@PDLA or PHBV/PLLA/KNN, on mice [90], [92]). US is a mechanical wave which propagates through medium (water, tissue) with two main physical effects, thermal and mechanical, intensity of each depends on the parameters. Principle of mechanical deformation by using US bath and water as a medium is presented in Fig. 11a. Disturbance caused by US causes an oscillation (compression and expansion) in the ambient pressure, leading to bubble formation due to the present gases, which grow to the point of implosion with continuation of US, therefore bubbles release energy (temperature and light) [93]. Cavitation and temperature release are more frequent at low frequencies, when bubbles have time to grow (kHz). Typically, US baths are used for cleaning, so a high destructive power is desired with the resulting bubbles further increasing the destructive/heating effect [94], so some optimization (power reduction if possible) is required for the *in vitro* tests with cells. For *in vivo* therapeutic use, low intensity pulsed ultrasound (LIPUS) is used to reduce the thermal effect (heating of tissue) and still transfer the proper stimuli inside (oscillation of the particles), usually in 1-3 MHz frequency range, depending on the penetration depth needed [95]. Lower frequency (kHz) result in deeper penetration depth, usually used for drug delivery and palliative treatment (provide relief from pain of a serious illness), while higher frequencies (1-3 MHz) are used for therapeutic and diagnostic medicine [95]. The heating effect of US is closely related to intensity and also varies if an aqueous medium is used or if dense tissue is to be penetrated.

Therefore, I believe that both stimulation methods, US bath and low power therapeutic US probe, are suitable for *in vitro* experiments with some optimization (time, frequency, cooling system), since the required penetration is not deep and a small piezoelectric output is desired, so even a lower stimulation power is sufficient. Fig. 11b illustrates the proposed behavior of thin polymer film excited with US bath, where the film is wrinkled/twisted (mechanically deformed). This excitation was successful for piezoelectric PVDF polymer with parallel piezoelectric properties [16]. I believe that using this method, due to the mechanical twisting of the film, shear piezoelectric can be properly deformed to generate charge on the surface. Fig. 11c demonstrates the idea of using such biocompatible piezoelectric polymers *in vivo*, where the film is externally mechanically deformed by US. Our group is the first to develop an US-active PLLA biomaterial, where we showed and measured the generated piezoelectric properties of stretched polymer films or composites using a frequency of 80 kHz (US bath) or 1 MHz (US probe) and tested for the interactions of our material with the cells during the mentioned stimulations [96].

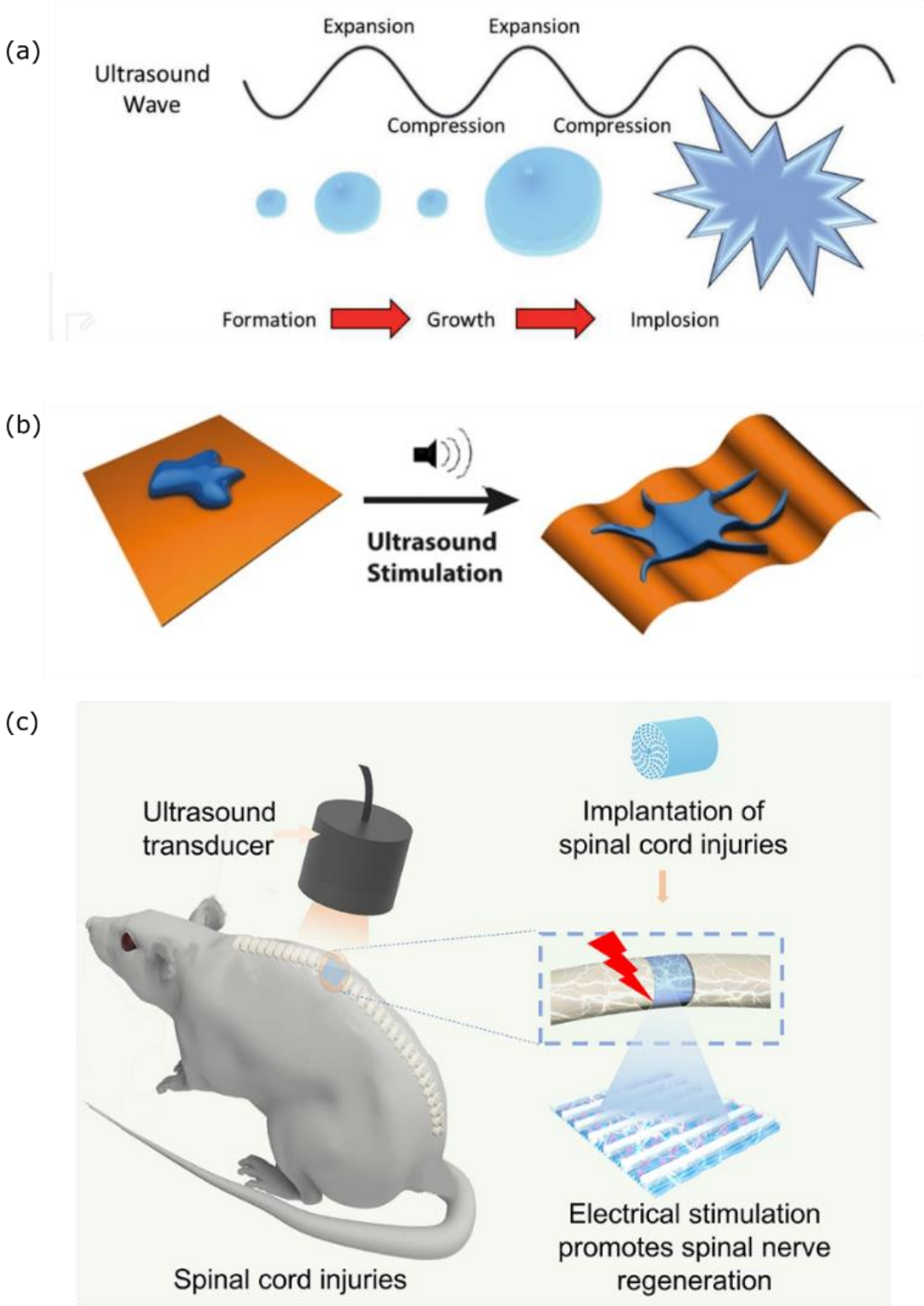

Figure 11: Demonstrating (a) the development of forming bubbles in water, as US stimulation continues, bubbles grow and when they reach the critical size, they collapse and release captured energy, adapted from ref. [93]; (b) the proposed behavior of polymer film in US bath; (c) external excitation of piezoelectric material in an *in vivo* test using an US transducer.

Chapter 2

Objective and Outline of This Work

2.1 Aim

This dissertation focuses on acquiring novel knowledge in the area of biomaterials science related to designing and optimizing innovative organic piezoelectrics and their use in piezo-stimulation as a novel tool in biomedicine applicable for healing and tissue engineering. The acquired knowledge is expected to allow predicting piezoelectric properties of organic polymers like PLLA characterized by shear piezoelectricity, identifying surface and bulk properties of organic piezoelectric films essentially needed for piezo-stimulation as well as tailoring their properties toward selective interactions with bacterial and mammalian cells that will stimulate human cell regeneration and eliminate infection. Piezo-stimulation is expected to be developed as a new noninvasive approach for wound regeneration, particularly during post-operative and post-traumatic recovery, able to offer minimized or eliminated antibiotic treatment. The latter is of the highest interest against the lack of effective antibiotics and developing resistant strains as one of the main global health threats as well as preventing chronic wounds toward better health and improved quality of life.

The main goal of the dissertation is to design, optimize and evaluate PLLA films as innovative biomaterial tools applicable for piezo-stimulation. The aim of the doctoral work is on:

(i) designing innovative organic piezoelectrics made of PLLA as biocompatible, biodegradable, and soft polymer, mechanically compliant to human cells and tissues;

(ii) understanding the mechanism behind piezoelectric properties of PLLA polymer to be able to optimize the process of film preparation;

(iii) optimizing mechanical deformation of PLLA film to obtain piezoelectric signal that will stimulate specific phases in cell life and finding the best way of its transfer from films surface to cells;

(iv) understanding the influence of PLLA piezoelectricity on bacterial and human cells and the main mechanism behind them.

For that purpose, in the proposed doctoral dissertation, I would like to answer the following questions:

- Which are the critical properties of polymeric films that enable and regulate their piezoelectricity?
- How to evaluate piezoelectricity of films with a complex structure?
- How to stimulate piezoelectricity of films in a water environment?
- Which ultrasound stimulation is appropriate not to damage human keratinocyte cells, red blood cells, or bacteria cells?

- How to improve close contact between the film and cells to achieve the best possible effect that the film can provide?
- What kind of effect will be observed when films are in contact with bacteria cells?
- How piezoelectricity influences red blood cells (suspended cells) and human epidermal cells (adherent cells)?
- How do immune cells (macrophages) respond to the electric stimulation, smooth or nanotextured polymer film?

2.2 Hypotheses

Using the processes of high temperature-drawing and templating, PLLA can be processed into optimal piezoelectric films (high crystallinity, orientation, hydrophilicity, etc.) that could be mechanically deformed to provide piezo-stimulation with selective influence to mammalian and bacterial cells.

Hypothesis 1: Optimizing piezoelectricity in PLLA films.

It is well known that drawing polymer above the glass transition results in strain-induced crystallization, therefore film with high crystallinity and oriented polymer chains is achieved [42]. With additional annealing, crystallinity is improved and with this expected piezoelectric properties [39]. Such film is capable to produce piezoelectric effect upon mechanical stimulation. However, each polymer with a different molecular mass is responding differently to drawing and temperature conditions. Different optimization procedure is needed for preparing melt-drawn film or film with self-standing nanotubes on the surface. For high temperature-drawing, effect of temperature, draw ratio, draw rate and post processing annealing was correlated to final properties. For the preparation of NT film using the template-assisted method, process conditions (such as temperature, time, pressure and post-treatment annealing) were investigated to see how they affect the final properties of PLLA with 250 kDa molecular weight. *I expect that with the precise optimization I can find the proper conditions under which the polymer would have optimal piezoelectric properties.*

Hypothesis 2: Piezo-PLLA films processed as hydrophilic surfaces.

Hydrophobic property is the main drawback of otherwise often used PLLA for medical applications, since it can lead to poor cell attachment. PLLA is polyester, ending with carboxylic and alcohol end group on each side, with long hydrophobic polymer backbone in-between. Using alkaline etching, ester bonds can be hydrolyzed, resulting in shorter polymer chains with more hydrophilic end groups present. *I expect that by using alkaline etching as post-treatment of prepared films, an obstacle such as hydrophobicity can be overcome to induce more hydrophilic carboxyl end groups on the surface and at the same time preserving piezoelectric properties.*

Hypothesis 3: Piezo-properties during polymer degradation in water or in enzyme solution as simulation of natural environment.

PLLA polymer is insoluble in water, but it can swell in such conditions, however this process is very slow. If we simulate the actual situation in wound area, it is possible that enzymes capable of cleavage of ester bonds are present in such an environment. Proteases are present at the site of injury towards the end of healing. They are responsible for remodeling the extracellular matrix, clearance of damaged protein and destruction of the provisional matrix, facilitation of cellular migration to the wound area and granulation tissue formation [97]. Those enzymes are able to rapidly cleave ester bonds, resulting in

degradation of the polymer film at the contact. Therefore, it is important to approach the mechanism of degradation for PLLA polymer. Upon the bulk degradation of the polymer, it is expected to lose piezoelectric properties of the film with the rate of degradation. *I expect unfazed piezoelectric property change of PLLA film in water medium, however increased degradation when the enzyme (proteinase K) is present.* I researched the effect of changing the surface hydrophilicity of PLLA films prepared with melt-drawing and achieved that proteases are focused only on the surface, starting with the surface and edge erosion of the polymer, lowering the degradation rate. *Due to additional modifications into more hydrophilic PLLA film on the surface I expect preservation of piezoelectric properties for a longer time since mostly surface is to be exposed to enzyme degradation.*

Hypothesis 4: Deforming film for efficient signal transfer to cells.

For piezoelectric film to generate charge on the surfaces, mechanical deformation is needed. When considering the site of injury where the film would be placed, deformation can occur by body movements, cell seeding or using wireless stimulation from the outside using ultrasound. US can work with different frequencies and amplitudes, from which mechanical deformation on the film is dependent. It was shown that using US, piezoelectric effect of properly prepared PVDF film can be activated, therefore charge on the surface was observed [16], [80]. However, PLLA and PVDF have different forms of piezoelectricity (shear or transverse), therefore US can stimulate PLLA differently. *I believe that using US as an exogenous mechanical wave can trigger piezoelectric effect for PLLA melt-drawn and nanotextured films.* Optimization of US conditions is needed to discharge negative or positive effect of only US on bacteria or human cells, but still enough to mechanically deform PLLA.

Hypothesis 5: Determining piezoelectric properties of polymer films with complex topography.

Piezoelectric material can be used for catalytic redox reaction of hydrogen peroxide oxidation into ROS. Generated ROS species are able to decompose organic dies such as methylene blue (MB) [98], therefore through absorbance measurement, efficiency of piezo-potential can be observed. *I believe that through piezo-catalyzed organic dye (MB) degradation in the presence of hydrogen peroxide as a provider for ROS species, piezoelectric efficiency of PLLA stretched and nanotextured films can be compared and evaluated.*

Hypothesis 6: Interacting films with bacterial and mammalian cells (epidermal and immune cells).

Physical stimuli as piezo stimulation affect bacterial life in a different, cell non-specific manner in comparison to biochemical stimuli (i.e. antibiotics), presenting an interesting alternative and preventing bacteria to develop resistance [4]. Piezo stimulation results in accumulation of generated charge on the surface of mechanically deformed film, which could affect the potential in the cell membrane, leading to destroying their membrane. Preparing PLLA in stretched and NT form, piezoelectricity differs between them, therefore different response on bacteria is expected. With predicting improved piezoelectricity for NT film combined with the negative effect of surface morphology, bacteriocidic properties are expected against bacteria cells. For piezoelectric materials, usually ROS are responsible for achieved antibacterial effect, however for that, high piezoelectric constant of the material is needed (>100pC/N) [75], therefore PLLA with at least one order of magnitude lower value is incapable of forming ROS by itself. *I believe that the piezoelectric feature of the PLLA film is responsible for the bactericidal effect against Gram negative and Gram*

positive bacteria due to the generation of charges on the surface upon mechanical deformation, affecting the cell membrane integrity.

Literature shows many beneficial effects of piezo stimulation on mammalian cells (i.e. cell proliferation, differentiation or migration, increased specific gene expression), usually in combination with added stem cells, growth factors or using differentiation medium [99]. Some beneficial effects of using piezoelectric PLLA were already observed (PLLA rods inserted in fractured bone improve healing time [54]; improve wound closure due to maintaining moister microenvironment [100]; improve cell attachment [101]), however little was studied for PLLA in general in terms of the wound healing effect and its mechanism. *I believe that using piezoelectric PLLA film in stretched and nanotextured form leads to improvement in cell attachment, proliferation or migration for human keratinocyte cells, as the most dominant cell type constitutes 95% of the epidermal cells which play multiple roles in skin repair.* Beforehand, optimization of US conditions is needed to achieve optimum between mechanical deformation of the film and not damaging cells. Also, I do not expect any excessive immune response in case of PLLA film implementation inside the human body, therefore differentiation of non-adherent monocytes into adherent macrophages will be observed with or without electric stimulation activated by US. *I believe that differentiation from monocytes into macrophage will be minimal and the material will act as biocompatible.*

2.3 Thesis Outline

The thesis is divided as follows: a short introduction in **Chapter 1**, which presents the existing literature on the highlighted issues in this thesis, followed by a presentation of the purposes, goals and hypotheses in **Chapter 2**. In **Chapter 3**, I described the optimized preparation of piezoelectric PLLA stretched films, the characterization of the samples in detail, and the measurement system set up to measure the total piezoelectric properties for shear piezoelectric in the form of a thin film. The degradation process of the polymer film is followed by a comparison between the more hydrophilic (etched) and hydrophobic samples in water or in the enzyme system in **Chapter 4**, where the piezoelectric properties were preserved due to the displacement of the degradation to the surface for the more hydrophilic films. **In Chapter 5**, a new method was used for the preparation of piezoelectric films with a nanotextured surface, a new total piezoelectric measurement mechanism for samples with challenging surfaces was proposed, antibacterial properties were evaluated and linked to electrical stimulation or topography changes. **Chapter 6** presents the response of human epidermal and immune cells to smooth or nanotextured piezoelectric polymer films, related to potential medical applications. At the end, **Chapter 7** contains conclusions with final remarks and offers answers to the questions raised, opens a new discussion on future work, and suggests possible improvements and possibilities for further research.

Chapter 3

Preparation and Characterization of Drawn Piezoelectric Polymer Film and Surface Modification

This chapter provides an overview of optimization of operating conditions to achieve the most efficient tensile-drawn piezoelectric film from biodegradable PLLA polymer beads. In theory, crystallinity and orientation are the main factors for mentioned polymer influencing the piezoelectric properties. Therefore, the film was tensile-stretched into crystalline and oriented fibrous sheet. Film characteristics were observed by using X-ray diffraction (XRD), differential scanning calorimetry (DSC), Fourier transform infrared (FTIR) and Raman spectroscopy, showing semi crystalline (55%) and oriented structure of the film. I modified the method for piezoelectric measurements to measure shear piezoelectric properties (following a confirmed procedure by another research group) and I directly correlated piezoelectric measurements to the conditions of polymer stretching, and more importantly, how additional modifications (annealing and surface etching) alter piezoelectricity. PLLA is defined by specific hydrophobic properties. Since hydrophilicity is one of the main factors determining cell adhesion, surface modification such as alkaline etching was performed on prepared piezoelectric PLLA films. I designed piezoelectric PLLA film with high potential for strong interactions with cells in further biomedical applications. This study is the first in the literature to demonstrate the preserved piezoelectric properties of a stretched PLLA film with improved surface hydrophilicity.

The changes on the polymer surface were later confirmed by a surface-sensitive X-ray photoelectron spectroscopy (XPS) method, where a comparison before and after surface etching confirmed a higher concentration of hydrophilic end chains on the PLLA surface (Appendix A1).

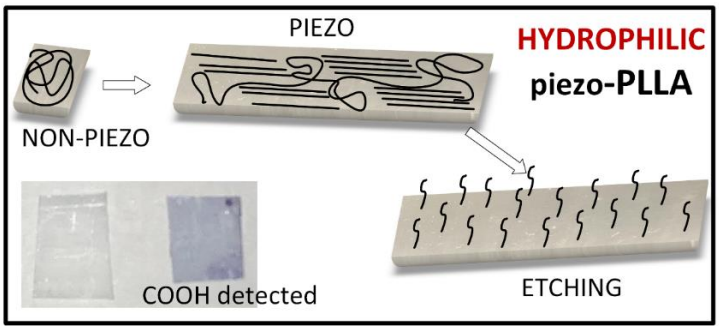

Figure 12: Showing the concept of using a drawing approach to obtain oriented and crystalline piezoelectric PLLA films and its combination with surface etching to release COOH groups on the surface and reaching hydrophilicity, image taken from the published article [39].

3.1 Towards Hydrophilic Piezoelectric Poly-L-Lactide Films: Optimal Processing, Post-heat Treatment and Alkaline Etching

Polymer Journal (2020) 52:299–311
https://doi.org/10.1038/s41428-019-0281-5

ORIGINAL ARTICLE

Towards hydrophilic piezoelectric poly-L-lactide films: optimal processing, post-heat treatment and alkaline etching

Lea Udovč[1,2] · Matjaž Spreitzer[1] · Marija Vukomanović[1]

Received: 28 June 2019 / Revised: 18 September 2019 / Accepted: 7 October 2019 / Published online: 21 October 2019

Abstract

Piezoelectric poly-L-lactide (PLLA) films are highly applicable for designing soft electronics in biomedicine. However, due to a lack of reactive side-chain groups, PLLA is characterized by a chemically inert and hydrophobic surface. Although compatible with biological environments, this polymer has very poor interactions with cells. This work is the first report on piezoelectric PLLA films with hydrophilic surfaces. We performed a systematic study that correlated processing parameters (drawing ratio, drawing temperature, drawing rate) with postprocessing steps (annealing and etching) to produce active, hydrophilic, piezoelectric PLLA surfaces. During processing, the optimal drawing ratio, temperature and rate increase the crystallinity and crystallite size and provide chain orientation. Postprocessing annealing and etching afford further improvements in structural properties and optimized surface characteristics. Consequently, the resulting PLLA films possess piezoelectric properties in combination with hydrophilic surfaces and specifically patterned topography. Using this approach, we designed active PLLA films with high potential for strong interactions with cells in further biomedical applications, including exploring the effect of piezoelectricity on cell proliferation. This study provides novel insight into designing synthetic piezoelectric polymers with significantly improved interactions with cells and tissues, which are particularly important for their application in biomedicine.

Introduction

Polylactic acid (PLA) is a synthetic biodegradable polymer characterized by piezoelectric responsiveness. For the last few decades, this polymer has been intensively studied for a range of different applications, such as electronics and sensors [1], components in food packaging [2] and a wide range of uses in biomedicine, including drug delivery systems, meshes, patches, plasters for wound healing [3], and scaffolds and coatings in tissue regeneration [4], among many others. As a biocompatible and biodegradable polyester, PLA is approved by the Food and Drug Administration (FDA) and European Medicines Agency (EMA) as appropriate for medical applications [5].

✉ Marija Vukomanović
marija.vukomanovic@ijs.si

[1] Advanced Materials Department, Jozef Stefan Institute, Ljubljana, Slovenia

[2] Jozef Stefan International Postgraduate School, Ljubljana, Slovenia

Monomers of PLA exist in two optical isomers (left-handed and right-handed), among which left-handed polylactic acid (PLLA) is used for biological applications owing to its similarity with biomolecules (proteins, amino acids, nucleic acid). PLLA forms different crystalline phases (α, α', β, and γ) [6]. The most common crystal phase is α with an orthorhombic crystallographic unit cell, produced at a high crystallization temperature (140 °C) or after annealing near the melting temperature [7]. Another crystal phase is α' with a similar orthorhombic unit cell but larger unit cell parameters, produced at low crystallization temperatures (80 °C) or through strain crystallization from an amorphous polymer [8].

Piezoelectricity in PLA originates from its helical structure; therefore, the polymer exhibits shear piezoelectricity in all crystal forms. The magnitude of the piezoelectric constant is proportional to the degree of orientation of molecular chains and crystallinity [9, 10]. A simple method to impart orientation to the polymer is drawing polymeric films or fibers to align chain molecules in the same direction throughout the entire film. The drawing process leads to molecular orientation in the crystalline and amorphous regions, which also influences mechanical properties and induces structural changes such as crystallinity, crystal shape and crystal size due to strain-induced crystallization

above the glass transition temperatures (T_g) [11–13]. Additional postprocessing heat treatment can improve crystallinity and decrease roughness and porosity. Because of their low dielectric value (2.7), PLLA films have a low charge (d) but high piezoelectric voltage coefficient (g), which is an important parameter for sensor applications and imparts an electrical field that develops under the applied force. This property means that the sensitivity of PLLA is very high, which is also required for various medical applications. The most commonly reported piezoelectric value of PLLA for d_{14} is $-10\,\mathrm{pC\,N^{-1}}$, which was mentioned for oriented piezoelectric PLLA films [14].

Piezoelectric biofilms should be active materials with the ability to promote cell attachment and protein adhesion. Therefore, their surface properties, such as roughness [15, 16] and hydrophilicity, are of crucial importance and should favor interactions with cells [17]. However, due to a lack of reactive side-chain groups, PLLA is characterized by a chemically inert and hydrophobic surface. Although compatible with biological environments, this polymer has very poor interactions with cells. Recently, a procedure based on alkali etching has been developed to enable very efficient surface modification of PLLA [17]. Alkylates accelerate the hydrolysis of ester linkages in PLLA backbone chains on the surface of the film, producing reactive carboxylic and hydroxyl end groups on the polymer chains that enable new possibilities for its design.

Starting from the previously mentioned points, the main goal of our work was to design PLLA as a piezoelectric biofilm with a hydrophilic surface. PLLA, as biodegradable, biocompatible and mechanically resistant polymer, is one of the most promising synthetic candidates for the design of such biofilms. However, its inert hydrophobic surface is a limiting factor. We focused our work on establishing an optimal procedure that will allow optimization of piezoelectricity in PLLA along with activation of the functional groups at the PLLA surface to form piezoelectric and hydrophilic PLLA films. For the first time, these characteristics in PLLA films are systematically correlated with processing parameters (drawing ratio, drawing temperature, drawing rate) and with postprocessing steps (annealing and etching). This study provides novel insight into designing synthetic piezoelectric polymers with significantly improved possibilities for interactions with cells and tissues, which are particularly important for their application in biomedicine.

Experimental

Materials

Left-handed polylactic acid (PLLA) polymer with a molecular weight of ~150 kDa, stored in a freezer at −4 °C, was purchased from Goodfellow, England. Sodium hydroxide and methanol were used to etch the polymer surface. Methylene blue (high purity, biological stain) was purchased from Alfa Aesar, Karlsruhe, Germany. Distilled water was purified using a Milli-Q system (Purelab Option-Q, ELGA).

Processing PLLA films

Formation of PLLA films

Amorphous PLLA films were prepared by compressing polymer pellets (Fig. 1a) between two heated metal plates at 200 °C under a pressure of 56 kN for 3 min using a manual lab press from Weber (Fig. 1b) and quenching in cold water to prevent thermally induced crystallization, which would restrict the subsequent process of drawing. To prepare a polymer with a desired thickness, thick aluminum foil was used for molding. It was protected on both sides with Teflon foil, appropriate for hot pressing. Amorphous PLLA films were obtained with ≈0.200 mm thickness.

Uniaxial drawing of PLLA films

To prepare oriented and crystalline polymer films, samples were cut into dumbbell shapes and drawn at different draw ratios, draw temperatures and draw rates using a homemade drawing device (Fig. 1c). One side of the polymer was fixed with an immobile clamp, and the other side was fixed with a mobile clamp, which was used for uniaxial stretching. The whole device was placed inside a Heraeus Vacutherm dryer (Thermo Scientific) at different temperatures. The film was drawn to a selected draw ratio, and then the stretcher was placed outside and allowed to cool to room temperature.

Crystallization of PLLA films

To improve the crystallinity of the polymer films and to induce a change in crystal structure, they were also annealed in a dryer at higher temperatures (140 or 160 °C) for 20 h while being pressed by 900-g weights (Fig. 1d). The weights were placed on top of the films to prevent wrinkling. Another form of postprocessing heat treatment used was hot pressing after drawing at 140 °C using a pressure of 40 kN and leaving the films to be pressed until the temperature dropped to room temperature.

Surface etching of PLLA films

To improve the wettability of the polymeric surface, films were alkaline etched for 20 h in a 0.04 M solution of NaOH in a water/methanol mixture (70/30 V/V). Methanol was used to increase the kinetics of surface degradation (as

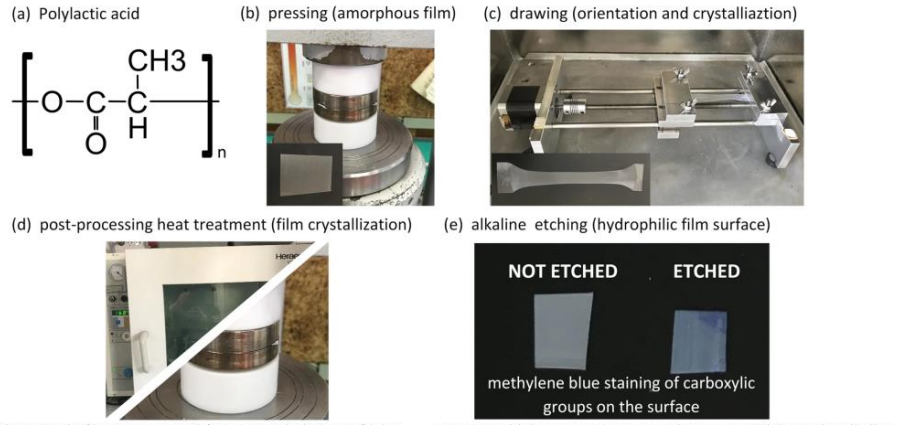

Fig. 1 Piezoelectric film was prepared from **a** PLLA that was (**b**) hot-pressed to obtain an amorphous film, **c** drawn at high temperatures to induce orientation and crystallinity, **d** annealed in a dryer or hot-pressed at higher temperatures to enhance crystallinity and **e** alkaline etched to improve the hydrophilicity of the surface, as confirmed with methylene blue staining

suggested in a previous work [12]), followed by washing with distilled water and drying. Newly formed carboxylic end groups were confirmed with methylene blue staining (0.1% aqueous solution) for 1 h (Fig. 1e) [18]. Schematics of the film preparation procedure are presented in Fig. 1.

Methods of characterization

X-ray diffraction (XRD) analysis

The crystal structure and crystallite size were determined with an X-ray powder diffractometer (Bruker AXS D4 Endeavor) using Cu Kα radiation ($\lambda = 1.54$ Å) in the 2Θ range of 5–50° with a 0.04° step size and a 5 s time of capture. Crystallite size was calculated from XRD diffractograms with the equation $L = \frac{K\lambda}{\beta 1/2\, cos\alpha}$, where $\beta_{½}$ is the full width at half maximum of a peak, λ is the wavelength of Cu Kα and K is the broadening constant (0.9) for the imperfect polycrystals.

Fourier transform infrared (FTIR) and Raman spectroscopy

Crystal structure and crystallinity were also analyzed using a Fourier transform infrared spectrometer in attenuated total reflectance (ATR) mode (PerkinElmer Spectrum 100). Spectra were recorded in a 600–4000 cm^{-1} wavenumber range with a spectral resolution of 4 cm^{-1}. Captured spectra were normalized to the maximum peak intensity for comparisons between samples. Films were also characterized using a polarized Raman spectrometer (NTEGRA Spectra NT-MDT) in the frequency range of 200–1800 cm^{-1} with a He–Ne polarized laser (633 nm). To observe the orientation of the crystal structure in the polymer films, the order ratio was determined for the peak corresponding to C–COO stretching at 871 cm^{-1} by changing the laser and analyzer polarization to observe the peak aligned along the fiber direction (∥) and the peak perpendicular to it (⊥), where the polarization of the analyzer is always aligned parallel to the laser polarization. For calculations, the following equation was used: $R = \frac{A_{\parallel}}{A_{\perp}}$, where R is the absorbance ratio between the parallel and perpendicular measurements [19].

Thermal analysis

Crystallinity was determined using a NETZSCH STA 449 thermal analyzer (Jupiter) for differential scanning calorimetry (DSC) analysis in an Ar/O atmosphere (40/10). A 3–4 mg sample was placed in platinum crucibles and heated from 40 °C to 200 °C at a heating rate of 20 °C min^{-1} due to temperature calibration under these conditions. The enthalpy of cold crystallization (ΔH_c) and enthalpy of melting (ΔH_m) were determined by calculating the area under the crystallization or melting peak, respectively. The bulk crystallinity was determined with the following expression: $X_c(\%) = \frac{\Delta H_n - \Delta H_c}{\Delta H_{100\%}} \times 100\%$, where the value for $\Delta H_{100\%}$ is taken as 93.6 J g^{-1}, which is a theoretical value for 100% crystalline PLLA films in α crystalline form [20].

Sessile drop method

The wetting angle was measured using a Theta Lite contact angle meter, Biolin Scientific. To determine the hydrophilic properties of the polymer film surfaces, distilled water with a droplet volume of 5 µl was used.

Microscopy

The surface of polymer films was investigated with a polarized optical microscope (Zeiss imager) and scanning electron microscope (SEM-JSM 7600F). For scanning electron microscopy (SEM) microscopy, samples were sputtered with gold using a BAL-TEC SCD 005 sputter coater to prevent charges on the surface. Samples were observed under a low voltage (2.5 kV) since higher energies led to melting of the polymer due to focused heating.

Piezoelectric measurements

Polymer films were cut at an angle of 45° from the stretching axis because shear stress reaches it maximum value when measured at this angle, as reported by Bernard et al. [21]. The measurement was made by a PiezoMeter System PM300, which was adapted for thin-film d_{31} measurements. First, gold electrodes were sputtered on both surfaces of polymer films, and the edges were cut to prevent short-circuiting between the electrodes. Then, the film was clamped on both sides, and the clamps were attached to the original machine to stretch the film at a specific frequency (110 Hz) and force (0.15–0.5 N). Voltage was measured with a voltmeter (Tenma multimeter) over a reference capacitor of 1000 pF, and the g_{13} piezoelectric coefficient was calculated rather than d_{13} to avoid errors from measuring the sample thickness. When the film is cut at 45°, according to the study of Bernard et al. the value of g_{14} is $2 \times g_{13}$ [21]. With this method, the g_{13} coefficient for the piezoelectric polymer film was calculated with the following equation: $g_{13} = \frac{d_{13}}{\varepsilon_{33}\varepsilon_0} = \frac{\frac{Q/(w \cdot h)}{F/(w \cdot t)}}{\frac{C \cdot t}{w \cdot h \cdot \varepsilon_0} \cdot \varepsilon_0} = \frac{Q \cdot w}{F \cdot C}, \left(\frac{Vm}{N}\right)$, where Q is the charge, C is the capacitance, w is the width of the electrode, h is the height of the electrode, t is the thickness of the film and F is the force. This method was confirmed by measuring a reference polyvinylidene fluoride (PVDF) piezoelectric film with known piezoelectric properties.

Results and discussion

Effect of draw ratio on the crystallinity and orientation

Amorphous polymeric films were drawn at different draw ratios (DRs) (defined as a ratio of the film length after and before stretching) to observe their effect on crystallinity and orientation in the polymeric chains and subsequently on piezoelectric properties (Fig. 2).

Crystallinity was determined by DSC measurements of thermal transitions in drawn polymers by considering changes in the melting and crystallization enthalpies. DSC thermograms of films drawn at 90 °C and a drawing rate of 40 mm min^{-1} with lower DRs (Fig. 2a) show the same transitions, namely, glass transition temperature (T_g), cold crystallization temperature (T_c), and melting temperature (T_m), as those observed in the thermogram of an undrawn polymer film (DR1), indicating. We observed that T_g is shifted to higher values for higher DRs and is barely detected at DRs of 4 and 5, indicating a decrease in the amorphous phase content and orientation of the chains in the amorphous part. Moreover, at DRs of 4 and 5, no crystallization exotherms are observed, which also suggests that the amorphous regions are transformed into crystalline regions as a result of the mechanical drawing of the polymer. The T_c is moved to lower temperatures with higher DRs due to more oriented molecular chains in the amorphous region, so crystallinity can occur at lower temperatures. We also observed a difference in T_m between undrawn films (crystallized by thermal analysis) and drawn films (crystallized by straining). The undrawn polymeric films (DR of 1) are thermally crystallized into the ordered α crystalline phase and have higher T_m values than those of the strain-crystallized films that grow into the less ordered α' phase with lower T_m values. However, at very high DRs, overstretching of the polymeric film and fibrillation of polymer chains are expected, leading to a loss in crystallinity [22]. This behavior was indeed observed at a DR of 7 when a small T_c peak appeared, and the T_g temperature was lower than that at a DR of 5, meaning less orientation of the chains in the amorphous regions, probably due to the polymer chains being shorter and therefore more mobile.

Molecular chain orientation was studied by polarized Raman spectroscopy, where the ratio of perpendicular or parallel intensities for the peak at a wavenumber of 871 cm^{-1}, corresponding to C–COO stretching (Fig. 2b), was calculated to determine the change in orientation in response to different DRs. Based on Raman analysis, the intensities for parallel and perpendicular measured peaks of films that were thermally crystallized at 140 °C (DR1 ANN) to obtain crystalline but non-oriented films versus strain-crystallized films (DR5) are reversed, indicating chain orientation in the drawing direction (Fig. 2b).

The calculated crystallinity changes, observed based on the DSC results from samples drawn at 90 °C and 40 mm min^{-1} (Fig. 2c), reveal an increase in crystallinity with higher DR to a maximal crystallinity of 55% at DR 5 as a result of the drawing alignment of chains in the drawing direction. With further drawing (DR6), the crystallinity is slightly lowered to 53%. A similar trend was also found in a previous study [11]. The calculated order ratio from the Raman spectra (Fig. 2c) is in agreement with the crystallinity results. Chain alignment is improved after drawing to only three times the initial length (DR3) and reaches a maximum at a DR of 5 (1.94). For higher DRs, alignment is

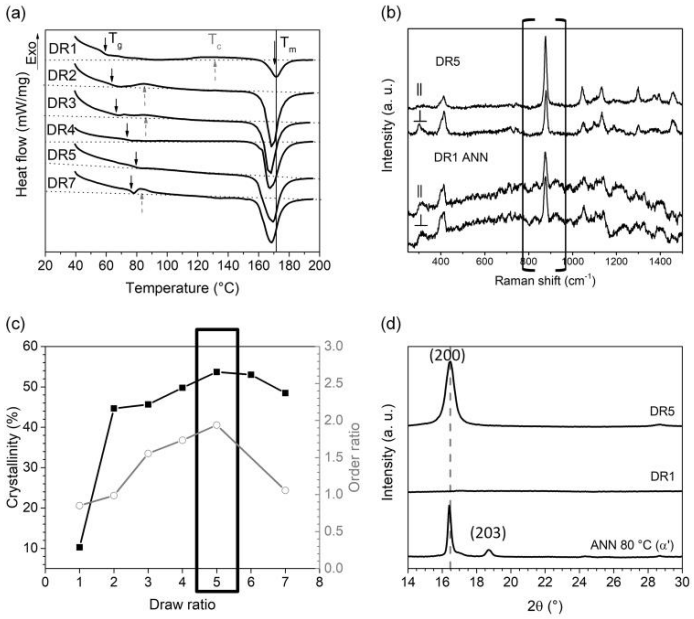

Fig. 2 **a** DSC thermograms of polymer films drawn at different draw ratios but the same temperature and rate; **b** Raman shifts of samples in measurements performed in parallel (ɪɪ) and perpendicular (⊥) geometry to the drawing direction for the undrawn and annealed sample (DR1 ANN) and the sample drawn to five times its initial length (DR5); **c** percentage of crystallinity calculated from DSC data (■) and Raman order ratio (○) plotted as a function of draw ratio at the same temperature and drawing rate; **d** XRD diffractograms of thermally crystallized(ANN 80 °C), undrawn (DR1) and drawn (DR5) films. The square in **c** indicates the optimal conditions

lowered, probably due to chain fibrillation, which is also a cause of loss of crystallinity.

Drawing-induced crystallization was confirmed by XRD analysis. The results (Fig. 2d) reveal the crystallinity of the sample when it was drawn to five times its initial length compared with the amorphous undrawn sample (DR1). All drawn films crystallize in the α' crystal structure (DR5), whereas the sample thermally crystallized at 80 °C (ANN 80 °C) is known to crystallize into the α' form.

The highest crystallinity of PLLA was obtained for drawing at a DR of 5. Accordingly, we concluded that a DR of 5 was the optimal stretching condition for which the highest piezoelectric constant was obtained. This conclusion was also supported by polarized Raman spectroscopy, which showed that highly oriented PLLA sheets were obtained after drawing to five times the initial length.

Effect of drawing temperature on crystallinity of the polymer

We observed that the polymer drawn at 70 °C exhibits all thermal transitions during the DSC study and that its maximal DR before the collapse of the film is four times the initial length. However, its crystallinity is much lower than that of the films drawn to four times their initial lengths at 80 or 90 °C. Processing at higher temperatures (90 °C) allows a higher DR without collapsing. The maximal average crystallinity, according to DSC results (Fig. 3a), for the samples drawn to five times their initial lengths, except at 70 °C, was achieved for the PLLA films drawn at 90 °C, which was selected as the optimal processing temperature. For the films drawn at 100 °C, the crystallinity is lower than that of the films drawn at 90 °C, which is probably due to the higher relaxation rate at higher temperatures, as at 90 °C, the orientation of the molecular chains predominates over the relaxation.

The results are also in agreement with the literature, where for strain-induced crystallization, it was confirmed that a polymer needs to be drawn at temperatures above its glass transition point and well below its melting point to induce molecular orientation of the polymer chains, where the orientation and relaxation rate are balanced [23, 24].

Effect of drawing rate on crystallinity and crystallite size

During the study, we observed that the rate of drawing has a major effect on crystallinity and crystallite size. It is essential to emphasize that for this purpose, the DR was fixed at 5. As shown in Fig. 3b, drawing a polymeric film

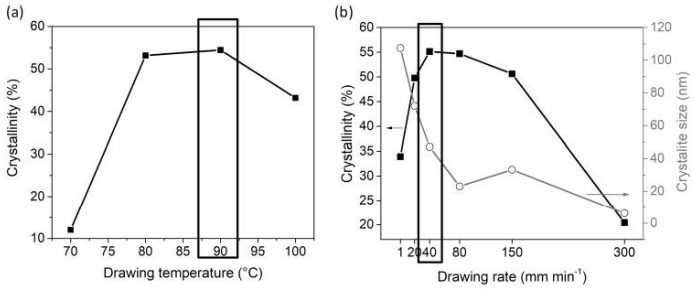

Fig. 3 **a** The effect of drawing temperature on crystallinity in samples drawn to five times their initial length, except for the film drawn at 70 °C, which was drawn to four times its initial length, as determined by DSC, and **b** the effect of drawing rate on crystallinity (■), as determined with DSC, and crystallite size (○), as determined from XRD diffractograms. The squares in **a** and **b** indicate the optimal conditions

at a 1 mm min^{-1} rate provides low crystallinity (34%). Since the polymer crystallizes thermally, a short drawing time at higher temperatures results in low crystallinity. However, when the polymer is drawn at faster rates, the crystallinity improves, with the maximum obtained at a drawing rate of 40 mm min^{-1}. This is probably due to the orientation of the polymer chains, where chains drawn more quickly remain oriented and achieve strain-induced crystallization. There is a limit (40 mm min^{-1}) at which a further increase in drawing rate has a negative influence on both crystallite size and crystallinity. An additional increase in rate results in a decrease in crystallinity, and the lowest crystallinity (20%) was achieved as a result of drawing at 300 mm min^{-1} due to the breaking of the already formed partial crystallites; therefore, shorter chains with higher relaxation rate remain.

For all drawing rates, the polymer crystalizes into the α' crystal form. We observed a difference in crystallite size during the XRD study: the FWHM for the (200) peak of PLLA films drawn at different rates narrowed. Chen et al. showed that a higher rate of drawing results in more uniform film morphology and orientation [23]; however, we observed that higher rates, namely, 150 mm min^{-1} or more, result in lower crystallinity and smaller crystallite size, probably due to high strain that breaks the formed crystallites into smaller parts (Fig. 3b). In contrast, for very low drawing rates (i.e., 1 mm min^{-1}), the polymer chains have time to crystallize into large crystals due to thermally induced crystallization.

Yoshida et al. [25] found that larger crystallites in PLLA films generate greater shear displacement; therefore, a higher piezoelectric coefficient can be achieved. Due to the ability to provide the best crystallization, we selected a drawing rate of 40 mm min^{-1} as optimal compared with 80 mm min^{-1}. In addition, according to Raman spectroscopy measurements, a higher order ratio was obtained (data not presented) at the selected drawing rate.

Effect of postprocessing heat treatment

To realize the maximal crystallization of PLLA films, we explored the possibility of additional ordering of the structure during postprocessing annealing. After stretching to the desired draw ratio (DR5) at 90 °C, 40 mm min^{-1}, films were annealed at different temperatures (140 or 160 °C) to crystallize during the next 20 h. Changes in crystallinity, crystal structure and crystallite size obtained as a consequence of the postprocessing heat treatment are observed in XRD diffractograms (Fig. 4a). For the films annealed at 140 °C, the crystallinity was improved by ~10% according to DSC measurements, with small ordering of the crystal structure indicated by a shift in the XRD peak position for the (200) crystal plane. For the PLLA films annealed at 160 °C, the polymer achieved the highest crystallinity of 78% as well as a change into a more ordered α structure, as observed by a shift in the (200) crystal plane at 16.72°, which is the experimental value for the α crystalline structure, obtained by only annealing overnight at 140 °C. However, these films were too brittle to withstand any stretching for piezoelectric measurement.

Figure 4b shows improved crystallization and crystal growth (indicated by narrowing of the FWHM 2θ values) after combined drawing and postprocessing heat treatment through annealing at 140 or 160 °C or annealing with hot pressing at 140 °C. For PLLA films drawn using the optimal parameters (DR 5, 90 °C and 40 mm min^{-1}), the crystallites grow from 48 nm to 86 nm when annealed at 140 °C. However, after annealing at 160 °C, as the temperature closer to T_m, there is a decrease in crystallite size (78 nm), which could be explained by crystal transformation into the α phase with a denser crystal structure. After annealing the films at 160 °C, orientation loss was observed, along with a decrease in Raman order ratio from 1.94 (DR5) to 1.78 (DR5, ANN 160 °C), which was not detected after annealing the films at 140 °C (1.93).

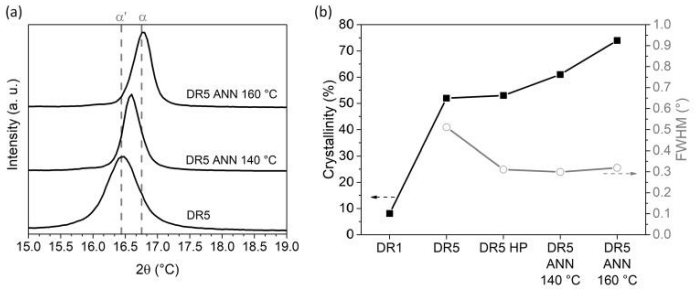

Fig. 4 **a** XRD diffractograms of the drawn polymer film (DR5), the polymer films further annealed at 140 °C (DR5 ANN 140 °C) or 160 °C (DR5 ANN 160 °C) and drawn at 90 °C, a DR of 5, and 40 mm min^{-1}, The positions of the (200) peaks for the α' (thermally crystallized at 80 °C) and α (thermally crystallized at 140 °C) crystalline phases are marked. **b** The change in crystallinity (■) and FWHM (○), which indicates a change in crystallite size, for the undrawn (DR1) films, the drawn films (DR5) and the films post-processing heat-treated with hot pressing at 140 °C (DR5 HP) or annealing at 140 °C (DR5 ANN 140 °C) or 160 °C (DR5)

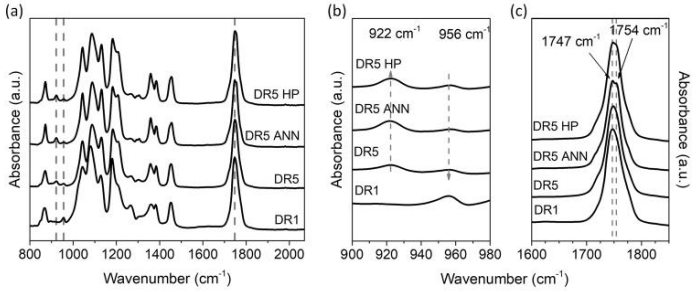

Fig. 5 **a** IR spectra of the undrawn PLLA film (DR1), drawn PLLA film (DR5) and further postprocessing heat-treated PLLA films (DR5 ANN and DR5 HP) and a closer view of the spectra in the wavenumber regions of **b** 900–980 cm^{-1} and **c** 1600–1850 cm^{-1}

More importantly, for the drawn PLLA films post-processed with hot pressing, we observed no changes in crystallinity and crystal structure compared with those of the films that were only drawn (a high piezoelectric value, compared with that of the films subjected to postprocessing heat treatment with annealing, is observed later). Although an increase in crystal growth was observed and higher crystallinity was expected, due to the high temperature and pressure, melting on the surface occurred, which was later confirmed when observing the surface morphology.

The contributions of the drawing and postprocessing heat treatment to the crystalline phase and crystallinity were further analyzed using the ATR method. The ATR spectra of amorphous PLLA films (DR1), films drawn with a DR of 5 at 90 °C and 40 mm min^{-1} (DR5) and films drawn and postprocessing heat treated at 160 °C (DR5 ANN) or hot pressed at 140 °C (DR5 HP) were compared. The observed peaks (Fig. 5a) correspond to C=O stretching (1700–1780 cm^{-1}), C–H bending (1300–1500 cm^{-1}), C–O–C stretching (1000–1300 cm^{-1}) and C–C stretching coupled with CH_3 rocking (800–1000 cm^{-1}), according to the literature [26, 27].

With a closer look at the peaks between wavenumbers of 900 and 980 cm^{-1} (Fig. 5b), corresponding to C–C stretching coupled with CH_3 rocking, a difference is observed between the amorphous (DR1) and semicrystalline polymer states (DR5s). Rangari et al. and Wang et al. documented that the band at 923 cm^{-1} is present only for crystalline polymers, so it can also be used as an indication of induced crystallization, while the band at 955 cm^{-1} decreases in intensity with increased crystallization and can be used to detect the amorphous phase [28, 29]. Similarity in the changes in all modified samples, both drawn and postprocessing heat treated, compared with the undrawn samples was observed. In the C=O carbonyl region of the spectra (Fig. 5c), splitting of a peak into two dominant peaks at 1747 cm^{-1} and 1757 cm^{-1} is observed after annealing at 160 °C due to a smaller space between two

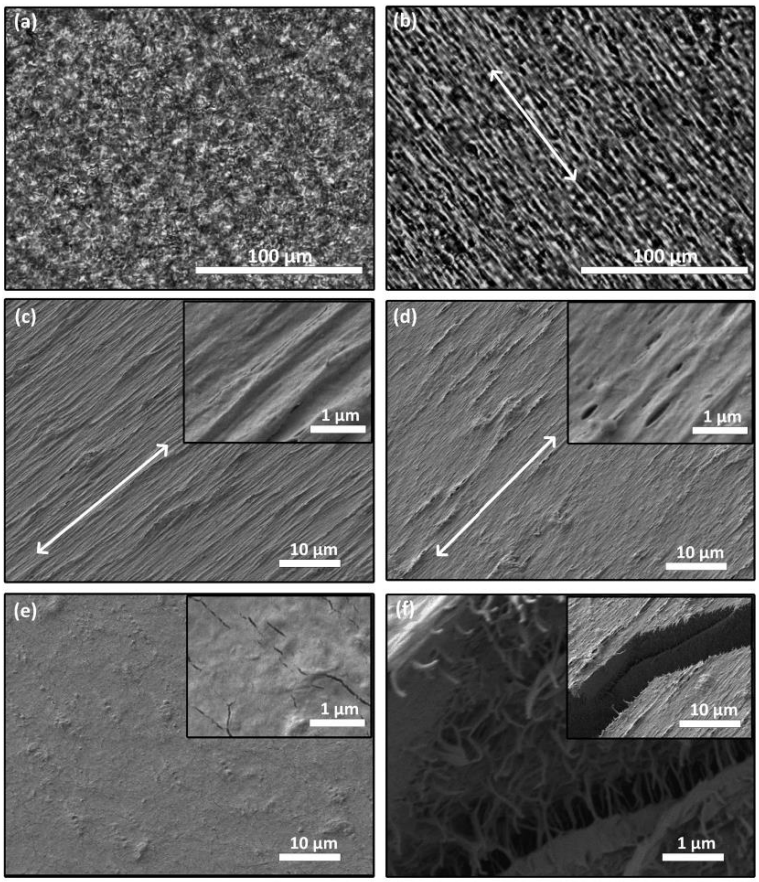

Fig. 6 Surface morphology observed by polarized optical microscopy for **a** thermally crystallized (spherulite growth) and **b** strain-crystallized (DR5) PLLA films and by SEM for **c** a drawn sample (DR5), **d** a sample post-treated with annealing at 140 °C, **e** a sample post-treated with hot pressing at 140 °C and **f** a tear in the sample shown in **d** with clearly observable fibers

C=O groups, corresponding to a change in the crystalline form to α, according to the literature [30]. This phenomenon is a good indicator of the compact α crystalline phase since the α' phase has a looser structure and splitting of the peak does not occur.

The most promising properties are shown by the drawn films (DR 5) annealed at 160 °C; however, these films are too brittle to withstand piezoelectric measurements or to be used for the predicted applications. Therefore, the samples subjected to postprocessing heat treatment with annealing at 140 °C or hot pressing were further analyzed.

Effect of drawing on the microstructure

Changes in microstructure were observed by polarized optical microscopy and SEM, where differences in the surface among the drawn, undrawn, and thermally treated polymer films were observed. Using polarized optical microscopy to observe the semicrystalline PLLA films, a difference in molecular chain orientation between the polymer that crystallized into non-oriented spherulite crystals (Fig. 6a) through thermally induced crystallization and the polymer subjected to strain-induced crystallization

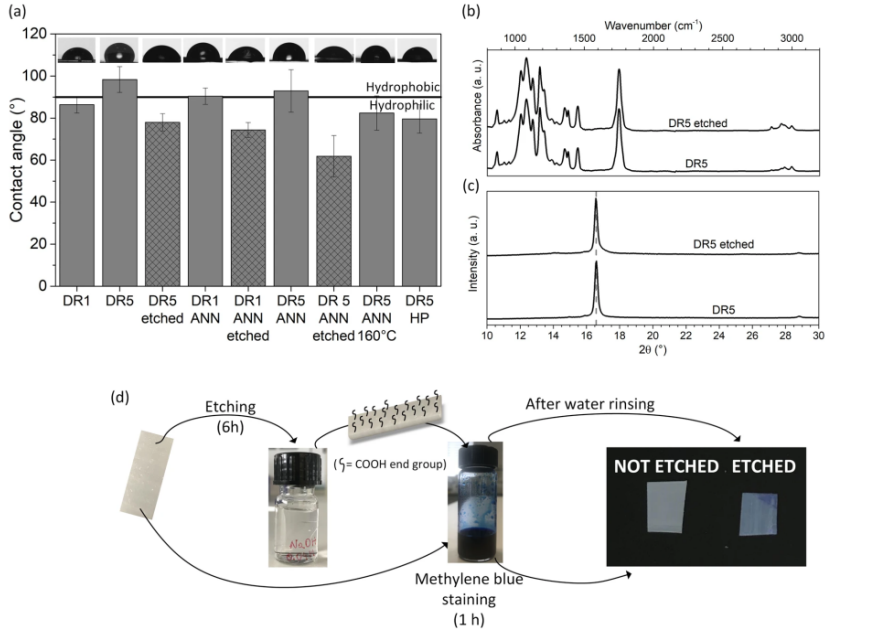

Fig. 7 **a** Wetting angles for an amorphous PLLA film, a drawn PLLA film, and PLLA films further annealed at 140 °C (ANN) and 160 °C (ANN 160 °C) and alkali etched (etched). The marked value indicates border between hydrophilic versus hydrophobic surfaces at a 90° angle. **b** IR spectra of drawn and further etched samples; **c** XRD diffractograms of drawn and further etched samples; **d** demonstration of methylene blue staining of nonetched and etched samples

(Fig. 6b), where molecular chain orientation was observed, was found. SEM images also confirm the macroscopic orientation of chains, which is revealed by sample tilting for better texture representation. The chains are aligned with the drawing direction, as indicated with arrows in the images. The roughness on the surface is clearly observed for the drawn films (Fig. 6c) and the films post-heat treated with annealing at 140 °C (Fig. 6d). On the other hand, post-heat treatment with hot pressing provides a smoother surface (Fig. 6e) than that of the films that were only drawn or annealed. There is also a difference in surface porosity, which is decreased after postprocessing heat treatment. The fiber structure in the volume of the films is also confirmed by observing the tear created on the drawn and annealed sample (Fig. 6f). The observed fibers are aligned and have nanoscale thickness.

Effect of drawing and posttreatment on the hydrophilic properties of PLLA films

For medical applications, cell attachment is important so that cells can actually exploit material functionality and is more common for materials with a hydrophilic surface than those with a hydrophobic surface. PLLA is, however, hydrophobic, which limits its interactions with cells. Figure 7a presents the effect of drawing, annealing, and alkali etching on the wetting angle of the films with deionized water. The contact angle is increased from the amorphous sample to above 90° upon drawing, which indicates the more hydrophobic behavior of the more crystalline samples, probably as a consequence of the difference in surface roughness between these two systems. However, the wetting angle is lowered for the annealed films, most notably for the smooth films post-treated with hot pressing, which could be explained by the reduction in surface roughness due to some chain reorganization on the surface. The last finding is in accordance with the previously observed amplifying effect of roughness, as a surface covered with a hydrophobic molecular coating become more hydrophobic if its roughness is increased [31]. For all the etched samples, the wetting angles are lower than 90°, which makes the polymer hydrophilic and therefore more attractive for cell attachment. Our polymeric films were alkali treated with 0.04 M NaOH. The strongest etching effect was observed

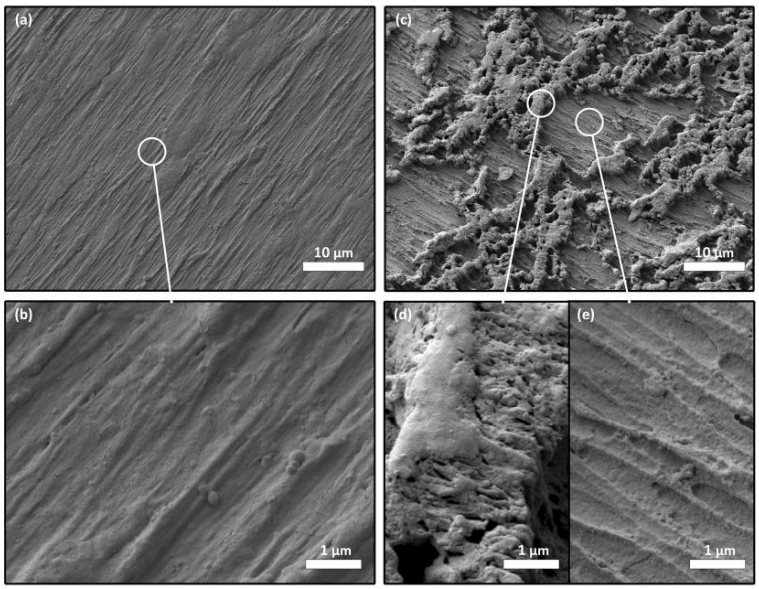

Fig. 8 **a** Surface of a drawn PLLA film (DR5) etched for 20 h in NaOH solution; **b** enlarged image of the etched sample in **a**; **c** surface morphology of a drawn (DR5) and annealed PLLA film sample that was etched (20 h at 140 °C); **d** enlarged image of islands formed on the etched surface of annealed samples; **e** enlarged view of the surface of an etched and annealed sample. All images were captured with SEM

for the annealed samples, with the lowest value of 62° obtained for sample DR 5, ANN 140 °C, possibly due to its more amorphous surface after annealing, which is easily etched. As observed before [17], upon etching PLLA, more carboxylic end groups are exposed on the surface, which improves the hydrophilic properties.

High improvement in wettability was observed for all etched samples, but no changes in crystallinity or crystal structure occurred simultaneously. No changes were observed in the IR spectra (Fig. 7b), which show no additional peaks or frequency shifts due to etching, or in the XRD data (Fig. 7c), which show no change in the crystal structure or crystallite size of the polymer films.

The increase in hydrophilicity after etching our polymer films was confirmed by staining with methylene blue (Fig. 7d), which interacts with the free carboxylic groups on the surface. In addition, we observed the surface topography of the etched samples. After etching of the drawn films, no changes in the surface were observed (Fig. 8a, b). With etching of the annealed films, changes in the surface topography and roughness were observed, which also contribute to their wettability (Fig. 8c). As observed in the SEM images, an island-like texture is formed on top of the post-treated annealed films after etching (Fig. 8d). The missing parts are probably etched due to degradation of the amorphous polymeric phase, which was present due to the annealing process at high temperatures. This observation confirms the amplifying effect of roughness on the hydrophilicity of surfaces with hydrophilic molecular coatings (in this case, through etching) if the surface roughness is increased. Due to the change in surface roughness observed on the etched and annealed samples, where an increase in hydrophilicity also occurred, better cell adhesion than that on the smooth surface of the non-annealed samples is expected.

Alkaline etching of poly-lactide is considered strictly a surface hydrolysis reaction that does not have effect on the bulk polymer and excludes bulk degradation [32]. Consequently, this process is not expected to lead to a change in molecular weight or a decrease in mechanical properties. It should both remove amorphous areas at the surface and modify the surface chemistry, leading to hydrophilicity. However, since mechanical characteristics are of ultimate importance for the biomedical applications of piezo-PLLA films, more investigations are needed in the future to explore the mechanical properties of these films and their changes after aging under physiological conditions.

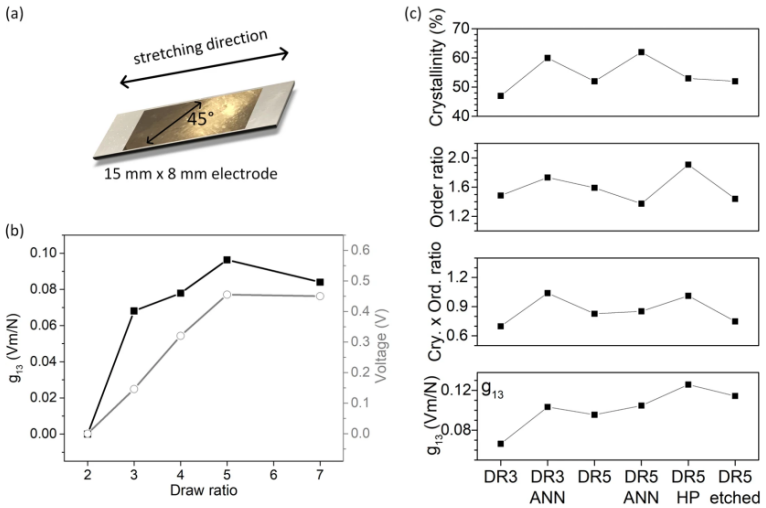

Fig. 9 **a** Symbolic depiction of the film sputtered with gold electrodes with a marked 45° fiber direction indicated with an arrow and the stretching direction for piezoelectric measurements; **b** the effect of the drawing ratio on the piezoelectric voltage coefficient g_{13} (■) and measured voltage signal on the surface of a 15 mm × 8 mm electrode in response to mechanical stress (○); **c** comparison of crystallinity, order ratio, crystallite size and order ratio and piezoelectric coefficient g_{13} measurements among differently prepared samples

Piezoelectric measurement of PLLA films

Our measured piezoelectric coefficients are determined as the effective macroscopic piezoelectric values, calculated from the voltage generated on the surface of a film cut at 45° relative to the stretching direction, needed to achieve shear deformation of the fibers when the films were stretched in the longitudinal direction under a known force and frequency. For shear piezoelectricity, Ochiai et al. measured piezoelectric coefficients by the quasi-static method, similar to the one we used, for films cut at 45° and confirmed the values with the self-resonant method [33], which provides comparable results; therefore, our method should be appropriate for macroscopic measurements. They measured the charge coefficient (d_{14}) as 10 pC N^{-1} and piezoelectric voltage coefficient as (g_{14}) 0.332 V m N^{-1} for elongated and annealed samples cut at 45° relative to the stretching direction.

When a film is drawn to a different DR, the piezoelectric voltage increases up to the point at which the sample is drawn to five times its initial length, which provides the highest piezoelectric value of 0.096 V m N^{-1}, and is lowered with a further increase in DR. The measured voltage, generated on the surface of a 8 mm × 15 mm × 0.1 mm film (Fig. 9a), shows a maximum value of 455 mV (4550 mV/mm), which should sufficient for use in medical applications (Fig. 9b). The human body generates biological electrical fields (EFs) by stress-generated potential (biological piezoelectricity), endogenous EFs (100–400 mV/mm) and transmembrane potentials (−10 to −90 mV), which are responsible for natural electrostimulated regeneration [34]. Some of the experimentally measured EFs are ~40 mV/mm in corneal wounds and 100–200 mV/mm in mammalian skin wounds [35]. Different cells and tissues can respond to electrostimulation in different ways. Therefore, designing medical devices with electrical output that is particularly characteristic of the natural EFs in a specific area of interest (specific type of cells or tissues) is the best way to mimic natural healing processes. The optimization of the processing parameters shown in the present study enables tailoring output EFs, which provides a very useful tool for further designing piezo-PLLA films for specific biomedical applications.

Interesting results are observed when the properties of the PLLA films post-treated with heating or etching are measured (Fig. 9c). When the films are post-heat treated at 140 °C, the crystallinity is increased to 62% for films drawn to different DRs (DR of 3 and DR of 5); however, the order ratio is increased for annealed samples with lower DRs. This increase could be a result of the crystalline form changing to a denser, almost α crystal structure with an increased number of oriented crystallites and reduced crystallite size. Compared with the drawn polymer that was only drawn, the polymer post-heat treated with hot pressing at 140 °C shows the same

crystallinity but an increase in the order ratio; consequently, the piezoelectricity is improved. This behavior could be explained by the denser structure arising from filling of the pores with melted polymer from pressing and from the growth of the oriented crystallites observed previously. Compared with the nonetched or even the annealed sample, the alkali-etched DR5 sample shows a slightly higher piezoelectric coefficient with no changes in material properties (crystallinity and order ratio), most likely due to a change in the surface active groups. The change in piezoelectricity follows the same trend as the crystallinity and orientation values presented in Fig. 9b, which are also in accordance with the results of Lovell et al. [10].

Our highest piezoelectric value for g_{13} is 0.125 Vm N^{-1}, which is equivalent to a g_{14} of 0.250 Vm N^{-1}. The piezoelectric properties and ability to crystallize with stretching are also dependent on the molecular weight and L-content in PLLA, which also leads to easier or more limited molecular orientation and crystallization with stretching. These results indicate that PLLA piezoelectricity strongly depends on the processing method used during film preparation and the polymer physical properties.

The processing and postprocessing treatments were optimized to obtain active PLLA films with an optimal balance among piezoelectricity, hydrophilicity and surface roughness. For higher crystallinity, orientation, and piezoelectric properties, PLLA films need to be drawn to five times their initial length at a drawing temperature of 90 °C and a drawing rate of 40 mm min^{-1} to achieve more uniform structural properties. Postprocessing heat treatment and alkali etching finally optimize film crystallinity and provide critically important optimization of the surface, leading to hydrophilic properties. The highest measured piezoelectric voltage coefficient g_{13} was 0.125 V m N^{-1}, which in theory corresponds to a g_{14} value of 0.250 V m N^{-1}, is a high value among polymers and is much higher than that of ceramic materials. The high piezoelectric voltage coefficient (g), which indicates that small strain is needed for the generation of an induced electrical field on the surface, opens interesting possibilities for the use of PLLA in biomedical sensors and wound healing applications.

In summary, postprocessing annealing and alkali etching of drawn PLLA films led to optimized combinations of hydrophilicity, roughness and piezoelectricity. Using this approach, we designed active PLLA films with high potential for strong interactions with cells, which are very important in further biomedical applications, including exploring the effect of piezoelectricity on cell proliferation. A very important aspect of the present work is its applicability as a useful tool for adjusting the properties of piezo-PLLA films to the specific needs of cells and tissues and for modulating their properties for specific biomedical applications. The summary of the processing methods presented in this work is directly applicable to a variety of polymers similar to PLLA (characterized by shear piezoelectricity), including a range of natural polymers. It can also be applied as a part of the processing route towards other types of polymers (similar to PVDF) in combination with electrical poling.

Acknowledgements The authors are grateful to David Fabijan and Damjan Vengust, Advanced Materials Department, Jozef Stefan Institute, for the piezoelectric and Raman spectroscopy measurements, respectively. We also acknowledge the CENN Nanocenter for the use of the NTEGRA Spectra I confocal Raman spectrometer. The work has been funded by the Slovenian Research Agency (ARRS) (grants J2-8169 and PR-08338).

Compliance with ethical standards

Conflict of interest The authors declare that they have no conflict of interest.

Publisher's note Springer Nature remains neutral with regard to jurisdictional claims in published maps and institutional affiliations.

References

1. Curry EJ, Ke K, Chorsi MT, Wrobel KS, Miller AN, Patel A, Kim I, Feng J, Yue L, Wu Q, Kuo C-L, Lo KW-H, Laurencin CT, Ilies H, Purohit PK, Nguyen TD. Biodegradable piezoelectric force sensor. Proc Natl Acad Sci USA. 2018;115:909–14. https://doi.org/10.1073/pnas.1710874115.
2. Lagarón J-M (editor). Polylactic acid (PLA) nanocomposites for food packaging applications. In: Multifunctional and nanoreinforced polymers for food packaging, Woodhead Publishing, Cambridge, UK; 2011. p. 485–97. https://doi.org/10.1533/9780857092786.4.485.
3. Miyazaki H, Kinoshita M, Saito A, Fujie T, Kabata K, Hara E, Satoshi O, Takeoka S, Saitoh D. An ultrathin poly(L-lactic acid) nanosheet as a burn wound dressing for protection against bacterial infection. Wound Repair Regen. 2012;20:573–9. https://doi.org/10.1111/j.1524-475X.2012.00811.x.
4. Ikada Y, Shikinami Y, Hara Y, Tagawa M, Fukada E. Enhancement of bone formation by drawn poly(L-lactide). J Biomed Mater Res. 1996;30:553–8. https://doi.org/10.1002/(SICI)1097-4636(199604)30:4<553:AID-JBM14>3.0.CO;2-I.
5. Abd Alsaheb RA, Aladdin A, Othman NZ, Abd Malek R, Leng OM, Aziz R, Enshasy HAEl. Recent applications of polylactic acid in pharmaceutical and medical industries. J Chem Pharm Res. 2015;7:51–63.
6. Lotz B. Crystal polymorphism and morphology of polylactides. In: Di Lorenzo ML, Androsch R, editors. Synthesis, structure and properties of poly(lactic acid). Springer, Cham, Switzerland; 2017. p. 273–302. https://doi.org/10.1007/12_2016_15.
7. Takahashi K, Sawai D, Yokoyama T, Kanamoto T. Crystal transformation from the a- to the b-form upon tensile drawing of poly (L-lactic acid), 45 (2004) 4969–76. https://doi.org/10.1016/j.polymer.2004.03.108.
8. Chen X, Kalish J, Hsu SL. Structure evolution of a α'-phase poly (lactic acid). J Polym Sci Part B Polym Phys. 2011;49:1446–54. https://doi.org/10.1002/polb.22327.
9. Fukada E. History and recent progress in piezoelectric polymers. IEEE Trans Ultrason, Ferroelectr, Freq Control. 2000;47:1277–90.

10. Lovell CS, Fitz-Gerald JM, Park C. Decoupling the effects of crystallinity and orientation on the shear piezoelectricity of polylactic acid. J Polym Sci Part B Polym Phys. 2011;49:1555–62. https://doi.org/10.1002/polb.22345.
11. Singh AA, Wei J, Herrera N, Geng S, Oksman K. Synergistic effect of chitin nanocrystals and orientations induced by solid-state drawing on PLA-based nanocomposite tapes. Compos Sci Technol. 2018;162:140–5. https://doi.org/10.1016/j.compscitech.2018.04.034.
12. Singh AA, Geng S, Herrera N, Oksman K. Aligned plasticized polylactic acid cellulose nanocomposite tapes: effect of drawing conditions. Compos Part A Appl Sci Manuf 2018;104:101–7. https://doi.org/10.1016/j.compositesa.2017.10.019.
13. Tajitsu Y. Basic study of controlling piezoelectric motion of chiral polymeric fiber. Ferroelectrics. 2009;389:83–94. https://doi.org/10.1080/00150190902987871.
14. Fukada E. New piezoelectric polymers. Jpn J Appl Phys. 1998;37:2775–80. https://doi.org/10.1143/JJAP.37.2775.
15. Zareidoost A, Yousefpour M, Ghaseme B, Amanzadeh A. The relationship of surface roughness and cell response of chemical surface modification of titanium. J Mater Sci Mater Med. 2013;23:1479–88. https://doi.org/10.1007/s10856-012-4611-9.
16. Tandon B, Blaker JJ, Cartmell SH. Piezoelectric materials as stimulatory biomedical materials and scaffolds for bone repair. Acta Biomater. 2018;73:1–20. https://doi.org/10.1016/j.actbio.2018.04.026.
17. Tham CY, Abdul Hamid ZA, Ahmad Z, Ismail H. Surface modification of poly(lactic acid) (PLA) via alkaline hydrolysis degradation. Adv Mater Res. 2014;970:324–7. https://doi.org/10.4028/www.scientific.net/AMR.970.324.
18. Yanagida H, Okada M, Masuda M, Ueki M, Narama I, Kitao S, Koyama Y, Furuzono T, Takakuda K. Cell adhesion and tissue response to hydroxyapatite nanocrystal-coated poly (L -lactic acid) fabric. J Biosci. 2009;108:235–43. https://doi.org/10.1016/j.jbiosc.2009.04.003.
19. Adar F, Noether H. Raman microprobe spectra of spin-oriented and drawn filaments of poly (ethylene terephthalate). Polymers. 1985;26:1935–43. https://doi.org/10.1016/0032-3861(85)90171-5.
20. Farah S, Anderson DG, Langer R. Physical and mechanical properties of PLA, and their functions in widespread applications —a comprehensive review. Adv Drug Deliv Rev. 2016;107:367–92. https://doi.org/10.1016/j.addr.2016.06.012.
21. Bernard F, Gimeno L, Viala B, Gusarov B, Cugat O. Direct piezoelectric coefficient measurements of PVDF and PLLA under controlled strain and stress. Proceedings. 2017;1:335 https://doi.org/10.3390/proceedings1040335.
22. Turner JF, Riga A, O'Connor A, Zhang J, Collis J. Characterization of drawn and undrawn poly-L-lactide films by differential scanning calorimetry. J Therm Anal Calorim. 2004;75:257–68. https://doi.org/10.1023/B:JTAN.0000017347.08469.b1.
23. Chen Z, Zhang S, Wu F, Yang W, Liu Z, Yang M. Motion mode of poly(lactic acid) chains in film during strain-induced crystallization. J Appl Polym Sci. 2016;133:1–10. https://doi.org/10.1002/app.42969.
24. Larrañaga A, Lizundia E. Strain-induced crystallization. In: Thomas S, Arif PM, Gowd B, Kalarikkal N, editors. Crystallization in multiphase polymer systems. 1st ed., Elsevier, Amsterdam, Netherlands; 2018. p. 471–508. https://doi.org/10.1016/B978-0-12-809453-2.00015-3.
25. Yoshida M, Onogi T, Onishi K, Inagaki T, Tajitsu Y. High piezoelectric performance of poly(lactic acid) film manufactured by solid-state extrusion. Jpn J Appl Phys. 2014;53:PC02-1–PC02-6. https://doi.org/10.7567/JJAP.53.09PC02.
26. Kister G, Cassanas G, Vert M, Pauvert B, Térol A. Vibrational analysis of poly(L-lactic acid). J Raman Spectrosc. 1995;26:307–11. https://doi.org/10.1002/jrs.1250260409.
27. Vasanthan N, Ly O. Effect of microstructure on hydrolytic degradation studies of poly (l-lactic acid) by FTIR spectroscopy and differential scanning calorimetry. Polym Degrad Stab. 2009;94:1364–72. https://doi.org/10.1016/j.polymdegradstab.2009.05.015.
28. Wang Y, Zhang H, Li M, Cao W, Liu C, Shen C. Orientation and structural development of semicrystalline poly(lactic acid) under uniaxial drawing assessed by infrared spectroscopy and X-ray diffraction. Polym Test. 2015;41:163–71. https://doi.org/10.1016/j.polymertesting.2014.11.010.
29. Rangari D, Vasanthan N. Study of strain-induced crystallization and enzymatic degradation of drawn poly (l-lactic acid)(PLLA) films. Macromolecules. 2012;45:7397–403. https://doi.org/10.1021/ma301482j.
30. Meaurio E, Zuza E, López-Rodríguez N, Sarasua JR. Conformational behavior of poly(L-lactide) studied by infrared spectroscopy. J Phys Chem B. 2006;110:5790–5800. https://doi.org/10.1021/jp055203u.
31. Quéré D. Rough ideas on wetting. Physica A. 2002;313:32–46.
32. Sun SP, Wei M, Olson JR, Shaw MT. Alkali etching of a poly (lactide) fiber, ACS Appl Mater Interfaces. 2009. https://doi.org/10.1021/am900227f.
33. Ochiai T, Eiichi Fukada. Electromechanical properties of poly-L-lactic acid. Jpn J Appl Phys. 1998;37:3374–6. https://doi.org/10.1143/JJAP.37.3374.
34. Meng S, Rouabhia M, Zhang Z. Electrical stimulation in tissue regeneration, In: Appl Biomed Eng. 2011. https://doi.org/10.5772/18874.
35. Wang ET, Zhao M. Regulation of tissue repair and regeneration by electric fields. Chin J. Traumatol.(English Ed.) 2010. https://doi.org/10.3760/cma.j.issn.1008-1275.2010.01.011.

Chapter 4

Effect of Surface Hydrophilicity on Polymer Degradation

This chapter provides an overview of the degradation process of polymer films with a hydrophobic or more hydrophilic surface as a result of alkaline surface treatment. Degradation in water was not observed for either type of sample, therefore the process was accelerated by adding the enzyme proteinase K (directed to cleave ester bonds) to the medium, where I observed the difference within 5 days of degradation. The improved surface hydrophilicity causes a change in the degradation process of the PLLA drawn film, from bulk to more surface-oriented erosion, maintaining mechanical stability and, consequently, piezoelectric properties for longer. The observed correlations are very important for further predictions during the interactions of piezoelectric PLLA films with living surroundings, particularly during electro-stimulated regeneration and wound healing, where the gradual loss of piezoelectric properties is beneficial. This paper is the first publication on the piezoelectric degradation of PLLA to show how the piezoelectricity changes with degradation, and the first to find that by increasing the hydrophilicity of the surface, the degradation moves from the bulk to the surface, preserving the piezo-properties typical for bulk polymer films [40].

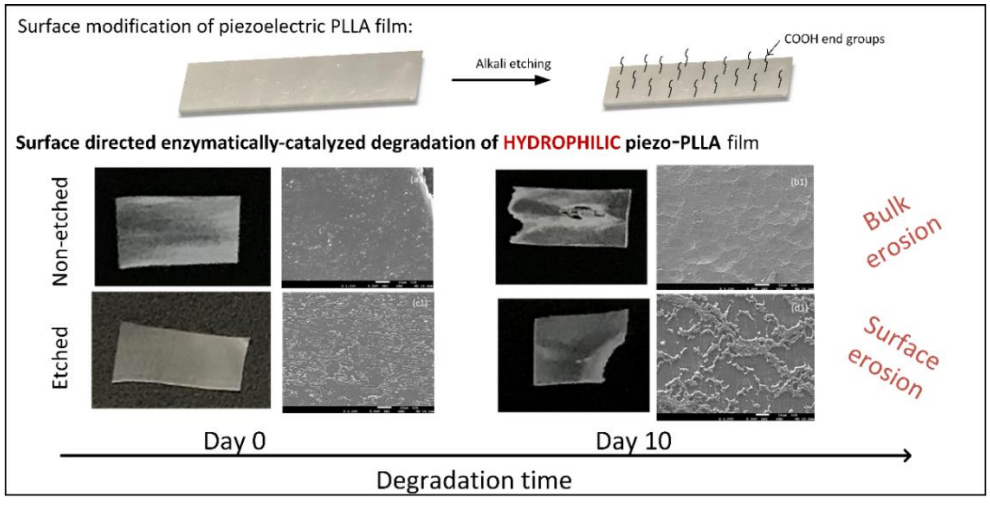

Figure 13: Demonstration of surface modification of PLLA film after alkaline etching to release COOH groups on the surface and achieve hydrophilicity of PLLA (etched sample) which shifts degradation to surface erosion instead of bulk [40].

4.1 Hydrophilicity Affecting the Enzyme-Driven Degradation of Piezoelectric Poly-L-Lactide Films

polymers

MDPI

Article

Hydrophilicity Affecting the Enzyme-Driven Degradation of Piezoelectric Poly-L-Lactide Films

Lea Gazvoda [1,2], Bojana Višić [3,4], Matjaž Spreitzer [1] and Marija Vukomanović [1,*]

[1] Advanced Materials Department, Jožef Stefan Institute, 1000 Ljubljana, Slovenia; lea.udovc@ijs.si (L.G.); matjaz.spreitzer@ijs.si (M.S.)
[2] Jožef Stefan International Postgraduate School, 1000 Ljubljana, Slovenia
[3] Condensed Matter Physics Department, Jožef Stefan Institute, 1000 Ljubljana, Slovenia; bojana.visic@ijs.si
[4] Institute of Physics Belgrade, University of Belgrade, Pregrevica 118, 11080 Belgrade, Serbia
* Correspondence: marija.vukomanovic@ijs.si; Tel.: +386-1-477-3547

Abstract: Biocompatible and biodegradable poly-L-lactic acid (PLLA) processed into piezoelectric structures has good potential for use in medical applications, particularly for promoting cellular growth during electrostimulation. Significant advantages like closer contacts between cells and films are predicted when their surfaces are modified to make them more hydrophilic. However, there is an open question about whether the surface modification will affect the degradation process and how the films will be changed as a result. For the first time, we demonstrate that improving the polymer surface's wettability affects the position of enzyme-driven degradation. Although it is generally considered that proteinase K degrades only the polymer surface, we observed the enzyme's ability to induce both surface and bulk degradation. In hydrophilic films, degradation occurs at the surface, inducing surface erosion, while for hydrophobic films, it is located inside the films, inducing bulk erosion. Accordingly, changes in the structural, morphological, mechanical, thermal and wetting properties of the film resulting from degradation vary, depending on the film's wettability. Most importantly, the degradation is gradual, so the mechanical and piezoelectric properties are retained during the degradation.

Keywords: poly-L-lactic acid; enzymatically catalyzed degradation; piezoelectricity; bulk erosion; surface erosion

Citation: Gazvoda, L.; Višić, B.; Spreitzer, M.; Vukomanović, M. Hydrophilicity Affecting the Enzyme-Driven Degradation of Piezoelectric Poly-L-Lactide Films. *Polymers* **2021**, *13*, 1719. https://doi.org/10.3390/polym13111719

Academic Editor: Roman A. Surmenev

Received: 29 April 2021
Accepted: 21 May 2021
Published: 24 May 2021

1. Introduction

Poly-L-lactic acid (PLLA), a biosynthetic thermoplastic polyester, is widely used in the biomedical field because it is biocompatible and biodegradable [1,2]. It can also be formed into different shapes (2D coatings and films, micro- and nano-powders, 3D scaffolds, etc.) with different properties, depending on the requirements [3]. Accordingly, PLLA is used in drug-delivery systems [4], tissue engineering [5], wound dressing [6], implantation [7] and many more [8,9].

A very poorly explored and particularly important aspect of PLLA's application in biomedicine is associated with the possibility of processing it into a piezoelectric material. Due to its helix structure, PLLA exhibits shear piezoelectricity [10]. When PLLA is oriented and crystalline, usually as fibers or films, the chains are strained, the molecular dipoles are aligned, and a voltage difference is observed [11]. Such a structure, formulated as a piezoelectric scaffold, can be applied for piezo-stimulation and promoting cell proliferation. The low piezoelectric effect of PLLA (compared to piezoceramics) is comparable to the piezoelectricity of natural biomacromolecules (i.e., collagen) [12] and can be efficient enough to relate with biological systems [13]. It makes this polymer particularly appropriate for regenerative medical use to accelerate the wound-healing process. When applied for wound healing, the safe biodegradation of piezoelectric PLLA films is very important. The process needs to be steady, and the biodegradation (followed by a change of mechanical,

structural, morphological and piezoelectric properties) should follow the kinetics of the tissue regeneration so that at the end, no material residues are left in the system when the new tissue is formed.

When PLLA is in contact with biological media, cleavage of the ester bonds occurs in the bulk matter, usually by hydrolysis, into lactic acid, carbon dioxide and water [14]. Under in vivo conditions, due to the inflammation process during the injury, the degradation process is enhanced by the enzymes present that degrade the polymer matrix [1]. Since PLLA is more hydrophobic, swelling of the polymer film occurs with the diffusion of water inside the polymer bulk, which triggers the degradation inside the material [14]. However, when enzymes are present, it is generally considered that surface degradation is favorable since the diffusion of enzymes inside the film is aggravated [15]. Proteinase K catalyzes the degradation of PLLA several times faster in amorphous than in crystalline regions [16]. At the surface, degradation is limited to just the amorphous parts [15]. Crystalline residues, remaining after the degradation of the connected amorphous areas, are released into the surrounding liquid medium or accumulate on the surface and increase crystallinity [15]. Polymer crystallinity and chain orientation have been determined to have an important role in the process of enzyme-induced PLLA degradation. H. Tsuji et al. showed that the initially higher crystallinity of the PLLA films slows the degradation process and that the higher polymer-chain orientation also limits the enzyme intake into the bulk [15]. In addition, Rangari et al. observed that during the hydrolysis of the amorphous part on the surface in uniaxially prepared crystalline PLLA films, crystallinity plays the dominant role in determining the extent of the degradation, compared to the orientation of the polymer chains [16].

Understanding the degradation mechanism in biologically relevant surroundings is a key issue for using a piezoelectric polymer in biomedical applications. Although there is a detailed study of the structural changes that follow enzymatic degradation (change in crystallinity, chain orientation, chain mobility, etc.), very little knowledge is available on the change in the piezoelectric and mechanical properties of PLLA films during the degradation process. All the information regarding PLLA degradation is available for polymers with a hydrophobic surface. However, the hydrophobic surface is the main disadvantage of PLLA, potentially resulting in a low cell affinity and an inflammatory response [17]. A particular lack of information was observed for the case of the degradation of surface-modified PLLA hydrophilic films. With that in mind, we focused our investigations on two questions:

(i) How will the degradation be affected if the surface of the PLLA film is modified from hydrophobic to hydrophilic (more favorable to cells)?
(ii) What will happen to the mechanical and piezoelectric properties of the PLLA once the film is immersed in a liquid medium containing proteinase K (as an imitation of the inflammation response at the site of a wound)?

Therefore, in this study, we compare the enzymatically catalyzed degradation process of a uniaxial drawn piezoelectric PLLA film with and without surface modification, and with it the mechanical and piezoelectric changes that occur during the degradation process to achieve a more stable and gradual loss of piezoelectric properties during the process. Films with improved wettability should have greater potential for medical applications due to the proposed better affinity of the cells for the film.

2. Materials and Methods

2.1. Materials

Poly-L-lactic acid (PLLA) having a molecular weight with an approximate value of 150 kDa (Goodfellow, Cambridge, Ltd., UK), bovine serum albumin (BSA) (Fisher scientific, Leics, UK), methylene blue (MB) (Alfa Aesar, Thermo Fisher GmbH, Kandel, Germany) were used. Enzyme proteinase K was purchased from ITW Reagents (AppliChem GmbH, A3830,0500, Darmstadt, Germany) and was used as received. TRIS buffer, sodium hydroxide (NaOH), methanol (MeOH), hydrochloride acid (HCl), were purchased from

Sigma-Aldrich Chemie GmbH, Steinheim, Germany. Distilled water was purified using a Milli-Q system (Purelab Option-Q, ELGA, High Wycombe, UK).

2.2. Processing PLLA Films

Piezoelectric polymer films were prepared using the following procedure, optimized in our previous study [18]. PLLA granules (1 g) were melt-pressed between two metal plates at 200 °C under a pressure of 56 kN for 3 min and immediately quenched in cold water (4 °C) (amorphous sheet). To prepare piezoelectric films, the amorphous sheet was cut into a dumbbell-shape film and uniaxially stretched with a homemade tensile stretcher to a draw ratio of 5 at a temperature above the glass transition (90 °C), using a drawing rate of 40 mm/min. Surface modification, such as alkaline etching, was performed to prepare hydrophilic films. Films were submerged overnight in a 0.04 M NaOH medium, prepared in a water/MeOH mixture (70/30 *V/V*) to cleave the ester bonds on the surface.

2.3. Enzymatic Degradation

The drawn films were immersed in 0.1 mg/mL proteinase K solution with pH 8.5. The enzyme solution was prepared using a 0.5 M TRIS buffer, adding HCl to adjust the pH value. 5 mL of enzyme solution containing films was maintained at 37 °C in a water bath while gently shaken. The degradation study was carried out for 10 days. Films were washed with water and left to dry before the analyses. Enzymatic activity during the degradation process was monitored using an absorbance multiplate reader (Synergy H1, BioTek, Bad Friedrichshall, Germany). A sample of 500 µL of enzymatic medium taken from the degrading sample was added to 500 µL of 1 mg/mL BSA protein and digested for 2 h. Absorbance at 290 nm was continuously measured to determine the half-time needed for protein degradation. Measurements were made in two parallel samples for enzymes with different polymer films and a bare enzyme. Further enzymatic activity was stopped by heating the sample at 90 °C. A total of 15 µL of the sample with 3 µL of added loading buffer were put on 15% polyacrylamide gel to separate the degraded BSA proteins based on size using SDS-page electrophoresis.

2.4. Characterization Methods

Gravimetric determination, crystallinity and orientation changes were calculated using the following equation:

$$\Delta X\ (\%) = 100\% \times (X_{t0} - X_t)/X_{t0}, \quad (1)$$

where ΔX represents the weight changes (w), crystallinity (X) and orientation ratio (D) from the beginning ($t0$) to a certain time of degradation (t).

Orientation was determined using a Fourier-transform infrared spectrometer in attenuated total reflectance (ATR) mode (PerkinElmer Spectrum 100, Waltham MA, USA). Spectra were recorded in the 600–4000 cm^{-1} wavenumber range with a spectral resolution of 4 cm^{-1} and the accumulation of 10 spectra using a polarizer. Changes in the orientation were determined using the previous equation, where D represents the ratio between changes of the vertical ($\parallel$) and horizontal ($\perp$) absorbance (A) of the C=O peak (1756 cm^{-1}) using the following equation [19,20]:

$$D = A_{\parallel}/A_{\perp}. \quad (2)$$

Crystallinity was determined using a NETZSCH STA 449 (Jupiter) thermal analyzer for differential scanning calorimetry (DSC) in an Ar/O atmosphere (40/10). A total of 3–4 mg of each sample were put in platinum crucibles and heated from 40 °C to 200 °C with a 20 °C/min heating rate due to the temperature calibration under these conditions. The enthalpy of cold crystallization (ΔHc) and the enthalpy of melting (ΔHm) were determined

by calculating the surface under the peak of the crystallization or melting, respectively. Bulk crystallinity was determined with the following expression:

$$X_c\ (\%) = 100\% \times (\Delta H_m - \Delta H_c)/\Delta H_{100\%}, \quad (3)$$

where the value for $\Delta H_{100\%}$ is taken as 93.6 J/g, which is a theoretical value for 100% crystalline PLLA films in the α crystalline form [21].

Morphological changes during degradation were observed with a scanning electron microscope (JSM-7600 F, Jeol Ltd., Tokyo, Japan). To observe changes in the hydrophilic properties, methylene-blue staining was used to observe the color change due to more carboxylic groups on the surface [22]. Water wetting angles were measured using a Theta Lite contact-angle meter, Biolin Scientific.

Dynamic mechanical properties of the PLLA samples were studied under tension mode on the films in a rectangular shape (9 mm long, 3–3.5 mm wide and 0.1 mm thick). The measurements were performed with a Mettler Toledo DMA/SDTA861e. The dynamic responses were tested from 0 °C to 130 °C at the heating rate of 3 K/min. The dynamic force amplitude was 1 N, and the validity of Hooke's law (linearity measurement) was tested on every sample to determine the displacement amplitude, which was 2–5 µm. The chosen frequency was 1 Hz. The storage modulus, loss modulus and tan δ were recorded as a function of the sample temperature. Since the measurements were made in the tension mode, the storage modulus corresponds to Young's modulus.

The piezoelectric properties were measured according to the description in a previous article [18]. Polymer films were cut at an angle of 45° from the stretching axis, seeing that the shear stress has a maximum value when measured at this angle [23]. The measurement was made using a PiezoMeter System PM300 (Piezotest Pte. Ltd., International Plaza, Singapore), which was adapted for thin-film d_{31} measurements. First, gold electrodes were sputtered on both surfaces of the polymer film. Then the film was clamped on both sides to stretch the film (frequency of 110 Hz and force 0.15–0.5 N). The voltage was measured with a voltmeter (Tenma multimeter) over a reference capacitor of 1000 pF. The piezoelectric coefficients g_{14} and d_{14} were calculated.

3. Results

PLLA films were made with a hydrophilic surface using alkali etching to improve their water wettability, which is favored for interactions with cells [24]. Before being applied for the degradation study, the stretched, oriented, and etched films remained stained after immersion in the methylene-blue solution, indicating a larger amount of carboxylic end groups on the surface (Figure 1a). Degradation was performed using a proteinase-K-buffered solution under simulated physiological conditions (gently shaking at 37 °C). After aging for 5 and 10 days in the enzyme solution, the polymeric films had macroscopically observable damage (Figure 1b). Normally, for PLLA polymers, proteinase K acts as a hydrolysis catalyzer, and degradation follows the surface mechanism [15]. For the case of non-etched, hydrophobic films, we initially observed the occurrence of surface erosion, along with some evidence of bulk erosion induced by autocatalysis (day 10). This result was more following the available literature on hydrophobic PLLA film degradation without any enzyme present [17]. However, in the case of more hydrophilic PLLA films, it was observed that the films were macroscopically more compact, without signs of bulk erosion, indicating a contribution of the surface modification to the degradation process and the following mechanism (Figure 1b).

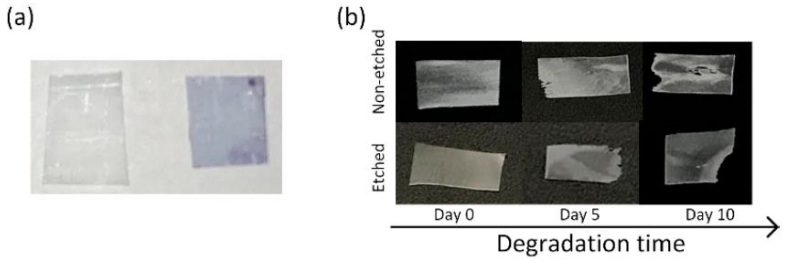

Figure 1. (**a**) Methylene blue staining of non-etched (**left**) and etched (**right**) PLLA films; (**b**) samples of enzymatic degradation of the non-etched (**top**) and etched (**bottom**) films after 0, 5 and 10 days.

3.1. Enzymatic Activity

Since all of the polymeric films were degraded in the same solution for the whole 10 day period, the enzyme activity was periodically monitored to follow the progress of degradation. By lowering the pH value, as a result of the release of lactic acid residues into the medium during the degradation progress, the activity of the proteinase K was also expected to decrease. The detected degradation products (based on an SDS-page test) (Figure 2a) and the half time of the enzyme's degradation activity (Figure 2b) show a lowering of the activity along with the film's degradation. The enzyme activity was also decreased in a reference enzyme solution (without films); however, this drop was more pronounced when films were present. Figure 2c presents the activity of the initial enzyme solution with the reference BSA protein, observed with a continuous absorbance measurement, from where the half time of the total protein degradation was determined. After 10 days of degradation, the enzyme activity is significantly reduced compared to day 1 (from 5 to 50 min), even without the films being present. This was expected since no fresh enzymes were added during the degradation. Despite the observed decreases, it should be noted that the enzyme was active for the whole period during which the degradation progress was observed. Accordingly, all the observed changes in the aged PLLA films could be assigned to the process of degradation.

3.2. Structural Changes (Crystallinity and Orientation)

After 10 days of degradation, the weight losses, indicating the progress of the degradation, were similar for both the etched (35%) and non-etched (37%) films. Additionally, the drops in the pH, directly correlated with the degradation process, were comparable for the etched and non-etched films (from 8.5 to 4.6) since the equally released lactic acid residues lower the initial pH value. The initial hydrophilicity was changed only on the surface of the films, which could affect the location of the degradation; however, the total progress of the degradation remained the same.

The main differences in the degradation of the etched and non-etched films were the crystallinity and orientation. These properties were detected by comparing the FTIR spectra of the enzymatically degraded films with the spectra of the film reference (corresponding to films aged in a medium without the enzyme present), as presented in Figure 3. Typical changes in the surface crystallinity are observed closely at normalized spectra in the wavelength range 900–980 cm^{-1}. Following previous studies [16,18], the increase in the intensity of the peak at 922 cm^{-1} represents an increase in the crystallinity of the PLLA, which we also observed in the case of the non-etched (hydrophobic) films (Figure 3, left).

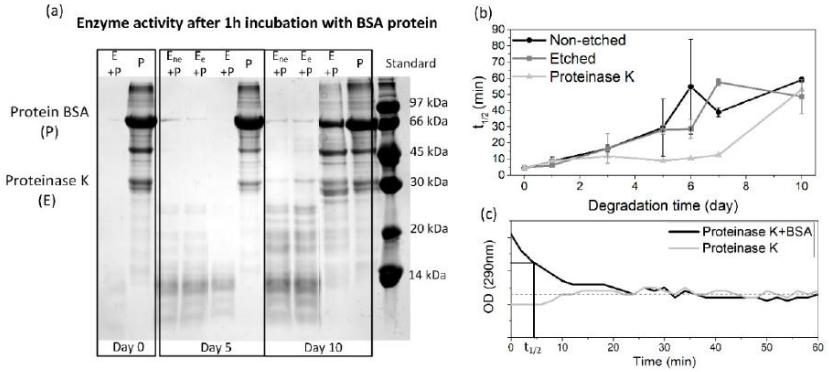

Figure 2. (**a**) SDS-page results for the enzymatic activity of the initial solution and after 5 and 10 days of degradation for enzymes in non-etched (Ene), etched (Ee) and control solutions (E), where activity was verified with degradation of the BSA protein (P); (**b**) calculated half time needed for BSA protein degradation for enzymes in non-etched, etched and control solutions, determined from measured optical density at 290 nm for each solution, where graph (**c**) presents the absorbance measurements for initial proteinase K solution with a marked half time of total degradation ($t_{1/2}$).

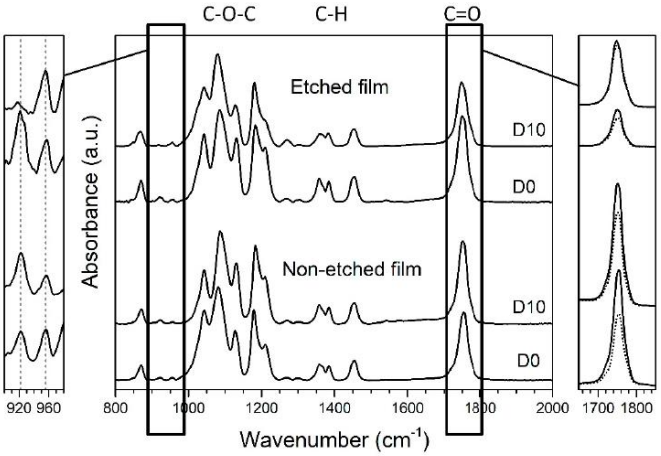

Figure 3. ATR FT-IR spectra (normalized to maximum peak absorbance) for non-etched and etched PLLA films (**middle**), degraded for 10 days in enzymatic solution (D10), compared to initial PLLA film (D0). On the (**left**), an enlarged, normalized spectrum between 900 and 980 cm^{-1} is presented to observe changes in the intensity of peaks that are specific for more crystalline (921 cm^{-1}) or more amorphous (956 cm^{-1}) films. On the (**right**), a polarizer was used to determine the changes in orientation of the C=O peak, comparing the intensities of horizontal (solid line) and vertical (dotted line) orientations without normalization of the spectra.

Orientation for the polymeric chains within the film was confirmed based on an observable peak at 1755 cm^{-1} that corresponds to the C=O stretching in the ester carbonyl group. As noted earlier, high anisotropy is obtained for oriented polymeric films when comparing the vertical and horizontal positions [19]. For our oriented PLLA films, the intensities of the C=O and C–O–C peaks are enhanced in the drawing direction (horizontal)

compared to the perpendicular direction (vertical) and shifted to slightly lower values (Figure 3, right). Comparable changes in the C=O and C–O–C peaks were also observed by T. Nobeshima et al. [20]. Regarding the influence of the water wettability, the orientation was decreased for both the hydrophobic non-etched and hydrophilic etched films during degradation (Table 1 and Figure 3).

Table 1. Summarized properties of degraded PLLA films over 10 days in solution with proteinase K.

Up to 10 Days of Degradation	PLLA Non-Etched	PLLA-Etched
pH change	From 8.5 to 4.6	From 8.5 to 4.6
Weight loss	37 wt %	35 wt %
Crystallinity change (DSC)	+27%	+5%
Orientation change (FT-IR: 1750 cm^{-1})	−24% of the initial ratio	−18% of the initial ratio
Piezo change	**After 5 days:**	**After 5 days:**
d_{14} g_{14}	2.68 pC/N (68.8% of initial) 0.092 Vm/N	2.32 pC/N (50.4% of initial) 0.066 Vm/N
	After 10 days	**After 10 days**
d_{14} g_{14}	Non-measurable with applied method	Non-measurable with applied method

Similar structural changes were revealed during the XRD study (Figure 4). As with the FTIR analysis, the XRD results clearly indicate the large increase in crystallinity of the non-etched samples. The polymer is in the α′ phase since the specific (200)/(110) peak appears at the 2-theta position lower than 16.6°, following a previous report [25]. After 10 days, the additional, more ordered α phase is observed only for the etched film, detected as an additional XRD peak at 16.9° (Figure 4b).

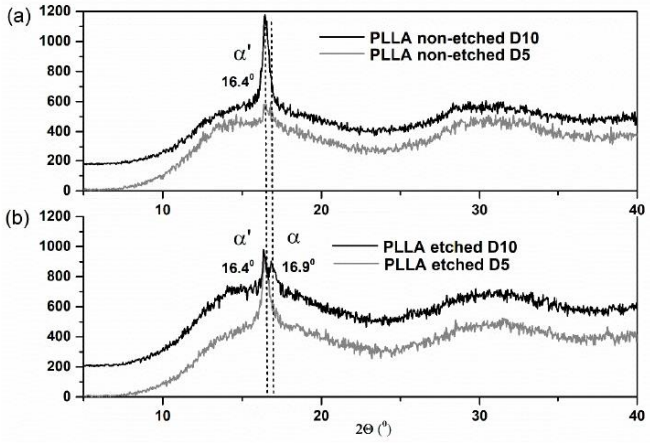

Figure 4. XRD patterns of hydrophobic non-etched (**a**) and hydrophilic etched (**b**) PLLA films obtained after 5 and 10 days of degradation by proteinase K (labeled with D5 and D10).

Investigating the thermal properties of PLLA films also revealed different responses to enzyme-catalyzed degradation for the etched and non-etched samples (Table 1, Table 2 and Figure 5). For the etched samples, the melting peaks are broad for all the measured

samples, indicating the presence of both crystalline forms: α′ and α. Degradation promotes recrystallization (α′ to α) since they are both detected in the final degradation stage, as seen in the XRD data. The crystallinity of the etched films, measured using DSC, is initially high (since etching removes part of the amorphous regions), and it was not changed much during the degradation. However, for non-etched samples, even though it starts at a lower value, the crystallinity increased significantly after 10 days of degradation, as also observed from the FTIR and XRD analyses. While the glass and melting temperatures (T_g and T_m) were shifted for non-etched films during degradation, similar changes were not observed in the etched films. H. Tsuji et al. also observed increased T_g values for the oriented and un-oriented films; therefore, T_g changes respond to the degradation process, like changes in the highly ordered structure, such as crystallinity or orientation [15].

Table 2. DSC data for etched and non-etched PLLA films for different periods of degradation.

Up to 10 Days of Degradation	T_g	ΔH cryst. (J/g)	T_c	ΔH melt (J/g)	T_m	Crystallinity %
PLLA-non-etched	69 °C	21	117 °C	51	173 °C	31
PLLA-non-etched D5	72 °C	35	118 °C	50	173 °C	16
PLLA-non-etched D10	75 °C	/	/	55	167 °C	58
PLLA-etched	71 °C	/	/	49	172 °C	52
PLLA-etched D5	72 °C	/	/	57	170 °C	61
PLLA-etched D10	72 °C	5	109 °C	59	170 °C	57

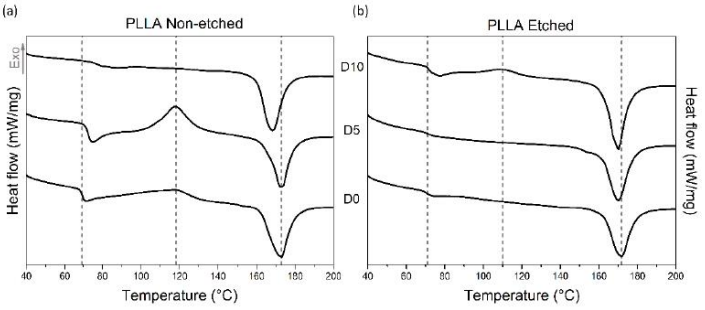

Figure 5. DSC curves of hydrophobic non-etched (**a**) and hydrophilic etched (**b**) PLLA films obtained after different periods of degradation by proteinase K, labeled by D0, D5 and D10.

3.3. Mechanical Properties

DMA measurements were performed for degraded samples to determine the changes in the mechanical properties. Since the non-etched films were very torn and porous after 10 days of degradation, measurements were not feasible. Therefore, the mechanical properties were measured only for the 5 day degradation period. On the other hand, in the case of the hydrophilic etched films, the compactness of the film was less damaged by degradation, so the mechanical measurements were normally made after 5 and 10 days of degradation.

Both etched and non-etched PLLA films have the same initial Young's modulus measured at 23 °C (2.4 GPa), comparable to values observed in the literature for PLA polymer [26], which confirms that alkali etching was performed only on the surface without compromising the inner parts (Figure 6a). After the enzymatic degradation, the values are significantly lowered for the non-etched samples, even after 5 days of degradation,

where the modulus is lowered by 92% (190 MPa), while it is only 1% for the etched samples (Figure 6a). As the degradation induces swelling and increased porosity in the bulk of the hydrophobic films (where degradation occurs), they cause a drop in the mechanical properties (observed through a drop in the storage modulus). These changes are not so pronounced in the case of the etched films before and after degradation since the dominant degradation events are taking place at the surface. In the case of the etched, hydrophilic PLLA films, Young's modulus drop occurs very slowly, only 16% for a degradation time of 10 days, clearly showing the lack of dominant bulk-erosion effects observed in non-etched films.

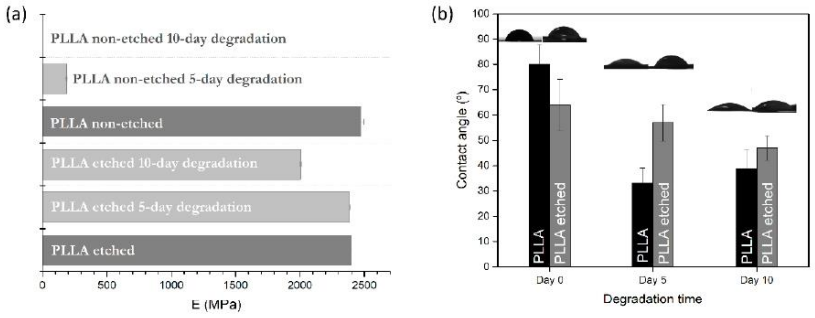

Figure 6. (**a**) changes in Young's modulus (at 23 °C) and (**b**) changes in wetting angle for water drop on polymer, for non-etched and etched samples after 0, 5 and 10 days of degradation.

3.4. Wetting-Angle Changes

Contact-angle measurements were made for pristine films and the films obtained after degradation. Interesting changes were observed for the non-etched films, where the wetting angle decreases more drastically than for the etched sample after 5 and 10 days of degradation (Figure 6b).

Alkali etching improved the hydrophilicity of the polymer surface by 25%, which resulted in more carboxylic end groups on the surface. During the degradation, a small lowering (−20%) of the initial wetting angle was observed in the etched films. The change could be associated with the change in the roughness observed in the SEM images for the etched films. On the other hand, due to the significant increase in the roughness and porosity of the non-etched hydrophobic films after degradation, their wetting angles decreased by 50%.

3.5. Piezoelectric Properties

Piezoelectric properties are highly dependent on the polymeric structure, the orientation of the polymer chains and the degree of crystallinity. Therefore, it was expected that the previously observed changes would affect them. According to those changes, proteinase-K-induced changes in the piezoelectric properties were lowered to 68% of the initial values for the non-etched sample and 50% for the etched polymer films (Table 1) after 5 days of aging. Further measurements after 10 days of degradation could not be performed since the degradation, with a mechanically unstable and porous film over the whole surface, did not allow measurements using the applied method.

3.6. Morphological Properties

After 10 days of degradation for the non-etched hydrophobic films, the main changes were observed in the cross-sections that reveal their inner (bulk) parts (Figure 7(a2,a3,b2,b3)). The initially dense and smooth layered structure in the cross-section of the starting films

before degradation (Figure 7(a2,a3)) turned into a porous, sphere-like structure obtained after the degradation progressed (Figure 7(b2,b3)). Both surfaces of the films, before and after the degradation (Figure 7(a1,b1)), are generally smooth, with a bubble structure observed on top of the degraded samples (Figure 7(b1)), indicating degradation events inside the film's bulk, such as progressive and intensive water swelling.

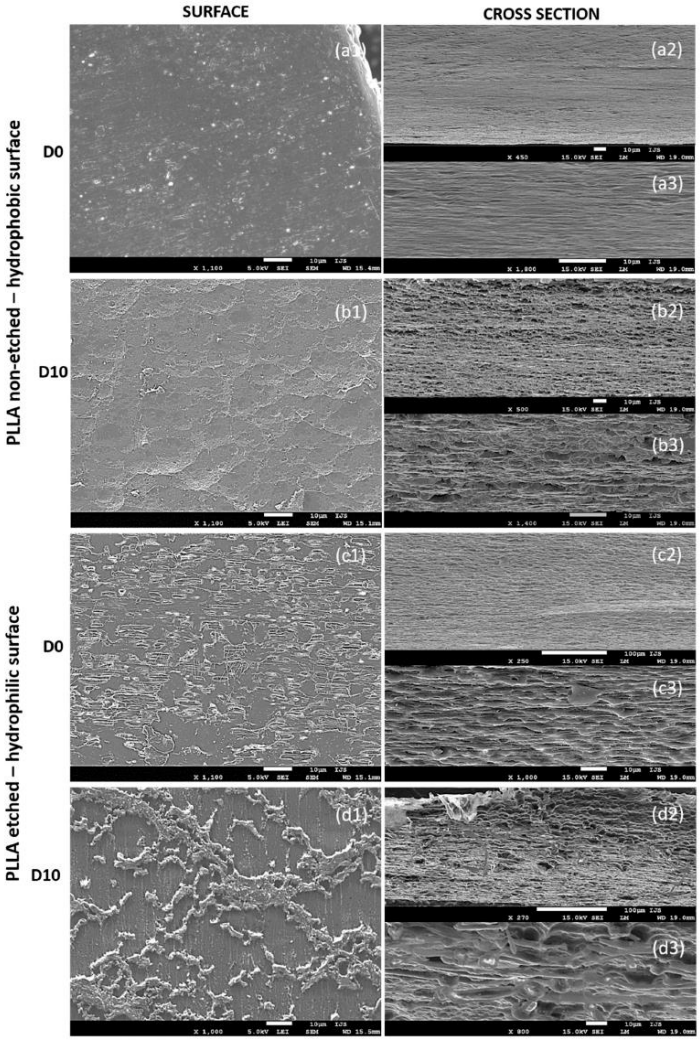

Figure 7. SEM images showing surfaces (1) and cross-sections (2, 3) of PLLA films with non-etched hydrophobic (**a1**–**a3**,**b1**–**b3**) and etched hydrophilic (**c1**–**c3**,**d1**–**d3**) surfaces before (D0) and after (D10) degradation with proteinase K.

Due to alkali etching, the hydrophilic films initially had a rougher surface with visible amorphous islands having short-edged chains (Figure 7(c1)). Such a structure is ideal for enzymatic degradation. As the degradation progressed, the roughness of the surface changed (Figure 7(d1)), indicating surface-erosion events. The inner parts of the films (observed in cross-sections, Figure 7(c2,c3,d2,d3)) did not change significantly and showed signs of delayed water swelling.

4. Discussion

Piezoelectric PLLA films were designed to optimize their applicability in electrostimulation, such as promoting mammalian cell growth. For the occurrence of effective electrical stimulation, film-cell contact is crucial, and surface properties are important. Therefore, to improve its properties for intended medical use and to ensure better cell affinity, hydrophilicity was improved by 25% using alkali etching of the polymer film, which resulted in more carboxylic end groups on the surface. The idea of the current study was to investigate the structural, mechanical, electric and surface properties of piezoelectric PLLA, with a hydrophobic and hydrophilic surface, in the presence of proteinase K as a degrading enzyme and a model of in vitro inflammation. This study is important since it can predict or explain further interactions of the surface-modified PLLA with living surroundings.

PLLA is a hydrophobic polymer that in general degrades through a hydrolysis reaction that occurs inside the bulk, driven by the swelling mechanism [14]. In the case of enzyme-driven degradation, when the enzyme proteinase K is present, surface erosion is reported as the main mechanism of degradation [15,16]. The reason is associated with the limited intake of the enzyme inside a polymer film.

According to our results, the structural, morphological, mechanical and piezoelectric changes obtained during the proteinase-K-induced degradation in PLLA films, two different degradation mechanisms are revealed due to the surface modification. In the case of the non-etched hydrophobic films, changes were mainly taking place in the polymer bulk. Due to the smooth surface and the strained, oriented chains observed with the electron microscope, enzyme–polymer contact is less probable; therefore, surface degradation is limited, and water diffusion inside the bulk is faster. Swelling occurs, which allows the enzymes to enter inside, meaning that bulk erosion is preferential. Enzymes cleave the tied and free amorphous parts from inside the bulk since proteinase K cannot degrade crystalline parts, resulting in increased overall crystallinity. Similar observations were made by Rangari et al., who also reported a slight increase in the crystallinity for oriented PLLA films due to the enzyme-catalyzed degradation of amorphous parts [16] but at the surface. The observed changes in crystallinity for the non-etched samples can be explained by the degradation of the free end and tie amorphous parts and possible accumulation of the cleaved crystalline parts trapped inside the film (increased crystallinity for day 10), as the degradation occurs there. However, the loss of crystallinity observed for day 5 can be associated with chain relaxation during the swelling mechanism. In both cases, for etched and non-etched films, the orientation of the polymeric films is lowered, which is expected since the swelling of the polymer in a water solution is inevitable after some time, making reorganization and mobility of the chains possible.

When observing etched films, their surface is hydrophilic with more amorphous end chains directly exposed to the outer water surroundings with the proteinase K enzyme. During the degradation, the film changes predominantly at the surface-with-surface erosion as the preferred mechanism. Therefore, only small changes are observed for bulk crystallinity and mechanical properties. Since the dense film is under amorphous clusters (as observed 7d1), the accumulation of crystalline residues is also less likely, and the loss of crystallinity is observed only on the surface.

F. Iñiguez-Franco et al. showed that increasing the hydrophilic properties of PLLA film using a chain extender, which incorporates more hydrophilic chain ends to form a branched structure, can result in hydrogen bonding between them and prevent the diffusion of water molecules inside the polymer matrix to start the bulk process [27]. This explanation can

be used to understand the changes we observed with the hydrophilic samples. In our case, the diffusion of water inside the films was slower, and enzyme travel inside the bulk was prevented. Therefore, enzymatically catalyzed hydrolysis occurs only at the surface (FTIR-921 cm^{-1} peak drop), inducing surface erosion. The loss of crystallinity for the etched sample occurred due to cleavage of the tie amorphous chain parts at the surface, releasing crystalline residues into the solution. Similar phenomena during degradation were previously explained by H. Tsuji et al. [15] on surface-eroded hydrophobic PLLA films. We also observed lowering the temperature of cold crystallization for the etched sample compared to non-etched films, which implies better orientation of the amorphous chains since the presence of oriented amorphous chains induces crystallization at a lower temperature. An interesting partial change from the α' to the α structural phase was observed only for etched films and further indicates the difference in degradation induced by surface wettability. This phenomenon could be explained by the recrystallization of polymer chains due to annealing in the medium at 37 °C since water can act as a plasticizer for PLLA. This was explained by H. Tsuji et al. as a possible event during degradation [15]. Since most of the degradation events in our etched films occur on the surface, this should also be the case for recrystallization.

The use of PLLA films for piezo-stimulation depends on their mechanical properties. PLLA is a semi-crystalline polymer; therefore, its properties depend largely on its crystalline phase. However, the balance of crystalline and amorphous regions is desirable since it enables the elasticity required for deformation in ultrasound that generates the voltage needed for promoting cell growth during stimulation. A difference in mechanical properties also implied a bulk-degradation event for non-etched and a surface-erosion event for the etched films during degradation. A huge loss of modulus, observed for non-etched films, could be connected to the swelling of the polymer film, as observed before [28], which could indicate that the degradation process was greater than that, which was evident with the weight loss. Due to swelling, there is an internal cleavage of the molecular bonds inside the film, which affects their compactness and strength, promoting degradation without the evident weight loss [1]. A similar situation was not detected in the etched films as their degradation took place at the surface.

Piezoelectricity in PLLA is a consequence of oriented and crystalline polymer chains inside the film [11]. A simple method like uniaxial drawing was used for preparing piezoelectric PLLA films. The drawing process above T_g aligns the chain molecules in the same direction in the entire film, inducing structural changes, such as crystallinity, due to the strain-induced crystallization [18]. Compared to the literature (10pC/N) [29], smaller values for d_{14} were obtained for our films (4–4.6 pC/N); however, negligible changes were observed after the surface modification with etching to improve the hydrophilic properties of the film (results presented in a previous article [18]). It is very important that the films retained their piezoelectric properties despite all the structural and mechanical changes during degradation. Changes in the piezoelectric properties after the degradation were observed for the first time. The preservation of piezoelectric properties is a consequence of changes in crystallinity and orientation. Bulk changes are not so pronounced in hydrophilic films, where most of the degradation events and the consequent modifications are taking place at the surface. However, the detected recrystallization, loss of surface crystallinity and relaxing orientation cause the loss of half of the initial piezoelectricity (50.4%, Table 1). In hydrophobic films, most of the degradation events and the following changes occur inside the films. Although there is a decrease in the orientation and an observed increase in the porosity, a smaller drop in the piezoelectric properties (68.8% of initial value remain, Table 1) was observed, possibly due to an increase in the crystallinity and the reorientation of fibers after drying the sample. However, our estimation is for the non-etched film to have a lower piezoelectric value during the degradation since the polymer is swollen from the start, compared to the etched sample, where the swelling was not observed after 5 days of degradation.

A combination of a hydrophilic surface with gradual changes to the films during degradation that maintains their piezoelectric properties is the optimal design for polymeric films initially developed for interactions with mammalian cells. With such a design, we could expect that the high affinity of cells for hydrophilic surfaces will enable close contact between the cells and films and provide the effective electrostimulation required for applying piezo-films in regeneration processes, particularly in wound healing.

5. Conclusions

Proteinase K can induce both bulk and surface degradation in PLLA films. The surface properties of the polymer films play a significant role in their degradation. As shown in the present study, their change is a powerful tool and makes it possible to change where the degradation occurs and defines the dominant degradation mechanism. If films are hydrophilic, enzyme-driven degradation occurs at the film surface, where they degrade the accumulated amorphous areas. On the other hand, if they are hydrophobic, water uptake and polymer swelling make it possible to transfer the enzyme to the bulk where the degradation occurs. When the surface chemistry is well balanced by degradation progress, so the mechanical, structural and piezoelectric changes to the films occur gradually, and very effective interactions with the cells are expected. The observed correlations are very important for further predictions during the interactions of piezoelectric PLLA films with living surroundings, particularly during electro-stimulated regeneration and wound healing, where the gradual loss of piezoelectric properties is useful for following the tissue regeneration.

Author Contributions: Research conceptualization, L.G. and M.V.; mechanical measurements and interpretation, B.V.; data curation, L.G., B.V. and M.V.; writing—original draft preparation, L.G.; writing—review and editing, B.V., M.V. and M.S.; visualization, L.G., B.V. and M.V.; supervision, M.V.; funding acquisition, M.V. and M.S. All authors have read and agreed to the published version of the manuscript.

Funding: The work was funded by the Slovenian Research Agency (ARRS) with grants J2-8169, N2-0150 and PR-08338 and research programs P2-0091 and PR-0099.

Institutional Review Board Statement: Not applicable.

Informed Consent Statement: Not applicable.

Data Availability Statement: The data presented in this study are available on request from the corresponding author.

Acknowledgments: The authors are grateful to Mario Kurtjak and David Fabian from Advanced Materials Department, IJS, for performing FTIR and piezoelectric measurements. Sara Pintar from Biochemistry and Molecular Biology Department, IJS, for performing gel electrophoresis.

Conflicts of Interest: The authors declare no conflict of interest. The funders had no role in designing the study; in the collection, analyses, or interpretation of data; in the writing of the manuscript, or in the decision to publish the result.

References

1. De Silva, D.; Kaduri, M.; Poley, M.; Adir, O.; Krinsky, N.; Shainsky-Roitman, J.; Schroeder, A. Biocompatibility, biodegradation and excretion of polylactic acid (PLA) in medical implants and theranostic systems. *Chem. Eng. J.* **2018**, *340*, 9–14. [CrossRef] [PubMed]
2. Pappu, K.L.; Pickering, V.K. Thakur, Manufacturing and characterization of sustainable hybrid composites using sisal and hemp fibres as reinforcement of poly (lactic acid) via injection moulding. *Ind. Crop. Prod.* **2019**, *137*, 260–269. [CrossRef]
3. Rajabi, A.H.; Jaffe, M.; Arinzeh, T.L. Piezoelectric materials for tissue regeneration: A review. *Acta Biomater.* **2015**, *24*, 12–23. [CrossRef] [PubMed]
4. Jelonek, K.; Li, S.; Kaczmarczyk, B.; Marcinkowski, A.; Orchel, A.; Musial-Kulik, M.; Kasperczyk, J. Multidrug PLA-PEG filomicelles for concurrent delivery of anticancer drugs—The influence of drug-drug and drug-polymer interactions on drug loading and release properties. *Int. J. Pharm.* **2016**, *510*, 365–374. [CrossRef]
5. Mushtaq, F.; Torlakcik, H.; Vallmajo-martin, Q.; Can, E.; Zhang, J.; Röhrig, C.; Shen, Y.; Yu, Y.; Chen, X.; Müller, R.; et al. Magnetoelectric 3D scaffolds for enhanced bone cell proliferation. *Appl. Mater. Today* **2019**, *16*, 290–300. [CrossRef]

6. Gomaa, S.F.; Madkour, T.M.; Moghannem, S.; El-sherbiny, I.M. New polylactic acid/cellulose acetate-based antimicrobial interactive single dose nanofibrous wound dressing mats. *Int. J. Biol. Macromol.* **2017**, *105*, 1148–1160. [CrossRef]
7. Barroca, N.; Marote, A.; Vieira, S.I.; Almeida, A.; Fernandes, M.H.V.; Vilarinho, P.M.; Odete, A.B. Electrically polarized PLLA nanofibers as neural tissue engineering scaffolds with improved neuritogenesis. *Colloids Surf. B Biointerfaces* **2018**, *167*, 93–103. [CrossRef]
8. Shin, D.; Hong, S.W.; Hwang, Y.-H. Recent Advances in Organic Piezoelectric Biomaterials for Energy and Biomedical Applications. *Nanomaterials* **2020**, *10*, 123. [CrossRef]
9. Ates, B.; Koytepe, S.; Ulu, A.; Gurses, C.; Thakur, V.K. Chemistry, Structures, and Advanced Applications of Nanocomposites from Biorenewable Resources. *Chem. Rev.* **2020**, *120*, 9304–9362. [CrossRef]
10. Tajitsu, Y. Basic study of controlling piezoelectric motion of chiral polymeric fiber. *Ferroelectrics* **2009**, *389*, 83–94. [CrossRef]
11. Lovell, C.S.; Fitz-Gerald, J.M.; Park, C. Decoupling the effects of crystallinity and orientation on the shear piezoelectricity of polylactic acid. *J. Polym. Sci. Part B Polym. Phys.* **2011**, *49*, 1555–1562. [CrossRef]
12. Minary-Jolandan, M.; Yu, M. Nanoscale characterization of isolated individual type I collagen fibrils: Polarization and piezoelectricity. *Nanotechnology* **2009**, *20*, 085706. [CrossRef] [PubMed]
13. Murillo, G.; Blanquer, A.; Vargas-estevez, C.; Barrios, L.; Ibáñez, E.; Nogués, C.; Esteve, J. Electromechanical Nanogenerator-Cell Interaction Modulates Cell Activity. *Bioelectronics* **2017**, *29*. [CrossRef]
14. von Burkersroda, F.; Schedl, L.; Gopferich, A. Why degradable polymers undergo surface erosion or bulk erosion. *Biomaterials* **2002**, *23*, 4221–4231. [CrossRef]
15. Tsuji, H.; Ogiwara, M.; Saha, S.K.; Sakaki, T. Enzymatic, alkaline, and autocatalytic degradation of poly (L-lactic acid): Effects of biaxial orientation. *Biomacromolecules* **2006**, *7*, 380–387. [CrossRef]
16. Rangari, D.; Vasanthan, N. Study of Strain-Induced Crystallization and Enzymatic Degradation of Drawn Poly (l-lactic acid) (PLLA) Films. *Macromolecules* **2012**, *45*, 7397–7403. [CrossRef]
17. Casalini, T.; Rossi, F.; Castrovinci, A.; Perale, G. A Perspective on Polylactic Acid-Based Polymers Use for Nanoparticles Synthesis and Applications. *Front. Bioeng. Biotechnol.* **2019**, *7*, 1–16. [CrossRef]
18. Udovc, L.; Spreitzer, M.; Vukomanovic, M. Towards hydrophilic piezoelectric poly-L-lactide films: Optimal processing, post-heat treatment and alkaline etching. *Polym. J.* **2020**, *52*, 299–311. [CrossRef]
19. Vogel, C.; Wessel, E.; Siesler, H.W. FT-IR Spectroscopic Imaging of Anisotropic Poly (3-hydroxybutyrate)/Poly (lactic acid) Blends with Polarized Radiation. *Macromolecules* **2008**, *41*, 2975–2977. [CrossRef]
20. Nobeshima, T.; Sakai, H.; Ishii, Y.; Uemura, S.; Yoshida, M. Polarized FT-IR Study of Uniaxially Aligned Electrospun Poly (DL-Lactic Acid) Fiber Films. *J. Photopolym. Sci. Technol.* **2016**, *29*, 353–356. [CrossRef]
21. Farah, S.; Anderson, D.G.; Langer, R. Physical and mechanical properties of PLA, and their functions in widespread applications—A comprehensive review. *Adv. Drug Deliv. Rev.* **2016**, *107*, 367–392. [CrossRef] [PubMed]
22. Yanagida, H.; Okada, M.; Masuda, M.; Ueki, M.; Narama, I.; Kitao, S.; Koyama, Y.; Furuzono, T.; Takakuda, K. Cell adhesion and tissue response to hydroxyapatite nanocrystal-coated poly (L-lactic acid) fabric. *JBIOSC* **2009**, *108*, 235–243. [CrossRef] [PubMed]
23. Bernard, F.; Gimeno, L.; Viala, B.; Gusarov, B.; Cugat, O. Direct Piezoelectric Coefficient Measurements of PVDF and PLLA under Controlled Strain and Stress. *Proceedings* **2017**, *1*, 335. [CrossRef]
24. Webb, K.; Hlady, V.; Tresco, P.A. Relative importance of surface wettability and charged functional groups on NIH 3T3 fibroblast attachment, spreading, and cytoskeletal organization. *J. Biomed. Mater. Res.* **2009**, *41*, 422–430. [CrossRef]
25. Chen, X.; Kalish, J.; Hsu, S.L. Structure Evolution of a α'-Phase Poly (lactic acid). *J. Polym. Sci. Part B Polym. Phys.* **2011**, *49*, 1446–1454. [CrossRef]
26. Leluk, K.; Frackowiak, S.; Ludwiczak, J.; Rydzkowski, T.; Thakur, V.K. The Impact of Filler Geometry on Polylactic Acid-Based Sustainable Polymer Composites. *Molecules* **2021**, *26*, 149. [CrossRef]
27. Iñiguez-franco, F.; Auras, R.; Ahmed, J.; Selke, S.; Rubino, M.; Dolan, K.; Soto-valdez, H. Control of hydrolytic degradation of Poly(lactic acid) by incorporation of chain extender: From bulk to surface erosion. *Polym. Test.* **2018**, *67*, 190–196. [CrossRef]
28. Subramani, R.; Izquierdo-alvarez, A.; Bhattacharya, P.; Meerts, M. The Influence of Swelling on Elastic Properties of Polyacrylamide Hydrogels. *Front. Mater.* **2020**, *7*, 1–13. [CrossRef]
29. Fukada, E. New Piezoelectric Polymers. *Jpn. J. Appl. Phys.* **1998**, *37*, 2775–2780. [CrossRef]

Chapter 5

Preparation of a Nanotextured Polymer Film Using a Template-Assisted Method and the Response of Bacteria or Human Non-Adherent Cells to Drawn or Nanotextured Piezoelectric Films

This chapter provides an overview of a new method of preparation (template-assisted method) to prepare NT PLLA films. To obtain such films, the template is chemically etched, so some by-products may remain trapped inside and interfere with the results, but I subsequently confirmed the purity of the polymer using surface-sensitive XPS, shown in Appendix A1. Due to the nanosized topography on PLLA polymer film, piezoelectric properties are expected to improve significantly, consequently also the desired biological response. What is really missing from the fiber and complex surface structure of polymer films (NT topography on the one side), where the piezoelectricity is usually measured locally, on a single wire, is a piezoelectric measurement of the total contribution of the film. Many authors provide values for the individual fibers, so the overall piezoelectric properties may vary. Therefore, I proposed an alternative method for determining the piezoelectric properties of materials with a complex structure through the decomposition of an organic dye. Materials with a high piezoelectric constant (such as ceramics) can generate ROS from water molecules, but this is less possible for a polymer [102]. However, with hydrogen peroxide added, the piezoelectric polymer can act as a catalyst for the decomposition of peroxide into ROS species. ROS have been shown to successfully degrade MB or other similar organic dyes, so I used MB degradation to confirm and compare overall piezoelectric properties of differently prepared PLLA films (stretched, NT).

I also observed the antibacterial effect of the polymer on Gram negative and Gram positive bacteria, originating from the piezoelectric properties of the film, and found US stimulation conditions that lead to proper piezoelectric excitation, resulting in a bactericidal effect for the NT samples. Toxicity to non-adherent cells was also discarded, making the films suitable for therapeutic use in the case of antibacterial agents or for the wound healing process. I obtained clear evidence that the piezoelectricity of PLLA induces antimicrobial activity in a manner that damages the bacterial cell wall, which is the first

reported in the literature [49]. This paper also clearly shows that ROS is not the reason for the antimicrobial activity as interpreted in the literature so far. The results were first presented at the Conference of the European Society for Biomaterials (ESB2021) and was then invited for publication in a journal.

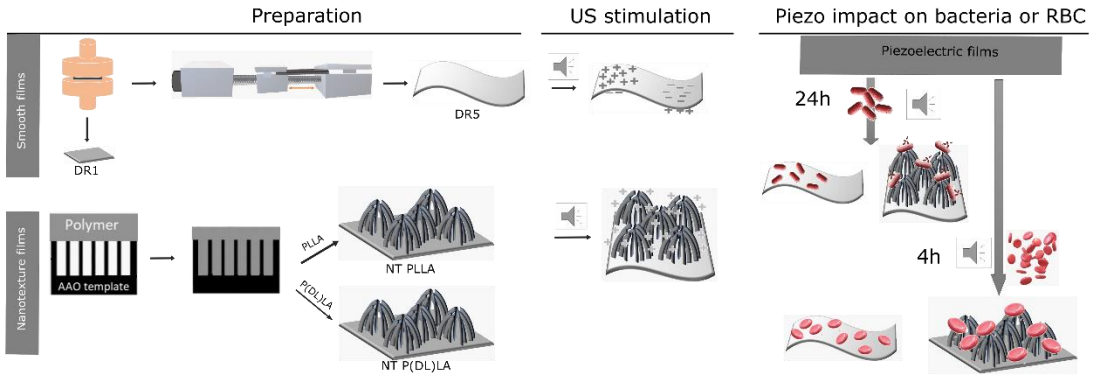

Figure 14: Demonstration of the preparation of a PLLA polymer film that acquires piezoelectric properties (smooth film: hot pressing to obtain an amorphous sheet, which is later stretched to a draw ratio of 5; nanotextured film: pressing a nanoporous template into a polymer melt and later removing the template), which was later ultrasonically deformed to generate a charge on the surface of the film/tube and observing a destructive piezo/electric effect on bacteria or a non-toxic effect on red blood cells [49].

5.1 Antimicrobial Activity of Piezoelectric Polymer: Piezoelectricity as a Reason for Damaging Bacterial Membrane

Biomaterials Science

ROYAL SOCIETY OF CHEMISTRY

PAPER

View Article Online
View Journal | View Issue

Check for updates

Cite this: *Biomater. Sci.*, 2022, **10**, 4933

Antimicrobial activity of piezoelectric polymer: piezoelectricity as the reason for damaging bacterial membrane†

Lea Gazvoda,[a,b] Milica Perišić Nanut,[c] Matjaž Spreitzer [a] and Marija Vukomanović [a]*

Cell stimulation using piezoelectric polymers, which is known as piezostimulation, is an innovative approach for designing antimicrobial protection. As an antibiotic-free and inorganic nanoparticle-free approach, it uses physical stimuli to target bacterial cells in a non-specific manner, which may be of great importance, particularly in the context of avoiding resistant bacterial strains. In this study, we prepared fully organic piezoelectric biodegradable films composed of poly-L-lactide (PLLA) and demonstrated their antimicrobial effect on *S. epidermidis* as a model of Gram-positive and *E. coli* as a model of Gram-negative bacteria. The PLLA films were either smooth and fabricated using simple melt- drawing or nanotextured, as self-standing nanotubes formed using the template-assisted method. The morphological differences between nanotextured and smooth films resulted in a larger surface area and better surface contact in nanotextured films, together with improved structural properties and better crystallinity, which were the main reasons for their better piezoelectric properties, and consequently stronger bactericidal effect. The comparison between the nanotextured surfaces with and without piezoelectric nature excluded the main role of morphology and directly confirmed piezoelectricity as the main reason for the observed antimicrobial affect. We also confirmed that piezo-stimulation using the antibacterial nanotextured film could damage the bacterial membrane as the main mechanism of action, while the contribution of pH changes and ROS generation was negligible. More importantly, the effect was selective toward the bacterial membrane and the same damage was not observed in human red blood cells, making the therapeutic use of these films possible.

Received 26th April 2022,
Accepted 4th July 2022
DOI: 10.1039/d2bm00644h
rsc.li/biomaterials-science

Introduction

Physical stimuli (mechanical, magnetic, and electrical) affect bacteria cells in different, non-specific manners in comparison to biochemical stimuli (*i.e.*, antibiotics), presenting an interesting treatment alternative.[1] Given that physical forces keep the structure of a cell together, targeting the structure of the cellular envelope is a common mechanism of action. Piezo-stimulation implies the application of a charge, which accumulates at the surface of mechanically deformed materials, thus affecting the potential in the cell envelope. It contributes to disassembling and destroying the bacterial cell envelope, thus achieving an antimicrobial effect. Accordingly, as antibiotic-free and inorganic nanoparticle-free approach, the main benefit of providing an antimicrobial effect using piezo-stimulation is the limited ability of bacteria to develop resistance to it. Piezo-stimulation is mostly investigated for stimulating mammalian cell growth and its contribution to faster wound healing.[2–5] However, optimizing piezo-stimulation for achieving bacterial cell death is important given that it can be effectively used in preventing acute and chronic wound infections and decreasing the application of antibiotics during post-surgical and post-traumatic recovery.

In comparison to electrostimulation, which uses a similar mechanism, piezo-stimulation has self-powering activation (produces charge simultaneously upon mechanical deformation) and does not rely on external electrical sources and application of electrodes. Furthermore, the advantages of fully organic piezoelectrics, including biocompatibility, biodegradability and simple processing, are the main reasons for the use of poly-L-lactic acid (PLLA) in their design. This polymer has a similar left-handed helix orientation as the natural piezoelectrics in the human body (collagen, chitin, and elastin[6]). It is characterized with shear mode piezoelectricity and an electric dipole component distributed throughout the molecule.

[a]*Advanced materials Department, Jožef Stefan Institute, Ljubljana, Slovenia. E-mail: marija.vukomanovic@ijs.si*
[b]*Jožef Stefan International Postgraduate School, Ljubljana, Slovenia*
[c]*Department of Biotechnology, Jožef Stefan Institute, Ljubljana, Slovenia*
†Electronic supplementary information (ESI) available. See DOI: https://doi.org/10.1039/d2bm00644h

Twisting of the polymer film leads to the orientation of molecular dipoles and generation of an electrical charge,[7] which can provide an antimicrobial effect.

However, to date, the antimicrobial properties of fully organic piezoelectrics are very poorly explained, and consequently ineffectively exploited. In general, it has been proposed that piezoelectric materials can affect bacteria through a variety of processes, such as transmembrane current-induced electroporation,[8,9] disruption of metabolic system/membrane potential,[10] positive surface charge[10,11] and generation of reactive oxygen species (ROS).[12] In contrast to inorganic piezoelectrics,[12,13] where ROS generation has been experimentally detected and associated with the antimicrobial activity observed mainly at the cationic Poles, the investigation of the electrical effect of piezoelectric polymers (such as PLLA[7,8] and polyvinylidene fluoride (PVDF)[10,13,14]) in bacteria is in its infancy. Ando *et al.* suggested that three different mechanisms are responsible for the antibacterial effect for PLLA (electroporation due to high-voltage output, electric current and less likely ROS), which lead to the formation of pores through which the bacterial contents leak, thus killing bacteria.[7] In contrast to piezoceramics, polymeric piezoelectrics such as PLLA or PVDF do not possess sufficient piezoelectric properties (d_{33} > 100 pC N^{-1}) to hydrolyse water into ROS products, using ultrasound as a source of mechanical deformation.[15] Therefore, achieving antibacterial properties due to the production of ROS is less likely to be the mechanism. In the case of ultrasound-stimulated piezoelectric PVDF films, different effects have been observed, including bacterial proliferation/growth inhibition and adhesion/antifouling on both the positive and negative poled sides depending on the applied ultrasound frequency (4 or 40 Hz) used for film deformation. The surface charge (under static condition, without ultrasound) resulted in antifouling at cationic and adhesion at anionic pole. The damaging effect of the positive surface charge was detected in Gram-positive *S. epidermidis* and Gram-negative *E. coli* bacteria.[10,16,17] However, a systematic approach for the investigation of bacterial piezo-stimulation using PLLA films is still lacking in the literature. Particularly this type of investigation is needed due to the difference in deformation required for achieving polarization in these two polymers, *i.e.*, shear in PLLA and compression/stretching in PVDF.

The topological and morphological characteristics of surface of films are other factors contributing to antimicrobial effects. Some findings suggest that films prepared with nanotextured patterns on their surface, which initially have no antibacterial properties, exhibit a damaging effect on bacterial cells by mimicking the natural defence mechanism observed in cicada wings.[18–21] Due to the physical topography movements, the cell walls of the attached bacteria stretch and disfigure when they are in contact with the film, leading to cell rupture and death.[19] It has been observed that piezoelectric PLLA films with a nanotextured surface affect mammalian cells and promote their attachment during piezo-stimulation.[22] However, the effects of these films combining nanotexturing and piezoelectricity on bacterial cells still remains unexplored.

Considering the above-mentioned description, the main goal of this work was finding clear evidence correlating the piezoelectricity of fully organic PLLA films with their antimicrobial effect and optimizing the film design toward higher bactericidal efficacy and better compatibility in mammalian cells. Accordingly, the antimicrobial properties of piezoelectric and non-piezoelectric PLLA films with smooth and nanotextured surfaces were evaluated for (i) their impact on ROS formation, (ii) the impact of their topography, and (iii) direct influence of charge generated due to piezoelectricity. The piezo-stimulation resulting in the bactericidal nature of their effect was confirmed in both Gram-positive and Gram-negative bacterial strains and the selectivity was examined in blood cells.

Materials and methods

Materials

Chemicals and materials used during the experiments: poly-L-lactic acid polymer L207 S (PLLA, Evonik, Germany); poly(D,L-lactide-*co*-glycolide) RG-505, 50 : 50 (P(DL)LA, Evonik, Germany); piezoelectric polyvinylidene difluoride metallised film (PVDF, Goodfellow, Germany); anodised aluminium oxide plates on aluminium substrate with 200 nm × 30 μm pores (AAO, Topmembranes, China); methylene Blue (MB, Alfa Aesar, Germany); hydrochloric acid, HCl (J.T. Baker, Poland); hydrogen peroxide solution 30% (Carlo Erba Reagents, Germany); copper(II) chloride, $CuCl_2{\cdot}2H_2O$ (Riedel-de Haën AG, Seelze-Hannover, Germany); orthophosphoric acid 85% (VWR Chemicals BDH, France); sodium chloride, NaCl (Carlo Erba Reagents, Germany); HEPES (Fisher Scientific, Taiwan); Luria/Miller Broth (LB, Carl Roth, Germany); agar (Fluka, Spain); glutaraldehyde solution 25% in H_2O (Sigma-Aldrich, Co., USA); bacterial strains *Escherichia coli* (*E. coli*, ATCC 47076) and *Staphylococcus epidermidis* (*S. epidermidis*, ATCC 12228); labelling dye FM™ 4-64 (*N*-(3-triethylammoniumpropyl)-4-(6-(4-(diethylamino)phenyl)hexatrienyl) pyridinium dibromide, Invitrogen, Thermo Fisher Scientific, USA); DAPI (diamidino-2-phenylindole, Biotium, Fremont, CA) in Hank's balanced salt solution (Invitrogen, Thermo Fisher Scientific, USA); Live/Dead BacLight Bacterial Viability kit (L7007, Molecular Probes, Life Technologies, USA) and PrestoBlue™ Cell Viability Reagent (PB, Invitrogen by Thermo Fisher Scientific, USA). In all cases MIlliQ (Purelab Option-Q, Elga) pure water was used.

Film fabrication

Piezoelectric films were prepared using two approaches. Drawn films (DR) were prepared using the same conditions for stretching presented in our previous work.[23] Briefly, the polymer was hot-pressed above its melting temperature (250 °C) into amorphous films and quenched in a cold water bath (DR1). These films were cut into a dumbbell shape and

clamped in a drawing machine, stretched at 80 °C to a draw ratio of 5 (DR5) at a speed of 40 mm min^{-1}. Nanotextured films (NT) were prepared using a one-side-closed AAO porous template on an aluminium substrate, containing pores with a size of 200 nm thick and 30 μm long. The preparation route was similar to that for the previously reported films by Smith *et al.*[24] The was melted on glass covered with aluminium foil at 250 °C using a magnetic stirrer with hot plate (MSH-20D). After, the AAO template with open pore side was lowered on the polymer melt and pressed using a 1 kg weight and left to fill for 2–3 min. Subsequently, the films were removed from the heater and left to cool (NT as-prepared). To achieve improved crystallinity, the whole polymer inside the AAO template was annealed in a furnace at 160 °C for 1 h and left to cool slowly (NT ANN). The template was removed in 3 steps according to the manufacturer's instructions with slight modification. The back closed side of AAO was removed by immersing the film in 40% orthophosphoric acid for 6 h, and then the aluminium capping was etched using $CuCl_2{\cdot}2H_2O$/HCl (4%/2%) solution overnight, and then transferred again to 40% orthophosphoric acid to remove the aluminium oxide pore walls in the membrane. After complete removal, self-standing nanotubes on the excess polymer substrate were left as a nanotextured film (NT). The obtained films were washed with water and ethanol and left to dry.

Extracted nanotubes were prepared with additional grinding of the excess of polymer filling before removing the template. When only filled pores remained in the template, membrane was removed with the same step explained above. Between steps, washing and changing the solutions were performed by centrifuging the samples in Eppendorf tubes at 12 500 rpm for 20 min. The nanotubes were washed with water at least 5 times and left in the wet state for further XRD and Raman analyses.

Physicochemical characterization

A drop of the extracted nanotubes was dried on a silica substrate. Silica was used to enhance the signal of a small single nanotube. To estimate the orientation of the polymeric chains inside the single nanotube, Raman spectroscopy with polarized light was performed using an NTEGRA Spectra NT-MDT and polarised 488 nm laser source in the frequency range of 100–3200 cm^{-1}. The acquisition was set to 100 s with a laser power of 5 mW, under which we did not observe signs of degradation. The results were labelled HHH and HVV, where the first letter corresponds to the fibre direction (horizontal), while the second and third are the orientation of the polariser and analyser (H-horizontal, V-vertical), respectively. All peaks were normalized to [0,1] relative to the silica main peak at 970 cm^{-1}. For the orientation of the C–COO groups, the intensities were compared in the horizontal (HHH) and vertical (HVV) directions for the peak value at 875 cm^{-1}. For the stretched samples, the observed peak intensities were normalized to the CH_3 asymmetric bending mode at 1454 cm^{-1}. The orientation factor (R) was calculated as (HHH) *versus* (HVV) value for the C–COO peak.

Differential scanning calorimetry (DSC) analysis was performed using a NETZSCH STA 449 thermal analyser (Jupiter). Around 8 mg of sample was placed in platinum crucibles and heated in an Ar/O atmosphere (40/10) in the temperature range of 40 °C to 600 °C at a heating rate of 20 °C min^{-1}. In the case of the nanotextured films, the excess polymer outside the AAO template was ground off to measure only the properties of the inner nanotube pores. The enthalpy of cold crystallization (ΔH_c) and enthalpy of melting (ΔH_m) were determined by calculating the surface under the peak of crystallization or melting, respectively. Bulk crystallinity was determined using the following expression: $X_c\ (\%) = (\Delta H_m - \Delta H_c)/\Delta H_{(100\%)} \times 100\%$, where the value for $\Delta H_{100\%}$ was taken as 93.6 J g^{-1}, which is the theoretical value for 100% crystalline PLLA films in the α-crystalline form.[25] The weight fraction of polymer in the sample was calculated using thermogravimetric (TG) analysis and used for correction of the measured enthalpy initially normalized to the weight of the whole sample.

X-ray diffraction (XRD) analysis was performed on a BRUKER AXS D4 ENDEAVOR (Cu Kα radiation (λ = 1.54 Å), 2θ range 10°–40°, 0.04° step size with 5 s capture time) and EMPYREAN (2θ range 15°–18°, 0.026° step size with 400 s capture time) to confirm the crystallinity of the prepared films and nanotubes. To perform measurements on the films, the edges of the samples were taped to the surface of the holder. For the extracted nanotubes, a suspension was added to a monocrystalline holder and the XRD patterns were measured focusing on the 2θ peak at around 16.5°.

The morphology of the polymer films was investigated using a scanning electron microscope (SEM-JSM 7600F, Jeol). For SEM microscopy, the samples were sputtered with gold using a BAL-TEC SCD sputter coater to prevent charging on the surface. The samples were observed under a low voltage (5 kV).

The wetting angle was measured using a Theta Lite-Biolin, Scientific contact angle meter. To determine the hydrophilic properties of the surface of the polymer films, a 5 μL drop of distilled water was used. The results are presented in the ESI.†

Direct and indirect voltage output measurements

Direct voltage output measurement. The voltage output was measured when the films were subjected to mechanical stimulus using an ultrasonic bath (Elmasonic P, Elma, Germany). The films were sputtered with gold, acting as electrodes on both sides and connected to cables. The cables were attached to the electrodes using a protective adhesive polyimide film (3M, USA) on both sides with extremely low electrostatic discharge properties, which covered the sample. The edges were coated with nail Polish to ensure sealing against water intrusion during measurement. After impregnation against water intrusion the samples were placed in the US bath and stimulated at 37 kHz or 80 kHz. We used the listed frequencies according to the ultrasonic bath device settings due to the simplicity and usability of the system to mechanically stimulate the samples. Cables was routed through the piezo-film to a Kaysight MSOX3034T oscilloscope to record the signal.

Indirect voltage output measurements (ROS generation potential). A stock solution of methylene blue (MB) (1 mg mL^{-1}) was prepared in MilliQ clean water and kept in the dark for further use. The films were washed in water, placed in a 1 : 1 V/V mixture of MB and water (0.5 mg mL^{-1}) with or without 5% of peroxide (0.5 M H_2O_2) and sonicated with 37 kHz or 80 kHz ultrasound during the measurement. During the testing, all the samples (piezoelectric films DR5 and NT ANN and as-prepared films, PVDF as the working reference, and non-piezoelectric films NT P(DL)LA and DR1) were protected from light using amber 15 mL tubes. Every 20 min, 100 μL aliquots were transferred on a transparent 96-well plate for absorbance measurement at 665 nm on a microplate reader (H1 Hybrid Multi-mode Microplate Reader, Synergy). Degradation was calculated as follows:

$$\text{Degradation } (\%) = 100\% - \left(\frac{(A_{\text{time}} - A_{\text{empty}})}{(A_{\text{initial}} - A_{\text{empty}})} \times 100\% \right)$$

All samples were tested in duplicate and for each, the absorbance was measured twice.

Antibacterial testing

Susceptibility tests during piezostimulation. Gram-negative (*E. coli*) and Gram-positive (*S. epidermidis*) bacteria were tested in saline (0.9% NaCl) and Luria-Bertani (LB) growth medium to observe the effect of the piezoelectric film and ultrasonic piezo-stimulation on bacteria. In saline solution, an ~10^8 CFU mL^{-1} (OD 0.1 for *E. coli* and OD 1 for *S. epidermidis*) stock suspension was used for testing in suspension or following the ISO22196 standard for testing the antimicrobial properties of the non-porous and non-absorbing surfaces.[26,27] To prepare bacteria in saline solution, bacteria were centrifuged (6000 rpm, 5 min) and the growth medium was discarded and replaced with saline solution. Prior to all antimicrobial assays, the films were sprayed with 70% ethanol solution and allowed to dry under laminar flow for sterilization. The films (0.5 cm × 1 cm) were immersed in the bacteria suspension and stimulated using an ultrasonic bath for 30 min using 80 kHz frequency. After sonication (US), the samples were incubated at 37 °C, while gently shaking using a MAX Q 4000 (Thermo Scientific) shaker. For bacteria counting, the sample solution was further diluted and drop-casted (10 μL) in triplicate on solid agar plates for counting. The plates were incubated overnight in an bacterial incubator (Kambič I-105 CK UV) at 37 °C before counting. The adjusted drop test (following the ISO22196 standard) was performed to observe the bacteria in full contact with the film, tested in saline solution (NaCl), where a 15 μL drop was placed inside the wells of a 24-well plate and covered with the prepared films. After US stimulation of the plate, the samples were incubated at 37 °C, while maintaining high humidity, and thus no water evaporated from the drop. After 24 h, the films were washed with saline solution (500 μL) and dilutions was placed on solid LB agar plates for counting. Part of the film with attached bacteria was put in LB growth medium (200 μL) in a 96-well plate and Presto blue indicator (5%) added to observe if any surviving and viable bacteria remained. Part of the washed bacteria solution was also transferred to a plate with added LB growth medium (1 : 1) and Presto blue indicator added to confirm if any remaining viable bacteria were left. For testing the kinetics in growth medium (LB), 10^5 CFU mL^{-1} bacteria stock solution was prepared. The films (0.5 cm × 1 cm) were placed upright in 200 μL bacteria suspension on a 96-well plate in triplicate and incubated in a microplate reader (H1 Hybrid Multi-mode Microplate Reader, Synergy) to follow the growth curve by measuring the absorbance at 600 nm (OD600) for 20 h. Live/dead testing was performed according to the manufacturer's instructions. A 20 μL drop of a die mixture (propidium iodide (PI) and Syto 9) was put on the film and observed under a fluorescence inverted microscope (Nikon Eclipse Ti-U inverted microscope).

Observing ROS effect during piezostimulation. Sterile films were immersed in saline solution with bacteria (~10^8 CFU mL^{-1}) in a 2 mL Eppendorf tube. A 20× diluted stock solution of ascorbic acid (0.7 mg mL^{-1}) was added to each well as an antioxidant to prevent any possible ROS to disturb the bacteria. After 30 min of sonication followed by 24 h of incubation, the diluted bacteria were spread on agar plates and grown for an additional 24 h at 37 °C for counting colonies.

SEM morphology in piezo-stimulated bacteria. Samples containing bacteria were fixed in 2 wt% aqueous solution of glutaraldehyde for 1 h and washed with saline solution. This was followed by a dehydration step to exchange the water inside the cells with ethanol. For this, the samples were subsequently immersed in series of ethanol solutions (30%, 50%, 70%, 90% and 3× 100% EtOH) and incubated for 15–30 min in each of them. In the final phase, the samples in ethanol were dried under CO_2 critical conditions using a critical point dryer (K850, Quorum Technologies). The dry samples were coated with a 10–15 nm gold layer and analysed using a JEOL JSM-7600F SEM.

Bacterial membrane integrity after piezostimulation. After piezostimulation of the bacteria with the films and incubation for 24 h, 100 μL was centrifuged for 5 min at 6000 rpm, and the supernatant was replaced with 50 μL of FM 4-64/DAPI containing 0.4 μL of 5 mg mL^{-1} (FM 4-64 and 1 μL of 125× DAPI). After a short staining period, the bacteria were visualized with an LSM-710 confocal microscope (Carl Zeiss, Germany) equipped with UV (405 nm), Argon (488 nm and 514 nm), and HeNe (543 nm and 633 nm) lasers under 63× magnification. The images were acquired and processed using the ZEN software (Carl Zeiss).

Influence on red blood cells (hemolysis)

Hemolysis after piezostimulation. Films was incubated with red blood cells (RBC) using the same piezostimulation conditions as that for bacteria (80 kHz) with 100% and 30% power. For this, RBCs were diluted in 20 mM HEPES/0.9% NaCl buffer to 2.5% cells mL^{-1}. The films were immersed in 300 μL prepared RBC solution in Eppendorf tubes and sonicated in an ultrasonic bath at 80 kHz for 30 min. After piezosti-

mulation, the films and RBCs were incubated at 37 °C for 4 h. Hemolysis was measured as absorbance reading at 540 nm for the supernatant after centrifugation (800 rcf, 5 min), using RBC in water as the positive control and non-treated RBC in HEPES/NaCl as the negative control.

RBC membrane integrity after piezostimulation. Staining of the membrane in RBC was performed following the same protocol as that for the bacteria using FM 4-64/DAPI fluorescent dyes.

Statistical analysis

Data are expressed as mean ± SD of one or two experiments performed in duplicate or triplicate. All graphs were plotted using OriginPro or GraphPad Prism. Statistical analysis was done using the GraphPad Prism software and standard one-way ANOVA test (a p value of <0.05 was considered statistically different).

Results and discussion

Structural properties of PLLA nanotextured films

Herein, we present the difference in morphological and piezoelectric properties of PLLA polymer films prepared in nanotextured (NT) or smooth (DR) form, focusing on the impact of these films on Gram-negative and Gram-positive bacteria and their selectivity. Fig. 1 illustrates the process for the preparation of the piezoelectric NT or smooth drawn (DR5) films and the non-piezoelectric reference samples of NT P(DL)LA and smooth non-drawn (DR1) film, respectively, and their predicted behavior under ultrasound (US) and towards bacteria and blood cells (RBC).

Initially, the prepared films were morphologically and structurally analysed to determine their crystallinity and orientation properties required to execute a piezoelectric effect.

Morphological study of prepared films. The organic films formed using PLLA (with more than 90% L-lactic acid stereoisomer) and produced by mechanical drawing (DR5) (Fig. 2(a)) and using a porous template (NT ANN) (Fig. 2(b)) exhibited a significantly different surface morphology. The PLLA DR5 films had a rough surface with respect to the non-drawn films, but flat with respect to the NT films, with amorphous clusters covering the oriented polymer chains in the drawing direction (Fig. 2(a)).

Alternatively, texturing (Fig. 2(b)) and tube formation (Fig. 2(c)) were confirmed by closely observing the surface of NT PLLA, where nanotubes were arranged in island-liked groups on the polymer substrate at the bottom of the film (as indicated in Fig. 2(d)). The tubes on the surface of the annealed film possessed an average radius of 177 ± 28 nm and length of 27 ± 2 μm (Fig. 2(c) and (d)), indicating the filling of the pores inside the templates during their formation to the top. The same approach was applied to produce the non-piezoelectric nanotextured film reference (NT P(DL)LA) using a copolymer with a 50 : 50 ratio of poly(D,L-) lactide and poly-glycolide. The tubes on the surface of P(DL)LA possessed a diameter of 167 nm ± 24 nm (ESI S1 (Fig. S1†)), confirming their similar morphology to that of NT PLLA.

Crystallinity and crystal structure. The combination of high crystallinity and directional polymer backbone chain orientation is desirable to exploit the shear piezoelectric properties of the PLLA polymer,[28] and therefore these properties were investigated initially.

Additional processing of the NT and DR films improved their crystallinity, as observed in their XRD (Fig. 3(a and b)) and DSC (Fig. 3(c and d)) patterns, respectively. After applying stretching and the formation of DR5, strain-induced crystallization occurred, which resulted in (110)/(200)-oriented crystalline regions in their α-crystalline structure. In comparison to these films, the non-drawn films (DR1) were amorphous. Applying annealing induced crystallization, as observed in the case of the DR1 films annealed above 140 °C. In this case, the non-oriented and annealed film (DR1 ANN) showed high crystallinity with additional orientations of crystalline regions

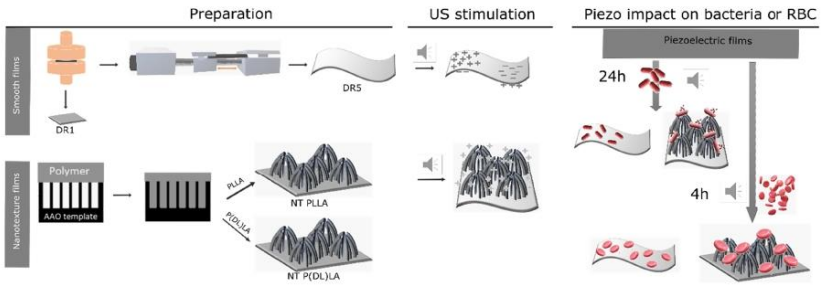

Fig. 1 Schematic presentation of the preparation of smooth piezoelectric (DR5) and non-piezoelectric (DR1) and nanotextured piezoelectric (NT PLLA) and non-piezoelectric (NT P(DL)LA) polymer films and their expected response to ultrasound stimuli as generation of positive charge on the stretched upper side of the down bent polymer and negative charge on the bottom bent side; and piezo-stimulated damaging impact on bacteria for nanotextured film and not harmful behaviour towards RBCs.

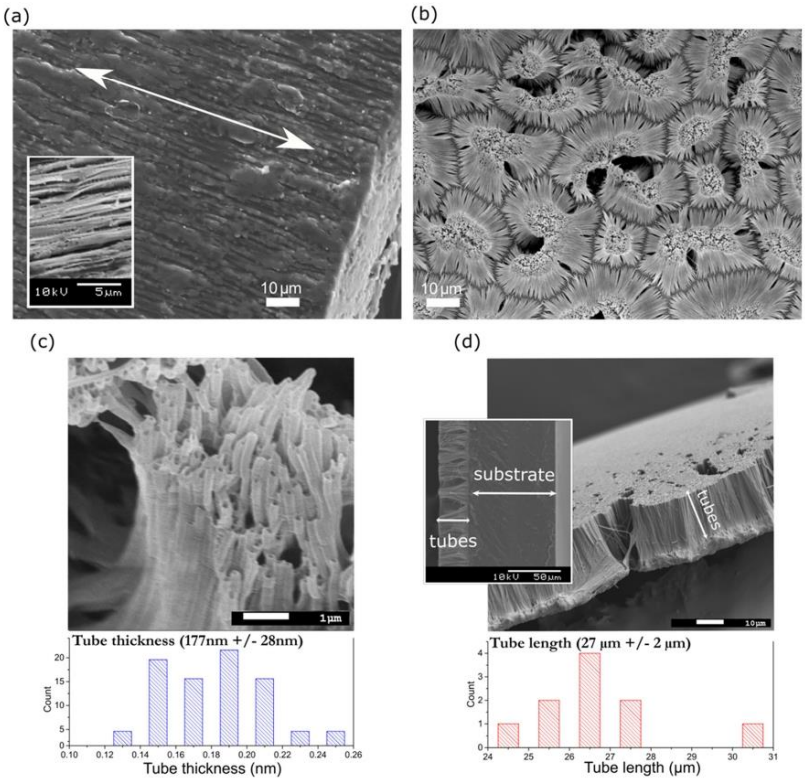

Fig. 2 Scanning electron microscopy analysis of (a) drawn film with a draw ratio of 5 (DR5) with arrow presenting the drawing direction and image of the cross-section in the white square, (b) surface of nanotextured annealed film (NT ANN), where tubes tend to form lean to island-like groups, (c) closer look of NT ANN film, confirming the formation of tubes and (d) cross-section to determine tube length from polished polymer substrate and image of actual prepared film in white square, and (c) and (d) show size distribution histograms of average tube thickness and length, respectively.

present in the α-crystalline structure, as identified based on.[29] The DR5 film was crystalline; however, due to the presence of a cold crystallinity peak, there is still room for improvement, and therefore after annealing, full crystalline potential was achieved (DR5 ANN), as observed by DSC (Fig. 3(c)).

The as-prepared NT film also possessed an amorphous structure (Fig. 3(a)). It crystallized only after annealing, with the appearance of the (110)/(200) crystalline peak. The position of this peak shifted to lower 2θ values compared to that of the smooth film, indicating the formation of a more disordered α′-crystalline structure. When the same approach was applied for the formation of the NT P(DL)LA film, even after annealing its structure remained amorphous.[30] For the non-drawn copolymer P(DL)LA film, the DSC results showed only an amorphous peak and lack of melting peak, indicating that the polymer could not crystalize at temperatures up to 200 °C (Fig. 3(c)). Therefore, this polymer was used as a non-piezoelectric reference in the case of the NT-prepared films.

It should be considered that for the NT films, nanotubes were formed on the substrate (bottom part of the film), which held them at their surface (as indicated in Fig. 2(d)). Given that the bottom part was thicker than the nanotubes, most of the XRD signals for the film come from the substrate. This is the reason why the nanotubes were extracted from the substrate and the XRD pattern of only the nanotubes was recorded (Fig. 3(b)). The results show that the as-prepared nanotubes had low crystallinity, while after annealing for 1 h at 160 °C, their crystallinity improved and shifted to the α′-crystal form. Considering that both the α and α′ PLLA structures possess piezoelectric properties[23] due to the helix structure of the

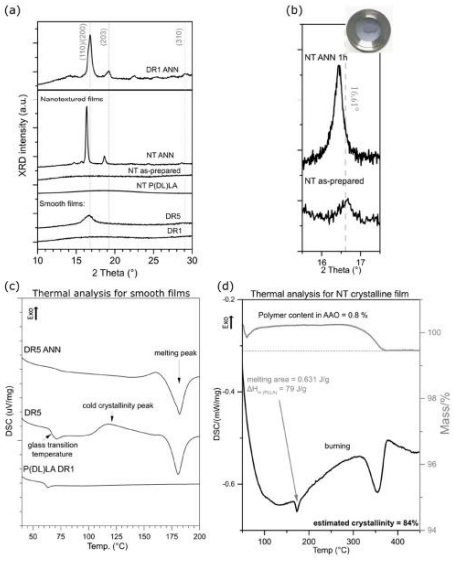

Fig. 3 (a) XRD diffractograms of nanotextured films (NT as-prepared, annealed (NT ANN) at 160 °C for 1 h and for P(DL)LA as-prepared (NT P(DL)LA)) and smooth films (non-drawn (DR1) and drawn (DR5) compared to unoriented annealed film (DR1 ANN) at 160 °C for 1 h. (b) XRD of mechanically extracted nanotubes for NT as-prepared and NT ANN tubes. Thermal analysis (DSC and mass lost) of (c) drawn films (DR5, DR5 ANN and P(DL)LA DR1) and (d) filled AAO template with polymer excess ground off on the bottom of the NT ANN sample.

polymer chain, annealing for 1 h was used for further analysis of the NT films with bacteria.

To quantify the crystallinity of the nanotubes, we applied thermal analysis and the DSC signal was measured for the AAO template with the polymer-filled pores and polymeric substrate removed (the substrate, as indicated in Fig. 2(d), was ground off). The DSC curve (Fig. 3(d)) does not show peaks corresponding to the cold crystallization and glass transition (which are properties of the low-ordered, amorphous phase), only a peak corresponding to melting, indicating an ordered structure with high crystallinity. We assumed that the entire peak area belongs to the polymer inside the pores, which represents only 0.8% of the mass of the whole sample. The estimated value was calculated to be around 84% crystallinity, which is extremely high compared to the smooth DR5 films, where upon annealing for 1 h, the maximum of 62% crystallinity was achieved.[23] Smith *et al.* measured 53% crystallinity for nanotube films prepared in a similar manner; however, they measured the whole film together with the substrate, meaning that most of the signal came from the larger bottom part.[24] Also, 70% crystallinity was obtained for PLLA fibres prepared from solution at 100 °C.[31] The DSC and XRD results also confirmed that annealing increased the crystallinity of the drawn films (DR5), and that P(DL)LA polymer only shows amorphous behaviour. The improved crystallinity after annealing of both the NT and DR films (detected by XRD and thermal analysis) indicates that this post-processing step also improved their piezoelectric properties.

Orientation properties of films. The chain orientation in the PLLA films was observed using Raman spectroscopy with polarized light. Due to the small dimensions of a single nanotube, its signal was enhanced using a silica substrate (Fig. 4(a)). The orientation of the thicker DR5 ANN film was also confirmed (Fig. 4(b)), where its intensities were higher. The intensities of the C–COO peak at 875 cm^{-1} were obtained using different, horizontal and vertical, directions of light and compared. In both films, the fibres were in the horizontal position; therefore, the signals from two light-directions were assigned to nanotube stretching (HHH) and nanotube perpendicular direction (HVV), which were used to calculate the nanotube orientation factor ($R = I^n_{HHH}/I^n_{HVV}$) (Fig. 5(c)). Using this approach, we confirmed that chain orientation in the nanotubes follows the longitudinal direction of the AAO pore, where they were formed (R = 1.31). In the AAO template, the melted polymer solidifies on the surface of nanopore wall. Due to the rapid growth along these nanopores, the polymer chain orientation follows the pore direction. A similar mechanism of nanotube formation and orientation was previously observed for the PS-*b*-PLLA copolymer and PAO nanotubes,[24,32] Besides the single nanotubes, the polymer chain orientation was also confirmed for the drawn films (DR5). The orientation factor obtained for the drawn films (R = 2.45) was distinctly different from that of the non-oriented annealed film (R = 0.80). Similar to the nanotubes, the chain orientation in the drawn films followed the direction of drawing used for their formation. This implies that both the capillary forces, which stretched the polymer inside the nanotube template, and mechanical forces used for film drawing had the same role in the formation of their structures.

Estimation of piezoelectric properties through piezo-degradation potential of organic dye

The films were mechanically deformed using US to measure their piezoelectric properties by measuring the voltage generated during their deformation. Using an ultrasonic bath, the direct voltage output was measured for the PLLA films and compared to the standard with known piezoelectric properties (PVDF film). According to Cafarelli *et al.*, US waves are mechanical waves that travel through the medium, and combined with US-responsive materials, US can be used for the stimulation of piezoelectric materials for the generation of a localized electric field due to the direct piezoelectric effect.[33] The effect of ultrasound on the film is dependent on the pressure it can produce through the cavitation of bubbles. Rashwan *et al.* explained that at a fixed intensity (in our case, the power of the ultrasonic bath was fixed), in a low ultrasonic frequency range (20–50 kHz), the difference between the minimum and maximum pressure is small compared to that

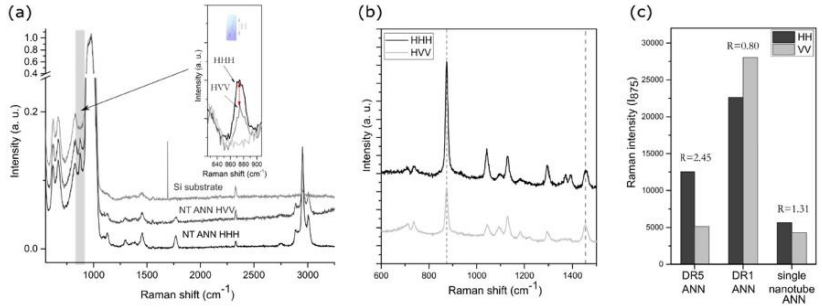

Fig. 4 Polarized Raman spectra of (a) extracted annealed nanotubes in pore length direction (HHH) and perpendicular (HVV) for orientation assessment with magnification of 875 cm^{-1} peak (b) and drawn film in drawing direction (HHH) and perpendicular (VVV). (c) Comparison of Raman intensities for horizontal and perpendicular values of 875 cm^{-1} peak for annealed drawn film (DR5 ANN), non-oriented film (DR1 ANN) and single nanotube, with calculated orientation ratio (*R*) as HHH normalized to VVV values.

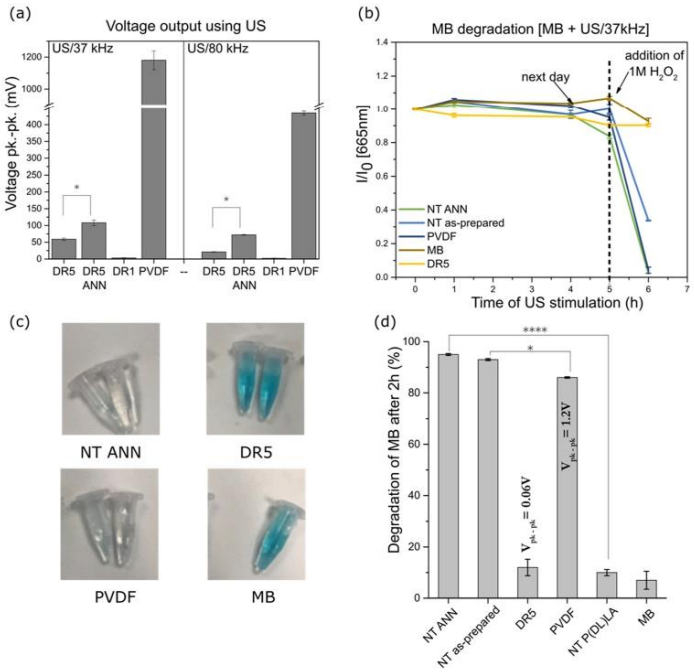

Fig. 5 (a) Voltage peak-to-peak output data collected for US-stimulated piezoelectric films at 37 kHz and 80 kHz for drawn (DR5), drawn and annealed (DR5 ANN), non-drawn (DR1) and PVDF reference sample; (b) methylene blue (MB) degradation observed through absorbance measurements (665 nm) under 37 kHz ultrasound stimulation with marked addition of 1 M hydrogen peroxide (H_2O_2) for nanotextured annealed film (NT ANN), as-prepared nanotextured film (NT as-prepared), smooth drawn film (DR5) and reference sample of PVDF film and clear MB solution; (c) visual presentation of colour change after MB degradation for above-mentioned samples; and (d) percentage of MB degradation after 2 h of ultrasonication with 0.5 M hydrogen peroxide as active species in contact with the above-mentioned samples and for non-piezoelectric nanotextured film (NT P(DL)LA); where * and **** annotate $p < 0.05$ and $p < 0.0001$, respectively.

at higher frequencies (55–80 kHz) where it is much larger. A larger difference means that the periodic time of the wave cycle is reduced, and therefore bubbles take more time to grow before collapsing. At lower frequencies, more bubbles cavitate and are more powerful, consequently generating a higher pressure and temperature on the films compared to that at higher frequencies.[34] Given that the changes in cells occur due to the US stimulation of the piezoelectric PVDF (which requires transverse deformation)[35] and PLLA (requiring shear deformation)[36] polymer, we believe that the application of ultrasound can excite both transverse and shear piezoelectricity.

PVDF showed the highest peak-to-peak output voltage of 1.2 V (Fig. 5(a)) at 37 kHz and less than half this value at 80 kHz (450 mV). A similar trend was observed for the DR5 films and films that were additionally annealed. The values were much lower at 37 kHz compared to that of the PVDF reference (59 mV and 108 mV for DR5 and DR5 ANN, respectively), while at two-times higher frequency, they were around two-times lower. Given that annealing of the DR5 film improved its crystallinity; consequently, its piezoelectric properties were at least 2-times higher at both frequencies (Fig. 5(a)). A clear difference was observed the between drawn (DR5) and non-drawn film (DR1), given that the shape of the curve differed from the noise, as presented in ESI S2 (Fig. S2†).

The same method was unsuitable for the NT films, given that the electrodes were difficult to adjust for the complex surface made of individual nanotubes. Therefore, we applied an indirect method to estimate their piezoelectric properties by measuring their piezo-degradation potential. We took advantage of the ability of hydrogen peroxide to catalytically decompose into reactive oxygen species (ROS), which degrade the organic dye methylene blue (MB). In this reaction, the piezoelectric film acts as the catalyst. As previously observed, the ROS formed by piezo-catalysed H_2O_2 oxidation were responsible for the discolouration of MB.[37,38] Fig. 5(b) shows the effect of US stimulation of the films on MB degradation by measuring the absorbance at 665 nm, which is presented as the normalized absorbance to the initial value. Without that addition of H_2O_2 and after 5 h of continuous US stimulation, no MB degradation was observed, confirming that the investigated polymers were not capable of producing ROS by themselves. ROS products originating from the hydrolysis of water are commonly obtained for ceramic materials with much higher piezoelectric properties.[39–41] However, with the addition of H_2O_2 with a redox potential lower than that of water, the investigated polymers could catalyse ROS, which allowed insight into their piezo-degradation capacity. Therefore, when highly concentrated H_2O_2 was added, the total degradation of MB is observed for the NT piezoelectric films (NT ANN and NT as-prepared) and PVDF reference as compared to the clear MB or DR5 film with low piezoelectricity, where degradation did not occur. The observed effect is illustrated in the photographs presented in Fig. 5(c), showing the partial or complete discolouration of MB solution at the end of the stimulating process for the different films. In addition, for the controls, we observed that MB/peroxide was not degraded by ultrasound without the films and that the films did not degrade MB/peroxide until ultrasound was turned on (ESI S3 (Fig. S3†)). This is direct evidence that the observed degradation processes were driven by the charge form on the surface of the films during their deformation and a direct consequence of their piezoelectricity. After the addition of a lower concentration of H_2O_2 (0.5 M) the degradation kinetics were slower (kinetic curves presented in ESI S4 (Fig. S4 and S5†), which clearly revealed the differences in piezo-degradation potential among the investigated films (Fig. 5(d)). The highest piezo-degradation potential was observed for the piezoelectric NT PLLA films with the highest rate of MB degradation (95%) among the piezoelectric films, including PVDF and DR5 (86% and 12%, respectively) (ESI S4 (Table S1†)). The clear contribution of the piezoelectricity to MB degradation was observed when the degradation by the piezoelectric NT PLLA films was compared that of the non-piezoelectric NT P(DL)LA films with the same morphology and surface area. Specifically, the degradation rate obtained for the drawn DR5 films was very slow and not significantly different compared to the non-treated MB or non-piezoelectric NT P(DL)LA film, which is due to their low piezoelectric effect and small available specific surface area.

For the thin films and films with complex a morphology of nanotexture on the surface, the piezoelectric coefficient was difficult to measure, and therefore it was confirmed through piezo-potential for organic dye degradation.

Antibacterial properties

After the detailed characterization of the structural, morphological and piezoelectric properties of the developed films, they were further investigated for their capacity to affect bacterial cells. Particularly we were focused on the individual contributions of different factors including film surface morphology, piezoelectricity, and ROS generation as the possible source of the antimicrobial effect. The tests were performed using *E. coli* as the representative Gram-negative and *S. epidermidis* as the Gram-positive bacteria.

Both piezoelectric PLLA films (NT ANN and DR5) initially possessed greater hydrophobic properties with a contact angle of around 110°; however, after wetting their surface, the contact angle decreased (70° and 45° for DR5 and NT ANN sample, respectively), indicating the better wettability of the NT films (ESI S5 (Fig. S6†)). Hydrophobic properties can play an important role in assessing the antibacterial properties of the samples due to the poor contact of the bacteria with the film surface.

Direct contact-based antibacterial effect. The antibacterial drop test, which is one of the standard tests to evaluate the antibacterial properties of non-porous and non-absorbing surfaces, was performed to assess the bacterial susceptibility to piezo-stimulation.[26,27] This test was the optimal choice given that it provides the best contact between the investigated bacteria and surface of the film, given that none of the antimicrobial agents are expected to be released in the surround-

ing medium. When a drop of bacteria (containing 10^6 cfu mL^{-1} or 10^8 cfu mL^{-1} of *E. coli* or *S. epidermidis*, respectively) was put on the piezoelectric NT PLLA films (both as-prepared and ANN), followed by US deformation, all the bacteria were killed after 24 h and no further survival was detected (Fig. 6(a) and (b)). In the case of the NT ANN films, with the highest piezoelectricity based on piezo-degradation potential (Fig. 5(d)), the antibacterial effect was observed even without US stimulation. Smith *et al.* demonstrated that the adhesion and further growth of human dermal fibroblasts on the surface of NT PLLA mechanically deformed the film, exhibiting a piezoelectric effect on the cells.[22] We also predicted the same after loading the bacteria on the NT PLLA films. This small deformation was high enough to activate the piezoelectric effect, providing a complete bactericidal effect on both bacterial strains (with 6 log 10 and 8 log 10 cfu reduction) even without the application of US deformation. The same was not observed for the drawn DR5 films with a much lower piezoelectricity. To clearly confirm death of the bacteria on the NT PLLA film surface, the washed solution and the films from the assay were also placed in growth medium to observe the viability of any surviving bacteria by following the 24-hour kinetics of PB fluorescence at 37 °C, finally confirming their bactericidal effect (ESI S6 (Fig. S7–S9†)).

The washed films after the contact test showed a clean surface without bacteria and their piezo-degradation potential toward MB dye degradation in the presence of peroxide was still observed (60% lower degradation compared to initial), indicating the possible reuse of the film, as presented in ESI S6 (Fig. S10†).

Influence of surface texturing on antibacterial properties. Another possible source of antimicrobial activity observed in the NT PLLA films could be potentially associated with their nanotextured morphology. A nanotextured morphology (in the case of short and tightly packed nanopillars[20,42]) can exhibit a bacteriocidic effect by itself.[20,21] This type of morphology can also exhibit superhydrophobicity towards liquids, resulting in an anti-fouling and self-cleaning effect[43] and consequently repelling the attachment of bacteria.[19] To evaluate the influence of the surface morphology on the bactericidal effect observed for the NT PLLA films, we compared the antimicrobial effect in piezoelectric PLLA and non-piezoelectric P(DL)LA with the same surface morphology. The CFU count between the US-treated *E. coli* and bacteria in contact with NT P(DL)LA was not statistically different, where no log reduction occurred for the non-piezoelectric nanotextured film (Fig. 6(a) black square). In the case of the non-piezoelectric NT P(DL)LA films, a killing effect was not observed, and therefore the effect of the surface morphology was discarded. It can be assigned to the formation of long nanotubes (27 μm in length) without dense packing (Fig. 3). This type of morphology enables bacteria to attach to the nanotube sides rather than their top, which is where their nanotexture-associated antimicrobial effect occurs.[20] The comparison between NT P(DL)LA and PLLA directly confirmed that piezoelectricity is the main reason for the observed antimicrobial effect.

Kinetics of antibacterial activity in saline solution and growth medium. The kinetics of killing bacteria in saline solution and the growth curves for the bacteria suspended in growth medium were also measured for *E. coli* and *S. epidermidis* bacteria. When the films were immersed and left to float in the bacteria saline suspension (*E. coli*), the NT ANN samples, US stimulated, still showed a clear bactericidal effect (Fig. 7(a)). After incubation for 1 h, we observed that after there was no difference between the non-treated bacteria and bacteria incubated with the films; while after 5 h at least

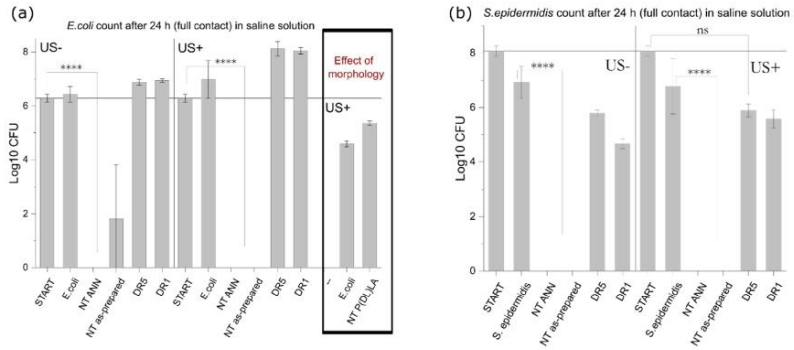

Fig. 6 Full contact-based testing of PLLA films with *E. coli* bacteria. (a) Graph of counted CFU of surviving *E. coli* bacteria on agar plate, after contact with PLLA films (nanotextured annealed (NT ANN) and non-annealed (NT as-prepared), drawn (DR5) and non-drawn film (DR1)) with or without US stimulation for 30 min (annotated with US+ and US–); black square indicating separate contact test between *E. coli* and non-piezoelectric nanotextured film (NT P(DL)LA). (b) Graph of counted CFU of survived *S. epidermidis* bacteria in contact with above-mentioned films on agar plates after 22h of incubation; where **** annotates $p < 0.0001$ and ns is statistically insignificant difference.

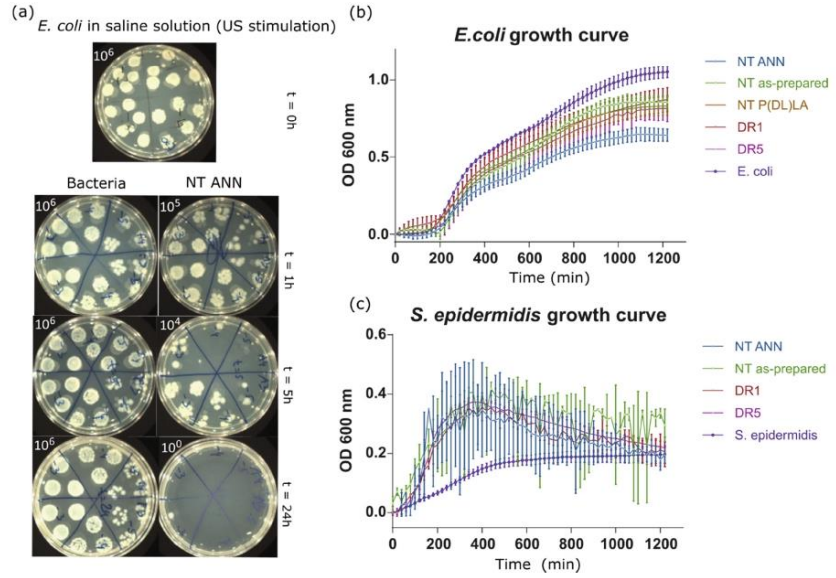

Fig. 7 (a) Agar plates with diluted bacteria growth for *E. coli* and bacteria in contact with NT PLLA film at start and after 30 min US stimulation following 1 h, 5 h and 24 h incubation in saline solution. Kinetics of bacteria growth in LB medium after initial US stimulation for (b) *E. coli* bacteria and (c) *S. epidermidis* bacteria (presented only average values).

2 log 10 reduction was observed; and after 24 h, clear death resulting in 6 log 10 reduction was confirmed for the bacteria incubated with the immersed NT ANN film (Fig. 7(a)).

In the case when films were immersed in LB bacterial suspension, the differences in bacteria growth were insignificantly lower. In the case of both bacterial strains, *E. coli* (Fig. 7(b)) and *S. epidermidis* (Fig. 7(c)), the growth kinetic curves showed a small decrease in OD values, which was the most pronounced in the case of incubation with NT ANN films with *E. coli* bacteria (50%) (Fig. 7(b)). Testing in saline solution confirmed that killing bacteria using piezo-stimulation is not a fast process (>5 h). Therefore, if bacteria have the possibility to grow, such as in nutrition LB medium, the piezo-effect will not be pronounced or have a significant effect on bacteria growth. A similar small or no effect was also observed after stimulating bacteria with piezoelectric PVDF films in planktonic growth.[10] The hydrophobicity of the prepared samples can also be a reason for the insufficient film-bacteria contact, and therefore the observed poor antibacterial properties in growth medium solution.

Influence of pH change and the effect of ROS. Another aspect of the antimicrobial effect obtained for the US-deformed NT PLLA films can be associated with polymer degradation and generation of ROS. PLLA is a polyester, which degrades through hydrolysis, releasing acidic products and consequently decreasing the pH, particularly in the microenvironment close to the film surface. However this process is not fast, and as we observed earlier, degradation in the presence of enzymes takes several days.[44] This period is longer than the time needed for obtaining an antibacterial effect, and therefore the contribution of pH changes due to the release of lactic acid was discarded. More importantly, with polymer degradation, the piezoelectric properties gradually decrease,[44] implying the prolonged availability of their surface for providing piezo-stimulation-induced antimicrobial activity.

Alternatively, the generation of ROS is the main reason for the antibacterial effects obtained by strong piezoelectrics (such as piezoceramics).[12] This is ascribed to their capacity to hydrolyze water, as confirmed using the MB degradation test.[39–41] Using a similar MB test, we confirmed that none of the investigated PLLA and even PVDF reference did not have capacity for the degradation of MB in water (Fig. 5(b)). Consequently, ROS formation cannot be associated with the antimicrobial effect observed for NT PLLA. This was further confirmed with the addition of an ROS scavenger during antimicrobial testing. Specifically, we applied 0.035 mg mL^{-1} ascorbic acid as a strong antioxidant to eliminate any potentially formed ROS during piezo-stimulation. Consequently, we did not observe any difference in bactericidal effect when bacteria were in contact with the NT-annealed films (Fig. 8(a)). This is clear proof that ROS were not responsible for killing the bacteria.

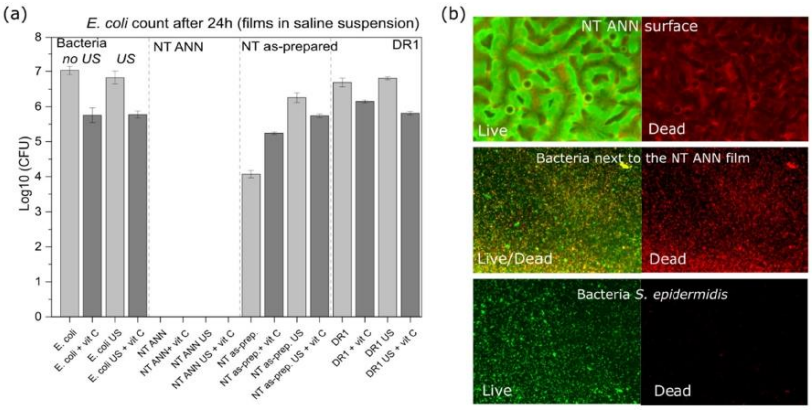

Fig. 8 *E. coli* count of grown bacteria on agar plate after 24 h incubation of films immersed in bacteria suspension in saline solution with added ascorbic acid (vitamin C; dark grey column) with or without US at start. (b) Live/dead imaging of NT ANN film with bacteria, solution of bacteria near the film and clear bacteria for *S. epidermidis* test in saline suspension.

Influence on membrane compactness. The fraction of dead bacteria obtained after US stimulation with the NT ANN films was also detected and visualized using the live/dead test. Fig. 8(b) shows the live/dead fraction of bacteria detected in case of *S. epidermidis*. The film itself adsorbed the dye mixture, which strongly limited the ability to detect the bacteria directly on the film. However, we were able to clearly detect bacteria in the saline medium above the film. Consequently, the intensive staining with propidium iodine (PI) showing red fluorescence indicates a very large fraction of dead bacteria.

The morphological characteristics of the bacterial cells attached to the film after testing in saline suspension were investigated using SEM microscopy. For this, the bacteria detected on the piezoelectric NT ANN films were compared with the bacteria on the NT as-prepared films with US stimulation. This study was performed using both Gram-negative *E. coli* and Gram-positive *S. epidermidis* bacteria. In both cases, we observed a damaged bacterial cell envelope when the bacteria were in contact with the piezoelectric NT ANN tubes and lack of morphological damage for the bacteria detected on the NT as-prepared film (Fig. 9(a and b)), confirming that the observed bacteriocidic effect for the NT ANN film in saline suspension in the antibacterial assay. Smith *et al.* showed that charge is present along the full length of each PLLA tube bent at the surface of NT films and that the top of the bent tubes holds a positive charge.[22] Accordingly, the whole presented surface of the ANN sample should have an effect on bacteria. We observed a lot of residual bacterial cells after complete damage of the cell structure (small dots on the tubes (Fig. 9(a)) observed for *E. coli*) and damaged cell envelope for *S. epidermidis* (Fig. 9(b)). This indicates that the long *E. coli* bacterial cells in contact with the top of the tubes were intensively raptured and disintegrated. Some of them that were aligned with the tube length maintained their compactness, however, membrane distortion was observed. For the shorter *S. epidermidis* bacteria, cell rupture did not occur; however, clear membrane distortion was observed. Similar membrane distortions were observed by Ando *et al.*, who showed a clear difference in bacterial cell surface morphology when their death was caused by piezoelectricity or with another stimuli (including heat, drying, or pH).[8] We also observed that US stimulation did not affect the orientation of the annealed PLLA tubes, which remained in the island formation as that at the before treatment. In contrast, sonication significantly changed the orientation of the tubes in the as-prepared films (Fig. 9(a and b) right and ESI S7 (Fig. S11†)). Due to their lower crystallinity, they were more elastic. Although the annealed and non-annealed NT PLLA films were detected to have a similar piezo-degradation potential (Fig. 7), the difference in their topography after US stimulation indicates that the annealed tubes were more stable and less mobile. Consequently, it is easier for bacteria to mechanically deform them just by landing on their surface, resulting in the generation of a piezo-signal and leading to the antibacterial effect observed even without US stimulation. Due to the movement of the tubes under US stimulation, a similar damaging effect was not detected on the NT as-prepared films when tested in suspension.

After 24 h of incubation of the immersed NT ANN film in *E. coli* saline solution, the membrane damage was optically observed using stain colours (FM 4-64 and DAPI) and a confocal microscope. Closer observation showed an intact membrane (red) for *E. coli* bacteria after incubation in saline solu-

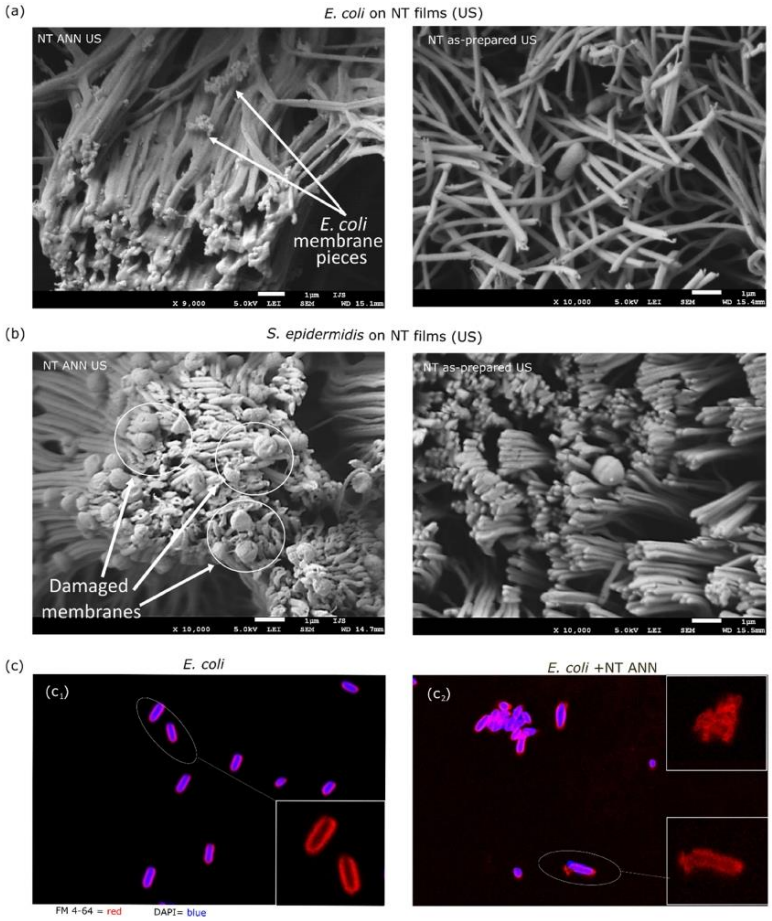

Fig. 9 SEM images of (a) *E. coli* and (b) *S. epidermidis* bacteria on the nanotextured film surfaces after US stimulation for 30 min following 24 h incubation in saline suspension after cell fixation for NT ANN sample (left) and NT as-prepared sample. (c) FM 4-64 (red) and DAPI (blue) staining of *E. coli* bacteria (c_1) and bacteria in contact with NT ANN film (c_2) after test in saline solution with US stimulation.

tion and US (Fig. 9(c_1)). However, for the bacteria in contact with the NT ANN film, an uneven distribution of the staining, indicating membrane damage, and rupture of the membrane were observed (Fig. 9(c_2)). Also, the observed agglomeration of bacteria indicated their death.

The bacteriocidic effect was confirmed for the NT ANN sample with or without US stimulation as a result of the detected piezoelectric properties of the sample in combination with the nanotextured topography, which allows better mechanical deformation using US and more available surface. Under mechanical stimulation, we presume that a positive charge is present on the surface and responsible for membrane damage in bacteria, leading to their death *via* only the contact-kill mechanism. Similar membrane damage and disruption of the transmembrane potential due to the exchange of cationic ions on the cell membrane and positively charged polymer surface was observed for positively charged quaternary ammonium compounds and proposed as the mechanism for bacteria death.[16] A positive charge can generate an electric field with the adhered bacteria, resulting in the removal of

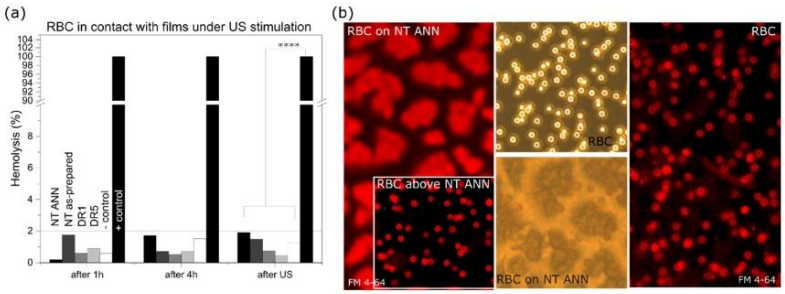

Fig. 10 Piezo-stimulation effect in red blood cells (RBC). (a) Test of hemolysis for films (nanotextured annealed (NT ANN), NT as-prepared, drawn (DR5) and undrawn film (DR1)) in contact with RBCs compared to +and − control (damaged RBC in water and undamaged RBC in HEPES medium, respectively) using US stimulation: 30 min, 80 kHz, 30% power and (b) FM 4-64 red staining of RBC membranes and optical pictures of RBC in contact with nanotextured annealed film (RBC + NT ANN) after US stimulation compared to intact RBC reference in HEPES.

their membrane lipids and the dramatic electron loss, causing a distortion in their cell shape and leading to cell death.[16,17] We believe that poor contact is the reason for the low antibacterial properties of the NT ANN film when tested in the growth medium (50% lower OD value for *E. coli* bacteria) as a result of the contact-kill mechanism alone. According to the proposed mechanism, our films can be considered as an alternative to the established antibacterial therapies given that electric stimulation can prevent the emergence of bacteria resistance.[1]

Hemolysis test and RBC membrane compactness

The effect of piezoelectricity was also investigated to determine if it damages red blood cells (RBC) through absorbance measurements of released hemoglobin (540 nm) and membrane staining. Less than 2% of released hemoglobin was detected after the films were in contact with RBC for 4 h for all the films with US stimulation (80 kHz, 30% power; Fig. 10(a)) and without US (ESI S8 (Fig. S12 and S13†)), compared to the positive control with RBC incubated in water. Disc-shaped RBC were detected both directly on the film surface and in the medium above the films (based on brightfield images in Fig. 10(b)). The potential damage in the RBC membranes was checked with the same FM 4-64 staining used for staining the bacterial membranes. Staining resulted in red fluorescence in membranes without penetration of the dye inside the cells, confirming their compactness and absence of any mechanical damage (Fig. 10(b)). Using full power at 80 kHz US, 40%–90% damage to the RBC was observed (ESI S8 (Fig S12†)) for all the films with a nanotextured surface. The effect was the most pronounced for the non-piezoelectric NT films (90% for NT P(DL)LA), which led to the conclusion that it was caused by the topographical effect. In contrast, this effect was not detected for the drawn films.

The bactericidal effect on the surface of the NT ANN films was observed after the bacteria landed on their surface (without US stimulation, Fig. 6) or if the films were additionally deformed in ultrasound (with US stimulation, Fig. 6). In this case, it can be concluded that for a suitable dose of ultrasonic deformation, piezo-stimulation with the use of fully organic polymers can be optimized. A wide range of mechanical deformations capable of inducing a piezoelectric response is needed for achieving an antimicrobial effect, and therefore a useful tool for attaining the required selectivity. Selective interactions with bacterial and mammalian cells are ultimately necessary for optimizing piezo-stimulation as a therapeutically applicable antimicrobial approach, which is highly efficient against bacteria and compatible with mammalian cells. Electric stimulation is also beneficial for mammalian cells,[45,46] and therefore the prepared biodegradable films with antibacterial properties can be applicable to increase cell proliferation, migration and differentiation for wound healing or tissue regeneration and preventing infections associated with chronic wounds. The main benefits of its application in infection control are expected from the non-specificity of the piezo-stimulation mechanism used to damage bacteria. This mechanism applies physical deformation, which does not leave them too many options to adopt and develop a resistance mechanism, as is the case with most of the currently used antimicrobial technologies.

Conclusion

Fully organic, biodegradable, polymeric films were designed as PLLA piezoelectrics with nanotextured or smooth surfaces. Nanotexturing combined with post-processing annealing resulted in a higher specific surface area and better crystallinity, which jointly affected their piezo-degradation potential, implying a significant improvement in their piezoelectric properties. Piezostimulation induced bacterial death in both Gram-positive and Gram-negative bacterial strains. The films were not capable of producing ROS and the antimicrobial effect on their surface was achieved even in the presence of an ROS scavenger. Either bacterial cells landing on their surface

or application of US stimulation, which caused mechanical deformation of the nanotextured PLLA piezoelectric films, generated a surface charge, affecting the bacterial membrane. In the case of the non-piezoelectric films, the long and flexible pillars on the nanotextured films could not cause an antimicrobial effect just by nanotexturing. Therefore, the detected damage in the cell bacterial membrane was due to the disrupted transmembrane potential, leading to cell death with time (>5 h). Due to the poor adhesion of the bacterial cells to the surface of the films, the effect was not fast. Further improvement in their efficacy is expected using adhesion molecules, which will enhance the bacterial attachment to the surface of the films, which we consider an interesting and potential option to be explored in the future. After optimization of the conditions of mechanical stimulation, high usability of these films for therapeutic use is expected.

Author contributions

Research conceptualization, L. G. and M. V.; fluorescence confocal microscope observations, M. P. N.; data curation, L. G., M. P. N. and M. V.; writing – original draft preparation, L.G.; writing – review and editing, M. P. N., M. V. and M. S.; visualization, L. G. and M. V.; supervision, M. V.; funding acquisition, M. V., M. S.

Conflicts of interest

The authors declare no conflict of interest. The funders had no role in the design of the study; in the collection, analyses, or interpretation of data; in the writing of the manuscript, or in the decision to publish the result.

Acknowledgements

The authors are grateful to Dr Urška Gabor, Msc. Damjan Vengust and David Fabian from Advanced Materials Department, IJS, for help with performing XRD, Raman and piezoelectric measurements.

The work has been funded by the Slovenian Research Agency (ARRS) within grants J2-8169, N2-0150 and PR-08338 and research programs P2-0091 and PR-0099.

References

1 M. M. Fernandes, E. O. Carvalho and S. Lanceros-Mendez, Electroactive Smart Materials: Novel Tools for Tailoring Bacteria Behavior and Fight Antimicrobial Resistance, *Front. Bioeng. Biotechnol.*, 2019, **7**, 277.
2 C. Ribeiro, S. Moreira, V. Correia, V. Sencadas, J. G. Rocha, F. M. Gama, *et al.*, Enhanced proliferation of pre-osteoblastic cells by dynamic piezoelectric stimulation, *RSC Adv.*, 2012, **2**, 11504–11509.
3 H. Miyazaki, M. Kinoshita, A. Saito, T. Fujie, K. Kabata, E. Hara, *et al.*, An ultrathin poly(L-lactic acid) nanosheet as a burn wound dressing for protection against bacterial infection, *Wound Repair Regen.*, 2012, **20**, 573–579.
4 H. Guo, Z. Li, S. Dong, W. Chen, L. Deng, Y. Wang, *et al.*, Piezoelectric PU/PVDF electrospun scaffolds for wound healing applications, *Colloids Surf., B*, 2012, **96**, 29–36.
5 S. N. Gorodzha, A. R. Muslimov, D. S. Syromotina, A. S. Timin, N. Y. Tcvetkov, K. V. Lepik, *et al.*, A comparison study between electrospun polycaprolactone and piezoelectric poly(3-hydroxybutyrate-co-3-hydroxyvalerate) scaffolds for bone tissue engineering, *Colloids Surf., B*, 2017, **160**, 48–59.
6 S. Guerin, S. A. M. Tofail and D. Thompson, Organic piezoelectric materials: milestones and potential, *NPG Asia Mater.*, 2019, 10.
7 M. Ando, S. Takeshima, Y. Ishiura, K. Ando and O. Onishi, Piezoelectric antibacterial fabric comprised of poly(l-lactic acid) yarn, *Jpn. J. Appl. Phys.*, 2017, **56**, 10PG01.
8 M. Ando, D. Tamakura, T. Inoue, K. Takumi, T. Yamanaga, R. Todo, *et al.*, Electric antibacterial effect of piezoelectric poly(lactic acid) fabric, *Jpn. J. Appl. Phys.*, 2019, SLLD09.
9 T. Wang, H. Chen, C. Yu and X. Xie, Rapid determination of the electroporation threshold for bacteria inactivation using a lab-on-a-chip platform, *Environ. Int.*, 2019, **132**(April), 105040.
10 E. O. Carvalho, M. M. Fernandes, J. Padrao, A. Nicolua, J. Marques-Marchan, A. Asenjo, *et al.*, Tailoring Bacteria Response by Piezoelectric Stimulation, *ACS Appl. Mater. Interfaces*, 2019, **11**(30), 27297–27305.
11 S. Kumar, R. Vaish and S. Powar, Surface-selective bactericidal effect of poled ferroelectric materials, *J. Appl. Phys.*, 2018, **124**, 014901.
12 G. Tan, S. Wang, Y. Zhu, L. Zhou, P. Yu, X. Wang, *et al.*, Surface-Selective Preferential Production of Reactive Oxygen Species on Piezoelectric Ceramics for Bacterial Killing, *ACS Appl. Mater. Interfaces*, 2016, **8**(37), 24306–24309.
13 I. S. Vatlin, R. V. Chernozem, A. S. Timin, A. P. Chernova, E. V. Plotnikov, Y. R. Mukhortova, *et al.*, Bacteriostatic Effect of Piezoelectric Poly-3-Hydroxybutyrate and Polyvinylidene Fluoride Polymer Films under Ultrasound Treatment, *Polymers*, 2020, **12**, 240.
14 D. V. Bayramol, N. Soin, A. Dubey, R. Kant, R. Priyadarshini, S. S. Roy, *et al.*, Evaluating the fabric performance and antibacterial properties of 3-D piezoelectric spacer fabric, *J. Text. Inst.*, 2018, **5000**, 1–7.
15 Y. Wang, Y. Xu, S. Dong, P. Wang, W. Chen, Z. Lu, *et al.*, Ultrasonic activation of inert poly(tetrafluoroethylene) enables piezocatalytic generation of reactive oxygen species, *Nat. Commun.*, 2021, **12**(3508), 1–8.
16 R. Kaur and S. Liu, Antibacterial surface design – Contact kill, *Prog. Surf. Sci.*, 2016, **91**(3), 136–153.
17 G. Wang, H. Feng, L. Hu, W. Jin, Q. Hao, A. Gao, *et al.*, An antibacterial platform based on capacitive carbon-doped

TiO2 nanotubes after direct or alternating current charging, *Nat. Commun.*, 2018, **9**(2055), 1613–1619.

18 E. P. Ivanova, J. Hasan, H. K. Webb, V. K. Truong, G. S. Watson, J. A. Watson, *et al.*, Natural Bactericidal Surfaces: Mechanical Rupture of Pseudomonas aeruginosa Cells by Cicada Wings, *Small*, 2012, **8**(16), 2489–2494.

19 A. Jaggessar, H. Shahali, A. Mathew and P. K. D. V. Yarlagadda, Bio-mimicking nano and microstructured surface fabrication for antibacterial properties in medical implants, *J. Nanobiotechnol.*, 2017, **15**, 64.

20 M. N. Dickson, E. I. Liang, L. A. Rodriguez, N. Vollereaux and A. F. Yee, Nanopatterned polymer surfaces with bactericidal properties, *Biointerphases*, 2015, **10**(2), 021010.

21 Y. Jang, W. T. Choi, C. T. Johnson, A. J. Garcia, P. M. Singh, V. Breedveld, *et al.*, Inhibition of Bacterial Adhesion on Nanotextured Stainless Steel 316L by Electrochemical Etching, *ACS Biomater. Sci. Eng.*, 2018, **4**, 90–97.

22 M. Smith, T. Chalklen, C. Lindackers, Y. Calahorra, C. Howe, A. Tamboli, *et al.*, Poly-L-Lactic Acid Nanotubes as Soft Piezoelectric Interfaces for Biology: Controlling Cell Attachment via Polymer Crystallinity, *ACS Appl. Bio Mater.*, 2020, **3**, 2140–2149.

23 L. Udovc, M. Spreitzer and M. Vukomanovic, Towards hydrophilic piezoelectric poly-L-lactide films: optimal processing, post-heat treatment and alkaline etching, *Polym. J.*, 2020, **52**, 299–311.

24 M. Smith, C. Lindackers, K. Mccarthy and S. Kar-narayan, Enhanced Molecular Alignment in Poly-L-Lactic Acid Nanotubes Induced via Melt-Press Template-Wetting, *Macromol. Mater. Eng.*, 2019, **304**, 1800607.

25 S. Farah, D. G. Anderson and R. Langer, Physical and mechanical properties of PLA, and their functions in widespread applications—A comprehensive review, *Adv. Drug Delivery Rev.*, 2016, **107**, 367–392.

26 ISO 21702 : 2019- Measurement of antiviral activity on plastics and other non-porous surfaces.

27 E. Pinho, L. Magalhães, M. Henriques and R. Oliveira, Antimicrobial activity assessment of textiles: standard methods comparison, *494 Ann. Microbiol.*, 2011, **61**, 493–498.

28 C. S. Lovell, J. M. Fitz-Gerald and C. Park, Decoupling the effects of crystallinity and orientation on the shear piezoelectricity of polylactic acid, *J. Polym. Sci., Part B: Polym. Phys.*, 2011, **49**(21), 1555–1562.

29 K. Takahashi, D. Sawai, T. Yokoyama, T. Kanamoto and S.-H. Hyon, Crystal transformation from the a- to the b-form upon tensile drawing of poly(L- lactic acid), *Polymer*, 2004, **45**(14), 4969–4976.

30 C. A. C. Erbetta, R. J. Alves, J. M. Resende, F. R. S. Freitas and R. G. de Sousa, Synthesis and Characterization of Poly (D,L-Lactide-co-Glycolide) Copolymer, *J. Biomater. Nanobiotechnol.*, 2012, **3**, 208–225.

31 M. Smith, Y. Calahorra, Q. Jing, S. Kar-narayan, M. Smith, Y. Calahorra, *et al.*, Direct observation of shear piezoelectricity in poly-l-lactic acid nanowires, *APL Mater.*, 2017, **5**, 074105.

32 M. Y. E. Yau, I. Gunkel, B. Hartmann-Azanza, W. Akram, Y. Wang, T. Thurn-Albrecht, *et al.*, Semicrystalline Block Copolymers in Rigid Confining Nanopores, *Macromolecules*, 2017, **50**, 8637–8646.

33 A. Cafarelli, A. Marino, L. Vannozzi, J. Puigmartí-Luis, S. Pané, G. Ciofani, *et al.*, Piezoelectric Nanomaterials Activated by Ultrasound: The Pathway from Discovery to Future Clinical Adoption, *ACS Nano*, 2021, 11066–11086.

34 S. S. Rashwan, I. Dincer and A. Mohany, Investigation of acoustic and geometric effects on the sonoreactor performance, *Ultrason. Sonochem.*, 2020, **68**, 105174.

35 M. Hoop, X. Chen, A. Fer, F. Mushtaq, G. Ghazaryan, T. Tervoort, *et al.*, Ultrasound-mediated piezoelectric differentiation of neuron-like PC12 cells on PVDF membranes, *Sci. Rep.*, 2017, **7**(4028), 1–8.

36 R. Das, E. J. Curry, T. T. Le, G. Awale, Y. Liu, S. Li, *et al.*, Nano Energy Biodegradable nanofiber bone-tissue scaffold as remotely-controlled and self-powering electrical stimulator, *Nano Energy*, 2020, **76**, 105028.

37 L. I. Jinga, G. Popescu-pelin, G. Socol, S. Mocanu, M. Tudose, D. C. Culita, *et al.*, Chemical Degradation of Methylene Blue Dye Using TiO2/Au Nanoparticles, *Nanomaterials*, 2021, **11**(1605), 1–10.

38 S. Liu, B. Jing, C. Nie, Z. Ao, X. Duan, B. Lai, *et al.*, Piezoelectric activation of peroxymonosulfate by MoS2 nanoflowers for the enhanced degradation of aqueous organic pollutants, *Environ. Sci.: Nano*, 2021, **8**, 784–794.

39 C. Lei, L. Song and S. Zhang, Study on the piezoelectric catalytic degradation dyes performance of three- dimensional bismuth tungstate microflower, *Ceram. Int.*, 2020, **46**(18), 29344–29351.

40 X. Xue, W. Zang, P. Deng, Q. Wang, L. Xing, Y. Zhang, *et al.*, Piezo-potential enhanced photocatalytic degradation of organic dye using ZnO nanowires, *Nano Energy*, 2015, **13**, 414–422.

41 T. Hou, F. Cao, M. Li, J. Wang and L. Lv, Harvesting the Vibration Energy with BaTiO3@Graphene for the Piezocatalytic Degradation of Methylene Blue, *J. Environ. Sci. Eng. Technol.*, 2020, **8**, 84–91.

42 M. Michalska, F. Gambacorta, R. Divan, I. S. Aranson, A. Sokolov, P. Noirot, *et al.*, Tuning antimicrobial properties of biomimetic nanopatterned surfaces, *Nanoscale*, 2018, **10**, 6639–6650.

43 G. Moran and R. Meallet-Renault, Superhydrophobic Surfaces Toward Prevention of Biofilm-Associated Infections, in *Bacterial Pathogenesis and Antibacterial Control*, ed. S. Kırmusaoğlu, IntechOpen, London, 2018, pp. 95–109.

44 L. Gazvoda, B. Višić, M. Spreitzer and M. Vukomanović, Hydrophilicity affecting the enzyme-driven degradation of piezoelectric poly-l-lactide films, *Polymers*, 2021, 1719.

45 M. Rouabhia, H. Park, S. Meng, H. Derbali and Z. Zhang, Electrical stimulation promotes wound healing by enhancing dermal fibroblast activity and promoting myofibroblast transdifferentiation, *PLoS One*, 2013, e71660.

46 M. R. Asadi and G. Torkaman, Bacterial Inhibition by Electrical Stimulation, *Adv. Wound Care*, 2014, **3**(2), 91–97.

Electronic Supplementary Material (ESI) for Biomaterials Science.

Supporting Information:

Antimicrobial activity of Piezoelectric Polymer: Piezoelectricity as a reason for damaging bacterial membrane

Lea Gazvoda [1,2], Milica Perišić Nanut [3], Matjaž Spreitzer [1], Marija Vukomanović [1]
[1] Advanced materials Department, Jožef Stefan Institute, Ljubljana, Slovenia
[2] Jožef Stefan International Postgraduate School, Ljubljana, Slovenia
[3] Department of Biotechnology, Jožef Stefan Institute, Ljubljana, Slovenia

S1. PDLLA nanotexture morphology.

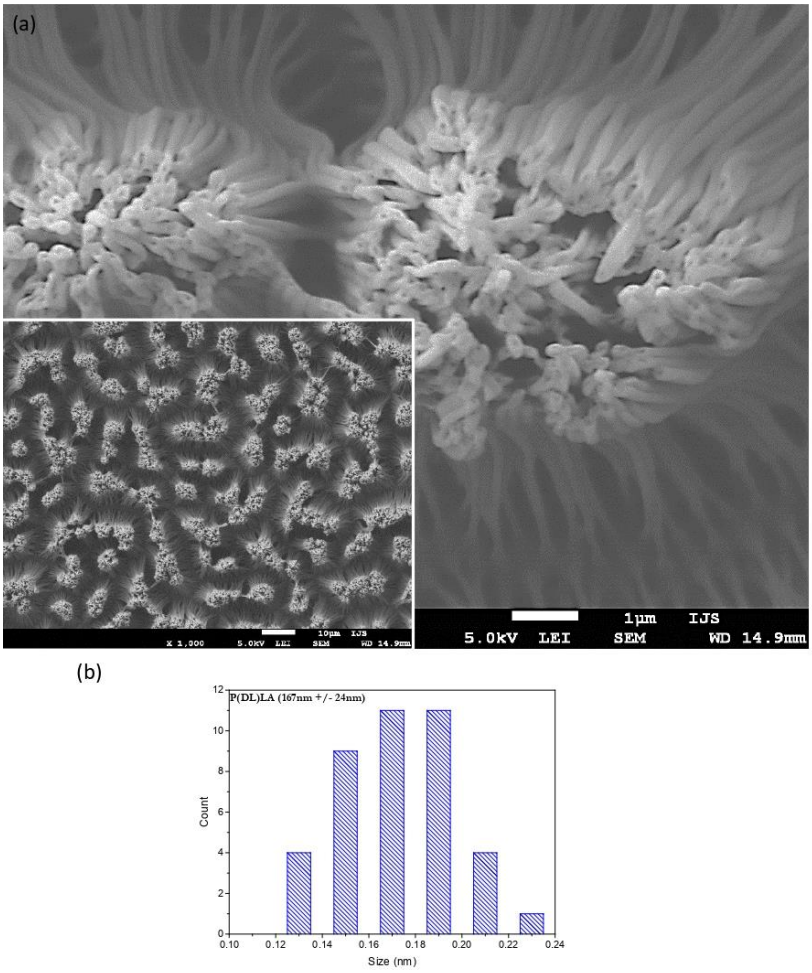

Figure S1. (a) SEM image of P(DL)LA nanotextured film and closer look confirming tube formation and (b) average diameter count from analysing SEM images.

Using the same template assisted method as we used to prepare piezoelectric nanotextured PLLA film we prepared reference sample as non-piezoelectric biodegradable nanotextured P(DL)LA film. Film was used for observing morphological effect on bacteria cells. After analysing some of the SEM images above 10,000x – 15,000x magnification, average pillar estimated diameter was 167 nm ± 24 nm, suggesting the full filling of the template pores (Fig. S1 (a,b)).

S2. Frequency signal comparison between piezoelectric and non-piezoelectric films under ultrasound (US) stimulation.

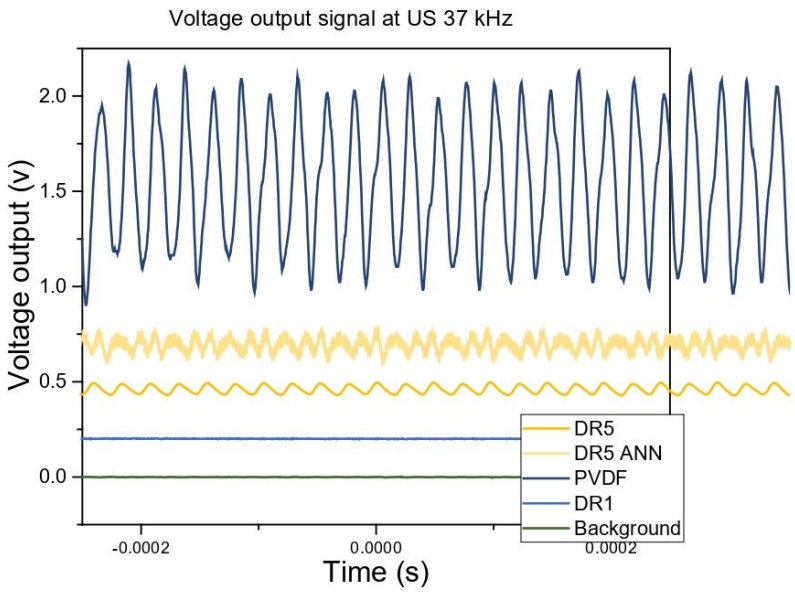

Figure S2. Voltage output as a function of time as frequency signal observed for different films (offset was used). Comparison of Voltage output for drawn film (DR5), non-drawn film (DR1), drawn and annealed (DR5 ANN), PVDF reference sample and background noise.

Clear difference is observed in voltage output frequency for non-drawn therefore non-piezoelectric film (DR1) or background noise compared to all other films, which shows some piezoelectricity (Fig. S2). Therefore, even the measured small signal from DR5 film is confirmed as piezoelectric property of the film.

S3. Methylene blue (MB) degradation in presence of hydrogen peroxide without ultrasound (US) stimulation.

For thin films and films with complex morphology as nanotexture on the surface, global piezoelectric coefficient is hard to be measured, therefore we confirmed it through the piezo potential for piezo-catalyzed organic dye degradation. Methylene blue (MB) acting as organic pollutant can be destroyed by reactive oxygen species (ROS), generated from H_2O_2 catalytic degradation [1]. Our polymer can be used as a piezo catalytic redox reagent to produce ROS (hydroxyl radicals (•OH), superoxide (•O2−), and singlet oxygen) from hydrogen peroxide medium. To activate piezoelectric properties ultrasound stimulation is one and very useful possibility to achieve mechanical deformation which result in polarization effect and charge generation on the film [2].

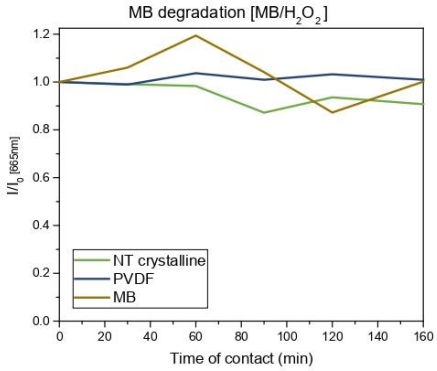

Figure S3. Methylene blue (MB) degradation curve in presence of active component (peroxide) and piezoelectric films without ultrasound (US) stimulation.

For MB degradation test, with 0.5 M H_2O_2 present, no degradation was observed for annealed NT film and PVDF reference, if no US stimulation was used after 2h of mixing, presented in the graph (Fig. S3). Those samples showed highest response with US stimulation under same addition of peroxide.

S4. Methylene blue (MB) degradation in presence of peroxide with US and added 0.5 M hydrogen peroxide as active component.

Methylene blue (MB) dye can be degraded with reactive oxygen species (ROS) over time. In our experiment, hydrogen peroxide is added as a source of formed ROS and piezoelectric films act as piezo-catalysers for peroxide reduction. Proposed mechanism of ROS production and MB degradation is:

$$ultrasound + piezo\ PLA \rightarrow e_{piezo} + h^{+}_{piezo}$$

$$H_2O_2 + e_{piezo} \rightarrow \boldsymbol{OH^{\cdot}} + OH^{-} + O_2$$

$$OH^{-} + h^{+}_{piezo} \rightarrow \boldsymbol{OH^{\cdot}}$$

$$H_2O_2 + h^{+}_{piezo} \rightarrow H^{+} + HOO^{\cdot}$$

$$\boldsymbol{OH^{\cdot} + MB \rightarrow CO_2 + H_2O}$$

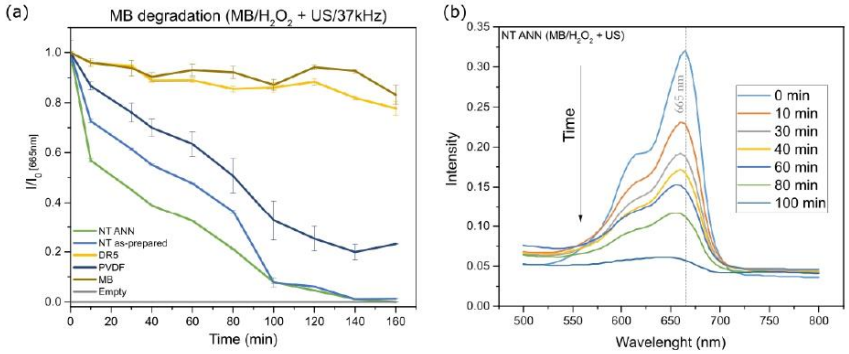

Figure S4. (a) Methylene (MB) degradation with added active component (peroxide) in presence of piezoelectric films (NT as prepared, NT annealed (NT ANN), drawn film (DR5), reference sample (PVDF)) under ultrasound (US) stimulation. (b) Associated absorbance spectra for NT ANN sample after different time of US stimulation.

By adding 0.5 M hydrogen peroxide (Fig. S4 (a,b)), the degradation process is slower and almost reaches 100 % degradation in 2 hours for nanotextured samples (NT ANN and NT as-prepared), compared to the previously added 1 M peroxide process completed before 1 hour of stimulation in the US for nanotextured samples and PVDF. Highest degradation rate is observed for nanotexture annealed sample, with similar end degradation after 2 h of US stimulation as NT as-prepared film. PVDF showed slower degradation rate, indicating lower piezoelectric potential compared to nanotextured films. Drawn piezoelectric film showed no degradation of MB dye.

Piezoelectric potential of prepared films is expected to be at least 2x higher at 37 kHz compared to higher frequency, since effect of mechanical stretching is higher. For piezoelectric properties films were measured at 37 kHz frequencies. Therefore, to see what is happening at conditions used for bacteria testing, which does not disturb bacteria growth, 80 kHz was used and observed the MB/H_2O_2 degradation (Fig. S5). Results again shows similar behaviour of the curves for NT ANN film and PVDF reference with slower degradation rate. Also confirming that piezoelectric effect is responsible for change in degradation rate, since at 37 kHz degradation is faster compared to 80 kHz.

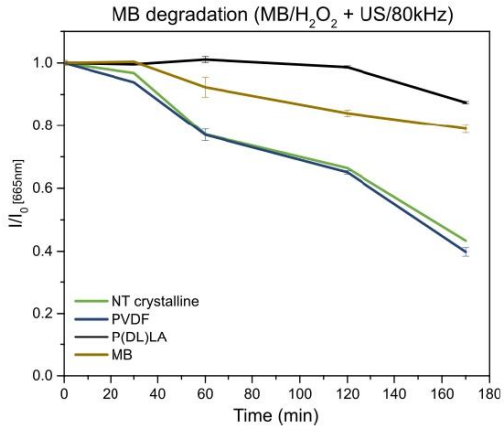

Figure S5. Methylene (MB) degradation with added active component (peroxide) in presence of piezoelectric films under ultrasound (US) stimulation at 80 kHz frequency.

Kinetics of MB degradation in presence of peroxide (0.5 and 1 M) and films under US stimulation (37 kHz and 80 kHz), and comparison with voltage output measurements for smooth films ($V_{pk-pk.}$) is presented in Table S1.

Table S1. Comparison of calculated degradation rate for different piezoelectric and non-piezoelectric films, with 0.5 or 1M hydrogen peroxide addition, stronger (37 kHz) or milder (80 kHz) ultrasound (US) stimulation, and measured direct voltage output under US stimulation.

Sample	H_2O_2 [**0.5M**] + US [**37kHz**]		H_2O_2 [**1M**] + US [**37kHz**]		H_2O_2 [**0.5M**] + US [**80kHz**]		Piezo with US mechanic stimulation (V_{p-p})	
	k (min^{-1})	Degradation at 1h of US	k (min^{-1})	Degradation at 1h of US	k (min^{-1})	Degradation at 1h of US	**37kHz**	**80kHz**
NT crystalline	0.0146	68 %	3.6154	97 %	0.0035	23 %	Not applicable	
NT amorphous	0.0136	52 %	1.0893	66 %	Not measured		Not applicable	
DR5	0.0013	11 %	Not measured		Not measured		59 mV	24 mV
PVDF	0.0098	34 %	3.1149	95 %	0.0037	23 %	1.2 V	450 mV
NT P(DL)LA film	0.0009	0 %	Not measured		0.0004	1 %	Not applicable	
MB	0.0008	7 %	0.14121	13 %	0,001	8 %	/	/

Values show faster kinetic for higher addition of peroxide (1M), since more ROS can be formed. However, it is also observed that with stronger US (37 kHz) compared to milder (80 kHz) for the same piezoelectric film (NT ANN for instance) degradation rate is 5 times higher (0.015 compared to 0.003

min^{-1}), indicating that piezoelectric properties effect degradation rate and ROS production from peroxide.

S5. Contact angle measurements of representative piezoelectric samples.

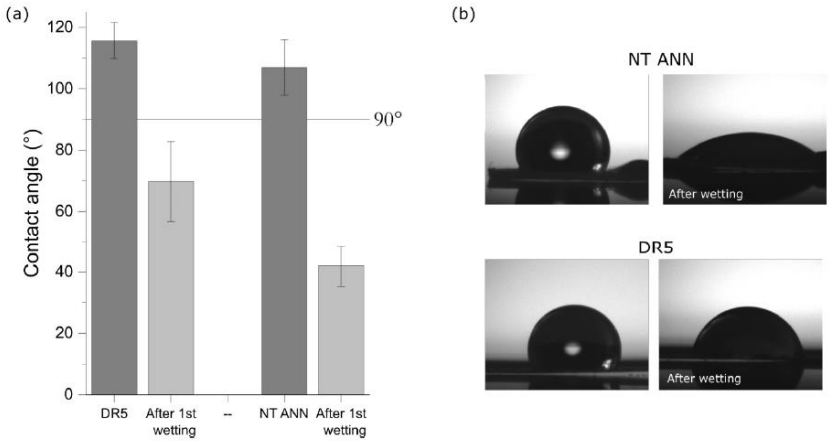

Figure S6. (a) Contact angle measurements of dry piezoelectric drawn (DR5) and nanotextured annealed film (NT ANN) and after wetted and wiped surface; (b) pictures of contact angle measurement for beforementioned samples.

For piezoelectric stretched (DR5) and nanotextured samples (NT ANN), contact angles were observed for 5 µl water dropped on the dry film surface (Fig. S6 (a,b)). We observe high angles of our samples, indicating more hydrophobic nature of the films. However, after the surface was initially wetted and wiped (not dried completely), observed angles were much lower (70° and 42° for DR5 and NT ANN films respectively), even more for NT sample. We believe in our assays after short time film is wetted and good contact is achieved between bacteria and suspension, however hydrophobicity can inhibit the contact of bacteria with film surface, suspecting mostly for the drawn DR5 films, where no effect of films was observed on bacteria viability and membrane integrity, even when ultrasound stimulation was used. Using US may improve needed bacteria-material contact and help to overcome hydrophobic properties.

S6. Antibacterial testing for *E. coli* and *S. epidermidis* in saline solution.

After contact test, where bacteria suspension was added on films, sonicated (80 kHz, 100% power, 30 min) and incubated in saline solution for 24 h, washed film solution was mixed with growth medium (LB) and viability of bacteria was estimated through fluorescence measurement of Presto blue indicator changing colour into more fluorescence after metabolic degradation of initial dye. It is clearly observed that only for non-piezoelectric film (DR1) and E. coli, bacteria freely grew and change colour into more fluorescent (Fig. S7). For nanotextured films no survival of bacteria was observed. Similar was confirmed when films were put on solid agar plate to really observe any remained bacteria on the

film (Fig. S7 right). Again, for nanotextured piezoelectric films no growth was observed. Since all bacteria on the films were dead, bacteriocidic effect of piezoelectric nanotexture film was confirmed.

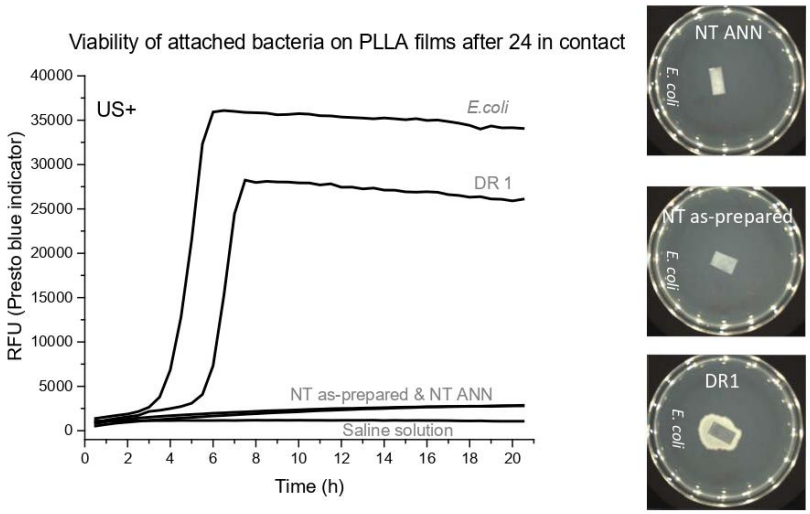

Figure S7. Viability of attached E. coli bacteria on tested films (DR1, NT as-prepared and NT ANN) after incubation at 30 min of US and in saline solution for 21 h, with pictures of petri dishes with films put on solid agar.

Similar was observed when contact test with *S. epidermidis* bacteria was performed. Observing the growth of only attached bacteria, for nanotextured films none colony was formed, when around DR1 film the growth is obvious (Fig S8).

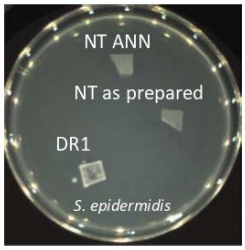

Figure S8. Agar plate presenting survival of attached S. epidermidis bacteria on tested films (DR1, NT as-prepared and NT ANN) after incubation at 30 min of US and in saline solution for 24h.

We also observed viability of washed bacteria (Fig. S9 (a,b)) after contact test to clearly confirm dead bacteria. For NT films with or without ultrasound stimulation, in close contact test, both bacteria (*E. coli* and *S. epidermidis*) was killed. No viability through presto blue fluorescence was observed, compared to smooth piezoelectric films or reference bacteria. Small effect of piezoelectricity for drawn film was observed (suspected less bacteria at start due to the shift of curve increase to later time), if US was used, compared to the curve without US stimulation. Since for the bacteria with or without stimulation, curve is the same.

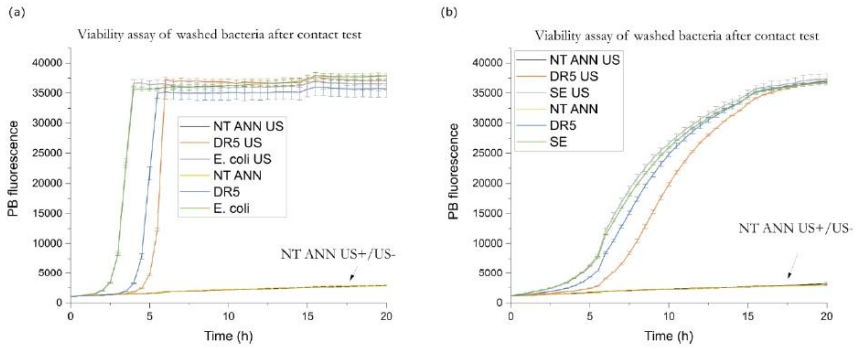

Figure S9. Viability assay through Presto blue fluorescence measurement. Washed bacteria after close contact with piezoelectric nanotextured (NT ANN), piezoelectric drawn (DR5) films and reference (a) E. coli and (b) S. epidermidis bacteria with or without US stimulation.

After contact testing, piezo-degradation potential for methylene blue dye was examined for NT ANN samples after the contact test preformed twice with *E. coli* bacteria and washed with 70% ethanol. If we observe washed sample under SEM without Glutaraldehyde fixation, most bacteria or bacteria leftovers are washed away, therefore active piezo-potential was expected (Fig S10 (a)). Conditions for piezo-potential testing were the same (0.5 mg/ml MB, 0.5 M peroxide), however samples were smaller, therefore reference samples with the same size were compared to assess the piezo-potential loss. Result show some decrease in piezo-potential (60 %), however still present (Fig. S10 (b)). Some degradation due to US or bacteria, ethanol spraying can be the reason for some loss in piezoelectric signal.

10

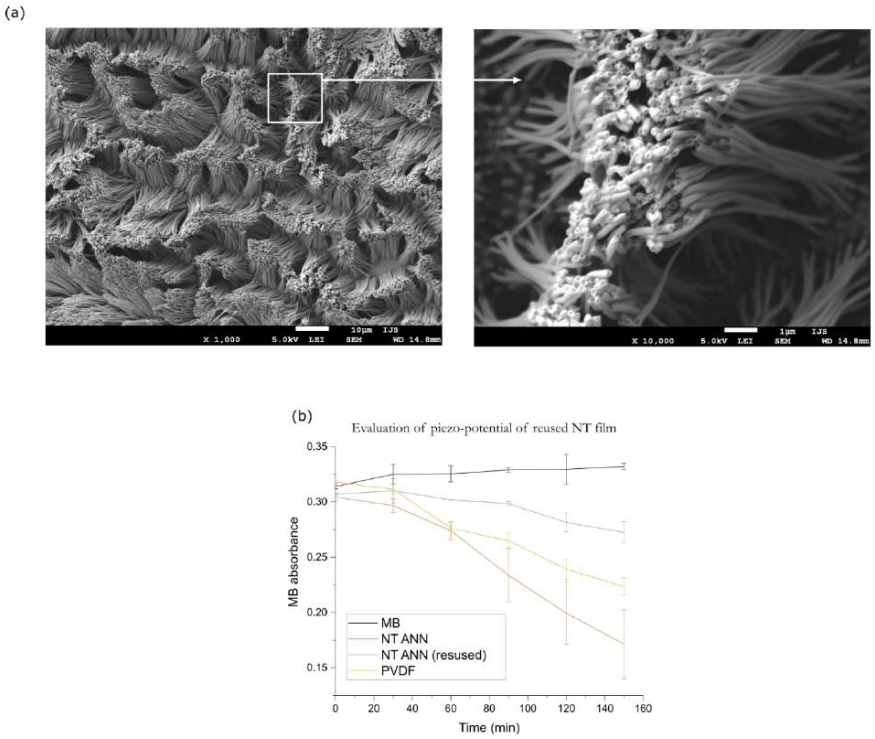

Figure S10 (a) SEM images of nanotextured annealed sample (NT ANN) after close contact test with E.coli and washing with 70% ethanol and closer look on the right; (b) methylene blue (MB) degradation potential assessment for NT ANN samples compared to non-used NT ANN sample, PVDF reference and MB dye.

S7. SEM observation of annealed and as prepared nanotubes after 30 min of ultrasound (US) sonication.

SEM analysis showed difference before and after sonication in ultrasonic bath at frequency 80 kHz for 30 minutes, as were the typical process parameter for bacteria testing. For as-prepared films (Fig. S11 (a)) fibers are all over the place after sonication for 30 minutes, when for annealed samples (Fig. S11 (b)), they stay in island formation, as was the initial construction for both samples. After 30 minutes of sonication, almost all fibers stay attached on the film substrate.

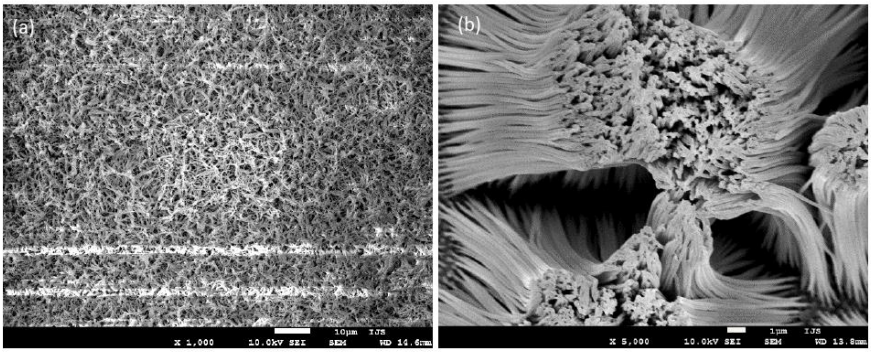

Figure S11. SEM images of nanotextured films after 30 min of US sonication (80 kHz) for (a) NT as-prepared sample and (b) NT ANN sample.

S8. Haemolysis test for piezoelectric films with references without US or US at 80 kHz with 100 % power.

Any damage of red blood cells (RBC) were excluded when nanotextured or smooth, piezoelectric or non-piezoelectric films were in contact with RBCs, if US was not implemented (Fig. S12, left part of the picture), observed through released haemoglobin detection (absorbance measurement) from damaged cells. Similar was observed (less than 2 % damage of RBC) for US stimulated under 80 kHz for 30 min and only 30 % power. Undamaged RBCs with films still inside were also visually confirmed with observing Eppendorf tubes right after US (Fig. S13), where turbid liquid for NT ANN, NT as-prepared and DR5 confirm undamaged RBC and clear red liquid (RBC in water) means dead RBCs. However, difference occur if full power US was used at 80 kHz, where 40 % (NT ANN and NT as-prepared) or 90 % (NT P(DL)LA) damaged cells were observed for nanotextured films, regardless of their piezoelectric properties. This observation clearly indicates negative morphological effect on RBC only after more powerful US stimulation. When comparing piezoelectric with non-piezoelectric films with same morphology, piezoelectricity help survive more RBC compared to more damaged cells in contact with non-piezoelectric samples (NT P(DL)LA and DR1).

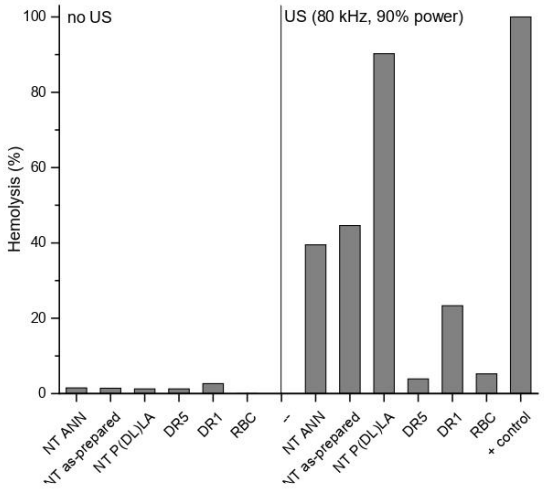

Figure S12. Hemolysis test for detecting damaged red blood cells (RBC) in contact with films (nanotextured piezoelectric- NT ANN, NT as- prepared and non-piezoelectric- NT P(DL)LA; or smooth piezoelectric- DR5 and non-piezoelectric- DR1) without US (left part) or with 80 kHz US for 30 min and 100 % power (right part).

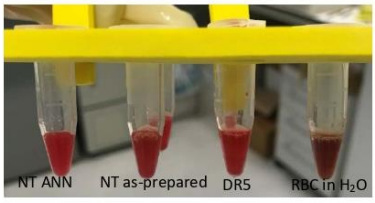

Figure S13. Visual observation of tested films in RBC solution (NT ANN, NT as-prepared, DR5 and fully damaged RBC in water) after US stimulation in Eppendorf tubes.

Literature:

[1] L. I. Jinga *et al.*, "Chemical Degradation of Methylene Blue Dye Using TiO2/Au Nanoparticles," *Nanomaterials*, vol. 11, no. 1605, pp. 1–10, 2021.

[2] G. G. Genchi *et al.*, "P (VDF-TrFE)/ BaTiO 3 Nanoparticle Composite Films Mediate Piezoelectric Stimulation and Promote Differentiation of SH-SY5Y Neuroblastoma Cells," 2016.

Chapter 6

Interactions of Drawn and Nanotextured Piezoelectric Films with Human Adherent and Immune Cells

This chapter provides an overview of the response of human adherent cells (keratinocyte, as representatives for human skin cellular response and macrophages derived from THP-1 monocytes, as representatives of the immune response) when in contact with piezoelectric or non-piezoelectric, drawn or NT PLLA films. With mechanical stimulation through US, the film is deformed to exhibit its piezoelectric properties. A high-power US bath at a frequency of 80 kHz or a low-power US probe at 1 MHz is used for stimulation, which causes a greater or lesser piezoelectric response of the film, respectively (presented in Appendix A2). Firstly, cell attachment is improved for drawn and NT surfaces compared to the glass or just pressed smooth film, due to the rougher surface topography. For the cells seeded on the film, a good transmission of stimuli is expected, so the effect of electrostimulation can be observed. When working with cells, the films were never additionally coated with poly-L-lysine (PLL), as noted in many other papers as a method to improve cell attachment, as a comparison between the films and films coated with PLL did not result in greater cell attachment (presented in Appendix A3) or later the change in proliferation. For keratinocytes, improved proliferation was not observed, however a significant difference in the shape of the attached bacteria was seen, where more elongated cells were observed after (piezo)electric stimulation, an increase in actin filament production was enhanced, and improved cell-to-cell connections through formed filopodia. Cell migration towards wound closure was mostly enhanced by mechanical stimulation (US) compared to electrical stimulation. An interesting observation was made in cells attached to piezoelectric NT films and US stimulated by an US bath, where damaged cell membranes were observed, but not under milder conditions using US probe. This indicates the excessive piezoelectric properties of the US bath-activated NT film, which produces a much higher output voltage compared to the drawn film.

Regarding the immune response, the differentiation of monocytes (white blood cells) into macrophages was near 25%, as determined by the viability of only adherent cells on the films. Subsequent stimulation did not result in increased cell proliferation compared to phorbol 12-myristate 13-acetatechemically (PMA) induced macrophages for control, pointing to a minimal immune response towards the PLLA polymer films, piezoelectric or not. When observing the morphology, M2 polarization of macrophages (towards wound

remodeling) was observed for the drawn film stimulated under mild conditions and more similar to M1 (inflammatory response) for piezoelectric NT samples, probably due to the nano size of the contact felt by the cells and due to the movement of the tubes under US, as macrophage fusion was observed.

Overall, the most promising effect on cells regarding wound healing through (piezo)electric stimulation was observed for drawn piezoelectric films when stimulated under mild conditions (US probe, 1 MHz).

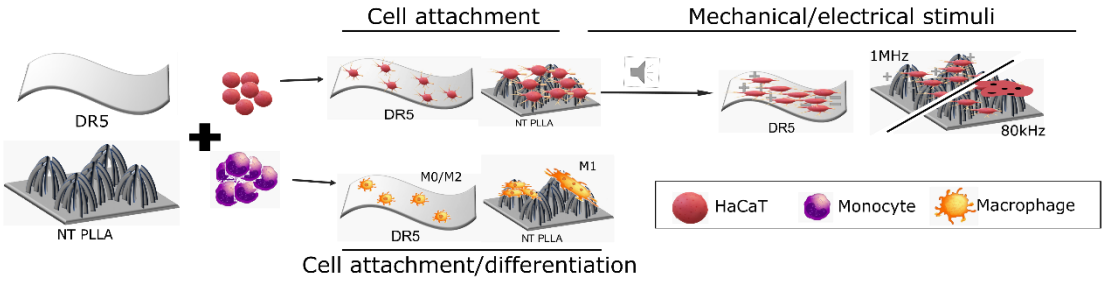

Figure 15: Demonstration of initial attachment of skin (HaCaT) cells or differentiation of monocytic cells (THP-1) into macrophages, indicating an immune response and further mechanical/electrical impact on the cells activated by 80 kHz or 1 MHz US stimulation. Damaged cells are observed only on the nanotextured film with enhanced piezoelectric properties, only when stimulated using high power conditions (80 kHz), which also results in a larger piezoelectric response, while beneficial effects were observed for piezoelectric drawn films.

6.1 Contact-Based Electrical Stimulation via Biodegradable Piezoelectric Poly-L-Lactic Acid Polymer to Promote Wound Healing

ABSTRACT:
Electrical stimulation with biocompatible piezoelectric materials is a novel battery-free, externally controlled method for transmitting electrical stimulation directly on the wound side. The use of poly-l-lactic acid (PLLA) as a piezoelectric film that is mechanically deformed externally by ultrasound (US) to allow electrical stimulation of cells in close contact has the main advantage of biodegradability and more suitable piezoelectric properties than other ceramic or polymer piezoelectrics. I prepared drawn and nanotextured (NT) PLLA films with confirmed piezoelectric properties to observe changes in cell behavior using external mechanical deformation in the form of US. Improved initial protein binding and cell attachment to the NT and drawn smooth film were observed as a result of more rough morphology. Increased formation and orientation of F-actin filaments show a positive effect of contact-based electrical stimulation with piezoelectric drawn films, while for NT samples US and tube movement has a predominant effect on cell behavior. A reduced proliferation relative to a non-piezoelectric reference was observed for the piezoelectric drawn film, suggesting cell differentiation in response to (piezo)electrical stimulation activated by low-power US probe. Some immune response of prepared piezoelectric, non-piezoelectric, NT or smooth films was observed. Similar initial binding of monocyte (THP-1)-derived macrophages was observed on all samples, with morphological changes occurring after US incubation. On NT piezoelectric PLLA samples, I observed an inflammatory type of macrophages in the form of fused macrophages as giant cell, observed as a film-like structure over the tubes. But a promising indication for M2 polarization was observed in cells attached on a drawn piezoelectric film. I have shown that the use of drawn piezoelectric film (DR5) made of PLLA provide contact-based and externally controlled electrical stimulation on cells which could promote wound healing with expected small initial immune response when inserted inside the body.

Keywords: piezoelectric polymer, poly-L-lactic acid, HaCaT keratinocytes, wound healing, cell proliferation, contact-based mechanism, monocyte differentiation, macrophage fusion

6.1.1 Introduction:

Electric charges are present all around us and also inside the human body and give great importance to the connection and signaling of cells. Human body generates biological electrical fields by stress-generated potential which are also responsible for natural regeneration, such as endogenous electric field [59]. Therefore, one of potential stimulation to accelerate healing process is electrical stimulation, which has been shown *in vivo* and *in vitro* to improve cell proliferation, migration or differentiation [103].

Wound healing starts with hemostasis to control bleeding, continues with the migration of inflammatory cells to the wound site, granulation tissue formation, collagen repair, vascularization and re-epithelization [104]. Briefly, when injury occurs and disrupts the

endogenous electric field, electric current between 100-150 mV/mm is produced between wound site and undamaged area, which promotes directional flow of important biological material towards the wound [105]. Since most wounds take a week or two to heal or is even greatly prolonged in case of chronic wounds, electric stimulation could accelerate the healing process. Electric stimulation is mostly explained through effect on voltage-gated ion channels of Ca^{2+} ions, which increases intracellular calcium concentration and triggers many paths (such as ERK ½ and Akt pathway) that leads to direct cell activity through increased growth factor and actin filament production to promote cell polarization, proliferation, differentiation and/or migration [58], [59].

Different cell response is expected when changing stimuli parameters or observing effect on different cells. Direct current (DC) treatment have high effect on directional cell migration [106], it can be replaced by pulsed current (PC) to reduce electrothermal and electrochemical hazards of DC [107]. Devendra showed that using alternating current, volume wound reduction was faster compared to DC simulated current for artificially created wound on rats and rabbits [108], therefore also appropriate to promote healing. Improper stimulation parameters such as high intensity electric stimulation (>100 V/cm) can cause membrane electroporation, increase in ROS, which induce cell apoptosis instead of wound healing [59]. How to impart electric stimulation is an important question, therefore to avoid invasive electrode implementation near the damaged tissue, electroactive materials are a suitable solution. They can convert different types of signals (mechanical, thermal, and magnetic) into electrical ones, which provides the opportunity to use them for the stimulation of cell growth in tissue regeneration [109]. One of such materials are piezoelectrics, which have no energy or power supply requirements to promote transient surface charge as response to mechanical deformation.

Using piezoelectric material, electrochemical self-stimulation can be easily achieved through cell adhesion [110], body movement or using outside source such as US [89]. By using piezoelectric devices in combination with US, remote control is achieved. Since low-voltage stimulation is required, piezoelectric biocompatible polymers are particularly suitable for such stimulation. Most promising material is PLLA due to its small piezoelectricity (d_{14} = 10 pC/N [44]) and most important its full biodegradability, leaving the advantage of not needed removal from the body.

Electrical stimulation has been shown to be effective in the regeneration of mammalian cells, but the applicability of piezoelectrics in such case is still at the beginning of research. Most promising cells, responsive to electrical stimulation, in case of tissue regeneration are nervous, bone and muscle cells [89], in case of epidermal wound healing, fibroblast and keratinocyte also shows response to electric stimulation. Ceramic piezoelectric materials with high piezoelectric properties (boron nitride nanotubes, barium titanite nanoparticles, zinc oxide nanomaterial) are having problem with cytotoxicity (ROS production), cytocompatibility, hydrophobicity, non-degradability, therefore many authors tend to prepare composites with biocompatible polymers to improve cell -material contact [89]. Using polymer coating over piezoelectrics lowers the piezoelectric value, however the range of needed excitation in biology is very low compared to electronic devices, therefore sufficient electrical stimulation can be expected. Some studies confirm beneficial effect of electrical stimulation using organic piezoelectrics to promote stimulation, such as bone tissue promotion through osteogenic differentiation of stem cells and enhanced mineralization [99], [111], neuronal growth elongation and differentiation [16], enhanced proliferation of pre-osteoblastic cells [112], differentiation of keratinocytes [62], stem cell differentiation [113], enhance migration, adhesion and secretion of fibroblasts [56], [101], [109], [114]. Mentioned promotions of used piezoelectric polymers are presented in Table 1 with information about stimulation of polymer to exhibit piezoelectric properties. Using biodegradable, biocompatible polymer piezoelectrics avoid many disadvantages of

electrostimulation, as reducing the electrothermal and electrochemical hazards which leads to cytotoxic effect [109].

Table 1: Collected data on piezoelectric polymers, their stimulation to exhibit piezoelectric properties and observed effect on investigated cells.

Application	**Material**	**Stimulation of polymer**	**Ref.**
Osteogenic differentiation of stem cells and enhanced mineralization (bone tissue)	Electrospun poly(3-hydroxybutyrate-co-3-hydroxyvalerate) scaffold (PHBV-SiHA)	/	[111]
	Electrospun PLLA (output voltage 25-30mV)	US: 40 kHz	[99]
Neuronal growth elongation and differentiation	Polyvinylidene difluoride (PVDF)	US: 132 kHz, 5 x per day for 10 min	[16]
Enhanced proliferation of pre-osteoblastic cells	Poled PVDF	Mechanical stimulation using vibrational module at 1 Hz	[112]
Differentiation of keratinocytes	Stimulated through carbon–silicone electrodes	PC current, 4.8 kHz, 3 V, 5 min per day	[62]
Enhance neurogenesis and osteogenesis (stem cell differentiation)	Electrospun PLLA fibers (generate 0.5-10 mV)	Cell-matrix adhesion through focal adhesion complexes	[115]
Enhance migration, adhesion and secretion of fibroblasts	PLLA nanotubes	Through cell attachment	[101]
	Polyurethane/polyvinylidene fluoride (PU/PVDF) piezoelectric scaffolds	Mechanical stretching with 0.5 Hz for 24 h	[56]
	Electrospun PVDF hydrogel patch	Loudspeaker stimulation	[109]
	Heparin bioactivated polypyrrol/PLLA conductive membranes	DC electrical stimulation of 50 or 200 mV/mm	[114]

When focused on epidermal wound healing effect, keratinocytes constitute 95% of the epidermal cells and play multiple roles in skin repair [116]. Usually they work in union with

fibroblast cells [117], where keratinocytes are the initiators and executors of the re-epithelization process. They migrate, proliferate and differentiate to restore epidermal barrier. HaCaT cells are immortalized human keratinocyte cell line which is usually used as a model for the study of wound healing [118]. For keratinocyte cells, some report about the increased proliferation for cells, other showed no significant change or delay in proliferation, however in most of the studies, growth factor enhancement is observed [104], [117]. Arai et al. showed that for keratinocyte cells under PC stimulation (3 V), differentiation rather occur which slows the proliferation process [62]. Change was detected through increase in differentiation markers, such as keratin 10, involucrin and filaggrin, through increase in intracellular-free Ca^{2+} concentration and inhibition of proliferation [62].

An important aspect to consider is also the immune response of the body (white blood cells, macrophages) to the introduced material. Macrophages play a crucial role in wound healing and implementation as a key factor of determining the balance between inflammatory or remodeling response [69]. Macrophages are adherent cells, differentiated from non-adherent monocytes from peripheral blood, which occur when tissue is damaged and they attach on the damaged surface and acts against bacteria, viruses or implant present and trigger inflammatory response (M1 type) [67], [68]. Later on, macrophage can change polarization (differentiate into M2 type) to help with the regeneration, re-establishing the tissue integrity, observed as macrophage proliferation [67]. A group from Germany observed *in vivo* that is possible that electric stimulation could shift the macrophage response to injury from healing/scarring to regeneration [73] after 7 days of stimulation.

In this context, I have prepared biodegradable piezoelectric PLLA smooth films and films with introduced NT topography on the surface to observe and compare the changes in HaCaT cell behavior after mechanical stimulation to activate (piezo)electric properties of the film. Since keratinocyte HaCaT cells can sensitively respond to electrical stimuli [116], these cells were chosen for the cell model in this study of piezoelectrically induced electrical stimulation on cells. For the NT films, some cell attachment improvements were expected, since the texture reminds on extracellular matrix (ECM, randomly dispersed actin filaments) which should mimic the natural cell environment. I also evaluated the immune response of monocyte-derived macrophages as their numerical attachment to the film surface and observe morphology changes after US stimulation.

6.1.2 Experimental

Poly-L-lactic acid polymer (PLLA) L207 S (Evonik, Germany) was used to prepare piezoelectric polymer film samples in NT and smooth form. For non-piezoelectric NT films, Poly (D,L-lactide-co-glycolide; PDLLA) RG-505, 50:50 (Evonik, Germany) polymer was used as it is incapable of crystallization. Chemicals that were used in template assisted method for template removal are hydrochloric acid- HCl (J.T. Baker, Poland), copper (II) chloride- CuCl2x2H2O (Riedel-de Haën AG, Germany) and orthophosphoric acid 85% (VWR Chemicals BDH, France).

For cell testing, HaCaT human keratinocyte cells were kindly provided by Biochemistry and Molecular and Structural Biology Department (B1) at Jožef Stefan Institute (ATCC PCS-200-011). Growth medium was prepared as mixture of Dulbecco's Modified Eagle Medium- high glucose (DMEM, Sigma-Aldrich, USA) supplemented with 10% Fetal Bovine Serum (FBS, Gibco, USA) and 1% of Penicillin-Streptomycin antibiotics 1:1 (Gibco, USA). Cells were washed using Dulbecco's Phosphate buffered saline (DPBS, Sigma-Aldrich, USA) and trypsinization by TrypLE select (Gibco, USA). PrestoBlue™ Cell Viability Reagent (PB, Invitrogen by Thermo Fisher Scientific) was used for cell viability observation and Live/Dead Viability/cytotoxicity Kit (L3224, Invitrogen, Life

technologies, USA) to optically observe cells. In all cases MIlliQ (Purelab Option-Q, Elga) clean water was used.

Smooth piezoelectric film was prepared by uniaxially drawing amorphous sheet at the temperature above the glass transition (80°C) at 40 mm/min draw rate to draw ratio 5 (DR5) (Fig. 16a) [39]. NT piezoelectric films were prepared by pressing polymer melt into well-defined nonporous anodized aluminum oxide template on aluminum substrate with 200 nm x 30 µm pores (AAO, Topmembranes, China [80]) [49]. Film was afterwards annealed at 160°C for 1 h in template to increase crystallinity. To separate NT polymer film, template was chemically etched in 40% phosphoric acid, next in $CuCl_2$/HCl (4%/2%) water solution and again in 40% phosphoric acid. At each step samples were washed with water (Fig. 16b).

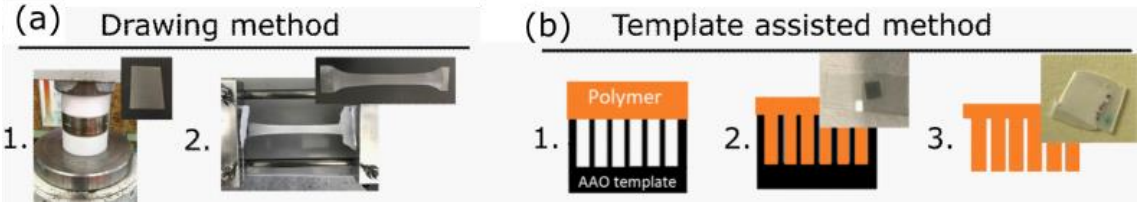

Figure 16: Schematic presentation of film preparation using (a) drawing (1. hot pressing and 2. drawing) or (b) template assisted method (1. AAO on polymer melt, 2. filled pores and 3. released nanotextured surface after chemically removed template).

To observe protein binding from FBS at the surface of 1 cm^2 of piezoelectric or non-piezoelectric, smooth or NT samples, films were analyzed using procedure and calibration curve from bovine serum albumin (BSA) kit. Films were incubated in 200 µl FBS for 24 h at 37°C in polystyrene (PS) plate. In next step they were washed three times in DPBS. To quantify attached proteins, washed films were incubated in 1 ml of 2% SDS solution in DPBS for 24 h at room temperature to release the proteins from the surface. The amount of released proteins was measured in triplicate as optical density read at 562 nm, based on bicinchoninic acid (BCA) colorimetric detection of the cuprous cation obtained by protein Cu^{2+} reduction in an alkaline medium, as reported in detail in [34]. PS plate was used for control surface.

To observe cell adhesion, proliferation or migration, HaCaT cells were initially cultured in recommended DMEM medium supplemented with 10% of FBS and 1% of antibiotic in humidified incubator at 37°C and 5% CO_2. For cell attachment, supplemented DMEM medium was used to observe 50 µl of trypsinized cells (5x 10^5 cells/ml in medium) attaching to exposed films in 24 h. In this step (after 24 h), cellular cytotoxicity was also evaluated by measuring the PB of cells incubated with the films from the beginning. After cell attachment, films were moved to a new plate and 40 µl of PB was added in 400 µl DMEM mixture and incubated for 1 h to measure cell viability of attached cells on the film surface through fluorescence measurement of metabolized non-fluorescent resazurin reduced to the fluorescent resorufin (excitation at 535 nm, emission at 590 nm). Values were normalized to surface area of film piece. To observe cell cytotoxicity, 50 µl of trypsinized cells (80% confluent growth) were seeded on cell culture PS plates for 3 days and covered with 1 cm^2 film sample in 400 µl cell medium for 24 h. Afterwards, PB was added to measure cell viability through fluorescence. To observe cell proliferation, 1 cm^2 films were immersed in cell solution in 24-well plate for 1 day for cells to attach. Afterwards, films were transferred into fresh medium and viability was measured daily using PB for the next 3 days with or without US stimulation. Each time PB was washed with DPBS and fresh medium was added. For US stimulation after the seeding, covered PS plate was additionally sealed with parafilm and sonicated each day in a) ultrasonic bath for 20 min

at 80 kHz (30% power), temperature not exciding 35°C and b) via ultrasonic probe for 3 min, 1 MHz frequency, 1:10 s pulsed current and with power of 1.8 W/cm^2 (schematics of stimulation presented in Appendix A2). For simplicity of understanding, Fig. 17a schematically shows the testing procedure on HaCaT cells to measure cytotoxicity, adhesion and subsequent cell proliferation.

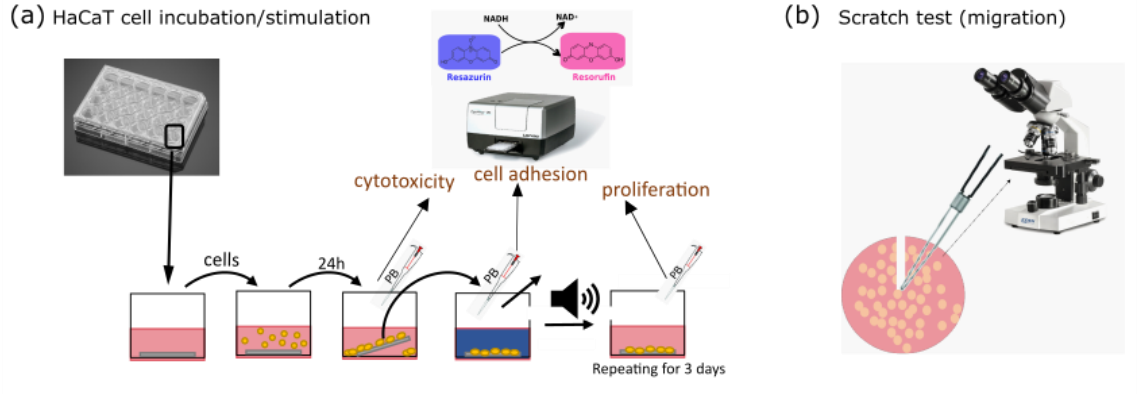

Figure 17: (a) Schematic of testing on HaCaT cells: initial incubation with film samples in 24-well PS plate for 24 h to determine cytotoxicity via measuring PrestoBlue^{TM} (PB) cell viability through cell metabolic activity reducing resazurin into resorufin, transferring the films with attached cells and measuring viability to determine cell adhesion, and US stimulating after washing the samples for the next 3 days, measuring PB viability daily to determine proliferation of cells; (b) presentation of a scratch assay to determine cell migration where a pipette tip creates a scar on confluent cells attached to a PS plate and observes cell migration towards wound closure with an optical microscope after 24 hours.

To observe cell migration, after confluent growth in 96-well PS plate, scratch was made using pipette tip and non-adhered cells were washed using DPBS twice. In the next step round films were prepared by hole punch to cover the entire cell seeded region (tissue cultured 96-well plate) in FBS low medium (1% FBS and 1% antibiotic in DMEM) and incubated for 24 h with or without 30 min US (80 kHz) stimulation. Next day, live/dead imaging was performed according to the provider of the test. A 100 µl drop of a die mixture (green-fluorescent calcein-AM and red-fluorescent ethidium homodimer-1) was put on film and observed under fluorescence inverted microscope (Nikon Eclipse Ti-U inverted microscope). Pictures were automatically analyzed in ImageJ using processing from Venter et al. [119] to calculate area reduction as area after 20 h of incubation normalized to area at start. The schematic of the test is shown in Fig. 17b.

For analysis of F-actin filament distribution in cells, I performed staining after 3-day incubation of cells, seeded directly on films. First, cells were fixed in 200 µl of 3.7% paraformaldehyde in DPBS (Sigma-Aldrich, Germany), washed twice in DPBS (200 µl) and permeabilized with 400 µl of DPBS containing 4 µl of 0.5% Triton X-100 (Sigma-Aldrich Life science, USA), during 15 minutes for each step at room temperature, followed by washing in DPBS (200 µl) two times. Samples were then stained with DAPI (diamidino-2-phenylindole, Biotium, Fremont, CA in Hank's balanced salt solution; 200 µl of stock, 5 µl/ml) for nucleus observation and Rhodamine Phalloidin (RP, Invitrogen by Thermo Fisher Scientific, USA; 200 µl of DPBS with 1 µl RP stock 200 µl/ml) for F-actin filament observation. Fluorescence images were obtained by fluorescence inverted microscope using red and blue filters. Using microplate reader, fluorescence of DAPI and RP were measured after 1 h of staining at Ex/Em 355/346 nm and 584/562 nm, respectively, and presented as fluorescence of number of cells (DAPI) and actin filaments normalized per cell number obtained through RP/DAPI fluorescence measurement.

For evaluating immune response, acute monocytic leukemia (THP-1, ATCC TIB-202) monocytes were kindly provided from Department of Biotechnology (B3), Jožef Stefan Institute. Cells were grown under ATCC-recommended culture conditions prior to use. Cells were defrosted and incubated for 10 days, when normal growth and shape was observed for further implementation. Cells were incubated in RPMI-1640 medium, supplemented with heat-inactivated FBS and 1% penicillin/streptomycin (obtained from Gibco, USA) and medium was replaced every second- or third-day using centrifugation. One set of cells were stained with CFSE CellTrace™ dye (Invitrogen by Thermo Fisher scientific) to observe under fluorescence inverted microscope using green filter. For testing, 5x10^4 monocyte cells per well were introduced with the material in 400 µl growth medium and incubated for 2 days. Non-adherent cells were washed and medium was replaced to observe attachment/differentiation into macrophages. For the control, THP-1 cells in presence of 100 nM phorbol 12-myristate 13-acetate (PMA, Sigma-Aldrich) were incubated for 2 days to initiate cell differentiation into attached macrophages. Viability was measured by PB same as for keratinocyte cells. After the attachment, films were subjected to US stimulation using same condition by US bath (80 kHz) and US probe (1 MHz) for 2 days. After the last stimulation, PB viability test was performed (value of empty PB dye in DMEM was subtracted from all measurements), actin filament and nucleus were stained and measured with the same protocol as for the keratinocyte cells and presented as F-actin production per number of nuclei.

Characterization of the film and film/cell morphology was performed using a scanning electron microscope (SEM-JSM 7600F, Jeol) to observe morphology changes of gold sputtered samples (BAL-TEC SCD) using accelerated voltage of 5 (films) or 10 kV (films with cells). Films with cells were prepared in advance according to the following protocol: cells were incubated for 2 hours in 2.5% glutaraldehyde (25% aqueous solution, Sigma-Aldrich, USA) and DPBS solution; washed with 3x DPBS and dehydrated with ethanol/water solutions (10%, 20%, 30%, 40%, 50%, 60%, 2x70%, 80%, 90% and 2x100%) for 5 minutes at each concentration; then a 50% hexamethyldisilazane (HMDS, Sigma-Aldrich, Germany) solution in ethanol was added and after 2x 100% HMDS for 10 min and allowed to air dry.

Statistics. The results were expressed as mean ± standard deviation. The statistical significance analysis of results between groups was carried out by one-way ANOVA at a confidence level of 95%. A probability value (p) of < 0.05 was considered to be statistically significant.

6.1.3 Results and discussion

The use of piezoelectric polymers, including PLLA, has been recently introduced for improved tissue healing. However, in most of these studies they included some additional factors to effect cell changes, such as growth factors, which in combination with electrical stimulation contribute to better cell differentiation [99]. The use of solely piezoelectric effect as the main stimulator to produce electrical stimulation on cells is still insufficiently researched.

''Remotely controlled and battery-free biodegradable electrical stimulator'' as Das et al. stated for theirs electrospun scaffolds [99], is in my case achieved by using prepared NT or drawn piezoelectric polymer films as contact-based mechanism of cell stimulation, remotely activated via US. In the tested human keratinocyte cells (HaCaT) as a model for wound healing, I mainly observed an effect on cell spreading, elongation and production of F-actin filaments in response to AC stimulation through drawn piezoelectric films (DR5) externally mechanically deformed by US with a promising indication towards cell differentiation and

for the immune response towards a healing type of macrophage polarization (M2) in the case of using 1 MHz US stimulation.

6.1.3.1 Film morphology

For PLLA to exhibit shear piezoelectric properties, main helix chains need to be oriented (similar C=O molecular dipole orientation after shear deformation results in generation of net charge on the surface) and crystalline (deformation can be imparted mostly on crystalline parts) [31], [39]. In both methods used for processing polymeric films, drawing and template assisted method, orientation and crystallization is induced via strain. In case of the drawn films they occur in drawing direction and for NT films in pore direction due to the capillary flow of viscous polymer melt inside the pores, as presented in more details in my previous studies [39], [49]. I also confirmed piezoelectric properties of both morphologically different films, with at least 10 times improved piezoelectricity for NT compared to drawn films (estimated values for US stimulation at 37 kHz are $V_{pk\text{-}pk} > 1$ V and 25 mV, respectively), using reference sample with known piezoelectric value, determined through indirect chemical method [49]. In this study, morphologically smooth (drawn DR5 films, Fig. 18a) compared to NT films (Fig. 18b) are being observed for interactions with human keratinocyte cells.

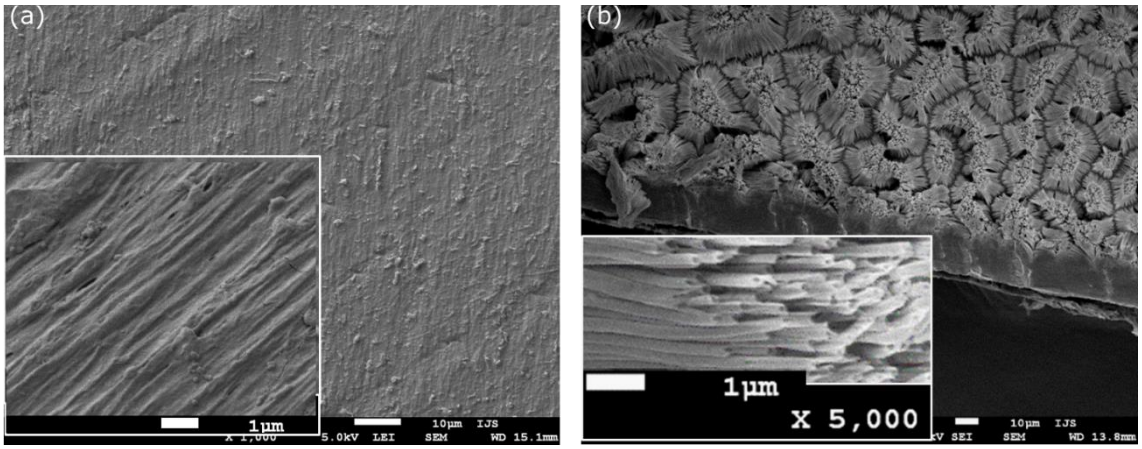

Figure 18: Observation of film morphology using SEM for (a) drawn films DR5 with smooth but rough surface and (b) NT films with 200 nm thick nanotubes on polymer surface.

6.1.3.2 HaCaT cell attachment

The biological response to electric stimulation demonstrates first in protein absorption, which is also a first step in interaction of cells with surrounding material [103]. This step could mediate cells attachment and subsequently tissue growth. Surface of the cell membrane usually carries negatively charged groups (carboxylates and phosphates) [120], therefore positive surface charge of material can also improve cell adsorption.

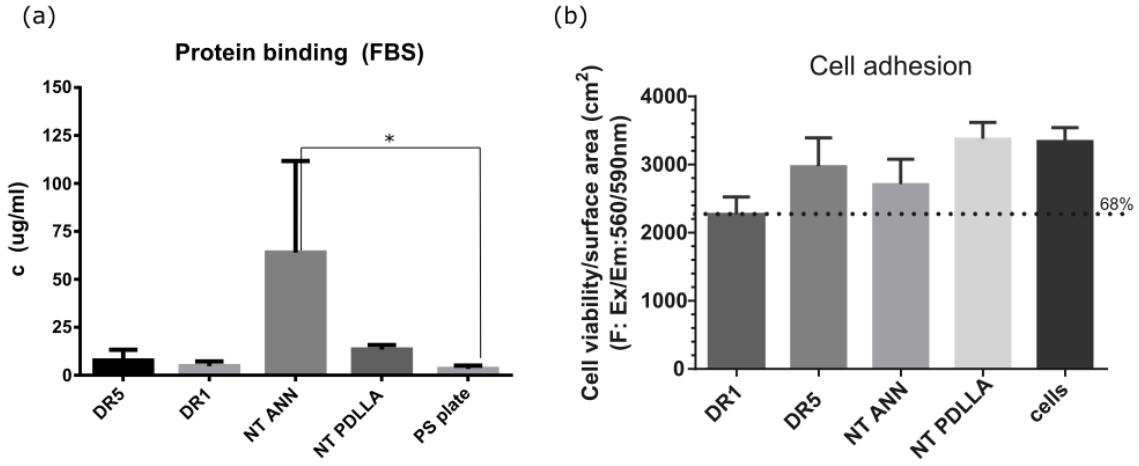

Figure 19: (a) FBS protein binding observation for piezoelectric smooth (DR5) and NT films (NT ANN) and non-piezoelectric smooth (DR1) or NT films (NT PDLLA) compared to PS plate; (b) cell attachment observation normalized to surface area of the inserted film, compared to values for all cells (the dotted line indicates the lowest value for attachment, which is 68% of the starting cells). * indicating significant statistical value $p < 0.05$.

Improved protein binding was observed for NT films (piezoelectric- NT ANN or non-piezoelectric- NT PDLLA) from FBS solution (Fig. 19a), expecting improved material-cell interaction later. Improvement can be explained by the increased surface area and rough topography for the NT films. Main difference between NT PLLA and NT PDLLA is that NT PLLA is crystalline and piezoelectric, while compared to PDLLA which is amorphous and non-piezoelectric, therefore improvement for NT ANN films can be also due to assumed charge on the surface of piezoelectric nanotubes. It may also include suspected influence of electrostatic edges, as several edges are exposed on the NT surface due to the presence of tubes (fixation of the fluorescent dye intended for cell staining was observed on edges of piezoelectric drawn PLLA film and on the tube endings, but not on DR1 or NT PDLLA samples, indicating increased reactivity of the edges). Small improvement of cell adhesion was observed when films were immersed in cell suspension for 24 h (Fig. 19b), compared to non-piezoelectric smooth reference DR1. I suspect that mostly surface had initial effect on cell adhesion, since NT samples and rougher drawn film have similar cell attachment (Fig. 19b). Jun et al. and Yang et al. observed that nano- or micro-scale surface of scaffolds positively promote cell-matrix and cell-cell interactions, due to the resembling of natural ECM environment [65], [121]. In my case also drawn film (DR5) has rougher surface (Fig. 18a) compared to non-drawn film (DR1), therefore a more favorable environment for cell adhesion.

6.1.3.3 Cytotoxicity to HaCaT cells

Cytotoxicity was evaluated for adhered cells on 24-well PS plate when they were covered with the films. It was compared to non-covered cells or cells covered with biocompatible microscopic slide glass used as a reference. No significant decrease was observed in cell viability when cells were covered with piezoelectric or non-piezoelectric, smooth or NT samples for 24 h (Fig. 20a). Even when cells were seeded directly onto the film (Fig. 20b), at least 80% of the cells survived. A small decrease in cell viability may be due to stress induced by the addition of new material or coverage. With continued US stimulation after (80 kHz), cell proliferation was similar in both cases, with films or not, as seen in optical images taken after 3 days of incubation of seeded cells on a PS plate (Fig. 20c) or drawn film (DR5, Fig. 20d), indicating confirmation of biocompatibility.

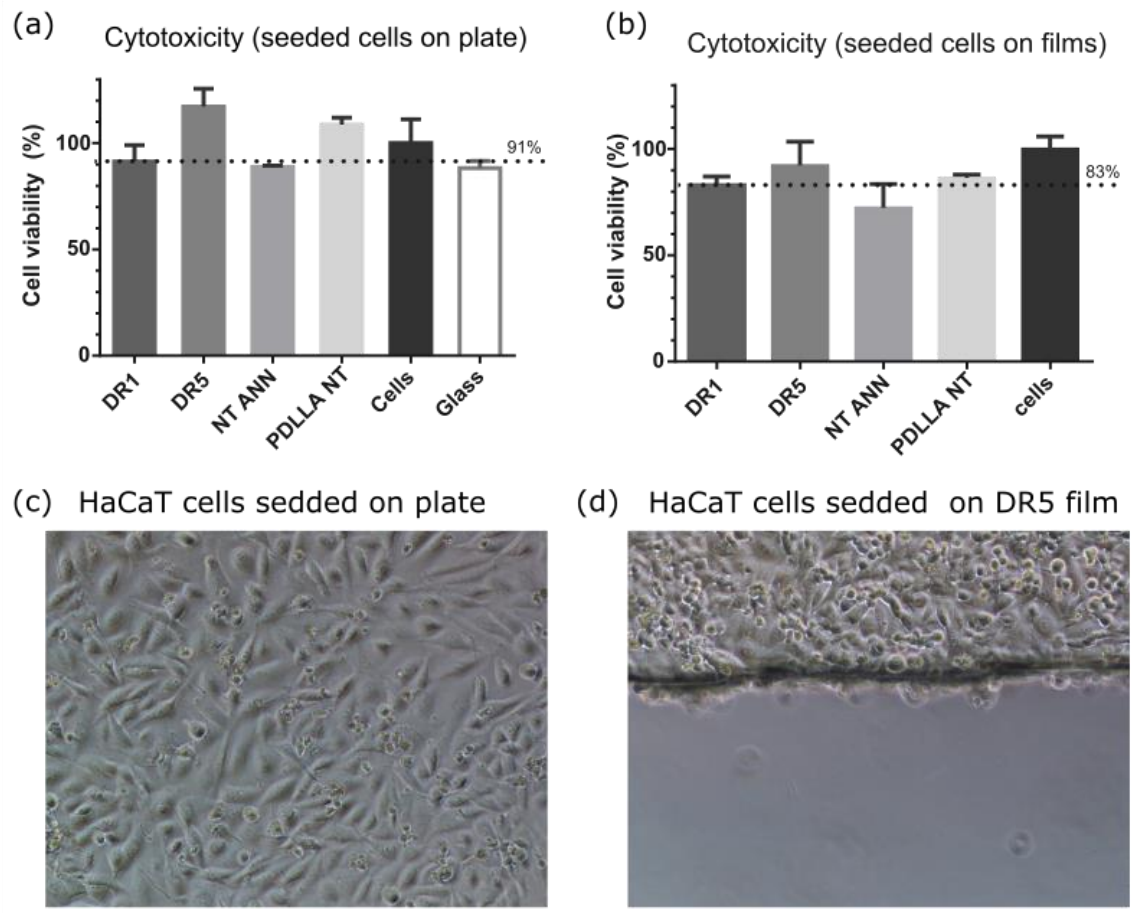

Figure 20: (a) Cytotoxicity of HaCaT cells seeded on PS plate and covered with PLLA film samples, (values of fluorescence measurement (Ex/Em:560/590 nm) normalized to values of non-covered cells); (b) cytotoxicity of HaCaT cells seeded directly on films, where dotted line indicate value for DR1 sample (83%); (c) optical image of cells seeded on PS plate after 3 days of incubation and (d) observed edge of cells seeded on DR5 film.

6.1.3.4 HaCaT cell proliferation

When testing with cells as living organisms, large fluctuations in behavior was expected, so in most cases direct interpretation does not have significant difference in values, but trends in behavior change can still be observed. In literature for this specific cells, small improvement in proliferation, migration or differentiation of HaCaT cells was observed in response to electric stimulation ([62], [68], [106], [118], [122]). When using US stimulation, a preliminary test (not presented) was performed to select the optimal conditions for stimulation, for example, for the US bath, a frequency of 80 kHz with 30% power of 100 W/3L for 20-30 min stimulation was used, and for the US probe, frequency 1 MHz with power 1.8 W/cm^2 in pulse mode 1:10 s.

Cell proliferation (Fig. 21a) was observed for cells seeded directly on films and incubated for a further 3 days with or without US bath (80 kHz, high power) or US probe stimulation (1 MHz, low power). In non-stimulated samples, the difference in cell proliferation between piezoelectric (DR5, NT ANN) and non-piezoelectric (DR1, PDLLA NT) films is not so observed (Fig. 21a). A slower proliferation is detected for the NT samples compared to the smooth films, possibly due to some initial cytotoxicity (20-30%) observed at the beginning (Fig. 20b). Since there is no difference between piezoelectric NT films and non-piezoelectric ones, I assume that the effect is topographic/initial. For stimulation in US bath (80 kHz),

proliferation after 3 days for smooth piezoelectric or not (DR1, DR5) is smaller compared to unstimulated cell growth, while for NT films is similar. One possibility for slower cell growth for NT films stimulated via US bath is also that topography effect and tube movement having an environmentally stressed effect on cells, since later on quite stressed/damaged surface morphology of cells is observed at 80 kHz US stimulation (Fig. 22e). For 1 MHz stimulation, after stimulation for the second day, number of cells is resting, which could indicate in cell differentiation, since differentiation and proliferation are mutually exclusive [62], however difference between piezoelectric or non-piezoelectric NT sample was not pronounced. An interesting observation was observed for the smooth films at 1 MHz stimulation, where fewer cells were observed on the piezoelectric films (DR5) compared to the non-piezoelectric reference (DR1), suggesting the possibility that electrical stimulation triggers cell differentiation, as the opposite behavior was observed where cells were not US stimulated.

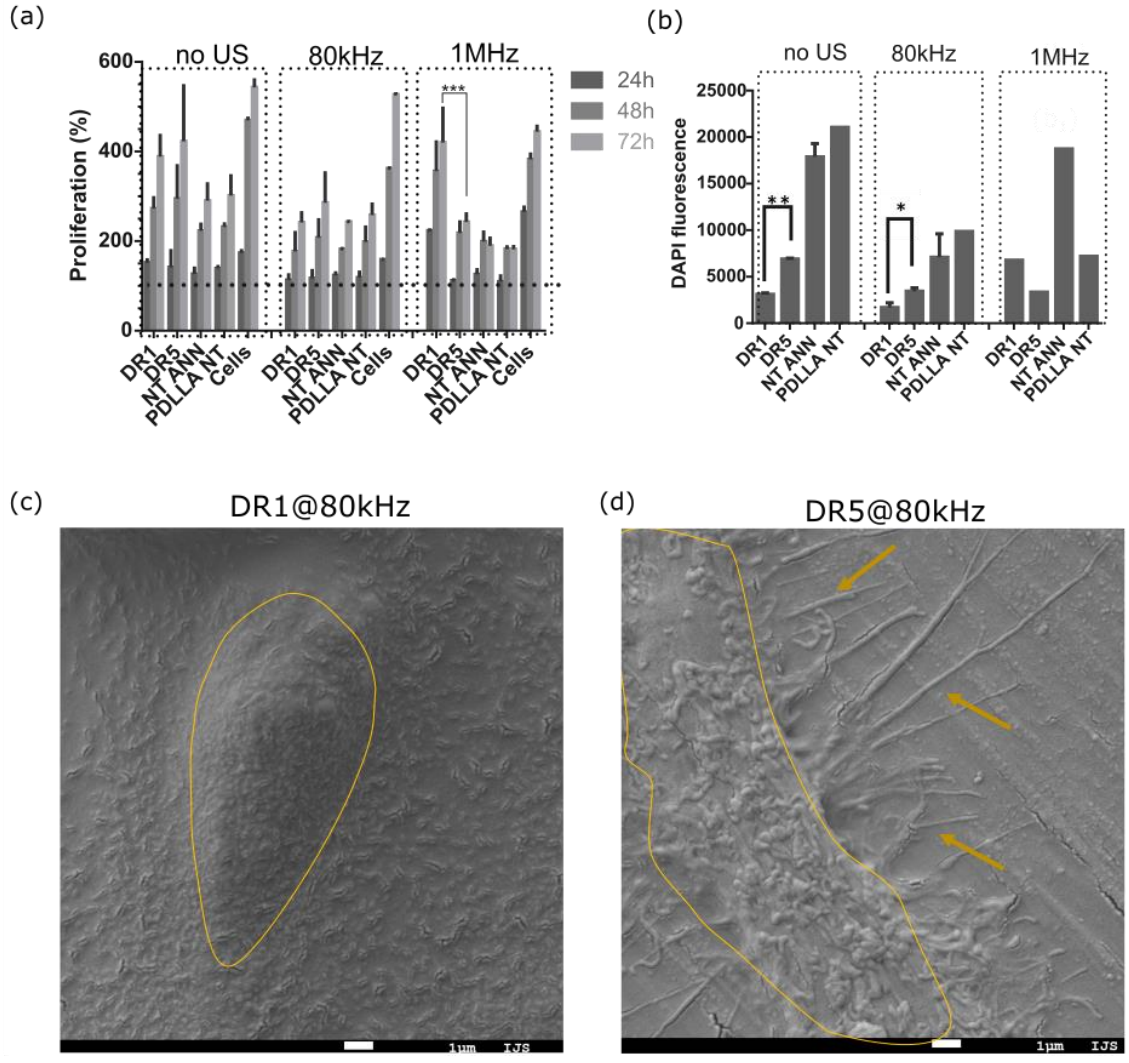

Figure 21: (a) Cell PrestoBlue™ viability normalized to fluorescence value of adhered cells obtained after seeding on films, continued with day 1, 2 and 3 to observe percentage of proliferation for non-drawn (DR1), drawn and piezoelectric (DR5), nanotextured piezoelectric (NT ANN) and non-piezoelectric (PDLLA NT) films with US stimulation of 80 kHz, 1 MHz or without; (b) measured DAPI stained nucleus fluorescence values for the same samples and stimulation conditions but only for the last day of incubation; morphological observation of attached and 3 days stimulated cells at 80 kHz US on the (c)

non-piezoelectric film (DR1@80 kHz) and (d) piezoelectric drawn film (DR5@80 kHz), with marked cell boundary and pronounced cell outgrowths/filopodia for better adhesion, observed only for piezoelectric film. *indicating significant statistical value $p < 0.05$.

When comparing the viability for the last day of stimulation/incubation (72 h) with number of cell nuclei (DAPI staining, Fig. 21b), very similar results were observed. With the same initial cell incubation at the beginning, the final number of cells on the DR5 films is higher compared to the DR1 film with 80 kHz US stimulation or without. Since I observed that the cells proliferate more on the DR5 films in both cases, US (80 kHz) or not, it is really difficult to suggest that this is actually the result of the (piezo)electric effect. However, at 1 MHz stimulation the situation is reversed, indicating possible cell differentiation in response to (piezo)electric stimulation.

The decrease in the number of cells for US bath stimulated NT samples is more pronounced when observing nuclei, however difference between piezoelectric or non-piezoelectric NT films was again not observed for no stimulated sample or using US bath. For NT films, the number of nuclei, therefore cell number is higher compared to smooth DR5 or DR1 films, which was the opposite when measured cell viability. It is possible, that stressed environment of nanotexture is slowing the cell metabolic activity, making cells less viable. Using US bath stimulation (80 kHz), combination of topography, tube movement and predicted high piezoelectric effect [49] results in smaller number of cells. The exception was again the 1 MHz stimulation, but in case of NT surface, proliferation is observed as a possible response to (piezo)electric stimulation (Fig. 21b).

In the case of the piezoelectric NT film, quite large differences in piezoelectric properties were observed compared to the drawn film [49], so it is understandable to observe different effects in the cells (proliferation or differentiation), which is probably related to the different intensities of (piezo)electric stimulation to which the cells are exposed at low power 1 MHz frequency.

6.1.3.5 Morphological changes of adhered HaCaT cells

When observing morphology on US bath stimulated piezoelectric (DR5) and non-piezoelectric (DR1) samples (80 kHz), no cell extensions are observed (Fig. 21c) in the non-piezoelectric film indicating poor attachment. For the piezoelectric film (Fig. 21d), larger and flattened cells are observed, indicating on improved cell adhesion. Elongated filopodia (actin rich cell outgrowths with an important role in cell migration, cell adhesion and wound healing [123], indicated by the yellow arrows on Fig. 21d) are observed only on stimulated piezoelectric film (DR5) compared to stimulated non-piezoelectric film (DR1), indicating improved connection with the material, cell-to-cell connections and indicating on cell migration. Although no significant difference in cell proliferation was observed between the piezoelectric sample and the non-piezoelectric reference, the DR5 piezoelectric film shows improvements in cell attachment and cell-to-cell connections compared to the non-piezoelectric film.

If I observe morphological changes on cell surface on piezoelectric smooth sample DR5 with or without US mechanical stimulation in more detail, difference is observed (Fig. 22). (Piezo)electrically stimulated cells look more deflated, larger, more spread and attached (Fig. 22 b, c) compared to no US stimulated (Fig. 22a). Similar was observed from Mojena-Medina et al. who showed SEM images for well attached cells as more spread and deflated in case of colonial growth of HaCaT cells [122]. Compering between stimulations, using US baths creates visible stress on the cell (observed round shapes on the cell surface, marked with a blue arrow on Fig. 22b) compared to using US probe with lower power, where larger and healthy cells are observed (Fig. 22c).

When comparing piezoelectric NT films (NT ANN: Fig. 22d, e, f) with non-piezoelectric (PDDLA NT: Fig. 22g, h, i), difference is mostly observed for 80 kHz US bath stimulation, where for piezoelectric sample, damaged and stressed cell surface is detected (Fig. 22e), which resembles the necrosis of cells (damaged membrane with large holes [124]). Many round shapes are observed on the piezoelectric NT surface, believed to be due to stress-related vacuolization, marked with a blue arrow, or start of the apoptosis (natural programmed cell death). When stimulated with 1 MHz US probe, the cells on both films are observed to be healthy (Fig. 22f, i). In all cases, the cells established good connections with both drawn and NT patterns, marked on the images with green arrows. Surface microvilli, indicated by white arrows in the images, are observed in all smooth and NT films, also for piezoelectric NT films stimulated at 80 kHz, when observed the other parts of the sample. It is also interesting that on NT piezoelectric film, cells are observed mostly on the surface of the tubes, while on the non-piezoelectric NT PDLLA sample, cells are also observed between the tubes. (Fig. 22i). This may be due to the greater flexibility of the long amorphous PDLLA tubes compared to the crystalline and less flexible PLLA tubes.

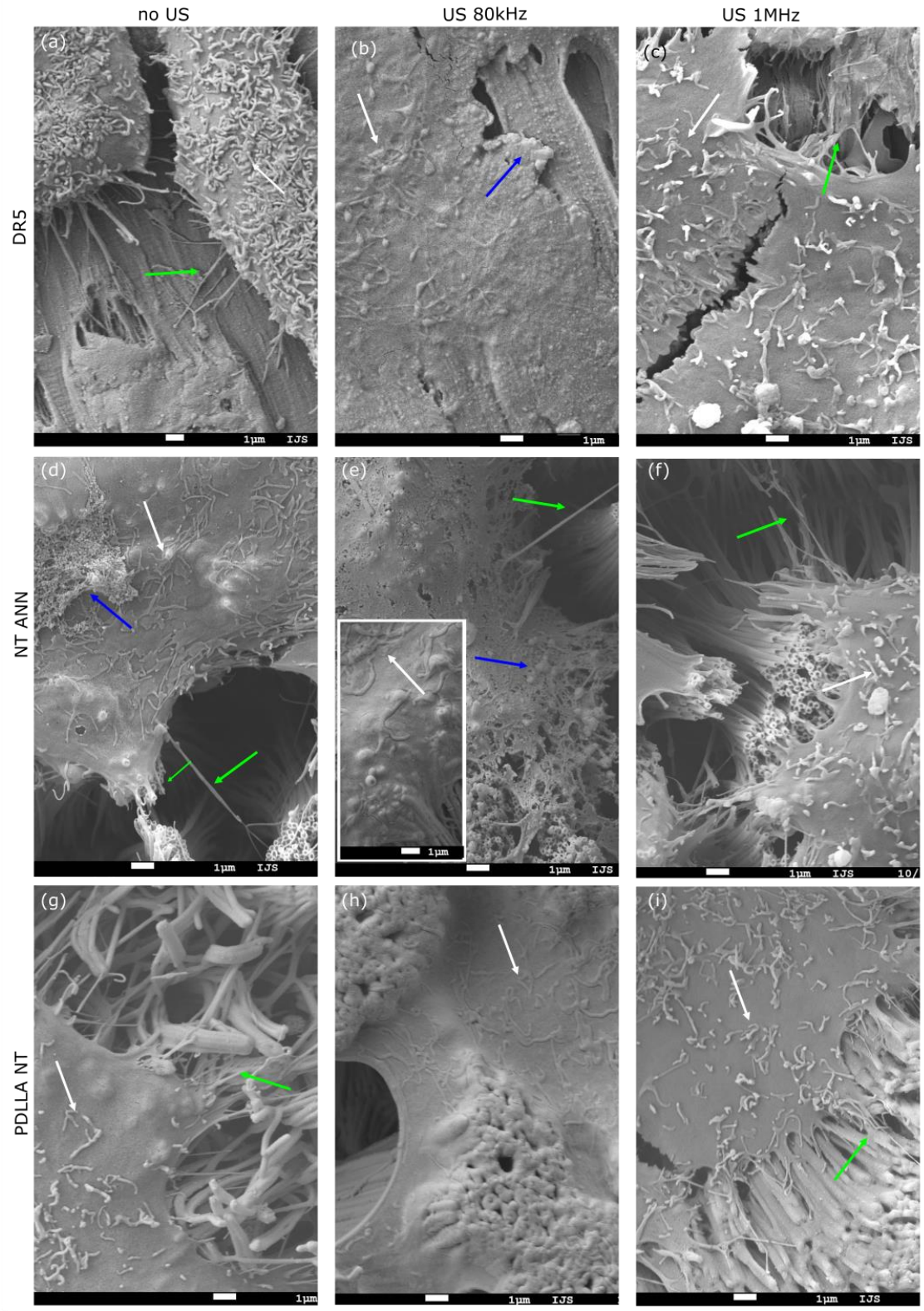

Figure 22: Images of piezoelectric drawn (PLLA DR5: a, b, c), nanotextured (PLLA NT ANN: d, e, f) and non-piezoelectric nanotextured films (PDLLA NT: g, h, i) showing the morphological changes of the cell surface, when the seeded cells were just incubated for 3 days (a, d, g), or stimulated with US bath (b, e, h) or US probe (c, d, i). Arrows showing good cell-material connections and cell outgrowths (green arrows), surface microvilli (white

arrows) and stress-related vacuoles (blue arrows) indicating the initial phase of apoptosis, observed on the cell surface.

6.1.3.6 Actin filament production of adhered HaCaT cells

Observation of actin filament alignment also indicate on cell morphology, polarization, adhesion and mostly directs cell migration in response to changes in calcium voltage gated ion channels [125]. As a result of electric stimulation, even small one (<10 V/cm), increased ion flow trigger cytoskeleton remodeling mostly to induce cell migration and has a significant effect on cell alignment [59]. When detecting actin filament production per cell as possible response of cells towards electric stimulation, in my case achieved by piezoelectric biodegradable PLLA polymer smooth or NT films, a noticeable difference was observed for US stimulated cells on drawn piezoelectric DR5 films compared to non-stimulated samples (Fig. 23a). Cells were seeded directly on films and incubated/stimulated for 3 days before fluorescence staining. Trend in increase of actin filament production per cell is observed for piezoelectric samples (DR5 and NT ANN) when stimulated via US bath (80 kHz), compared to the lower values observed when 1 MHz stimulation (US probe) was used. In optical observation using a fluorescence filter, compressed and small cells are observed for the non-piezoelectric sample (DR1) ultrasonically stimulated at 80 kHz (Fig. 23b) compared to larger and elongated cells stimulated on the piezoelectric smooth sample (DR5, Fig. 23c), with even more pronounced stretching at 1 MHz (Fig. 23d). I believe that on DR5 films, more spread actin filaments indicate better cell adhesion, elongated shape, where for DR1 sample rounded shape only around the nucleus indicate poor adhesion and limited spreading. Similar was observed from Xue et al., who demonstrated through F-actin staining improved cell adhesion and spreading for piezoelectric PVDF films when hydrophilicity was improved [110]. A possible related effect for cell stretching could also be the surface topography achieved by drawing the film, which gives it the specific unidirectional texture observed on the film surface (Fig 18a).

Increased actin filament production was observed for non-piezoelectric NT film (PDLLA NT) compared to piezoelectric NT film if stimulated or not. When analyzing fluorescence images for 1 MHz stimulation, actin filament was produced around the cell in all direction on crystalline nanotubes (Fig. 23e), probably due to the rigidity of the tubes, and tube movement in response to US deformation, limiting the stretching of the cell. However, for the non-piezoelectric NT PDLLA sample, I observed that the cells are elongated, probably because they are also located between the tubes and therefore can stretch in the created channels between the tubes (Fig. 23f). This is also probably the reason for more F-actin production per cell, since migration between the flexible tubes is easier, compared to crystalline piezoelectric sample where cells were mostly observed only on the surface.

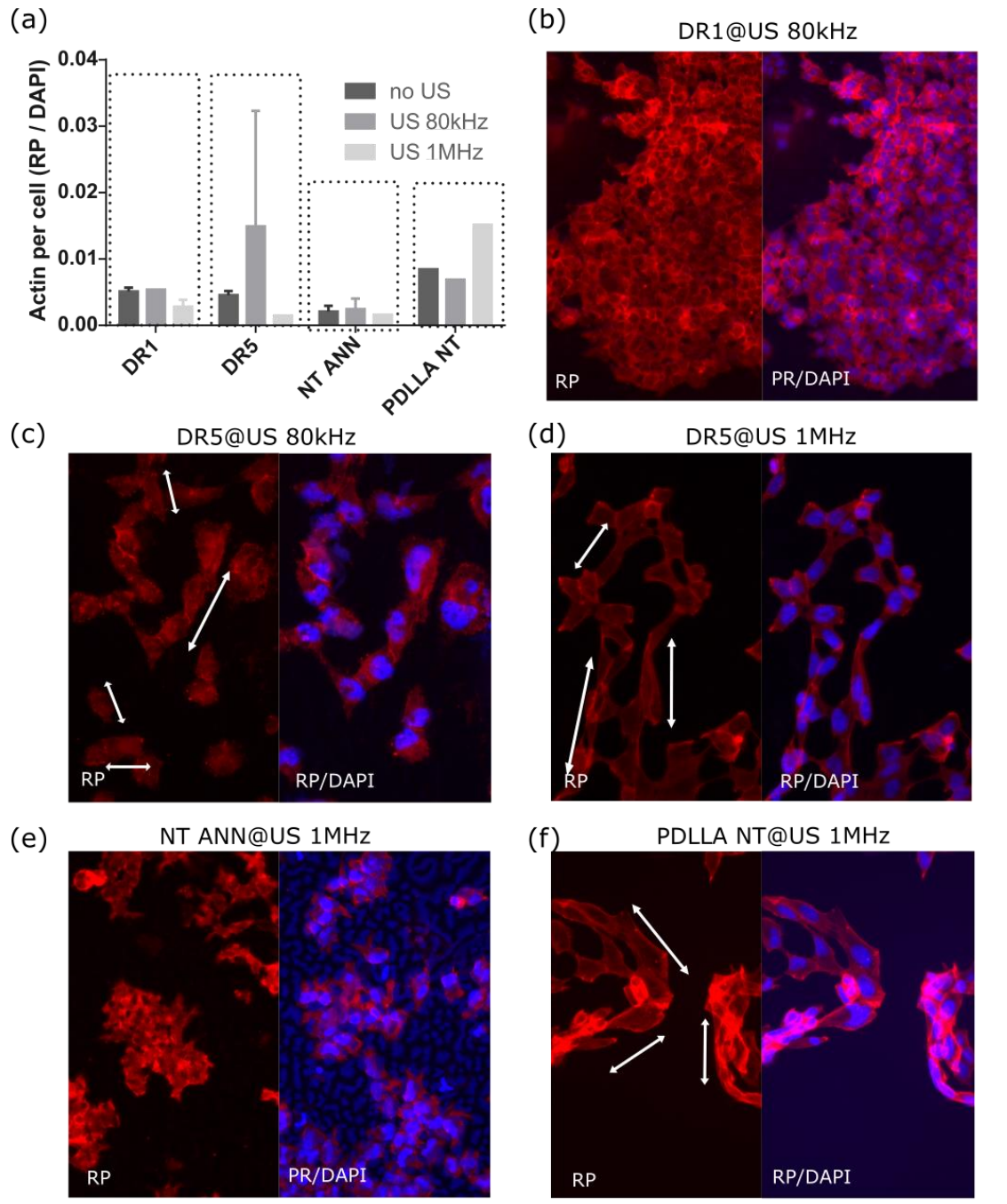

Figure 23: (a) Ratio between fluorescence measurements of Rhodamine Phalloidin (RP) F-actin staining compared to diamidino-2-phenylindole (DAPI) nuclei staining for the smooth and NT piezoelectric and non-piezoelectric samples after 3 days of stimulation/incubation, presented as ratio between produced actin filaments per number of nucleus (cells); images of F-actin and nucleus for US stimulated at 80 kHz for (b) non-piezoelectric (DR1) and (c) piezoelectric (DR5) film, (d) piezoelectric DR5 film stimulated at 1 MHz; and images of f-actin and nucleus for US stimulated at 1 MHz for NT (e) piezoelectric (NT ANN) and (f) non-piezoelectric (NT PDLLA) film.

6.1.3.7 HaCaT cell migration

Usually cell migration is directional and observed in case of direct current stimulation, therefore I am not expecting much improvement due to the way of expected electric stimulation through prepared films. It is important that we understand that source of stimulation I use is US, therefore we do not have directional current but more possible like alternating current (US generates alternating charge on the surface of the film, since due to shear piezoelectricity, upper bended part has positive charge and the lower part has negative charge, which shifts with film bending). Due to the limitation of making scratch directly on NT films (removal of polymer tubes from the surface) migration was observed for cells seeded on PS plate and covered with prepared films. Fig. 24a presents images of area reduction from the start and after 20 h for smooth and NT samples, piezoelectric and for their non-piezoelectric references. A high power 80 kHz US bath was used to produced highest piezo response of the films as they are not in direct contact with the cells. Using PLLA films on top of the scratched area, I observed that the influence of US prevails over the influence of (piezo)electrical stimulation, since no significant difference was observed between piezoelectric NT or smooth films compared to non-piezoelectric (Fig. 24b). I believe that the lack of firm contact is the reason I do not see a clearer difference. The effect of US alone was also confirmed, as US stimulation also increased cell migration by approximately 20% greater area reduction even when no film was added on the surface.

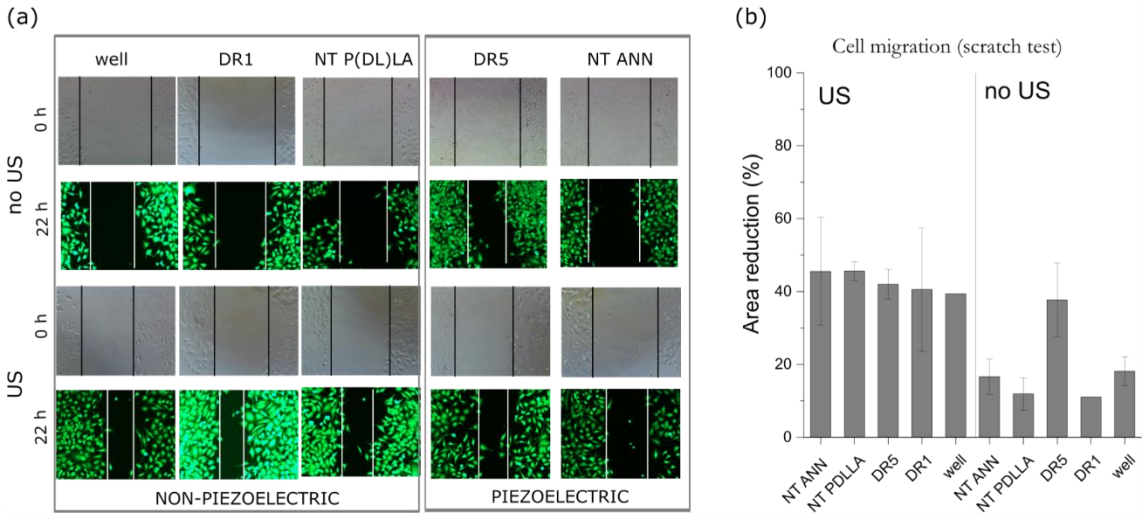

Figure 24: (a) Comparison of wound progression from start (optical images) and after 20 h (fluorescence images) for piezoelectric (smooth- DR5, and nanotextured- NT ANN), non-piezoelectric samples (smooth- DR1 and nanotextured- NT PDLLA) and for the well without the film on top, with or without external US@80 kHz stimulation; (b) graph showing the reduction in surface area of mentioned samples to observe changes for cell migration.

Using a piezoelectric drawn film (DR5), an improvement in cell migration was observed where no external mechanical stimulation was applied (Fig. 24b). This could be explained one way by the effect of surface-oriented topography parallel to the drawing direction, as I believe that piezoelectricity is difficult to activate without US in the case of drawn films or because of the DR1 film itself, as it is thicker and therefore heavier and exerts more unwanted pressure on the cells. For NT films, the migration is comparable to that of no covered cells and is enhanced when US is applied to either piezoelectric or non-piezoelectric samples, so the influence of US predominates.

6.1.3.8 Monitoring the immune response to a piezoelectric polymer film

I observed the immune response of monocyte-derived macrophages by analyzing the viability of attached cells on film using induced macrophagization (added PMA medium) only for the control sample. I understood that the monocyte cells, when in contact with the film, differentiate into macrophages as an immune response to the new material and attach to the surface. Over time, however, polarization of macrophages from inflammatory to non-inflammatory should occur. I observed that 26% of monocytes differentiated into macrophages when piezoelectric or non-piezoelectric, smooth or NT samples were added, compared to theoretically all differentiated monocytes when PMA medium was added (THP-1/PMA), presented in Fig. 25a. Optical observation of stained macrophage cells using CFSE dye show attachment of control sample on polystyrene plate (Fig 25b_1 and b_2) and small number of attached cells on piezoelectric smooth (Fig. 25b_3 and b_4) and NT film (Fig. 25b_5 and b_6). For NT sample, due to the thickness and loss of transparency, cells are not seen just by using optical microscope (Fig. 25b_5), however by using stained cells with fluorescent CFSE dye, attached cells are clearly observed under UV light and green dichroic filter (Fig. 25b_6).

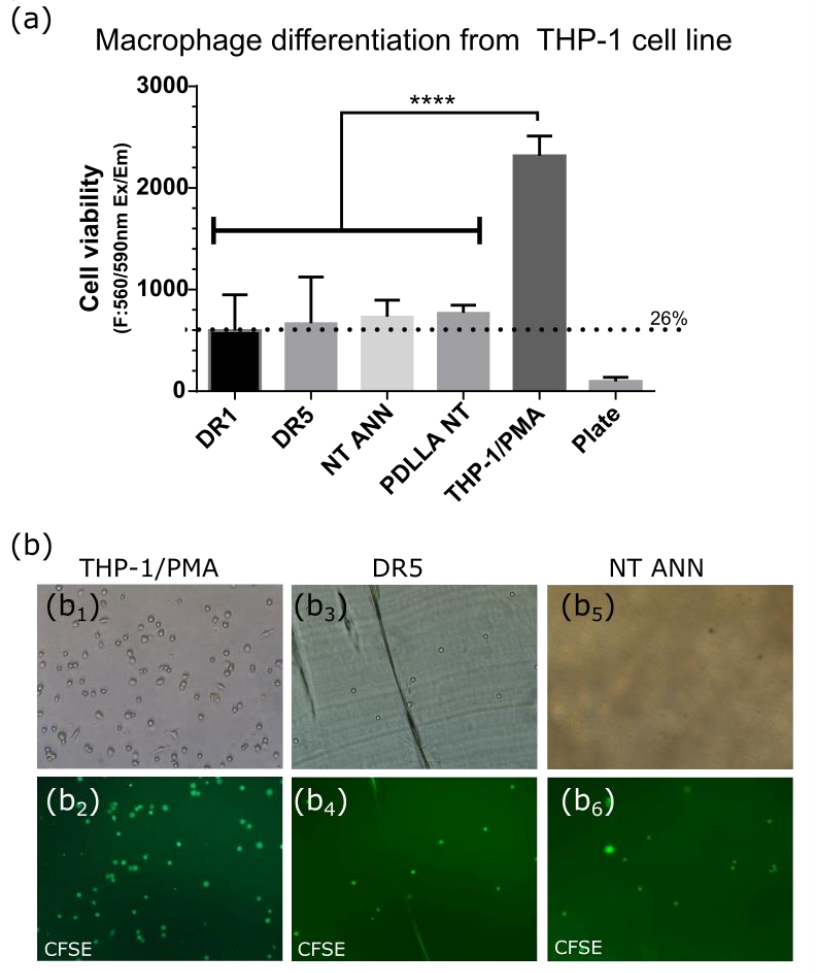

Figure 25: (a) Cell viability measurement of attached differentiated macrophages for piezoelectric samples (DR5, NT ANN), non-piezoelectric references (DR1, PDLLA NT) and control (THP-1/PMA, plate); (b) optical observation of attached cells after 2 days of incubation with THP-1 monocytes on PS plate (THP-1/PMA; b_1), piezoelectric smooth (DR5, b_3) and nanotextured films (NT ANN, b_5) and observation of CFSE stained

monocytes using green filter for control (b_2), piezoelectric smooth (b_4) and NT sample (b_6). **** indicating significant statistical value $p<0.0001$.

Viability of macrophages using PB was measured at the end of a 3-day incubation after initial attachment where they were stimulated with an US bath (80 kHz) or an US probe (1 MHz). Samples were also stained at the end to observe actin filaments production per cell and the number of cells. When observing proliferation after 3-day incubation of attached macrophages, no significant changes were observed among macrophages attached to PLLA polymer films. However, the observed proliferation was lower compared to the reference sample seen in Fig. 26a. When looking at cells alone, less proliferation was observed with 80 kHz stimulated samples compared to 1 MHz or unstimulated samples, similar was observed for smooth films (DR1, DR5) but not for NT samples, where both US stimulations slightly increased proliferation. When observing the number of cells whose nucleus was stained to represent the number of macrophages attached to the surface (Fig. 26b), a significant difference in the number of cells on the NT surface compared to the smooth films was observed, regardless of the piezoelectric properties. A pronounced increase was observed in non-piezoelectric NT sample (PDLLA NT). These results could just emphasize the small increase of initial attachment at the start of incubation for NT samples (Fig. 25a), since proliferation during the 3-day incubation was similar for all samples. Interestingly, highest proliferation was observed in the US probe-stimulated samples (1 MHz) compared to the US bath-stimulated or non-stimulated samples in all cases when films were involved.

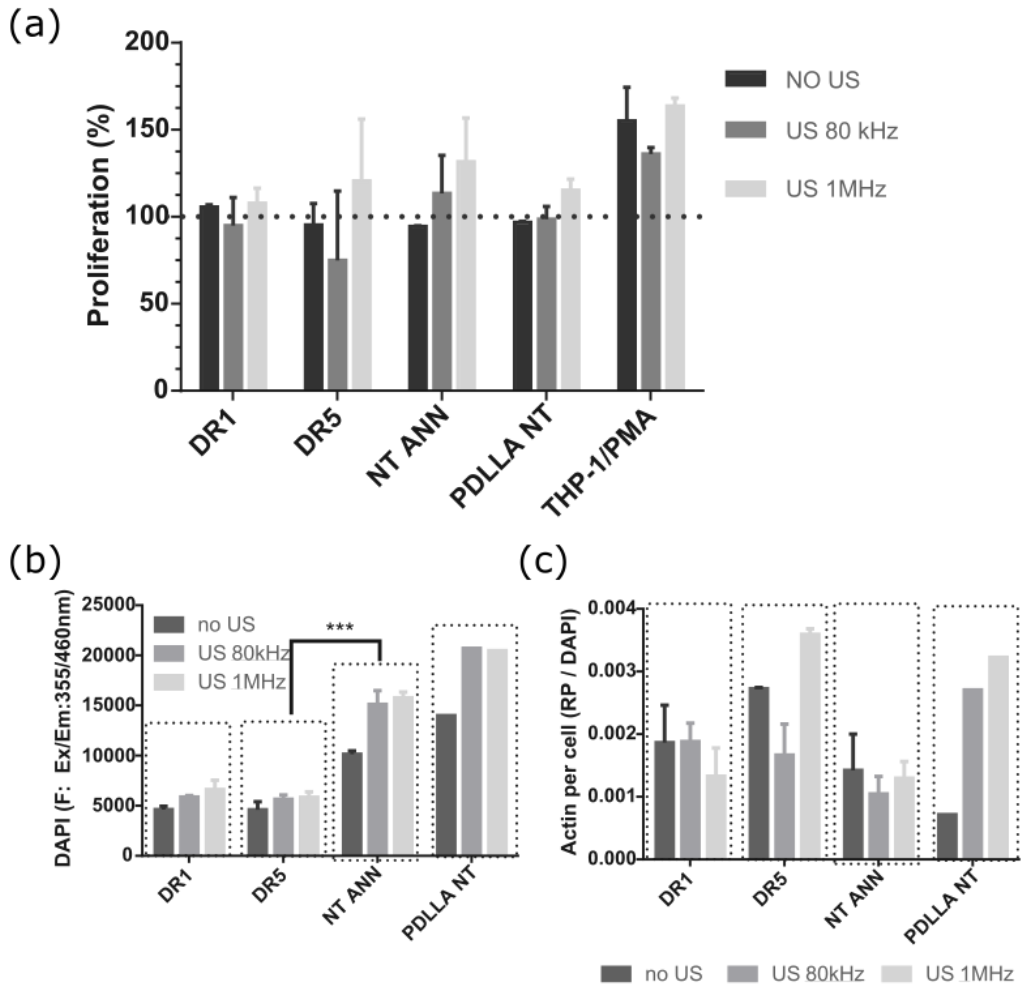

Figure 26: (a) Macrophage proliferation after 2-time (piezo)electric stimulation activated via US bath (80 kHz), US probe (1 MHz) or without US after 3 days of incubation after initial differentiation for piezoelectric drawn (DR5) or nanotextured film (NT ANN) or non-piezoelectric smooth (DR1) or nanotextured (PDLLA NT) samples, compared to cells attached on PS plate (THP-1/PMA); (b) fluorescence measurement of DAPI stained macrophages, indicating number of cells and (c) measured fluorescence for F-actin filament formation per number of cells (RP/DAPI). *** indicating significant statistical value $P<0.0002$.

When observing the actin filament production per cell (Fig. 26c), increased F-actin production per cell was observed for piezoelectric drawn film (DR5), especially for US stimulation at 1 MHz, compared to non-piezoelectric sample (DR1). The opposite was observed for NT samples, where piezoelectric NT ANN films show lower actin filament production compared to non-piezoelectric sample, when 80 kHz or 1 MHz US stimulation was used. Increase in actin filament production could mean migration, increased inflammatory response (M1 macrophage polarization) [126] or due to a fusion of many macrophages resulting in M1 or M2 macrophage polarization [127]. For piezoelectric NT film, a similar production of F-actin was observed with or without US stimulation, which may be due to the more crystalline and therefore stiffer tubes that are less mobile under US (combined mechanical effect), or possibly due to the piezoelectric properties, since some small decrease is observed when NT film were US stimulated. The opposite was observed for non-piezoelectric NT PDLLA sample when US stimulation increased actin filament

production per cell, which can again be attributed to a combined mechanical effect (combination of US and larger tube motion), whereas the effect of ultrasound alone was not pronounced in the DR1 sample.

6.1.3.9 Morphological observation of monocyte-derived macrophages

In the literature, direct observation of morphology was performed using an electron microscope between non-activated (M0), activated M1 or M2 polarization of macrophages, and a clear difference was observed in M1 activated samples compared to the other two types [128]. In M1 polarization, a more irregular and elongated shape of macrophages are observed compared to M2, where a similar round shape remains as in non-activated M0 initial macrophages [128]. Fig. 27 represents the observation of the morphology of monocyte-derived macrophages attached to a piezoelectric or a non-piezoelectric film with smooth or NT topography, using US stimulation or not. It should be noted that there were usually very few cells found on the film, so the general observation was difficult to assess.

However, in all cases of stimulation, on non-piezoelectric smooth samples (DR1, Fig. 27a_1, a_2, a_3), macrophages remain round with some outgrowths (white arrows), indicating an attached but presumably inactive form of macrophages. Since no changes were observed on the non-piezoelectric sample with or without US stimulation, I can state that US itself has a minimal effect. For the piezoelectric drawn sample (DR5, Fig. 27b_1, b_2, b_3), a difference in shape is observed after US stimulation, where more elongated (Fig. 27b_2) and irregular shapes (Fig. 27b_3) are observed compared to the unstimulated sample, where macrophages remain round (Fig. 27b_1), indicating on piezoelectric effect. The change in morphology was more pronounced for US bath stimulated sample (80 kHz), which I believe resulted in M1 polarization of the macrophages, whereas at the 1 MHz stimulated film, the macrophages are more like the M2 type, which is beneficial for wound healing applications.

For the non-piezoelectric NT film (PDLLA NT, Fig. 27c_1, c_2, c_3), macrophages are generally still round, but some macrophage fusion is observed when harsh 80 kHz US stimulation was used, and some indication towards the merging when stimulated at 1 MHz. A similar change was observed for actin filament production per cell for NT PDLLA sample, so I believe that tube movement under US is the main factor to activate macrophage M1 polarization and increase F-actin production. For crystalline piezoelectric PLLA samples with or without US stimulation, giant fused and flat macrophages are observed (Fig. 27d_1, d_2, d_3). Macrophages are thought to fuse with other macrophages to form the characteristic multinucleated giant cells as indicators of chronic inflammation [127], thus M1 polarization of macrophages is assumed. However according to their study of signaling pathways and cytokine detections of giant cells (fused macrophages), both inflammatory and anti-inflammatory type of giant cells can be formed from monocyte-derived macrophages with clear difference in number of merged macrophages (much higher number for inflammatory type) when incubated for longer time (7-10 days) [127]. In my case, macrophages probably appear in different stages, since fusion of more macrophages are observed from initial connection between two macrophages (Fig. 27d_1), close contact between 3 or more macrophages (Fig. 27d_2, d_3), and fusing the membrane together and creating film like appearance over the nanotubes (Fig. 27c_2). For both NT samples macrophages are also observed on the tube surface and between the tubes, creating craters in the NT topography (Fig 27 c_1). None of mentioned macrophage fusion was observed on smooth samples.

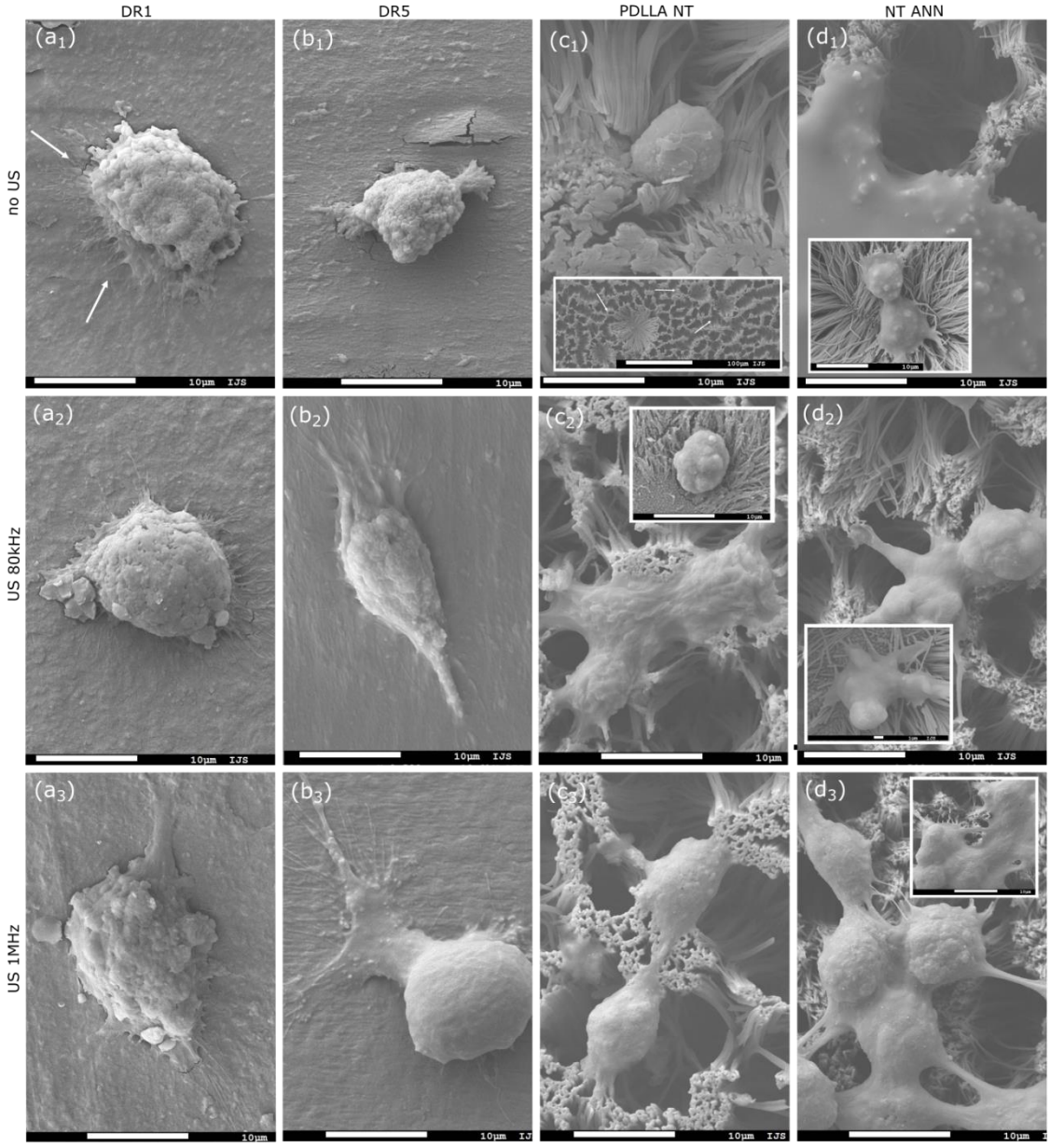

Figure 27: Microscopic observation of monocyte-derived macrophages after 3 days of incubation attached to: (a) non-piezoelectric PLLA films (DR1) without US stimulation (a_1) or stimulation using an US bath (a_2) or US probe (a_3); (b) DR5 piezoelectric drawn film without (b_1) or with US stimulation via US bath (b_2) or US probe (b_3); (c) non-piezoelectric NT PDLLA film without (c_1, with the general morphology of the film represented in the white rectangle) or with US stimulation via the US bath (c_2 with an additional image of the different morphology of the observed macrophage, represented in the white rectangle) or the US probe (c_3); (d) piezoelectric NT ANN film without (d_1) or with US stimulation via US bath (d_2) or US probe (d_3) with additional images in white squares presented the different observed morphology of macrophages.

6.1.4 Conclusion

Electrical stimulation is a novel tool for regulating cell behavior and shows a great potential in wound healing and tissue engineering. In theory, using piezoelectric biodegradable polymer such as PLLA, stimulation of cell proliferation and cell orientation can be achieved

without any additives which improve the wholesome healing process without any invasive therapies by only using US.

With previously confirmed piezoelectric properties of drawn and NT films, the effect of electric stimulation through them while mechanically stimulated with US was observed for cell behavior as cell attachment, proliferation and migration. Improved cell attachment was observed for all samples with rougher surface (NT and DR5) compared to non-piezoelectric smooth film (DR1). I observed no cytotoxic effect of piezoelectric or non-piezoelectric, smooth or NT films, and all further incubation resulted in cell growth, comparable to cell behavior without the films. No significant improvement was observed for proliferation under US stimulation, however clear improvement was observed in cell attachment. For drawn films, US bath and US probe are sufficient stimulation to activate piezoelectric properties and improve cell attachment, spreading and making connections. F-actin staining and microscopic images show better cell-to-film and cell-to-cell connection via increased number of filopodia for smooth films, cells are also more stretched and flattened, again indicating good connection and migration, but only when the films are piezoelectric (DR5) and US stimulated. Interesting observation for drawn piezoelectric films was for 1 MHz stimulation, where proliferation is noticeably less on the DR5 piezoelectric film, indicating differentiation as a possible response of the cells to (piezo)electric stimulation, which was not observed on the non-piezoelectric DR1 sample. However, for crystalline NT film with much improved piezoelectric properties, damaged morphology is clearly observed when using powerful US bath, but not for non-piezoelectric NT sample. I believe that high piezoelectricity with combination to crystalline tube movement under US is leading to observed cell necrosis. This is not observed when more mild 1 MHz stimulation via US probe was used, where cells morphology was intact and indicated towards increase in cell proliferation (DAPI staining). Mechanical stimulation using US bath creates stronger stimulation, producing a higher output voltage for drawn films, which is also assumed for NT films, compared to 1 MHz with low-power US probe stimulation, measured and validated on the stretched DR5 sample and PVDF reference, presented in Appendix A2. In the observation of cell migration, US plays a dominant role in enhancement, as I believe that the poor contact between the cell and the material is a reason for the cells to not sense the generated charge on the film surface to increase the response, as the cells are seeded on the plate and not directly on the films. In all cases with rougher surface, the cells established good associations with both NT samples and drawn oriented film, without the need to improve surface since cells attach to the samples in the same number as to film treated with cell-friendly poly-L-lysine, presented in Appendix A3.

I also observed the immune response to the prepared films, as PLLA can create a different microenvironment on the cells, due to the degradation of PLLA (decrease in pH), electrical stimulation, the appearance of small polymer shavings that could activate the immune response. In the literature, it is stated that, due to the environment, M0 macrophages are later activated into an inflammatory M1 or anti-inflammatory M2 polarization state, which is oriented towards attacking/healing or towards regeneration, respectively [67]. I observed some immune response for all samples, since 26% of monocyte differentiated into macrophages and attached on the films. After US stimulation, no changes were observed on macrophage morphology attached to the non-piezoelectric sample with or without US stimulation, therefore the effect of US can be discarded. For drawn piezoelectric film, indication towards M1 macrophage polarization was assessed due to the more elongated cell morphology, however M2 polarization could be result of 1 MHz stimulation, since cell stay more rounded. For NT samples I believe that tube movement under US and nanotexture topography is the main factor to activate macrophage M1 polarization, since macrophage fusion was observed in all cases of stimulation, more pronounced for piezoelectric sample (NT ANN). In all cases, I observed good macrophage

attachment/connection with the films as the cell outgrowths/filopodia extend towards the polymer tubes or rough surface of the drawn film. Kong et al. observed that piezoelectric effect (piezoelectric β-PVDF activated by US) enhances M1 polarization of macrophages, which in their case is favorable for cancer treatment [71]. However, another *in vivo* study showed that low voltage direct current electric stimulation can shift the immune response from healing/scaring to regeneration [73]. Therefore, it is important that in further studies using the as-prepared piezoelectric PLLA films, the differentiation of macrophages in response to electrical stimulation is more clearly determined, as currently a greater M1 polarization is indicated for the NT samples when stimulated with US and M2 for the drawn piezoelectric film, when 1 MHz frequency is applied.

In this study, I prepared piezoelectric drawn or NT polymer films that demonstrate a fully contact-based mechanism of providing electrical stimulation to cells activated externally via US. Drawn biodegradable piezoelectric film (DR5) shows the most promise for wound healing applications, given the observed improvements in cell behavior in response to electrical stimulation achieved using mild 1 MHz US stimulation. The most pronounced effect was on cell shape showing good attachment and improved actin filament production, indicating the improved cell-to-cell connection and migration. With further investigation, I believe that more favorable effect on cell behavior such as cell differentiation/maturation and contact-based migration will be confirmed when researching piezoelectric PLLA films further.

Chapter 7

Final Conclusions

During my study of the presented topic, I designed, optimized and evaluated PLLA drawn and nanotextured films as an innovative biomaterials tool, applicable to wireless piezo-stimulation by using ultrasound and found some of the important, previously unknown, answers on their properties and the way how they interact with bacterial and mammalian cells.

Which are the critical properties of polymeric films that enable and regulate their piezoelectricity? The critical parameters for piezoelectricity of PLLA are chain orientation and crystallization. When PLLA is stretched (oriented) and semi-crystalline, it can exhibit piezoelectric properties, which can be externally/wirelessly activated by using US (mechanical stimuli).

How to evaluate piezoelectricity of films with a complex structure? Exploring the piezo-catalytic activity of PLLA provides a possibility to correlate its ability to degrade organic dye (like methylene blue) indirectly with its piezoelectric properties and quantify it by comparison with piezoelectric standard. It leads to the unique method for measuring bulk piezoelectric properties of complex PLLA structures (like NT PLLA films) and enables a broader look from their local to bulk piezoelectricity.

How to stimulate piezoelectricity of films in a water environment? If the surface of the PLLA films is changed from inert hydrophobic to active hydrophilic, the degradation is transferred from the bulk to the surface, which keeps the PLLA piezoelectricity active for a long time even in an aqueous environment with hydrolytic enzymes. Films were successfully stimulated wirelessly using US in water/growth medium.

Which ultrasound stimulation is appropriate not to damage human keratinocyte cells, red blood cells, or bacteria cells? High frequency and low intensity US is found to be appropriate for stimulating cells without harmful effects directly induced by US waves. Their application in deforming drawn PLLA films is also not toxic for non-adherent (red blood cells) and adherent cells (keratinocytes). Deviations are noticeable for US-deformed NT PLLA films which can be assigned to a difference in their surface and piezo-stimulation capacity.

How to improve close contact between film and cells to achieve the best possible effect the film is providing? The piezostimulation was found to have contact-based mechanism. Therefore, growing cells directly on the films surface is found to lead to the most pronounced effects to their behavior.

What kind of an effect will be observed when films are in contact with bacteria cells? Piezoelectric stimuli imparted on bacteria through NT PLLA film and using US bath stimulation can depolarize and fibrillate the bacteria membrane or mechanically rapture the membrane, which leads to bacteria death.

How piezoelectricity influences red blood cells (suspended cells) and human keratinocyte cells (adherent cells)? Human cells can show some improvement in case of piezostimulation with drawn PLLA films (better cell attachment, increased actin filament production, proliferation/differentiation), however mechanical and piezoelectric signal overlap and it is hard to point to just one, and significant difference was not clear (trend is observed).

How do immune cells (macrophages) respond to the electric stimulation, smooth or nanotextured polymer film? Macrophages do attach and slightly proliferate on drawn or NT samples, however promising differentiation into M2 is emphasized for the most promising drawn PLLA films, beneficial to enhanced wound healing.

7.1 Final Remarks

Exploiting the piezoelectric properties of the chiral PLLA polymer and explaining the mechanism is challenging because the charge on the seeded cells moves from positive to negative with the US frequency, compared to the mostly investigated PVDF, where the charge is fixed on one side of the film, so the cells are exposed to the same electrical stimuli continuously. Therefore, the observation of the cell's response to the shear piezoelectric stimulation may differ from what is expected. Through detailed characterization and process optimization, piezoelectric drawn and nanotextured PLLA films were successfully prepared.

Using piezoelectric force microscopy (PFM) combined with finite element simulations and numerical analysis to determine the piezoelectric character on a single nanofiber is a common method used in research for determining piezoelectric properties [19], but it tells us little about the bulk properties of such films. The films with complex structures (electrospun fibers, NT film) affect the cells as a whole and not as individual fibers, so it is interesting to investigate the film's overall piezoelectric properties as well. I demonstrated a measurement method to compare changes in nanotexture or drawn PLLA films by measuring the piezoelectric properties of the entire film as their total piezoelectricity.

Due to the mentioned antibacterial effect of electrical stimulation, a number of antibacterial tests were carried out to determine whether the films were antibacterial. In most of the published literature, the antibacterial effect is presented in the percentage of cell viability (commonly as 60% lower number of bacteria in the presence of electrical stimulation compared to bacteria without the presence of stimuli (2x10^8)), but this is still an enormous number of surviving bacteria (still 10^8). Therefore, my research was more focused on investigating if the electrical potential could be the cause of bacterial death, so I performed the tests in physiological solution where bacterial growth is limited. Therefore, I directly confirmed that bacterial membrane fibrillation occurs due to electrical stimuli in NT films, where the piezoelectricity is higher.

Piezostimulation using PLLA is not a standard procedure for stimulating cells and very limited information without optimized protocols is available in the literature. Using ultrasound, I managed to develop an applicable experimental set up, standardize stimulation protocols and find optimal conditions for cell stimulation. However, I still intend to continue with biological testing on my samples to confirm a different hypothesized effect such as differentiation (the calcium gradient in the epidermis represents one of the most important triggers of keratinocyte differentiation) and to observe the behavior of different cells (like dermal fibroblasts) to electrical stimulation, as with the improvement of the equipment and by expanding my expertise, I can additionally contribute to solidifying knowledge in this area of research.

7.2 Proposed Improvements and Future Work

PLLA films developed in this work can serve as a basic platform, where I already set a starting point parameter and achieved good response from bacterial and mammalian cells

to piezoelectric stimulation. I believe that it can be further tailored and enhanced with upgrades or additions to strengthen the impact.

The idea of modifying or improving the prepared films, depending on the applications, is to add novel antibacterial particles, which were prepared in our group in a related research in which I also participated ([129], [130]), to the surface, which will improve the antibacterial properties, or by adding functional calcium phosphate biomaterials, working similarly as growth factors and would increase bone regeneration [130]. Some modifications should be incorporated onto the PLLA surface, such as surface plasma treatment or surface alkaline etching, to increase the number of possible attachment/reactive points.

By understanding the method of preparing a nanotextured surface, the literature shows that playing with the topography (size, length, shape of the nanopillars) can drastically change or create antibacterial properties. It would be interesting to use a template with different characteristics (pore depth, radius, spacing between pores) to prepare PLLA nanotubes, considering that this method achieves sufficient orientation and thus piezoelectric properties.

Due to its low piezoelectricity, I believe that the PLLA polymer can also be used as a sonoporator, where, in combination with an active component, it can allow the active material to enter the cell through an electrically created temporary hole, which greatly improves the effectiveness of antibiotics and reduces the required concentration.

The piezoelectric properties of stretch-prepared PLLA can be improved by adding a filler, which can be piezoelectric or not, where the first proposal would increase the piezoelectricity due to its properties, if possible for the filler to be activated by US. The next proposal would increase the orientation and crystallinity of the starting piezoelectric polymer during drawing or would cause increased deformation on the polymer during external US stimulation, resulting in increased piezoelectric properties of the film. The idea of adding a small amount (1wt.%) of high aspect ratio particles to affect orientation and crystallinity of the polymer was validated (20-fold higher voltage output) and researched within our group [96].

These possible upgrades open up new ideas about the use/model of such films, so there is still plenty of room for further exploration.

Appendix A

Additional Information for the Experimental and Characterization Methods

A.1 Observing Surface of the Nanotextured, Smooth and Hydrophilic Films by Using XPS

Additional surface analysis of prepared materials showed some new information relating to the surface modification by using a very surface-sensitive device, X-ray photoelectron spectroscopy (XPS). XPS spectra were recorded with the Versaprobe 3 AD (Phi, Chanhassen, US) using a monochromatic Al-Kα1 X-ray source. Spectra were acquired on a 200 µm spot size with the charge neutralizer turned on, as the films were put on a non-conductive double tape. The spectrum survey was acquired at 280 eV pass energy. The high-resolution core lines (C1s, O1s) were acquired at 55 eV pass energy, energy resolution of 0.2 eV. Spectra were analyzed with PHI MultiPak software, ESCA. First, linear-type background was subtracted, then the spectra were fitted using a non-linear least-squares fitting program adopting a Gaussian–Lorentzian peak shape. Due to air exposure, the C1s peak included environmental impurities. Therefore, after deconvolution of the C1s core line, the main peak at 285 eV, corresponding to hydrocarbon contamination combined to polymer backbone chain (C-C), was used as internal reference to correct the shift due to charging effects.

Surface analysis results showed some Teflon residue on the drawn and undrawn films, as Teflon foil was used for the initial hot-pressing process prior to drawing (Fig. 28a). A few Si ions are also observed, which are most likely impurities from the adhesive tape transferred with the tweezers. After surface etching of drawn PLA film (DR5) with Ar-cluster gun as a possible function of depth profiling, Teflon was not observed at all after the first cycle (Fig. 28b), therefore I confirmed that it came from the sheet used for initial hot pressing. Even though any response of bacteria and cell to Teflon was not observed. In the future, I will try to use a different foil (amide) for hot pressing polymer beads into uniform sheets. After observing NT films, no residues of the template or chemically removed aluminum oxide layer in contact (Al- or Cu-compounds) were indicated, therefore extracted NT polymer films were very clean (Fig. 28a).

After observing the alkali-etched and non-etched film surface, the ratio of COOH vs COH peak changed, additionally confirming the higher concentration of polymer hydrophilic end groups sticking out on the surface, which improved hydrophilicity of the polymer film (Fig. 28c, d). The analysis of spectra for the determination of surface

hydrophilicity was determined with the help of this article [34], where the surface was modified using plasma deposition and further treated using 1,2-diaminopropane (to add amino groups (NH_2)) or acrylic acid (to add carboxylic groups (COOH)). For the C1s region, not much difference is observed, other than lower C=O and C-OH intensities compared to the non-etched sample (Fig. 28c). More pronounced changes were observed for the O1s region after deconvolution of the peak. The intensity of the hydrophilic COOH peak increased greatly for the etched samples compared to non-etched (DR5), indicating improved surface hydrophilicity (Fig. 28d).

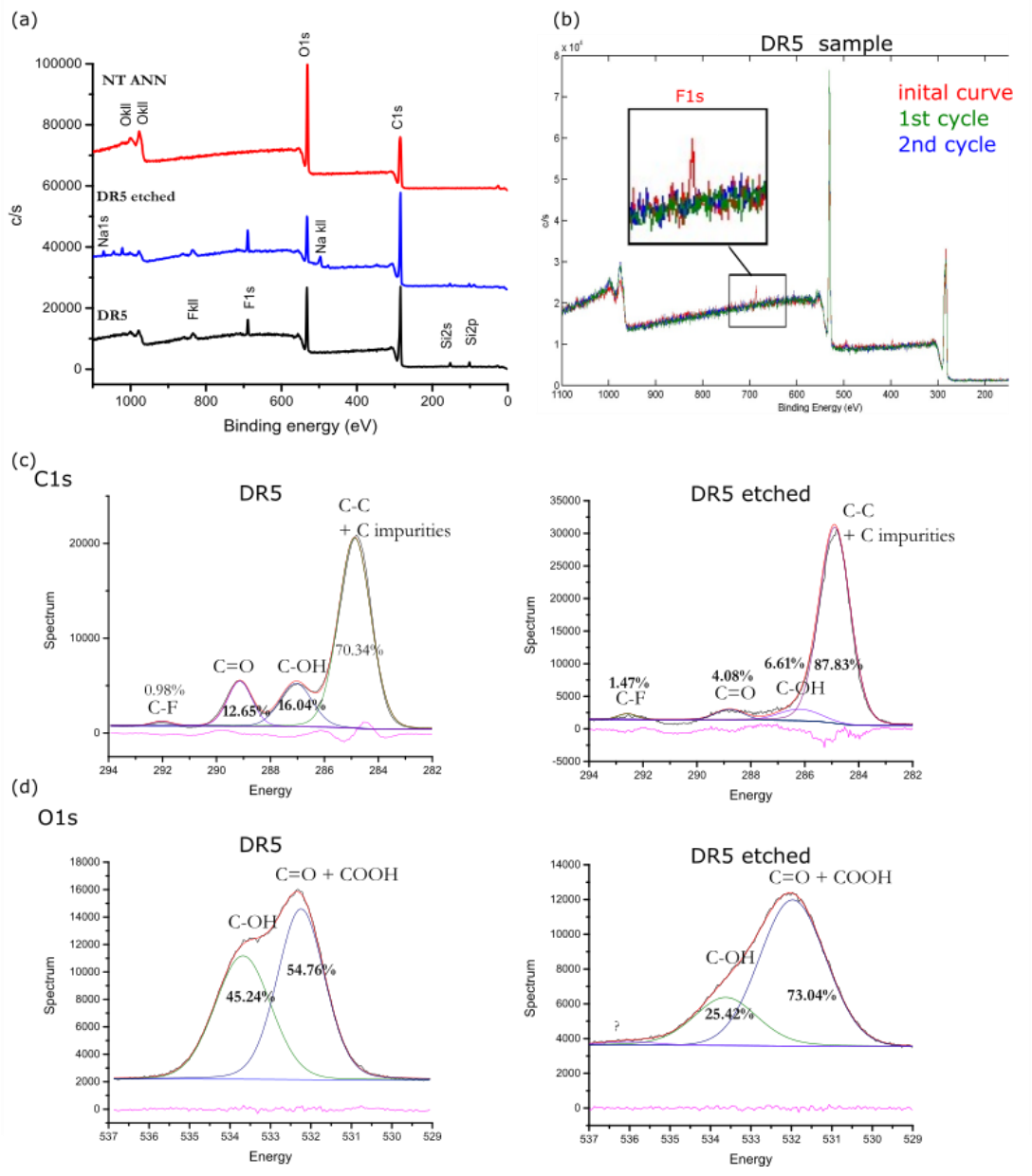

Figure 28: XPS spectra of nanotextured (NT), drawn (DR5) and additionally alkali-etched (DR5 etched) films present: (a) energy scan to identify elements, present on the surface; (b) Ar- surface etching of DR5 sample (2 cycles) to observe depth profiling, where clearly Flour disappear after the first etching cycle; (c) XPS spectra of C1s region, labeled with corresponding functional groups, and (d) XPS spectra of O1s region, labeled with corresponding functional groups for drawn sample (DR5) and drawn-etched sample (DR5 etched).

A.2 Comparing kHz and MHz Sound Stimulation on Possibility to Mechanically Deform Poly-L-Lactic Acid Film to Reveal Electric Potential

Piezoelectric measurements and following experiments on bacteria or human cells took place in an US bath with a manually controlled temperature that never exceeded 37°C (water flow while maintaining the water level). The usual excitation parameters for the measurements were a frequency of 37 kHz, 100% power of the US bath, while a frequency of 80 kHz (30-50% power) was used for the experiments with cells/bacteria, where the mechanical effect was less powerful (less bubble formation).

Less powerful 80 kHz range using US bath was used as it was mechanically more gentle for sensitive cells for near range excitation (cells/bacteria inside polystyrene sterile plate), but in real applicable use, the 1-3 MHz range is already used for therapeutic and diagnostic applications.

Table 2: Presented values of output potential in response to applied frequency excitation with US bath (37 or 80 kHz) or US probe (1 MHz) for piezoelectric (DR5) non-piezoelectric (DR1) films and the reference sample (PVDF).

ΔV	*Ultrasonic bath*		*Stimulating probe*
Frequency:	**37 kHz**	**80 kHz**	**1 MHz**
Drawn PLLA (DR5)	65 mV	25 mV	20 mV
PLLA DR1	0 mV	0 mV	0 mV
PVDF reference	1200 mV	400 mV	200 mV

By using US bath (Elmasonic P), presented in Fig. 29a, isolated films were immersed in a water-filled US bath and stimulated at different frequencies (37 or 80 kHz). Films were connected with electrodes to amplifier and to oscilloscope (Kaysight MSOX3034T) at the end, where generated voltage and responding film frequency was recorded. Through frequency measurement on the film, which corresponds to frequency of US bath, measurement method and material response was confirmed. For MHz stimulation, new machine (1 MHz US therapy machine Dynosound) was purchased and measurement was modified to be appropriate for later cell plate stimulation through water media. Fig. 29b presents the setup, where the stimulating probe is inserted under the glass petri dish, where a gel is used for better stimuli transfer and film or plate are in the water field petri dish, electrodes connected to the same oscilloscope in Fig. 29a.

Table 2 confirms that the film responds to both frequencies, kHz and MHz, and values for 80 kHz and 1 MHz are quite similar for PLLA, therefore using 80 kHz should be a good model to estimate the expected response of the cells if tested *in vivo*.

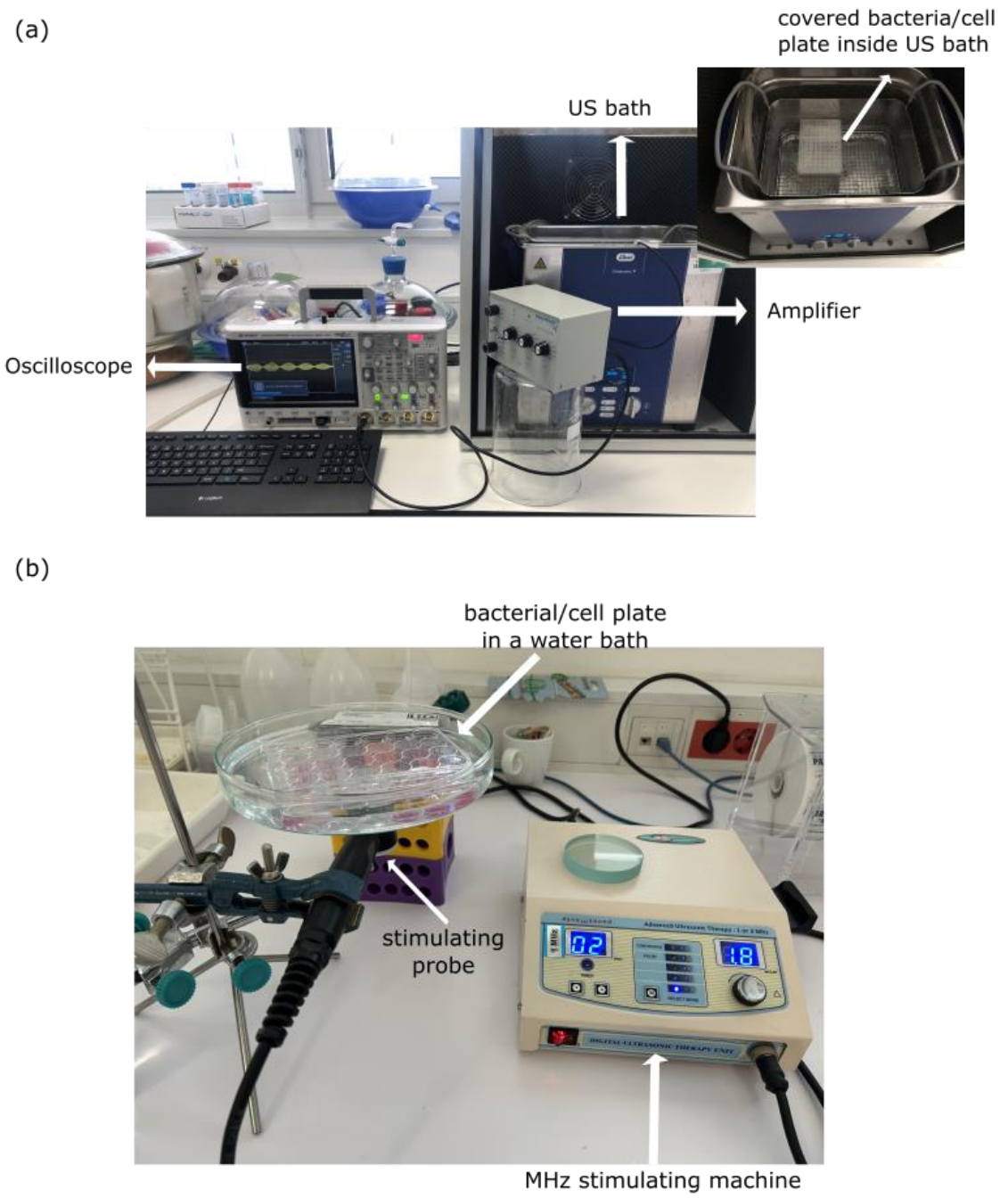

Figure 29: (a) Piezoelectric measurement/stimulating setup where the film (for measurement of piezoelectric properties) is submerged in water or the plate with cells (for testing) floats on water while the film is submerged in cell media inside a well, and sonicated, presented with named mechanical parts (ultrasonic bath, oscilloscope, amplifier); (b) MHz measurement setup using water as a medium to transfer the signal to the plate while stimulating with a probe touching a glass petri dish with gel applied in between for better stimuli transfer.

A.3 Observing Initial Attachment of Cells Due to Surface Modification (Alkaline Etching, Poly-L-Lysine Coating)

An improved hydrophilicity was observed for the surface-etched samples compared to the just drawn films, but the difference in cell attachment was not as pronounced as expected. Fig. 30a shows cell viability by PB absorbance measurements normalized to the surface showing a slight but not significant increase in cell attachment after 1 day of incubation compared to unetched samples, therefore post-etching was not used as a surface modification prior to testing.

Poly-L-lysine (PLL) is usually used in the literature as a standard method to improve the affinity of cells to the material. It is even used for polystyrene test plates intended for cells. In the presented case, the hot-pressed PLLA film was immersed in a prepared 0.01% sterile PLL solution (BioReagent, Sigma Life Science, UK) for 3 days and washed with DMEM before use. A cell solution (10^4 cells/well) was then added to the well, incubated for 1 day, and then the films were moved to a new well to measure the PB viability of the adherent cells alone. Values presented in Fig. 30b were normalized to surface area. DR1 film was chosen because it has the worst initial cell attachment, as this could emphasize the difference if observed. However, no difference in cell adhesion was observed when comparing the coated sample with the initial DR1 sample (Fig. 30b).

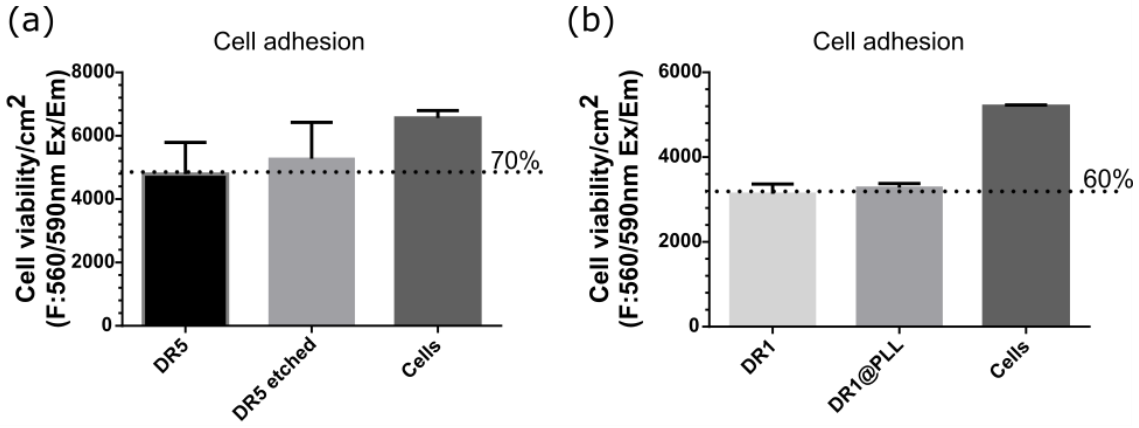

Figure 30: Comparison between PB cell viability normalized to surface area for (a) drawn (DR5) and surface-etched drawn films (DR5 etched), where the films achieved similar 70% adhesion compared to cells attached to the plate (dotted line); (b) PLLA DR1 sample and same sample coated with poly-L-lysin (DR1@PLL), where the films achieved similar 60% adhesion compared to cells attached to the plate (dotted line).

According to the results obtained, no post-etching or PLL coating was applied to the films prior the use with cells, as this does not provide any added value and the cell responses were observed in a shorter time, where polymer degradation does not yet occur.

References

[1] D. Kim, S. A. Han, J. H. Kim, J. Lee, S. Kim, and S. Lee, "Biomolecular Piezoelectric Materials: From Amino Acids to Living Tissues," *Adv. Mater.*, no. 1906989, pp. 1–16, 2020.

[2] S. E. B. Tyler, "Nature's Electric Potential: A Systematic Review of the Role of Bioelectricity in Wound Healing and Regenerative Processes in Animals, Humans, and Plants.," *Front. Physiol.*, vol. 8, p. 627, 2017.

[3] C. Ribeiro, V. Sencadas, D. M. Correia, and S. Lanceros-Mendez, "Piezoelectric polymers as biomaterials for tissue engineering applications," *Colloids Surfaces B Biointerfaces*, vol. 136, pp. 46–55, 2015.

[4] M. M. Fernandes, E. O. Carvalho, and S. Lanceros-Mendez, "Electroactive Smart Materials: Novel Tools for Tailoring Bacteria Behavior and Fight Antimicrobial Resistance," *Front. Bioeng. Biotechnol.*, vol. 7, no. 277, 2019.

[5] W. E. Prentice, "Tissue Response to Injury," in *Principles of Athletic Training: A Competency-Based Approach*, 2014, pp. 265–284.

[6] L. C. Shanley, "Harnessing the innate and adaptive immune system for tissue repair and regeneration: Considering more than macrophages," *Acta Biomater.*, vol. 133, pp. 208–221, 2021.

[7] S. Moon, J. Hong, S. Go, and B.-S. Kim, "Immunomodulation for Tissue Repair and Regeneration," *Tissue Eng. Regen. Med.*, vol. 20, no. 3, pp. 389–409, 2023.

[8] John D. Stroncek and W. Monty Reichert., "Chapter 1 Overview of Wound Healing in Different Tissue Types," in *Indwelling Neural Implants: Strategies for Contending with the In Vivo Environment*, 2008.

[9] Y. Qin, "Functional wound dressings," in *Medical Textile Materials*, Y. Qin, Ed. Woodhead Publishing, 2016, pp. 89–107.

[10] J. Hunckler and A. De Mel, "A current affair: electrotherapy in wound healing," *J. Multidiscip. Healthc.*, vol. 10, pp. 179–194, 2017.

[11] E. H. Kuzyk, P. R., & Schemitsch, "The science of electrical stimulation therapy for fracture healing," *Indian J. Orthop.*, vol. 43, no. 2, pp. 127–131, 2009.

[12] J. Wang, J. Lin, L. Chen, L. Deng, and W. Cui, "Endogenous Electric-Field-Coupled Electrospun Short Fiber via Collecting Wound Exudation," *Adv. Mater.*, vol. 34, pp. 2108325 (1–15), 2022.

[13] R. Nuccitelli, "A role for endogenous electric fields in wound healing.," *Curr. Top. Dev. Biol.*, vol. 58, pp. 1–26, 2003.

[14] G. Murillo *et al.*, "Electromechanical Nanogenerator-Cell Interaction Modulates Cell

Activity," *Bioelectronics*, vol. 29, p. 1605048, 2017.

[15] J. Jacob, N. More, K. Kalia, and G. Kapusetti, "Piezoelectric smart biomaterials for bone and cartilage tissue engineering," *Inflamm. Regen.*, vol. 38, no. 2, pp. 1–11, 2018.

[16] M. Hoop *et al.*, "Ultrasound-mediated piezoelectric differentiation of neuron-like PC12 cells on PVDF membranes," *Sci. Rep.*, vol. 7, no. 4028, pp. 1–8, 2017.

[17] C. G. T. Vance, D. L. Dailey, B. A. Rakel, and K. A. Sluka, "Using TENS for pain control: the state of the evidence.," *Pain Manag.*, vol. 4, no. 3, pp. 197–209, May 2014.

[18] K. E. Lampe, "Electrotherapy in tissue repair," *J. Hand Ther.*, vol. 11, no. 2, pp. 131–139, 1998.

[19] K. S. Ramadan, D. Sameoto, and S. Evoy, "A review of piezoelectric polymers as functional materials for electromechanical transducers," *Smart Mater. Struct.*, vol. 23, no. 3, 2014.

[20] P. Dineva, D. Gross, R. Muller, and T. Rangelov, "Piezoelectric materials," in *Dynamic Fracture of Piezoelectric Materials*, P. Dineva, D. Gross, R. Muller, and T. Rangelov, Eds. Springer International Publishing, 2014.

[21] Zeus, "Dielectric Properties of Polymers," 2005.

[22] C. Ribeiro, V. Sencadas, D. M. Correia, and S. Lanceros-Mendez, "Piezoelectric polymers as biomaterials for tissue engineering applications," *Colloids Surfaces B Biointerfaces*, vol. 136, pp. 46–55, 2015.

[23] A. H. Rajabi, M. Jaffe, and T. L. Arinzeh, "Piezoelectric materials for tissue regeneration: A review," *Acta Biomater.*, vol. 24, pp. 12–23, 2015.

[24] R. Wojnar, "Piezoelectric Phenomena in Biological Tissues," *Structure*, pp. 173–185.

[25] M. Smith *et al.*, "Direct observation of shear piezoelectricity in poly-l-lactic acid nanowires," *APL Mater.*, vol. 5, no. 074105, 2017.

[26] R. M. Rasal, A. V. Janorkar, and D. E. Hirt, "Poly(lactic acid) modifications," *Prog. Polym. Sci.*, vol. 35, no. 3, pp. 338–356, 2010.

[27] E. Lizundia, A. Larrañaga, J. L. Vilas, and L. M. León, "Three-dimensional orientation of poly(l-lactide) crystals under uniaxial drawing," *RSC Adv.*, vol. 6, no. 15, pp. 11943–11951, 2016.

[28] R. A. Abd Alsaheb *et al.*, "Recent applications of polylactic acid in pharmaceutical and medical industries," *J. Chem. Pharm. Res.*, vol. 7, no. 12, pp. 51–63, 2015.

[29] Y. Tajitsu, "Fundamental study on improvement of piezoelectricity of poly(L-lactic acid) and its application to film actuators," *IEEE Trans. Ultrason. Ferroelectr. Freq. Control*, vol. 60, no. 8, pp. 1625–1629, 2013.

[30] B. Lotz, "Crystal Polymorphism and Morphology of Polylactides," in *Synthesis, Structure and Properties of Poly(lactic acid)*, M. L. Di Lorenzo and R. Androsch, Eds. Cham: Springer International Publishing, 2018, pp. 273–302.

[31] C. S. Lovell, J. M. Fitz-Gerald, and C. Park, "Decoupling the effects of crystallinity and orientation on the shear piezoelectricity of polylactic acid," *J. Polym. Sci. Part B Polym. Phys.*, vol. 49, no. 21, pp. 1555–1562, 2011.

[32] B. Lotz, "Crystal Polymorphism and Morphology of Polylactides," in *Synthesis,*

Structure and Properties of Poly(lactic acid), M. L. Di Lorenzo and R. Androsch, Eds. Cham: Springer International Publishing, 2018, pp. 273–302.

[33] M. T. Chorsi *et al.*, "Piezoelectric Biomaterials for Sensors and Actuators," vol. 1802084, pp. 1–15, 2019.

[34] D. D. Angelo *et al.*, "Atmospheric Pressure Plasma Surface Modification of Poly (D,L-lactic acid) Increases Fibroblast, Osteoblast and Keratinocyte Adhesion and Proliferation," *Plasma Process. Polym.*, vol. 9, pp. 491–502, 2012.

[35] S. Sun, M. Wei, J. R. Olson, and M. T. Shaw, "Alkali Etching of a Poly(lactide) Fiber," *Appl. Mater. interfaces*, vol. 1, no. 7, pp. 1572–1578, 2009.

[36] C. Y. Tham, Z. A. A. Hamid, Z. Ahmad, and H. Ismail, "Surface Modification of Poly(lactic acid) (PLA) via Alkaline Hydrolysis Degradation," *Adv. Mater. Res.*, vol. 970, pp. 324–327, 2014.

[37] N. Yang *et al.*, "Immobilized Macrophage Colony-Stimulating Factor (M-CSF) Regulates the Foreign Body Response to Implanted Materials," *ACS Biomater. Sci. Eng.*, vol. 6, pp. 995–1007, 2020.

[38] M. Small *et al.*, "Nanostructure-Enabled and Macromolecule-Grafted Surfaces for Biomedical Applications.," *Micromachines*, vol. 9, no. 5, May 2018.

[39] L. Udovc, M. Spreitzer, and M. Vukomanovic, "Towards hydrophilic piezoelectric poly-L-lactide films: optimal processing, post-heat treatment and alkaline etching," *Polym. J.*, vol. 52, pp. 299–311, 2020.

[40] L. Gazvoda, B. Višić, M. Spreitzer, and M. Vukomanović, "Hydrophilicity Affecting the Enzyme-Driven Degradation of Piezoelectric Poly-L-Lactide Films," *Polymers (Basel).*, vol. 13, no. 1719, 2021.

[41] A. A. Singh, S. Geng, N. Herrera, and K. Oksman, "Aligned plasticized polylactic acid cellulose nanocomposite tapes: Effect of drawing conditions," *Compos. Part A Appl. Sci. Manuf.*, vol. 104, pp. 101–107, 2018.

[42] Z. Chen, S. Zhang, F. Wu, W. Yang, Z. Liu, and M. Yang, "Motion mode of poly(lactic acid) chains in film during strain-induced crystallization," *J. Appl. Polym. Sci.*, vol. 133, no. 6, pp. 1–10, 2016.

[43] Y. Tajitsu, "Basic Study of Controlling Piezoelectric Motion of Chiral Polymeric Fiber," *Ferroelectrics*, vol. 389, pp. 83–94, 2009.

[44] E. Fukada, "New Piezoelectric Polymers," *Jpn. J. Appl. Phys.*, vol. 37, pp. 2775–2780, May 1998.

[45] M. Smith, C. Lindackers, K. Mccarthy, and S. Kar-narayan, "Enhanced Molecular Alignment in Poly-L-Lactic Acid Nanotubes Induced via Melt-Press Template-Wetting," *Macromol. Mater. Eng.*, vol. 304, no. 1800607, 2019.

[46] M. Steinhart, J. H. Wendorff, and R. B. Wehrspohn, "Nanotubes a la Carte: Wetting of Porous Templates," *Chemphyschem*, vol. 4, pp. 1171–1176, 2003.

[47] J. Martín, J. Maiz, J. Sacristan, and C. Mijangos, "Tailored polymer-based nanorods and nanotubes by " template synthesis ": From preparation to applications," *Polymer (Guildf).*, vol. 53, no. 6, pp. 1149–1166, 2012.

[48] M. N. Dickson, E. I. Liang, L. A. Rodriguez, N. Vollereaux, and A. F. Yee, "Nanopatterned polymer surfaces with bactericidal properties," *Biointerphases*, vol. 10, no. 2, 2015.

[49] L. Gazvoda, "Antimicrobial activity of piezoelectric polymer: piezoelectricity as the reason for damaging bacterial membrane," *Biomater. Sci.*, vol. 10, pp. 4933–4948, 2022.

[50] J. Zhu, L. Jia, and R. Huang, "Electrospinning poly (l-lactic acid) piezoelectric ordered porous nanofibers for strain sensing and energy harvesting," *J. Mater. Sci. Mater. Electron.*, vol. 28, pp. 12080–12085, 2017.

[51] C. R. Gajjar, J. W. Stallrich, M. A. Pasquinelli, and M. W. King, "Process–Property Relationships for Melt-Spun Poly(lactic acid) Yarn," *ACS Omega*, vol. 6, no. 24, pp. 15920–15928, Jun. 2021.

[52] M. Yoshida, T. Onogi, K. Onishi, T. Inagaki, and Y. Tajitsu, "High piezoelectric performance of poly(lactic acid) film manufactured by solid-state extrusion," *Jpn. J. Appl. Phys.*, vol. 53, no. 9S, pp. PC02-1-PC02-6, 2014.

[53] R. P. Pawar, S. U. Tekale, S. U. Shisodia, J. T. Totre, and A. J. Domb, "Biomedical Applications of Poly(Lactic Acid)," *Rec. Pat. Regen. Med.*, vol. 4, pp. 40–51, 2014.

[54] Y. Ikada, Y. Shikinami, Y. Hara, M. Tagawa, and E. Fukada, "Enhancement of bone formation by drawn poly(L-lactide)," *J. Biomed. Mater. Res.*, vol. 30, no. 4, pp. 553–558, 1996.

[55] H. Miyazaki *et al.*, "An ultrathin poly(L-lactic acid) nanosheet as a burn wound dressing for protection against bacterial infection," *Wound Repair Regen.*, vol. 20, pp. 573–579, 2012.

[56] H. Guo *et al.*, "Piezoelectric PU/PVDF electrospun scaffolds for wound healing applications," *Colloids Surfaces B Biointerfaces*, vol. 96, pp. 29–36, 2012.

[57] E. T. Wang and M. Zhao, "Regulation of tissue repair and regeneration by electric fields," *Chinese J. Traumatol. - English Ed.*, vol. 13, no. 1, pp. 55–61, 2010.

[58] S. H. Bhang *et al.*, "Zinc Oxide Nanorod-Based Piezoelectric Dermal Patch for Wound Healing," *Adv. Funct. Mater.*, vol. 27, no. 1, 2017.

[59] C. Chen, X. Bai, Y. Ding, and I. Lee, "Electrical stimulation as a novel tool for regulating cell behavior in tissue engineering," *Biomater. Res.*, vol. 23, no. 25, 2019.

[60] K. Katoh, "Effects of Electrical Stimulation of the Cell: Wound Healing,Cell Proliferation, Apoptosis, and Signal Transduction," *Med. Sci.*, vol. 11, no. 11, 2023.

[61] A. Dascalu, A. Matithyou, Y. Oron, and R. Korenstein, "A hyperosmotic stimulus elevates intracellular calcium and inhibits proliferation of a human keratinocyte cell line.," *J. Invest. Dermatol.*, vol. 115, no. 4, pp. 714–718, Oct. 2000.

[62] K. Y. Arai *et al.*, "Pulsed electric current induces the differentiation of human keratinocytes," *Mol. Cell. Biochem.*, vol. 379, pp. 235–241, 2013.

[63] P. Martins, A. C. Lopes, and S. Lanceros-Mendez, "Electroactive phases of poly(vinylidene fluoride): Determination, processing and applications," *Prog. Polym. Sci.*, vol. 39, no. 4, pp. 683–706, 2014.

[64] T. Furukawa, "Piezoelectricity and Pyroelectricity in Polymers," *IEEE Trans. Electr. Insul.*, vol. 24, no. 3, pp. 375–394, 1989.

[65] Y. Yang and K. W. Leong, "Nanoscale surfacing for regenerative medicine," *WIREs Nanomedicine and Nanobiotechnology*, vol. 2, no. 5, pp. 478–495, 2010.

[66] M. Steinhart *et al.*, "Cellular interactions of biodegradable nanorod arrays prepared by nondestructive extraction from nanoporous alumina," *R. Soc. Chem. Soc. Chem.*,

vol. 20, no. 16, pp. 3117–3320, 2010.

[67] P. Italiani and D. Boraschi, "From monocytes to M1/M2 macrophages: phenotypical vs. functional differentiation," *Front. Immunol. /*, vol. 5, no. 514, pp. 1–22, 2014.

[68] J. Xu *et al.*, "Non-contact electrical stimulation as an effective means to promote wound healing," *Bioelectrochemistry*, vol. 146, p. 108108, 2022.

[69] C. R. Correia, J. Gaifem, M. B. Oliveira, R. Silvestre, and J. F. Mano, "Influence of surface modified poly (L-lactic acid) films on the differentiation of human monocytes into macrophages," *Biomater. Sci.*, vol. 5, no. 3, pp. 551–560, 2018.

[70] H. R. Caires, T. Esteves, P. Quelhas, M. A. Barbosa, M. Navarro, and C. R. Almeida, "Macrophage interactions with polylactic acid and chitosan scaffolds lead to improved recruitment of human mesenchymal stem/stromal cells: a comprehensive study with different immune cells," *J. R. Soc. Interface*, vol. 13, no. 20160570, 2016.

[71] Y. Kong *et al.*, "Wireless Localized Electrical Stimulation Generated by an Ultrasound-Driven Piezoelectric Discharge Regulates Proinflammatory Macrophage Polarization," *Adv. Sci.*, vol. 8, no. 13, p. 2100962, 2021.

[72] C. V Maduka *et al.*, "Polylactide Degradation Activates Immune Cells by Metabolic Reprogramming," *bioRxiv*, pp. 7–9, 2022.

[73] K. M. C. Oliveira *et al.*, "Electrical stimulation shifts healing/ scarring towards regeneration in a rat limb amputation model," *Sci. Rep.*, vol. 9, no. 11433, pp. 1–14, 2019.

[74] R. Kaur and S. Liu, "Antibacterial surface design – Contact kill," *Prog. Surf. Sci.*, vol. 91, no. 3, pp. 136–153, 2016.

[75] Y. Wang *et al.*, "Ultrasonic activation of inert poly(tetrafluoroethylene) enables piezocatalytic generation of reactive oxygen species," *Nat. Commun.*, vol. 12, no. 3508, pp. 1–8, 2021.

[76] S. K. Bardaweel, M. Gul, M. Alzweiri, and A. Ishaqat, "Reactive Oxygen Species: the Dual Role in Physiological and Pathological Conditions of the Human Body," *Eurasian J Med*, vol. 50, no. 3, pp. 193–201, 2018.

[77] M. Wu *et al.*, "Piezoelectric nanocomposites for sonodynamic bacterial elimination and wound healing," *Nano Today*, vol. 37, p. 101104, 2021.

[78] J. Feng, Y. Fu, X. Liu, S. Tian, S. Lan, and Y. Xiong, "Significant Improvement and Mechanism of Ultrasonic Inactivation to Escherichia coli with Piezoelectric Effect of Hydrothermally Synthesized t-BaTiO3," *ACS Sustain. Chem. Eng.*, vol. 6, no. 5, pp. 6032–6041, May 2018.

[79] S. Kumar, R. Vaish, and S. Powar, "Surface-selective bactericidal effect of poled ferroelectric materials," *J. Appl. Phys.*, vol. 124, no. 014901, 2018.

[80] E. O. Carvalho *et al.*, "Tailoring Bacteria Response by Piezoelectric Stimulation," *ACS Appl. Mater. Interfaces*, vol. 11, no. 30, pp. 27297–27305, 2019.

[81] C. Y. Calvet and L. M. Mir, "The promising alliance of anti-cancer electrochemotherapy with immunotherapy," *Cancer Metastasis Rev.*, vol. 35, no. 2, pp. 165–177, 2016.

[82] M. Ando, S. Takeshima, Y. Ishiura, K. Ando, and O. Onishi, "Piezoelectric antibacterial fabric comprised of poly(l-lactic acid) yarn," *Jpn. J. Appl. Phys.*, vol.

56, no. 10PG01, 2017.

[83] M. Ando *et al.*, "Electric antibacterial effect of piezoelectric poly(lactic acid) fabric," *Jpn. J. Appl. Phys.*, vol. 58, no. SLLD09, 2019.

[84] E. P. Ivanova *et al.*, "Natural Bactericidal Surfaces: Mechanical Rupture of Pseudomonas aeruginosa Cells by Cicada Wings," *Small*, vol. 8, no. 16, pp. 2489–2494, 2012.

[85] A. Jaggessar, H. Shahali, A. Mathew, and P. K. D. V Yarlagadda, "Bio-mimicking nano and micro-structured surface fabrication for antibacterial properties in medical implants," *J. Nanobiotechnology*, vol. 15, no. 64, 2017.

[86] Y. Jang *et al.*, "Inhibition of Bacterial Adhesion on Nanotextured Stainless Steel 316L by Electrochemical Etching," *ACS Biomater. Sci. Eng.*, vol. 4, pp. 90–97, 2018.

[87] M. Michalska *et al.*, "Tuning antimicrobial properties of biomimetic nanopatterned surfaces," *Nanoscale*, vol. 10, pp. 6639–6650, 2018.

[88] A. Cafarelli *et al.*, "Piezoelectric Nanomaterials Activated by Ultrasound: The Pathway from Discovery to Future Clinical Adoption," *ACS Nano*, vol. 15, pp. 11066–11086, 2021.

[89] Attilio Marino, G. G. Genchi, E. Sinibaldi, and G. Ciofani, "Piezoelectric Effects of Materials on Biointerfaces," *ACS Appl. Mater. Interfaces*, vol. 9, no. 21, pp. 17663–17690, 2017.

[90] X. Shi, Y. Chen, Y. Zhao, M. Ye, S. Zhang, and S. Gong, "Ultrasound-activable piezoelectric membranes for accelerating wound healing," *Biomater. Sci.*, vol. 10, pp. 692–701, 2022.

[91] J.-Y. Tsai, K.-H. Huang, J.-R. Wang, S.-I. Liu, and P.-C. Li, "Ultrasonic wireless power and data communication for neural stimulation," in *2011 IEEE International Ultrasonics Symposium*, 2011, pp. 1052–1055.

[92] P. Wu *et al.*, "Ultrasound-driven in vivo electrical stimulation based on biodegradable piezoelectric nanogenerators for enhancing and monitoring the nerve tissue repair," *Nano Energy*, vol. 102, p. 107707, 2022.

[93] H. L. de Mello, L. A. Alves, E. A. Dias, S. de Sá Pereira Magalhães, V. Cotta-de-Almeida, and R. da Cunha Bisaggio, "Sonodynamic and Photodynamics Used as a Combined Therapy in the Treatment of Malignant Neoplasms: Facts and Open Questions," in *Photodynamic Therapy*, N. M. Inada, H. H. Buzzá, K. C. Blanco, and L. D. Dias, Eds. Rijeka: IntechOpen, 2020.

[94] Y. Yao, Y. Pan, and S. Liu, "Power ultrasound and its applications: A state-of-the-art review," *Ultrason. Sonochem.*, vol. 62, p. 104722, 2020.

[95] Z. Xin, G. Lin, H. Lei, T. F. Lue, and Y. Guo, "Clinical applications of low-intensity pulsed ultrasound and its potential role in urology.," *Transl. Androl. Urol.*, vol. 5, no. 2, pp. 255–266, Apr. 2016.

[96] M. Vukomanović *et al.*, "Filler-Enhanced Piezoelectricity of Poly-L-Lactide and Its Use as a Functional Ultrasound-Activated Biomaterial," *Small*, vol. 19, no. 35, p. 2301981, 2023.

[97] S. M. Mccarty and S. L. Percival, "Proteases and Delayed Wound Healing," *Adv. Wound Care*, vol. 2, no. 8, pp. 438–447, 2013.

[98] L. I. Jinga *et al.*, "Chemical Degradation of Methylene Blue Dye Using TiO2/Au Nanoparticles," *Nanomaterials*, vol. 11, no. 1605, pp. 1–10, 2021.

[99] R. Das *et al.*, "Biodegradable nanofiber bone-tissue scaffold as remotely-controlled and self-powering electrical stimulator," *Nano Energy*, vol. 76, no. 105028, 2020.

[100] H. Bi, T. Feng, B. Li, and Y. Han, "In Vitro and In Vivo Comparison Study of Electrospun PLA and PLA/PVA/SA Fiber Membranes for Wound Healing," *Polymers (Basel).*, vol. 12, no. 839, 2020.

[101] M. Smith *et al.*, "Poly-L-Lactic Acid Nanotubes as Soft Piezoelectric Interfaces for Biology: Controlling Cell Attachment via Polymer Crystallinity," *ACS Appl. BIO Mater.*, vol. 3, pp. 2140–2149, 2020.

[102] T. Hou, F. Cao, M. Li, J. Wang, and L. Lv, "Harvesting the Vibration Energy with BaTiO3@Graphene for the Piezocatalytic Degradation of Methylene Blue," *J. Environ. Sci. Eng. Technol.*, vol. 8, pp. 84–91, 2020.

[103] C. Ning, Z. Zhou, G. Tan, Y. Zhu, and C. Mao, "Electroactive polymers for tissue regeneration: Developments and perspectives," *Prog Polym Sci*, vol. 81, pp. 144–162, 2019.

[104] S. B. Rajendran, K. Challen, K. L. Wright, and J. G. Hardy, "Electrical Stimulation to Enhance Wound Healing," *J. Funct. Biomater.*, vol. 12, no. 40, 2021.

[105] M. Zhao, "Electrical fields in wound healing—An overriding signal that directs cell migration," *Semin. Cell Dev. Biol.*, vol. 20, no. 6, pp. 674–682, 2009.

[106] C. Lu *et al.*, "Direct Current Electrical Fields Improve Experimental Wound Healing by Activation of Cytokine Secretion and Erk1/2 Pathway Stimulation," *Life*, vol. 11, no. 1195, 2021.

[107] J. C. Ojingwa and R. R. Isseroff, "Electrical stimulation of wound healing," *J Invest Dermatol.*, vol. 121, no. 1, pp. 1–12, 2003.

[108] D. Singh, "Comparative study of AC and DC fields on wound healing," *Environ. Conserv. J.*, vol. 21, pp. 173–175, 2020.

[109] S. Du *et al.*, "Bioinspired hybrid patches with self-adhesive hydrogel and piezoelectric nanogenerator for promoting skin wound healing," *Nano Res.*, vol. 13, no. 9, pp. 2525–2533, 2020.

[110] G. Xue *et al.*, "Cell Adhesion-Mediated Piezoelectric Self-Stimulation on Polydopamine-Modified Poly(vinylidene fluoride) Membranes," *ACS Appl. Mater. Interfaces*, vol. 13, no. 15, pp. 17361–17371, 2021.

[111] S. N. Gorodzha *et al.*, "A comparison study between electrospun polycaprolactone and piezoelecric poly(3-hydroxybutyrate-co-3-hydroxyvalerate) scaffolds for bone tissue engineering," *Colloids Surfaces B Biointerfaces*, vol. 160, pp. 48–59, 2017.

[112] C. Ribeiro *et al.*, "Enhanced proliferation of pre-osteoblastic cells by dynamic piezoelectric stimulation," *RSC Adv.*, vol. 2, pp. 11504–11509, 2012.

[113] Y. Tai, S. Yang, S. Yu, A. Banerjee, N. V Myung, and J. Nam, "Modulation of piezoelectric properties in electrospun PLLA nanofibers for application-specific self-powered stem cell culture platforms," *Nano Energy*, vol. 89, p. 106444, 2021.

[114] M. Rouabhia, H. Park, S. Meng, H. Derbali, and Z. Zhang, "Electrical stimulation promotes wound healing by enhancing dermal fibroblast activity and promoting myofibroblast transdifferentiation.," *PLoS One*, vol. 8, no. 8, p. e71660, 2013.

[115] Y. Tai, S. Yang, S. Yu, A. Banerjee, N. V Myung, and J. Nam, "Modulation of piezoelectric properties in electrospun PLLA nanofibers for application-specific self-powered stem cell culture platforms," *Nano Energy*, vol. 89, no. 106444, 2021.

[116] M. Piipponen, D. Li, and N. Xu, "The Immune Functions of Keratinocytes in Skin Wound Healing," *Int. J. Mol. Sci.*, vol. 21, no. 8790, 2020.

[117] S. Werner, T. Krieg, and H. Smola, "Keratinocyte – Fibroblast Interactions in Wound Healing," *J. Invest. Dermatol.*, vol. 127, no. 5, pp. 998–1008, 2007.

[118] I. Colombo *et al.*, "HaCaT Cells as a Reliable In Vitro Differentiation Model to Dissect the Inflammatory/Repair Response of Human Keratinocytes," *Mediators Inflamm.*, vol. 2017, 2017.

[119] C. Venter and C. U. Niesler, "Rapid quantification of cellular proliferation and migration using ImageJ," *Biotechniques*, vol. 66, no. 2, pp. 99–102, 2019.

[120] Y. Ma, K. Poole, J. Goyette, and K. Gaus, "Introducing Membrane Charge and Membrane Potential to T Cell Signaling.," *Front. Immunol.*, vol. 8, p. 1513, 2017.

[121] I. Jun, H. Han, J. R. Edwards, and H. Jeon, "Electrospun Fibrous Scaffolds for Tissue Engineering: Viewpoints on Architecture and Fabrication," *Int. J. Mol. Sci.*, vol. 19, no. 745, 2018.

[122] D. Mojena-Medina *et al.*, "Design, Implementation, and Validation of a Piezoelectric Device to Study the Effects of Dynamic Mechanical Stimulation on Cell Proliferation, Migration and Morphology," *Sensors*, vol. 20, p. 2155, 2020.

[123] P. K. Mattila and P. Lappalainen, "Filopodi[1] P. K. Mattila and P. Lappalainen, 'Filopodia: molecular architecture and cellular functions,' Nat. Rev. Mol. Cell Biol., vol. 9, no. 6, pp. 446–454, 2008.a: molecular architecture and cellular functions," *Nat. Rev. Mol. Cell Biol.*, vol. 9, no. 6, pp. 446–454, 2008.

[124] R. Ali, K. El-boubbou, and M. Boudjelal, "An easy, fast and inexpensive method of preparing a biological specimen for scanning electron microscopy (SEM)," *MethodsX*, vol. 8, no. May, p. 101521, 2021.

[125] B. Canales Coutiño and R. Mayor, "Reprint of: Mechanosensitive ion channels in cell migration," *Cells Dev.*, vol. 168, p. 203730, 2021.

[126] C. Pergola *et al.*, "Modulation of actin dynamics as potential macrophage subtype-targeting anti-tumour strategy.," *Sci. Rep.*, vol. 7, p. 41434, Jan. 2017.

[127] A. K. McNally and J. M. Anderson, "Macrophage fusion and multinucleated giant cells of inflammation.," *Adv. Exp. Med. Biol.*, vol. 713, pp. 97–111, 2011.

[128] A. R. B. Ribeiro, E. C. O. Silva, P. M. C. Araújo, S. T. Souza, E. J. da Silva Fonseca, and E. Barreto, "Application of Raman spectroscopy for characterization of the functional polarization of macrophages into M1 and M2 cells," *Spectrochim. Acta Part A Mol. Biomol. Spectrosc.*, vol. 265, p. 120328, 2022.

[129] M. Vukomanovic *et al.*, "Development of a ternary cyclodextrin–arginine–ciprofloxacin antimicrobial complex with enhanced stability," *Commun. Biol.*, vol. 5, no. 1, p. 1234, 2022.

[130] M. Vukomanovic *et al.*, "Multi-doped apatite: Strontium, magnesium, gallium and zinc ions synergistically affect osteogenic stimulation in human mesenchymal cells important for bone tissue engineering," *Biomater. Adv.*, vol. 140, p. 213051, 2022.

Bibliography

Journal Articles

L. Gazvoda, M. Spreitzer, M. Vukomanović, "Towards hydrophilic piezoelectric poly-L-lactide films: optimal processing, post-heat treatment and alkaline etching," *Polymer journal*, vol. 52, pp. 299-311, 2020.

L. Gazvoda, B. Višić, M. Spreitzer, M. Vukomanović, "Hydrophilicity affecting the enzyme-driven degradation of piezoelectric poly-L-lactic films," *Polymers*, vol. 13, no. 11, pp. 1719-1-1719, 2021.

L. Gazvoda, M. Peršić, M. Spreitzer, M. Vukomanović, "Antimicrobial activity of piezoelectric polymer : piezoelectricity as the reason for damaging bacterial membrane, " *Biomaterials science*, vol. 10, no. 17, pp. 4933-4948, 2022.

A. Motorzhina, S. Jovanović, V. K. Belyaev, D. Murzin, S. Pshenichnikov, V. G. Kolesnikova, A. S. Omelyanchik, L. Gazvoda, M. Spreitzer, L. Panina, V. Rodionova, M. Vukomanović, K. Levada, "Innovative gold/cobalt ferrite nanocomposite: physicochemical and cytotoxicity properties, ". *Processes* [Online ed.], vol. 9, no. 12, pp. 2264-1-2264-12, 2021.

M. Vukomanović, L. Gazvoda, M. Kurtjak, J. Hreščak, B. Jaklič, L. Moya-Anderico, M. del Mar Cendra, E. Torrents, "Development of a ternary cyclodextrin–arginine–ciprofloxacin antimicrobial complex with enhanced stability, " *Communications biology*, vol. 5, pp. 1234-1-1234-13, 2022.

M. Vukomanović, L. Gazvoda, N. Aničić, M. Rubert, D. Suvorov, R. Muller, S. Hofmann, "Multi-doped apatite: strontium, magnesium, gallium and zinc ions synergistically affect osteogenic stimulation in human mesenchymal cells important for bone tissue engineering, " *Biomaterials advances*, vol. 140, pp. 213051-1-213051-11, 2022.

M. Vukomanović, L. Gazvoda, M. Kurtjak, M. Maček, M. Spreitzer, S. Pane, et al., "Filler-enhanced piezoelectricity of poly-L-lactide and its use as a functional ultrasound-activated biomaterial, " *Small*, vol. 19, no 2301981, s. 1-16, 2023

Conference Paper

S. Nikolic, L.Gazvoda, R. M. Apetrei, M. Spreitzer, M. Vukomanovič, "Organic piezoelectric biomaterials for electrostimulation: poly-l-lactide films" in Proceedings of the 31st Conference of the European Society for Biomaterials, ESB2021 together with the 43rd Annual Congress of the Iberian Society of Biomechanics and Biomaterials (SIBB), Porto, Portugal (fully virtual): European Society for Biomaterials (EBS), 2021.

L. Gazvoda, M. Spreitzer, M. Vukomanović, "Use of piezoelectric Poly-L-lactic acid (PLLA) film to fight bacteria growth," in: 31st Conference of the European Society

for Biomaterials, ESB2021 together with the 43rd Annual Congress of the Iberian Society of Biomechanics and Biomaterials (SIBB), Porto, Portugal (fully virtual): European Society for Biomaterials, 2021.

L. Gazvoda, M. Spreitzer, M. Vukomanović, "Biomaterials for specific medical applications, " in: 11th World Biomaterials Congress (virtual): WBC 2020.

M. Vukomanović, L. Gazvoda, L. Moya-Anderico, M. del Mar Cendra, E. Torrents, "Boosting efficacy and decreasing toxicity of antimicrobial nanoparticles mediated by cyclodextrin, " in Abstracts of the 30th Annual Conference of the European Society for Biomaterials together with The 26th Annual Conference of The German Society for Biomaterials (DGBM), Dresden, Germany, 2019.

S. Jovanović, M. Vukomanović, L. Gazvoda, D. Peddis, M. Spreitzer, et al., "Synthesis of superparamagnetic zinc- and gallium-substituted cobalt ferrite nanoparticles, " in: M. Rivas (ed.), Book of abstract of the International Conference on Fine Particle Magnetism (ICFPM19), Gijón, Spain, Oviedo: Universidad de Oviedo, 2019.

L. Gazvoda, M. Spreitzer, M. Vukomanovič, "Wound healing using piezoelectric patch, " in: M. Topole (ed.), et al., Book of abstracts of the Science of the future how to stay up-to-date with your research!, 11th Jožef Stefan International Postgraduate School Students' Conference and 13th Young Researchers' Day, Planica, Slovenija, Ljubljana: Jožef Stefan International Postgraduate School: Jožef Stefan Institute, 2019.

S. Jovanović, L. Gazvoda, J. Rmuš, M. Spreitzer, M. Vukomanović, "Synthesis of antimicrobial cobalt ferrite/gold nanocomposites, " in: D. Uskoković, V. Radmilović (ed.), Programme and the book of abstracts of the Twentienth Annual Conference YUCOMAT, Herceg Novi, Montenegro, Belgrade: Materials Research Society of Serbia, 2018.

L. Gazvoda, M. Vukomanović, M. Štefanič, M. Spreitzer, "Influence of processing conditionson crystallinity and orientation of poly-L-lactic acid films prepared by tensile drawing, " in: M. Dežman (ed.), et al., Proceedings of the 10th Jožef Stefan International Postgraduate School Students' Conference and 12th Young Researchers' Day, Piran, Slovenia, Ljubljana: Jožef Stefan International Postgraduate School: Jožef Stefan Institute, 2018.

Biography

Lea Gazvoda obtained her first Criminal Justice and Security bachelor degree at the Faculty of Criminal Justice and Security, University in Maribor, in 2012. She transferred some useful knowledge, such as knowledge of working independently or in teams, social and psychological aspects of communication and an analytical, creative and innovative approach to problem solving to the equivalent study program Chemical Engineering, where she graduated in 2015 from the Faculty of Chemistry and Chemical Technology, University of Ljubljana. She continued her studies at the University of Ljubljana and received her Chemical Engineering master's degree in 2017. In the same year, she enrolled in the third-level study program of Nanosciences and Nanotechnologies at the Jožef Stefan International Postgraduate School in Ljubljana and started working as a Young Researcher at the Advanced Materials Department (K9).

Her research is focused on the biological field and on the preparation and characterizations of functional materials. Her experiences include sonochemical synthesis of nanoparticles, modulation of polymers into films and fibers, mechanical, thermal and electrical analysis of piezoelectric polymers, evaluation of surface properties, antibacterial properties and biocompatibility, with a knowledge of culturing cells and bacteria and biotesting with materials. Her latest research work is focused on preparing piezoelectric nanotextured or stretched films of biodegradable poly-L-lactic acid polymer, applicable as noninvasive contact delivery of on-demand electrical stimulation on the cells for improving wound healing with possible associated antimicrobial properties.